THE UNIVERSITY
of EDINBURGH

UNIVERSITY OF EDINBURGH

DOCTORAL THESIS

Deep and Intermediate Water Mass History of the Western Indian Ocean

---

Author:
Jamie Lyon MAXWELL

Supervisors:
Dr. Simon JUNG
Prof. Dick KROON

A thesis submitted in fulfillment of the requirements
for the degree of Doctor of Philosophy

January 7, 2019

Declaration of Authorship

I, Jamie Lyon MAXWELL, declare that this thesis titled, "Deep and Intermediate Water Mass History of the Western Indian Ocean" and the work presented in it are my own. I confirm that:

- This work has been composed by myself.
- This work has not been submitted for any other degree or professional qualification.
- Where I have consulted the published work of others, this is always clearly attributed.
- I have acknowledged all main sources of help.

Signed:

_____

Date:

_____

"This grand show is eternal. It is always sunrise somewhere; the dew is never all dried at once; a shower is forever falling; vapor is ever rising. Eternal sunrise, eternal sunset, eternal dawn and gloaming, on sea and continents and islands, each in its turn, as the round earth rolls."

John Muir

University of Edinburgh

School of GeoScience

Doctor of Philosophy

Abstract

Deep and Intermediate Water Mass History of the Western Indian Ocean

by Jamie Lyon MAXWELL

This research focuses on reconstructing the history of various oceanic conditions, ranging from surface to deep layers, in the Western Indian Ocean over the last glacial cycle.

A new data set is presented, composed of various palaeoceanographic proxies from marine sediment cores 64PE304-8 (752m), 64PE303-16 (1350m) and 64PE303-15 (1985m) retrieved along a depth transect during the "Tropical Temperature History During Paleogene Global Warming Events" (GLOW) **?** and "Indian – Atlantic Exchange" (INATEX) **?** expeditions of the research vessel Pelagia.

Interpretation of this new data, forming a vertical transect of geochemical proxies of terrigenous hydrological change and foraminiferal stable isotope records anchored in robust radiocarbon based age models, provides a significant contribution to an area of poor data coverage in the western Indian Ocean.

Geochemical records of eastern African hydrological change provide a record of monsoon driven rainfall changes. We show that orbitally driven cycles in the log (Ti/Ca) series are a direct response to regional equatorial insolation. We notice that the structure of the precessionally driven cycles shows no similarity with the widely cited monsoonal influenced Chinese cave speleothem records (**??**). The offshore Tanzanian records show a remarkable resemblance with the newly published Borneo cave speleothem record (**?**), both likely driven by near regional equatorial insolation patterns.

Millennial scale events are strongly manifest in the log(Ti/Ca) series in intervals where sedimentation rates are relatively high, punctuating the longer-term precessionally driven cycles. The log(Ti/Ca) series show a number of distinct dry events, which occurred synchronously with the northern hemisphere cold Heinrich events. The data show a strong coupling between changes in monsoon rainfall offshore Tanzania and the northern hemisphere Heinrich cold events, likely mediated by the average position of the intertropical convergence zone.

The stable isotope data helps our understanding of variability of surface, intermediate and deep ocean circulation in the western Indian Ocean on the millennial time-scale. The depth transect approach allows us to investigate time offsets between the individual stable isotope records of the surface, intermediate and deep waters during the late glacial-Holocene cycle. The time off sets are useful indicators of connections between changes in western Indian Ocean water masses and climate change in the high latitudes. Our new data highlights significant differences across the water column in the timing of deglaciation. We can robustly report that the intermediate depth ocean in the region of our cores was the first to record an oxygen isotope signal of the deglaciation. The rate of change records calculated further show the offsets and elucidate the apparent relationship between our surface records and Greenland in terms of timing of change.

The records presented here are also placed in a broader Indian Ocean/Arabian sea context to asses to role of the intermediate depths of the Indian Ocean in millennial scale change, particularly during Heinrich events. Using the combined insights provided by the new $\delta^{18}O$ and $\delta^{13}C$ records, the new transect of records highlights changes in the nature of intermediate depth Indian Ocean circulation changes over the last 40kyr. This contributes to the discussion of the origin of the oxygenation pulses in the Arabian Sea, that either reflect local changes in intermediate water properties, or indeed bear evidence of a larger, Indian Ocean wide expansion of glacial Antarctic Intermediate water. The new data are combined with published data to assess modes of ocean circulation in the Indian Ocean. This helps to elucidate the role played by this part of the global ocean system in the millennial-scale climate shifts - including the bipolar seesaw phenomenon - that occurred during this time period.

In particular, two valuable insights into past changes in ocean circulation in the western Indian Ocean are presented, with important implications for our understanding of the role of ocean circulation in millennial scale and deglacial climate

shifts. First, our new data supports the notion of expanded glacial AAIW at intermediate depths within the Indian Ocean during Heinrich events. Second, we see evidence of a deglacial reorganistaion of the ventilation pattern in the region across the deglaciation. This involves an chemically aged watermass reaching the upper 1000m of the western Indian Ocean via the Indonesian Through-flow and the SEC.

Acknowledgements

There are a number of people I should thank for a number of different contributions to my time as a doctoral student.

For their help on scientific matters:

- Jeroen van der Lubbe for important contributions of bulk sediment geochemical and stable isotope data
- Sam Carter for his help in picking foraminifera
- Simon Jung & Dick Kroon for their help throughout this project

For their help on a more personally supportive level:

- My wife Jessica for believing in me (and supporting me in ways too numerous to mention)
- My dog Shell for providing a constant reminder that this isn't all that important; walks are far more crucial
- My parents for their continued support for my overlong student career, despite never really knowing why

Contents

Chapter 1

Introduction & Background

1.1 Thesis Abstract

This research focuses on reconstructing the history of various oceanic conditions, ranging from surface to deep layers, in the Western Indian Ocean over the last glacial cycle.

A new data set is presented, composed of various palaeoceanographic proxies from marine sediment cores 64PE304-8 (752m), 64PE303-16 (1350m) and 64PE303-15 (1985m) retrieved along a depth transect during the "Tropical Temperature History During Paleogene Global Warming Events" (GLOW) Kroon and Party (2010) and "Indian – Atlantic Exchange" (INATEX) Brummer and Jung (2009) expeditions of the research vessel Pelagia.

Interpretation of this new data, forming a vertical transect of geochemical proxies of terrigenous hydrological change and foraminiferal stable isotope records anchored in robust radiocarbon based age models, provides a significant contribution to an area of poor data coverage in the western Indian Ocean.

Geochemical records of eastern African hydrological change provide a record of monsoon driven rainfall changes. We show that orbitally driven cycles in the log (Ti/Ca) series are a direct response to regional equatorial insolation. We notice that the structure of the precessionally driven cycles shows no similarity with the

widely cited monsoonal influenced Chinese cave speleothem records (Wang et al.; 2001; Cheng et al.; 2016). The offshore Tanzanian records show a remarkable resemblance with the newly published Borneo cave speleothem record (Carolin et al.; 2016), both likely driven by near regional equatorial insolation patterns.

Millennial scale events are strongly manifest in the log(Ti/Ca) series in intervals where sedimentation rates are relatively high, punctuating the longer-term precessionally driven cycles. The log(Ti/Ca) series show a number of distinct dry events, which occurred synchronously with the northern hemisphere cold Heinrich events. The data show a strong coupling between changes in monsoon rainfall offshore Tanzania and the northern hemisphere Heinrich cold events, likely mediated by the average position of the intertropical convergence zone.

The stable isotope data helps our understanding of variability of surface, intermediate and deep ocean circulation in the western Indian Ocean on the millennial time-scale. The depth transect approach allows us to investigate time offsets between the individual stable isotope records of the surface, intermediate and deep waters during the late glacial-Holocene cycle. The time off sets are useful indicators of connections between changes in western Indian Ocean water masses and climate change in the high latitudes. Our new data highlights significant differences across the water column in the timing of deglaciation. We can robustly report that the intermediate depth ocean in the region of our cores was the first to record an oxygen isotope signal of the deglaciation. The rate of change records calculated further show the offsets and elucidate the apparent relationship between our surface records and Greenland in terms of timing of change.

The records presented here are also placed in a broader Indian Ocean/Arabian sea context to asses to role of the intermediate depths of the Indian Ocean in millennial scale change, particularly during Heinrich events. Using the combined insights provided by the new $\delta^{18}O$ and $\delta^{13}C$ records, the new transect of records highlights changes in the nature of intermediate depth Indian Ocean circulation changes over

the last 40kyr. This contributes to the discussion of the origin of the oxygenation pulses in the Arabian Sea, that either reflect local changes in intermediate water properties, or indeed bear evidence of a larger, Indian Ocean wide expansion of glacial Antarctic Intermediate water. The new data are combined with published data to assess modes of ocean circulation in the Indian Ocean. This helps to elucidate the role played by this part of the global ocean system in the millennial-scale climate shifts - including the bipolar seesaw phenomenon - that occurred during this time period.

In particular, two valuable insights into past changes in ocean circulation in the western Indian Ocean are presented, with important implications for our understanding of the role of ocean circulation in millennial scale and deglacial climate shifts. First, our new data supports the notion of expanded glacial AAIW at intermediate depths within the Indian Ocean during Heinrich events. Second, we see evidence of a deglacial reorganistaion of the ventilation pattern in the region across the deglaciation. This involves an chemically aged watermass reaching the upper 1000m of the western Indian Ocean via the Indonesian Through-flow and the SEC.

1.1.1 Layman's Abstract

This work is part of a wider scientific effort to understand how our earth system operates. By looking into the past we can hopefully inform how the planet may change in the future. In order to achieve this we have built up records of past change using various indicators of different elements of the ocean and climate system in the western Indian Ocean and eastern African region. These records were obtained from sediment cores from the sea bed offshore Tanzania.

Two main types of indicators (or proxies) have been used. First, those representing change on the African continent. These were transported into the ocean by rivers and serve to record changes in the rainfall and climate on the continent,

nearby the core sites used here. Second, those representing changes in marine conditions. In this work these come from fossils of small creatures that lived in various different ocean conditions. From the chemistry of these fossils we can trace changes in, for example, the regional circulation and temperature of the oceans.

We document changes occurring along a transect from the African continent down to around 2km below the sea surface offshore Tanzania. The findings presented here are wide ranging. We have strengthened and contributed to much scientific debate surrounding the nature of change in the region during the past 150kyr and discussed how this change relates to climate elsewhere on the planet.

1.2 Introduction

Paleoclimate archives from across the globe provide significant insight into past changes in the global climate systems. These insights help us understand the climate system as it functions today and how it may change in the future. Of particular interest is the nature of variability during the Quaternary period ($\sim$2.6 million years ago until present day). This period has been characterised by relatively long-term glacial-interglacial type variability driven by orbital variations and feedbacks within the climate system. On shorter time-scales, millennial-scale variability occurred across the globe. The so called Dansgaard-Oeschger cycles represent recurrent and rapid temperature spikes over Greenland during the last glacial period (Dansgaard et al.; 1984). Embedded in this short-term variability are repeated occurrences of ice-rafted debris (IRD) layers within North Atlantic sediment, deposited during maximum cold conditions in the region (Heinrich; 1988; Broecker et al.; 1992). These events are termed Heinrich events. Melt-water events associated with IRD deposition led to reduced North Atlantic deep water (NADW) formation (Sarnthein et al.; 1994; Jung; 1996; Elliot et al.; 2002). Given that NADW is one of the most significant water masses of the deep ocean, this variability had implications

for ocean circulation and climate globally. The nature and spatial differences of this short-term variability are less well known.

An important feature of this short-term variability is the so-called bipolar seesaw, characterised by inter-hemispheric asynchrony in temperature variability (Stocker and Wright; 1996; Broecker; 1998). This was first documented in a comparison between Greenland and Antarctic ice core temperature records (Figure 1.1; Blunier et al. 1998; Blunier and Brook 2001). Our understanding of this phenomenon is poorly developed. A potentially significant role in the bipolar seesaw phenomenon comes from the intermediate and deep ocean circulation systems. The intermediate depth oceans provide a mechanism to connect climate change at high and low latitudes, sometimes termed the 'oceanic tunnel' mechanism (Liu and Alexander; 2007). Important feedbacks in terms of ocean-mediated global energy and greenhouse gas transport are associated with the intermediate depth circulation through 'oceanic tunnels'. For instance, it has been recently demonstrated that, in the modern systems, intermediate waters absorb a significant fraction of anthropogenic CO_2 (Mikaloff Fletcher et al.; 2006; Sabine et al.; 2004). Similarly, the deep portions of the world's oceans play a significant role in the storage of energy and carbon. Hence, an improved understanding of the role of intermediate and deep ocean circulation in past climate systems is important for our understanding of present and future roles of the ocean within the climate system.

Previous work suggests significant change in Indian Ocean intermediate and thermocline circulation patterns on the millennial time-scale, related to/part of the wider millennial-scale climate system (Böning and Bard; 2009; Kiefer et al.; 2006; Wang et al.; 2013; Romahn et al.; 2014; Jung et al.; 2009). Indeed, the intermediate depth oceans are thought to play a key role in transmitting a Southern type signal to lower latitudes via the oceanic tunnel mechanism (Liu and Alexander; 2007). Evidence of enhanced ventilation of Antarctic Intermediate Water (AAIW) during Heinrich 1 (H1) and the Younger Dryas (YD) periods has been found in the

Atlantic (Pahnke et al.; 2008), Pacific (Pahnke and Zahn; 2005) and Indian Oceans (Jung et al.; 2009). Although some studies find no evidence of this increased intermediate ventilation (Romahn et al.; 2014). Contrasting evidence has also been found showing a reduced influence of AAIW within the Atlantic during northern hemisphere cold events (Huang et al.; 2014).

Initial thinking around global millennial-scale climate change during the last glacial period assumed a high-latitude North Atlantic origin, propagated globally via NADW variability (Weyl; 1968; Broecker; 1998; Broecker et al.; 1990). More recently, improvements in ice core chronologies – based on alignment of methane concentrations – suggest that millennial-scale temperature variations occurred in Antarctica prior to Greenland (Blunier et al.; 1998; Blunier and Brook; 2001). Further, paired planktonic and benthic stable isotope records from marine sediments cores demonstrate a similar relationship in terms of high-latitude sourced water masses. Southern hemisphere derived Antarctic Bottom Water (AABW) variability leads NADW (Charles et al.; 1996; Shackleton et al.; 2000) by several thousand years. Further, improvements in the data coverage of low latitude regions suggest different millennial-scale change regimes. For instance, speleothem based records of monsoon rainfall from the mid-latitude northern hemisphere suggests correlation to Greenland temperature variations (Cheng et al.; 2016, 2009). Although a recent tropical record of monsoon rainfall shows a less clear relationship (Carolin et al.; 2016) and hints at a more independent tropical equatorial system of millennial-scale change. Low latitudinal monsoon areas may have a key role through greenhouse gas feedbacks in driving and/or perpetuating global millennial-scale change (Ivanochko et al.; 2005). Hence, current thinking on the wider millennial-scale climate system is unclear in terms of the overall drivers and responses of various parts of the globe.

Within the western Indian Ocean and in particular the Arabian Sea region, evidence suggests a coherence between surface ocean changes and high latitude

northern hemisphere climate change. This relationship is likely driven via changes in monsoon strength (Singh et al.; 2011; Schulz; 1998; Jung et al.; 2009; Ivanochko et al.; 2005; Altabet et al.; 2002; Deplazes et al.; 2014; Mohtadi et al.; 2014). Itself a consequence of changes in the position of the Inter-tropical Convergence Zone (ITCZ) as a response to high latitude temperature variability. Modelling studies show that the ITCZ will move towards the warmer hemisphere because of an increased inter-hemispheric temperature gradient (e.g. McGee et al. 2014; Broccoli et al. 2006; Chiang and Bitz 2005). However, some evidence has been found linking the tropical surface Indian Ocean to Antarctic climate patterns (Kiefer et al.; 2006). The subsurface ocean paints a more complex picture. Ventilation changes at intermediate water depth in the Arabian Sea appear connected to Southern Ocean circulation changes via glacial AAIW. There is suggestion of increased temperatures of intermediate waters in the Arabian Sea, during northern hemisphere cold events (Jung and Kroon; 2011; Jung et al.; 2009). Hence, there is much scope for improving our data coverage and understanding of this particular part of the climate system.

1.3 Objectives of Thesis

This research focuses on reconstructing the history of various oceanic conditions, ranging from surface to deep layers, in the western Indian Ocean over the last glacial cycle.

The primary objective of this project was to create a new data set of various palaeoceanographic proxies from marine sediment cores 64PE304-8 (752m), 64PE303-16 (1350m) and 64PE303-15 (1985m) retrieved along a depth transect during the "Tropical Temperature History During Paleogene Global Warming Events" (GLOW; Kroon and Party 2010) and "Indian – Atlantic Exchange" (INATEX; Brummer and Jung 2009) expeditions of the research vessel *Pelagia*.

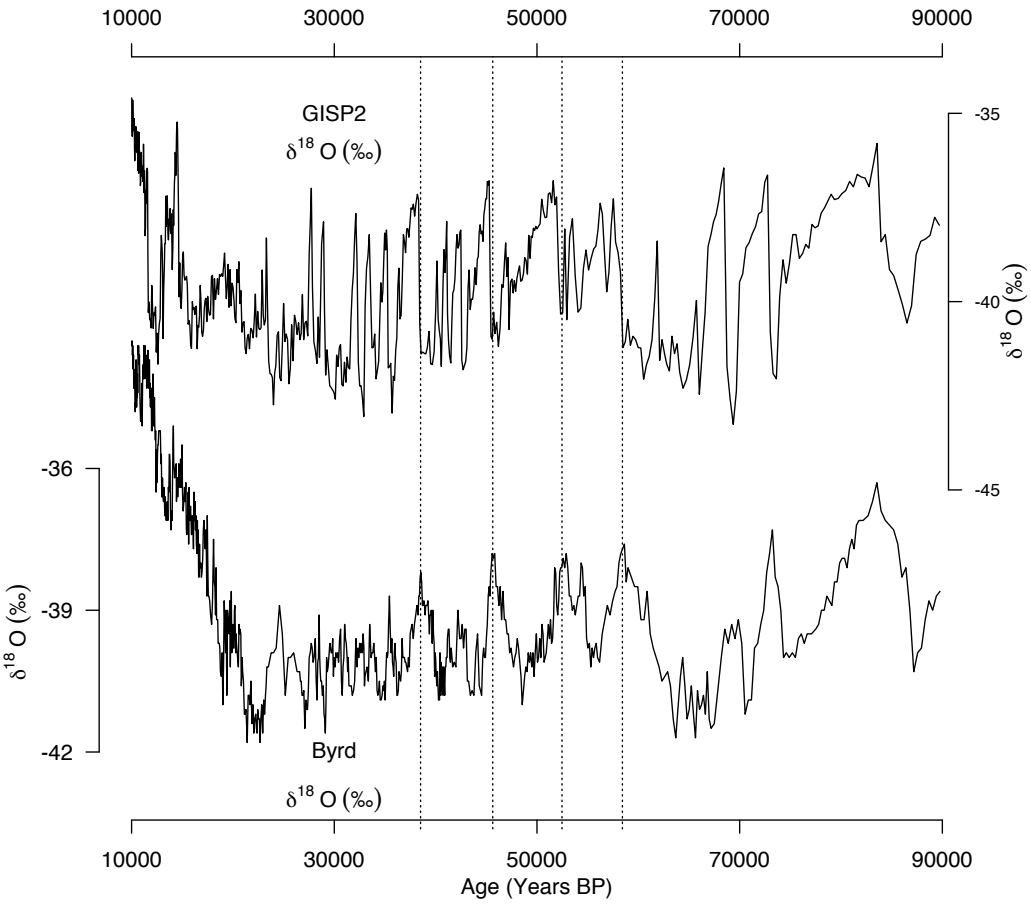

FIGURE 1.1: Oxygen isotope records from Greenland (top) and Antarctica (bottom), both plotted on GISP2 timescale. Modified after Blunier and Brook (2001). Vertical dashed lines illustrate onset of major Dansgaard-Oeschger (DO) events and the contrasting nature of change seen in the Byrd record at the same time. Greenland data from GISP2 ice core (Grootes et al.; 1993). Antarctica data from Byrd station, west Antarctica (Johnsen et al.; 1972).

The resultant data, forming a vertical transect of geochemical proxies of terrigenous hydrological change and foraminiferal stable isotope records anchored in robust radiocarbon based age models, will be described and interpreted with the aim of contributing to an area of poor data coverage in the western Indian Ocean.

The terrigenous-derived records of east African hydrological change provide a climatic record of monsoon driven rainfall changes. These records will help place the regional climate in the context of varying latitudinal regimes of climate change associated with long- and short-term changes over the last 150kyr. In doing so, we can assess the latitudinal dominance of the contrasting northern versus southern type climate variability that characterises the bipolar seesaw phenomenon. In terms of the wider discussion of the bipolar seesaw during millennial-scale climate shifts of the last glacial period, a better understanding of the atmospheric and hydrological climate regime is vital to understanding the surface ocean changes. Hence the combination of terrigenous and marine derived records of climate change makes for a powerful multi-proxy approach.

The stable isotope data helps our understanding of variability of surface, intermediate and deep ocean circulation in the western Indian Ocean on the millennial time-scale. The depth transect approach allows us to investigate time offsets between the individual stable isotope records of the surface, intermediate and deep waters during the late glacial-Holocene cycle. The time off sets are useful indicators of connections between changes in western Indian Ocean water masses and climate change in the high latitudes. Using the combined insights provided by the new $\delta^{18}O$ and $\delta^{13}C$ records, the new transect of records will help us to investigate changes in the nature of intermediate depth Indian Ocean circulation changes over the last 40kyr. This will allow assessment of the origin of the oxygenation pulses in the Arabian Sea, that either reflect local changes in intermediate water properties, or indeed bear evidence of a larger, Indian Ocean wide expansion of glacial AAIW. The new data will be combined with published data that are used to assess modes

of ocean circulation in the Indian Ocean based on time slice reconstructions. This will help to elucidate the role played by this part of the global ocean system in the millennial-scale climate shifts - including the bipolar seesaw phenomenon - that occurred during this time period.

1.4 Overview of Thesis

1.4.1 Chapter 1 - Introduction

The remainder of this chapter aims to give the reader a very brief overview of the regional setting of the sediment cores presented in this thesis and also of the sediment based proxies used to reconstruct the various oceanographic factors discussed here. This section is intentionally much more brief than it could be. I have tried to provide references for extra background where needed. Nearly all the proxies and methods used here are standard and well tested, hence little attention is given to discussing them. This approach is intended to keep the focus of this thesis on the new data and its interpretation. Further specific background is given where needed.

1.4.2 Chapter 2 - Methods

This chapter provides an overview of the procurement and preparation of the samples and of the analytical processes behind the data presented here. Once more, this section is kept succinct as the methods are standard. Note however this should not give the reader the impression that preparation of samples and collection of data occupied a minor part of the time and labour of this project; the very opposite is true.

1.4.3 Chapter 3 - Bulk sediment geochemical data

The monsoon system is key for understanding climate patterns in eastern equatorial Africa in a spatial and temporal sense. However, there is surprisingly little known about climate development in this area on long-term time-scales. This chapter presents geochemical changes (log(Ti/Ca) series) in four newly dated marine sediment cores (64PE304-8, 64PE304-34, 64PE303-16 and 64PE303-15) from ∼9°S in the western tropical Indian Ocean. These cores were retrieved along a depth transect offshore Tanzania, that reflect rainfall variability in the catchments of the Rovuma and Rufiji rivers in equatorial Africa on orbital and millennial time-scales for the last 150 kyrs. We show that orbitally driven cycles in the log (Ti/Ca) series are a direct response to regional equatorial insolation. We notice that the structure of the precessionally driven cycles, which are sinusoidal in nature, shows no similarity with the widely cited monsoonal influenced Chinese cave speleothem records (Wang et al.; 2001; Cheng et al.; 2016), which are box-shaped in nature. The offshore Tanzanian records show a remarkable resemblance with the newly published Borneo cave speleothem record (Carolin et al.; 2016), both likely driven by near regional equatorial insolation patterns. Millennial scale events are strongly manifest in the log(Ti/Ca) series in intervals where sedimentation rates are relatively high, punctuating the longer-term precessionally driven cycles. The log(Ti/Ca) series show a number of distinct dry events, which occurred synchronously with the northern hemisphere cold Heinrich events. The most distinct event is characterised by unusually dry conditions during the main melting phase of the stage 6 northern hemisphere ice sheet, which correlates to Heinrich event 11. Conversely, further south in the Zambezi area, similar geochemical data show that wetter conditions prevailed during the Heinrich events (van Der Lubbe et al.; 2014). The combined data show a strong coupling between changes in monsoon rainfall offshore Tanzania and the northern hemisphere Heinrich cold events, likely mediated by the

average position of the Intertropical Convergence Zone.

1.4.4 Chapter 4 - Stable oxygen isotope records

This chapter focuses on the oxygen isotope records derived from three foraminiferal species – representing a range of water column habitats – within cores 64PE304-8, 64PE303-16 and 64PE303-15. These cores form a depth transect offshore Tanzania. The oxygen isotope records provide insight into the timing of changes associated with the deglaciation and also millennial scale change over the last 40ka. We supplement the interpretation by calculating rates of change in oxygen isotope records, thus enabling a better understanding of the timing and succession of change in the water column at our sites. Our new data highlights significant differences across the water column in the timing of deglaciation. The depth transect approach allows us to robustly report that the intermediate depth ocean in the region of our cores was the first to record an oxygen isotope signal of the deglaciation.

The rate of change records calculated further show the offsets and strengthen the apparent relationship between our surface records and Greenland in terms of timing of change. The records presented here are also placed in a broader Indian Ocean/Arabian sea context to begin to test the idea that the intermediate depths of the Indian Ocean play a role in millennial scale change, particularly during Heinrich events

Overall this chapter provides important evidence of subsurface and surface ocean change during the deglaciation and last glacial period that suggest large time off-sets across the water column particularly during the deglaciation within the region. The planktonic and benthic $\delta^{18}O$ records presented in this chapter provide a basis for the next chapter – based on the equivalent carbon records – to further investigate and test the proposed surface and subsurface changes over the last 40kyrs.

1.4.5 Chapter 5 - Stable carbon isotope records

The main aim of this chapter is to evaluate the new stable oxygen and carbon isotope records in the wider context of subsurface changes in the Indian Ocean. Based on high-resolution stable oxygen and carbon isotope data from a set of new sediment cores retrieved from the sea bed off Tanzania, our data enable a better assessment of the origin of the oxygenation pulses in the Arabian Sea, that either reflect local changes in intermediate water properties, or indeed bear evidence of a larger, Indian Ocean wide expansion of glacial AAIW. The new data will be combined with published data that are used to assess modes of ocean circulation in the Indian Ocean based on time slice reconstructions.

In order to better visualize changes in carbon isotope distribution pattern off Tanzania on the millennial time scale, we use a water column-time transect that includes: the carbon isotope data from the new cores presented in this study; the benthic carbon isotope data of core GeoB12615-4 from Romahn et al. (2013), and; the respective data from nearby core WIND28k McCave et al. (2005). This approach highlights significant changes through time and across the water column and provides a basis from which to assess the changes recorded here in the context of wider millennial scale climate change and the bipolar seesaw.

1.4.6 Chapter 6 - Synthesis

This chapter provides a brief overview of the findings of this thesis. It is intended to highlight the most important contributions of this work. Particular focus is given to the insights gained by combining the Oxygen and Carbon Isotope data presented in chapters 4 and 5 respectively.

1.5 Oceanographic Setting

The Indian Ocean is an important part of the global ocean circulation system. It differs from the Atlantic and Pacific Oceans in that it is completely bounded to the north by the Eurasian continental landmass. This landmass prevents northward heat export and limits thermocline ventilation from the north (Schott et al.; 2009; Schott and McCreary; 2001). Further, the differing impact of seasonal changes in solar radiation on the ocean versus the continental land mass leads to the characteristic seasonally reversing monsoonal air flow at latitudes north of ∼10°S (Wyrtki; 1973). This monsoon system has significant impact upon the surface hydrography and leads to seasonally reversing surface ocean currents such as the Somali Current that flows along the coast of Somalia and Oman. South of the monsoon region, the southeast trade winds prevail. Their northern limit is dictated by seasonal shifts in the ITCZ; moving north during boreal summer

1.5.1 Modern Surface Circulation

The surface flow of the central western Indian Ocean is dominated by the trade wind driven, westward flowing South Equatorial Current (SEC; Schott et al. 2002). The SEC splits into two at the east coast of Madagascar (∼15°S) to form two western boundary currents, the North-East Madagascar Current (NEMC) and the South-East Madagascar Current (SEMC). The NEMC flows into the East African Coastal Current (EACC) which is the primary surface current at the core locations used here (Figure 2.1). North of ∼5°S the seasonally reversing winds control surface currents and result in strong seasonal upwelling at ∼4°N. To the south of our core sites (∼9°S), surface waters advect to the Atlantic supplying heat and salt to the South Atlantic (Gordon et al.; 1992), which eventually contribute to the formation of North Atlantic Deep Water (NADW). The regional average SST is ∼27.6°C (Fallet et al.; 2011) with a range of 25.5 to 28.7°C (Locarnini et al.; 2013).

1.5.2 Modern sub-surface circulation

Multiple sources contribute to the intermediate waters in the region. You (1998) reported intermediate waters along the western boundary at 5°N to be composed of 20% Antarctic Intermediate Water (AAIW), 70% Red Sea water and 10% Indonesian intermediate waters. AAIW – characterised by a salinity minimum (<34.7 psu) – flows northwards, from its formation region at the Sub-Antarctic Front (SAF; 45-55°S; Sloyan et al. 2010; Hartin et al. 2011, 2014). The subduction of AAIW at the SAF is influenced by air-sea exchanges and wind strength (Ribbe; 2001; Sloyan and Rintoul; 2001). The AAIW in the study region is thought to enter the Indian Ocean in the southwest (Fine et al.; 2008). AAIW and Sub-Antarctic Mode Water (SAMW; which forms between the subantarctic and subtropical fronts by vertical convection during winter (McCartney; 1982; Sarmiento et al.; 2004) are upwelled in the open ocean between 5-10°S due to Ekman upwelling associated with the northern boundary of the southeast trade winds (Schott and McCreary; 2001).

The deep circulation of the western Indian Ocean is strongly controlled by the regional bathymetry. The main feature of this flow is the northward flowing Circumpolar Deep Water (CDW) which penetrates north into the Somali basin (Toole and Warren; 1993; Warren; 1978; Wilson et al.; 2012). Near the northern limit of the Mascarene basin, the shallower portion of this water mass meets southwards flowing Indian deep water (IDW), which is essentially recirculated CDW (Johnson et al.; 1998) with an enriched nutrient content (You; 1997). More specific detail on Indian Ocean circulation is given in Chapter 5 in the context of discussion on past changes in circulation.

1.6 Proxies

1.6.1 Stable isotopes in planktonic and benthic foraminifera

Foraminifera are small (typically 0.05-0.5mm) marine organisms that live either on or within the sediment surface (benthic) or passively floating within the upper water column (planktonic). They belong to the phylum of amoebid protists (d'orbigny 1826). Key to their use in palaeoceanographic research, they form a shell composed of $CaCO_3$. The stable isotope composition of this shell is controlled by the temperature and stable isotope composition of the ambient seawater in which they live, sometimes with species specific vital effects on top.

The temperature dependency of oxygen isotope fractionation was first discovered in the late 1940's and early 1950's (Urey; 1947; Epstein and Mayeda; 1953). Following on from this, the relationship was applied as a tool for paleothermometry using fossil planktonic foraminifera by Emiliani (1955). The application was then refined by Shackleton (1967) who showed that the changes in $\delta^{18}O$ of seawater also reflect the preferential trapping of light oxygen (^{16}O) in continental ice sheets (hence, they display a signal of glacial-interglacial variability) and changes in the local evaporation-precipitation balance. These factors complicate the use of foraminifera based $\delta^{18}O$ records as pure paleothermometers.

The primary control on the $\delta^{13}C$ values of benthic and planktonic foraminifera is the carbon isotope composition of the dissolved inorganic carbon (DIC) of the ambient seawater in which these organisms calcified (Turner; 1982). The $\delta^{13}C$ of DIC is influenced by changes in the global carbon cycle and relative distributions between carbon reservoirs, local changes in the mixture and source of water masses, air-sea gas exchange, and the balance between photosynthesis and respiration in the water column (Kroopnick; 1985). These controlling factors lead to the $\delta^{13}C$ of foraminifera (particularly benthic species) being a useful tool to reconstruct changes in subsurface and deep ocean circulation (Curry and Oppo; 2005). The use

of $\delta^{13}C$ as a water mass tracer relies on an understanding of the factors influencing the $\delta^{13}C$ signature of the calcite and of the water from which it was calcified.

The average $\delta^{13}C$ of the atmosphere is 9‰ lower than the average surface ocean. The extent of fractionation between these two reservoirs is temperature dependent, with higher $\delta^{13}C$ and gas exchange at lower temperatures because of increased CO_2 solubility (Broecker and Maier-Reimer; 1992). Higher temperatures in the low latitudes lead to a net transfer of isotopically light CO_2 from the ocean to the atmosphere and a consequential enrichment in $\delta^{13}C$ of surface waters. The opposite is true for the high latitudes, where cold conditions lead to a net uptake of CO_2 by the oceans from the atmosphere. Hence surface waters become depleted in terms of $\delta^{13}C$ (Lynch-Stieglitz et al.; 1995). In cases where the surface water is advected to intermediate and deep layers of the ocean, this carbon isotope signature – indicative of conditions in its formation region – becomes the key component of using foraminiferal carbon isotope ratios as a tracer of past ocean circulation. The only subsequent influence on the $\delta^{13}C$ signature of a water mass is given the term 'ageing' and results in a gradual decrease in the $\delta^{13}C$ value of the water as time increases (primarily due to remineralisation of isotopically light organic matter). Hence this provides another tool by which to reconstruct increases/decreases in the rate of ventilation of a water mass (Lynch-Stieglitz and G. Fairbanks; 1994; Curry and Oppo; 2005).

Another important influence of the $\delta^{13}C$ recorded by benthic foraminifera is regional productivity. For instance, in regions of upwelling, productivity is driven by supply of nutrients. This leads to an increased flux of isotopically light organic carbon to the sea floor. This can alter the ambient $\delta^{13}C$ of the deep waters.

1.6.2 Foraminifera species

The three foraminifera species used in this thesis were chosen to cover a range of depth habitats. The reasons for selecting these species are detailed below.

Globigerinoides ruber

Globigerinoides ruber is a typical warm water species. It is abundant in tropical-subtropical waters of the Indian Ocean. It is a spinose, symbiont-bearing species that inhabits the upper 50m of the water column (Fairbanks et al.; 1980; Erez and Honjo; 1981; Peeters and Brummer; 2002). This species calcifies within the mixed layer between 20-50m (Mohtadi et al.; 2009; Birch et al.; 2013). The chemistry of the shells reflects subtropical/tropical surface water conditions (Birch et al.; 2013; Hemleben et al.; 1989). Previous work in the region suggests the species is unbiased by seasonal changes (Fallet et al.; 2011, 2010).

Neogloboquadrina dutertrei

Neogloboquadrina dutertrei is a non-spinose, symbiont-bearing subtropical thermocline (or more specifically nutricline/ chlorophyll maximum) dwelling foraminifer (Be and Tolderlund; 1971; Field; 2004). This is dictated by the need for nutrients. The vertical habitat of *N.dutertrei* is variable over the course of their life cycle, as the species migrates vertically to follow the depth of the nutricline from which it takes its nutrients. This variability will have small impact upon the isotope signal and as such, The species has previously been used to infer past thermocline and nutricline conditions (Leduc et al.; 2009; Kiefer et al.; 2006).

Cibicidoides wuellerstorfi

Cibicidoides wuellerstorfi lives on the surface of the ocean floor, exhibiting an epibenthic lifestyle (Lutze and Thiel; 1989). This species avoids the pore water related stable isotope issues of infaunal species (Zahn et al.; 1986; Mackensen et al.; 1993) and fossils of this species record stable isotope conditions of ambient bottom water (Bemis et al.; 1998; Duplessy et al.; 1984).

1.6.3 Bulk Sediment Elemental ratios

X-ray Flouresence (XRF) is a non-destructive, non-invasive technique used to quantify the elemental composition of sediments (Ramsey et al.; 1995; Jenkins; 2006). The records obtained are near-continuous. The technique is based on the excitation of electrons by incident x-rays. Ejection of electrons from inner electron shells creates a vacancy. As electrons from outer shells fall inwards, surplus energy is emitted as a secondary x-ray. The wavelength of this secondary emission is characteristic of the specific element from which it came. This allows estimation of the relative abundance of desired elements (Weltje and Tjallingii; 2008). Results are presented as count rates or ratios of count rates. The application of XRF core scanning results to trace input of terrestrial material by varying riverine discharge to marine sediments has been used in the region before (e.g. van Der Lubbe et al. 2014; Romahn et al. 2013).

The titanium/calcium (Ti/Ca) ratio in marine sediments has been frequently used to reconstruct climate change in nearby continental settings (Lubbe et al.; 2011; van Der Lubbe et al.; 2014; Tjallingii et al.; 2007). Unlike other elements such as iron, the mobility of titanium is less sensitive to changing weathering conditions in continental settings. Hence, in the absence of any significant sources in the ocean, titanium concentrations in deep sea sediments reflect climate conditions on the nearby continent. In contrast, calcium overwhelmingly stems from marine biogenic carbonates such as foraminifera and coccoliths. The use of this ratio assumes a continuous high level of calcium in the sediment in order to highlight changes in the supply of titanium bearing terrigenous material. In sediment sections with low calcium levels the relative changes in titanium input may be muted, as such the proxy is unreliable in terrigenous settings or marine settings dominated by terrigenous input.

The Ti/Ca ratio is therefore a useful tracer of changes in terrigenous sedimentation in marine settings. The logarithmic form (log(Ti/Ca)) has been introduced to reduce potential sediment matrix effects related to variable water concentrations and grain-size (Weltje and Tjallingii; 2008; Hennekam and de Lange; 2012; Tjallingii et al.; 2007).

1.6.4 Radiocarbon dating of foraminiferal calcite

The age models applied to the data presented in this thesis are mainly based on radiocarbon dating of monospecific samples of foraminiferal calcite (*G.ruber*). Radiocarbon dating is a radiometric technique making use of the decay of ^{14}C with a half-life of 5730 years. It is useful and reliable for the period of the last 40kyr (Stuiver et al.; 1998).

Radiocarbon is formed in the atmosphere by neutron reactions between cosmic radiation and atmospheric nitrogen (^{15}N). The initial dates measured by AMS radiocarbon dating assume that the concentration of atmospheric radiocarbon has been constant through time (Pilcher; 1991). However, it is known that atmospheric radiocarbon has fluctuated markedly in the past due to changes in production (due to magnetic field intensity and solar variability; Stuiver and Braziunas 1993) and distribution amongst the various carbon reservoirs (Siegenthaler and Sarmiento; 1993). Hence dates must be calibrated to account for this variability.

Another complication when using radiocarbon dating on marine sediment samples is known as the marine reservoir effect. Mixing times between the surface and deep ocean are slow, and radiocarbon can decay without being replenished (Lowe and Walker; 1985). As a consequence, coeval terrestrial and marine samples have an average age offset of 400 years (Stuiver and Braziunas; 1993). This apparent ageing is spatially variable also, with factors such as upwelling of 'old' water masses (Mangerud; 1972) leading to marine carbonate appearing older than it really is. Across the globe, marine reservoir age varies from around 400 years in

the North Atlantic (Bard; 1988; Bard et al.; 1991) to around 2000 years in the deep Pacific Ocean. In the western Indian Ocean region the marine reservoir age varies between 500-650 (Southon et al.; 2002). For the radiocarbon dating in this thesis we have selected a ΔR value (where ΔR is the value added on to the standard marine reservoir age of 400 years) of 215 ± 52 based on Southon et al. (2002).

Bibliography

Altabet, M. A., Higginson, M. J. and Murray, D. W. (2002). The effect of millennial-scale changes in Arabian Sea denitrification on atmospheric CO_2, *Nature* **415**(6868): 159–162.

Bard, E. (1988). Correction of accelerator mass spectrometry ^{14}C ages measured in planktonic foraminifera: Paleoceanographic implications, *Paleoceanography* **3**(6): 635–645.

Bard, E., Arnold, M. and Duplessy, J. C. (1991). Reconciling the sea level record of the last deglaciation with the $\delta^{18}O$ spectra from deep sea cores, *Quaternary Proceedings* **1**: 67–73.

Be, A. and Tolderlund, D. (1971). Distribution and ecology of living planktonic foraminifera in surface waters of the Atlantic and Indian Oceans., *The Micropalaeontology of Oceans*, chapter Distributi, pp. 105–149.

Bemis, B. E., Spero, H. J., Bijma, J. and Lea, D. W. (1998). Reevaluation of the oxygen isotopic composition of planktonic foraminifera: Experimental results and revised paleotemperature equations, *Paleoceanography* **13**(2): 150–160.

Birch, H., Coxall, H. K., Pearson, P. N., Kroon, D. and O'Regan, M. (2013). Planktonic foraminifera stable isotopes and water column structure: Disentangling ecological signals, *Marine Micropaleontology* **101**: 127–145.

Blunier, T. and Brook, E. J. (2001). Timing of Millennial-Scale climate change in Antartica and Greenland during the last glacial period, *Science* **291**(2001): 109–112.

Blunier, T., Chappellaz, J., Schwander, J., Clausen, H., Hammer, C. U. and Johnsen, S. (1998). Asynchrony of Antarctic and Greenland climate change during the last glacial period, *Nature* **349**: 739–743.

Böning, P. and Bard, E. (2009). Millennial/centennial-scale thermocline ventilation changes in the Indian Ocean as reflected by aragonite preservation and geochemical variations in Arabian Sea sediments, *Geochimica et Cosmochimica Acta* **73**(22): 6771–6788.

Broccoli, A. J., Dahl, K. A. and Stouffer, R. J. (2006). Response of the ITCZ to Northern Hemisphere cooling, *Geophysical Research Letters* **33**(1).

Broecker, W. (1998). Paleocean circulation during the last deglaciation: A bipolar seesaw?, *Paleoceanography* **13**(2): 119–121.

Broecker, W., Bond, G., Klas, M., Clark, E. and McManus, J. (1992). Origin of the northern Atlantic 's Heinrich events, *Climate Dynamics* **6**: 265–273.

Broecker, W. S., Bond, G., Klas, M., Bonani, G. and Wolfli, W. (1990). A salt oscillator in the glacial atlantic? 1. the concept, *Paleoceanography* **5**(4): 469–477.

Broecker, W. S. and Maier-Reimer, E. (1992). The influence of air and sea exchange on the carbon isotope distribution in the sea, *Global Biogeochemical Cycles* **6**(3): 315–320.

Brummer, G. and Jung, S. (2009). RV Pelagia Cruise Report : Cruise 64PE304 SE African margin ,.

Carolin, S. A., Cobb, K. M., Lynch-Stieglitz, J., Moerman, J. W., Partin, J. W., Lejau, S., Malang, J., Clark, B., Tuen, A. A. and Adkins, J. F. (2016). Northern Borneo

stalagmite records reveal West Pacific hydroclimate across MIS 5 and 6, *Earth and Planetary Science Letters* **439**: 182–193.

Charles, C. D., Lynch-Stieglitz, J., Ninnemann, U. S. and Fairbanks, R. G. (1996). Climate connections between the hemisphere revealed by deep sea sediment core/ice core correlations, *Earth and Planetary Science Letters* **142**(1-2): 19–27.

Cheng, H., Edwards, R. L., Broecker, W. S., Denton, G. H., Kong, X., Wang, Y., Zhang, R. and Wang, X. (2009). Ice Age Terminations, *Science* **326**(5950): 248–252.

Cheng, H., Edwards, R. L., Sinha, A., Spötl, C., Yi, L., Chen, S., Kelly, M., Kathayat, G., Wang, X., Li, X., Kong, X., Wang, Y., Ning, Y. and Zhang, H. (2016). The Asian monsoon over the past 640,000 years and ice age terminations, *Nature* **534**(7609): 640–646.

Chiang, J. C. H. and Bitz, C. M. (2005). Influence of high latitude ice cover on the marine Intertropical Convergence Zone, *Climate Dynamics* **25**(5): 477–496.

Curry, W. B. and Oppo, D. W. (2005). Glacial water mass geometry and the distribution of $\delta^{13}c$ of $\sigma\mathrm{co}_2$ in the western atlantic ocean, *Paleoceanography* **20**(1). PA1017.

Dansgaard, W., Johnsen, S., Clausen, H., Dahl-Jensen, D., Gundestrup, N., Hammer, C. U. and Oeschger, H. (1984). h, *in* J. E. Hansen and T. Takahashi (eds), *Climate Processes and Climate Sensitivity, Geophys. Monogr. Ser., vol. 29*, AGU, pp. 288–298.

Deplazes, G., Lückge, A., Stuut, J.-B. W., Pätzold, J., Kuhlmann, H., Husson, D., Fant, M. and Haug, G. H. (2014). Weakening and strengthening of the indian monsoon during heinrich events and dansgaard-oeschger oscillations, *Paleoceanography* **29**(2): 99–114. 2013PA002509.

Duplessy, J. C., Shackleton, N. J., Matthews, R. K., Prell, W., Ruddiman, W. F., Caralp, M. and Hendy, C. H. (1984). $\delta^{13}C$ Record of benthic foraminifera in the last

interglacial ocean: Implications for the carbon cycle and the global deep water circulation, *Quaternary Research* **21**(2): 225–243.

Elliot, M., Labeyrie, L. and Duplessy, J. (2002). Changes in North Atlantic deep-water formation associated with the Dansgaard – Oeschger temperature oscillations (60 – 10 ka), *Quaternary Science Reviews* **21**: 1153–1165.

Emiliani, C. (1955). Pleistocene Temperatures, *The Journal of Geology* .

Epstein, S. and Mayeda, T. (1953). Variation of O^{18} content of waters from natural sources, *Geochimica et Cosmochimica Acta* **4**(5): 213–224.

Erez, J. and Honjo, S. (1981). Comparison of isotopic composition of planktonic foraminifera in plankton tows, sediment traps and sediments, *Palaeogeography, Palaeoclimatology, Palaeoecology* **33**(1-3): 129–156.

Fairbanks, R. G., Wiebe, P. H. and Ba, A. W. H. (1980). Vertical Distribution and Isotopic Composition of Living Planktonic Foraminifera in the Western North Atlantic, *Science* **207**(4426): 61–63.

Fallet, U., Brummer, G. J., Zinke, J., Vogels, S. and Ridderinkhof, H. (2010). Contrasting seasonal fluxes of planktonic foraminifera and impacts on paleothermometry in the Mozambique Channel upstream of the Agulhas Current, *Paleoceanography* **25**(4).

Fallet, U., Ullgren, J. E., Casta??eda, I. S., van Aken, H. M., Schouten, S., Ridderinkhof, H. and Brummer, G. J. A. (2011). Contrasting variability in foraminiferal and organic paleotemperature proxies in sedimenting particles of the Mozambique Channel (SW Indian Ocean), *Geochimica et Cosmochimica Acta* **75**(20): 5834–5848.

Field, D. B. (2004). Variability in vertical distributions of planktonic foraminifera in the California current: Relationships to vertical ocean structure, *Paleoceanography* **19**(2).

Fine, R. A., Smethie, W. M., Bullister, J. L., Rhein, M., Min, D. H., Warner, M. J., Poisson, A. and Weiss, R. F. (2008). Decadal ventilation and mixing of Indian Ocean waters, *Deep-Sea Research Part I: Oceanographic Research Papers* **55**(1): 20–37.

Gordon, A. L., Weiss, R. F., Smethie, W. M. and Warner, M. J. (1992). Thermocline and intermediate water communication between the South Atlantic and Indian Oceans, *Journal of Geophysical Research* **97**(C5): 7223.

Grootes, P. M., Stuiver, M., White, J. W. C., Johnsen, S. and Jouzel, J. (1993). Comparison of oxygen isotope records from the GISP2 and GRIP Greenland ice cores, *Nature* **366**(6455): 552–554.

Hartin, C. A., Fine, R. A., Kamenkovich, I. and Sloyan, B. M. (2014). Comparison of Subantarctic Mode Water and Antarctic Intermediate Water formation rates in the South Pacific between NCAR-CCSM4 and observations, *Geophysical Research Letters* **41**(2): 519–526.

Hartin, C. A., Fine, R. A., Sloyan, B. M., Talley, L. D., Chereskin, T. K. and Happell, J. (2011). Formation rates of Subantarctic mode water and Antarctic intermediate water within the South Pacific, *Deep-Sea Research Part I: Oceanographic Research Papers* **58**(5): 524–534.

Heinrich, H. (1988). Origin and consequences of cyclic ice rafting in the Northeast Atlantic Ocean during the past 13,000 years, *Quaternary Research* **29**: 142–152.

Hemleben, C., Spindler, M. and Anderson, O. (1989). *Modern planktonic foraminifera*, Vol. 22.

Hennekam, R. and de Lange, G. (2012). X-ray fluorescence core scanning of wet marine sediments: methods to improve quality and reproducibility of high-resolution paleoenvironmental records, *Limnology and Oceanography: Methods* **10**: 991–1003.

Huang, K.-F., Oppo, D. W. and Curry, W. B. (2014). Decreased influence of Antarctic intermediate water in the tropical Atlantic during North Atlantic cold events, *Earth and Planetary Science Letters* **389**: 200–208.

Ivanochko, T. S., Ganeshram, R. S., Brummer, G. J. A., Ganssen, G., Jung, S. J. A., Moreton, S. G. and Kroon, D. (2005). Variations in tropical convection as an amplifier of global climate change at the millennial scale, *Earth and Planetary Science Letters* **235**(1-2): 302–314.

Jenkins, R. (2006). X-Ray Techniques: Overview, *Encyclopedia of Analytical Chemistry*.

Johnsen, S. J., Dansgaard, W., Clausen, H. B. and Langway, C. C. (1972). Oxygen Isotope Profiles through the Antarctic and Greenland Ice Sheets, *Nature* **235**(5339): 429–434.

Johnson, G. C., Musgrave, D. L., Warren, B. A., Ffield, A. and Olson, D. B. (1998). Flow of bottom and deep water in the Amirante Passage and Mascarene Basin, *Journal of Geophysical Research: Oceans* **103**(13): 30973–30984.

Jung, S. (1996). *Wassermassenaustausch zwischen NE-Atlantik und Nordmeer wahrend der letzten 300 000/80 000 Jahre im Abbild stabiler O- und C-Isotope*, PhD thesis, Christian-Albrechts-Universitat Kiel.

Jung, S. J. A., Kroon, D., Ganssen, G., Peeters, F. and Ganeshram, R. (2009). Enhanced Arabian Sea intermediate water flow during glacial North Atlantic cold phases, *Earth and Planetary Science Letters* **280**(1-4): 220–228.

Jung, S. and Kroon, D. (2011). Quantifying rates of change in ocean conditions with implications for timing of sea level change, *Global and Planetary Change* **79**(3): 204–213.

Kiefer, T., McCave, I. N. and Elderfield, H. (2006). Antarctic control on tropical Indian Ocean sea surface temperature and hydrography, *Geophysical Research Letters* **33**(24).

Kroon, D. and Party, S. (2010). Tropical Temperature History during Paleogene GLObal Warming (GLOW) Events, NIOZ site survey cruise report (RV Pelagia cruise number 64PE303), *NIOZ Site* pp. 1–59.

Kroopnick, P. M. (1985). The distribution of $\delta^{13}C$ of ΣCO_2 in the world oceans, *Deep Sea Research Part A, Oceanographic Research Papers* **32**(1): 57–84.

Leduc, G., Vidal, L., Cartapanis, O. and Bard, E. (2009). Modes of eastern equatorial Pacific thermocline variability: Implications for ENSO dynamics over the last glacial period, *Paleoceanography* **24**(3).

Liu, Z. and Alexander, M. (2007). Atmospheric bridge, oceanic tunnel, and global climatic teleconnections, *Reviews of Geophysics* (2005): 1–34.

Locarnini, R. A., Mishonov, A. V., Antonov, J. I., Boyer, T. P., Garcia, H. E., Baranova, O. K., Zweng, M. M., Paver, C. R., Reagan, J. R., Johnson, D. R., Hamilton, M. and Seidov, D. (2013). World Ocean Atlas 2013. Vol. 1: Temperature., *Technical Report September*.

Lowe, J. J. and Walker, M. J. C. (1985). *Reconstructing Quaternary environments*, Vol. 4.

Lubbe, J. V. D., Tjallingii, R., Castañeda, I. S., Brummer, G., Kroon, D. and Jung, S. (2011). Major reorganization in the transport pathway of Zambezi River sediments along and across the Mozambique Shelf during the last glacial-interglacial transition, *Geophysical Research Abstracts* **13**: 8855.

Lutze, G. F. and Thiel, H. (1989). Epibenthic foraminifera from elevated microhabitats; *Cibicidoides wuellerstorfi* and *Planulina ariminensis*, *The Journal of Foraminiferal Research* (2): 153–158.

Lynch-Stieglitz, J. and G. Fairbanks, R. (1994). A conservative tracer for glacial ocean circulation from carbon isotope and palaeo-nutrient measurements in benthic foraminifera, **369**: 308–310.

Lynch-Stieglitz, J., Stocker, T. F., Broecker, W. S. and Fairbanks, R. G. (1995). The influence of air-sea exchange on the isotopic composition of oceanic carbon: Observations and modeling, *Global Biogeochemical Cycles* **9**(4): 653–665.

Mackensen, A., Hubberten, H. W., Bickert, T., Fischer, G. and Fütterer, D. K. (1993). The $\delta^{13}C$ in benthic foraminiferal tests of *Fontbotia wuellerstorfi* (Schwager) Relative to the $\delta^{13}C$ of dissolved inorganic carbon in Southern Ocean Deep Water: Implications for glacial ocean circulation models, *Paleoceanography* **8**(5): 587–610.

Mangerud, J. (1972). Radiocarbon dating of marine shells, including a discussion of apparent age of Recent shells from Norway, *Boreas* **1**(2): 143–172.

McCartney, M. S. (1982). The subtropical recirculation of mode waters, *J. Mar. Res* **40**: 427–464.

McCave, I. N., Kiefer, T., Thornalley, D. J. R. and Elderfield, H. (2005). Deep flow in the Madagascar-Mascarene Basin over the last 150000 years, *Philosophical Transactions of the Royal Society A: Mathematical, Physical and Engineering Sciences* **363**(1826): 81–99.

McGee, D., Donohoe, A., Marshall, J. and Ferreira, D. (2014). Changes in ITCZ location and cross-equatorial heat transport at the Last Glacial Maximum, Heinrich Stadial 1, and the mid-Holocene, *Earth and Planetary Science Letters* **390**: 69–79.

Mikaloff Fletcher, S. E., Gruber, N., Jacobson, a. R., Doney, S. C., Dutkiewicz, S., Gerber, M., Follows, M., Joos, F., Lindsay, K., Menemenlis, D., Mouchet, a., Müller, S. a. and Sarmiento, J. L. (2006). Inverse estimates of anthropogenic CO_2 uptake, transport, and storage by the ocean, *Global Biogeochemical Cycles* **20**: n/a—-n/a.

Mohtadi, M., Prange, M., Oppo, D. W., De Pol-Holz, R., Merkel, U., Zhang, X., Steinke, S. and Lückge, A. (2014). North Atlantic forcing of tropical Indian Ocean climate., *Nature* **509**(7498): 76–80.

Mohtadi, M., Steinke, S., Groeneveld, J., Fink, H. G., Rixen, T., Hebbeln, D., Donner, B. and Herunadi, B. (2009). Low-latitude control on seasonal and interannual changes in planktonic foraminiferal flux and shell geochemistry off south Java: A sediment trap study, *Paleoceanography* **24**(1).

Pahnke, K., Goldstein, S. L. and Hemming, S. R. (2008). Abrupt changes in Antarctic Intermediate Water circulation over the past 25,000 years, *Nature Geosci* **1**(12): 870–874.

Pahnke, K. and Zahn, R. (2005). Southern Hemisphere water mass conversion linked with North Atlantic climate variability, *Science* **307**(5716): 1741–1746.

Peeters, F. J. C. and Brummer, G.-J. a. (2002). The seasonal and vertical distribution of living planktic foraminifera in the NW Arabian Sea, *Geological Society, London, Special Publications* **195**(January): 463–497.

Pilcher, J. (1991). Radiocarbon dating for the Quaternary scientist, *Quaternary Proceedings* **1**: 27–33.

Ramsey, M. H., Potts, P. J., Webb, P. C., Watkins, P., Watson, J. S. and Coles, B. J. (1995). An objective assessment of analytical method precision: comparison of ICP-AES and XRF for the analysis of silicate rocks, *Chemical Geology* **124**(1-2): 1–19.

Ribbe, J. (2001). Intermediate water mass production controlled by southern hemisphere winds, *Geophysical Research Letters* **28**(3): 535–538.

Romahn, S., Mackensen, a., Groeneveld, J. and Pätzold, J. (2013). Deglacial intermediate water reorganization: new evidence from the Indian Ocean, *Climate of the Past Discussions* **9**(4): 4035–4063.

Romahn, S., MacKensen, A., Groeneveld, J. and Pätzold, J. (2014). Deglacial intermediate water reorganization: New evidence from the Indian Ocean, *Climate of the Past* **10**(1): 293–303.

Sabine, C. L., Feely, R. A., Gruber, N., Key, R. M., Lee, K., Bullister, J. L., Wanninkhof, R., Wong, C. S., Wallace, D. W. R., Tilbrook, B., Millero, F. J., Peng, T.-H., Kozyr, A., Ono, T. and Rios, A. F. (2004). The oceanic sink for anthropogenic CO_2., *Science (New York, N.Y.)* **305**: 367–371.

Sarmiento, J. L., Gruber, N., Brzezinski, M. A. and Dunne, J. P. (2004). High-latitude controls of thermocline nutrients and low latitude biological productivity, *Nature* **427**: 56–60.

Sarnthein, M., Winn, K., Jung, S., Duplessy, J., Labeyrie, L., Erlenkeuser, H. and Ganssen, G. (1994). Changes in east Atlantic deepwater circulation over the last 30 , 000 years : Eight time slice reconstructions, *Paleoceanography* **9**(2): 209–267.

Schott, F. A., Dengler, M. and Schoenefeldt, R. (2002). The shallow overturning circulation of the Indian Ocean, *Progress in Oceanography* **53**(1): 57–103.

Schott, F. A. and McCreary, J. P. (2001). The monsoon circulation of the Indian Ocean, *Progress in Oceanography* **51**(1): 1–123.

Schott, F., Xie, S. P. and Jr, J. P. M. (2009). Indian Ocean circulation and climate variability, *Reviews of Geophysics* **47**: 1–46.

Schulz, H. (1998). Correlation between Arabian Sea and Greenland climate oscillations of the past 110,000 years, *Nature* **393**(May): 23–25.

Shackleton, N. J. (1967). Oxygen isotope analyses and pleistocene temperatures re-assessed, *Nature* **215**: 15–17.

Shackleton, N. J., Hall, M. A. and Vincent, E. (2000). Phase relationships between millennial-scale events 64,000-24,000 years ago, *Paleoceanography* **15**(6): 565–569.

Siegenthaler, U. and Sarmiento, J. L. (1993). Atmospheric carbon dioxide and the ocean, *Nature* **365**(6442): 119–125.

Singh, A., Jung, S., Darling, K., Ganeshram, R., Ivanochko, T. and Kroon, D. (2011). Productivity collapses in the Arabian Sea during glacial cold phases, *Paleoceanography* **26**(3): 1–10.

Sloyan, B. M. and Rintoul, S. R. (2001). The Southern Ocean Limb of the Global Deep Overturning Circulation, *Journal of Physical Oceanography* **31**(1): 143–173.

Sloyan, B. M., Talley, L. D., Chereskin, T. K., Fine, R. and Holte, J. (2010). Antarctic Intermediate Water and Subantarctic Mode Water Formation in the Southeast Pacific: The Role of Turbulent Mixing, *Journal of Physical Oceanography* **40**(7): 1558–1574.

Southon, J., Kashgarian, M., Fontugne, M., Metivier, B. and Yim, W. W.-S. (2002). Marine reservoir corrections for the Indian Ocean and Southeast Asia, *Radiocarbon* **44**(1): 167–180.

Stocker, T. F. and Wright, D. G. (1996). Rapid changes in ocean circulation and atmospheric radiocarbon, *Paleoceanography* **11**(6): 773–795.

Stuiver, M. and Braziunas, T. F. (1993). Sun, ocean, climate and atmospheric $^{14}CO_2$: an evaluation of causal and spectral relationships, *The Holocene* **3**(4): 289–305.

Stuiver, M., Reimer, P. J., Bard, E., Beck, J. W., Burr, G., Hughen, K. A., Kromer, B., McCormac, G., Van Der Plicht, J. and Spurk, M. (1998). INTCAL98 Radiocarbon Age Calibration, 24000-0 cal BP, *Radiocarbon* **40**(3): 1041–1083.

Tjallingii, R., Röhl, U., Kölling, M. and Bickert, T. (2007). Influence of the water content on X-ray fluorescence corescanning measurements in soft marine sediments, *Geochemistry, Geophysics, Geosystems* **8**(2).

Toole, J. M. and Warren, B. A. (1993). A hydrographic section across the subtropical South Indian Ocean, *Deep-Sea Research Part I* **40**(10): 1973–2019.

Turner, J. V. (1982). Kinetic fractionation of carbon-13 during calcium carbonate precipitation, *Geochimica et Cosmochimica Acta* **46**(7): 1183–1191.

Urey, H. C. (1947). The Thermodynumic Properties of Isotopic Substances., *Journal of the Chemical Society (Resumed)* .

van Der Lubbe, J. H., Tjallingii, R., Prins, M. A., Brummer, G.-J. A., Jung, S. J. A., Kroon, D. and Schneider, R. R. (2014). Sedimentation patterns off the Zambezi River over the last 20,000 years, *Marine Geology* **355**: 189–201.

Wang, Y. J., Cheng, H., Edwards, R. L., An, Z. S., Wu, J. Y., Shen, C. C. and Dorale, J. a. (2001). A high-resolution absolute-dated late Pleistocene Monsoon record from Hulu Cave, China., *Science (New York, N.Y.)* **294**(5550): 2345–2348.

Wang, Y. V., Leduc, G., Regenberg, M., Andersen, N., Larsen, T., Blanz, T. and Schneider, R. R. (2013). Northern and southern hemisphere controls on seasonal sea surface temperatures in the Indian Ocean during the last deglaciation, *Paleoceanography* **28**(4): 619–632.

Warren, B. A. (1978). Bottom water transport through the Southwest Indian Ridge, *Deep Sea Research* **25**(3): 315–321.

Weltje, G. J. and Tjallingii, R. (2008). Calibration of XRF core scanners for quantitative geochemical logging of sediment cores: Theory and application, *Earth and Planetary Science Letters* **274**(3-4): 423–438.

Weyl, P. K. (1968). The Role of the Oceans in Climatic Change: A Theory of the Ice Ages BT - Causes of Climatic Change: A collection of papers derived from the INQUA—NCAR Symposium on Causes of Climatic Change, August 30–31, 1965, Boulder, Colorado, American Meteorological Society, Boston, MA, pp. 37–62.

Wilson, D. J., Piotrowski, A. M., Galy, A. and McCave, I. N. (2012). A boundary exchange influence on deglacial neodymium isotope records from the deep western Indian Ocean, *Earth and Planetary Science Letters* **341-344**: 35–47.

Wyrtki, K. (1973). *Physical Oceanography of the Indian Ocean*, Springer Berlin Heidelberg, Berlin, Heidelberg, pp. 18–36.

You, Y. (1997). Seasonal variations of thermocline circulation and ventilation in the Indian Ocean, *Journal of Geophysical Research: Oceans* **102**(C5): 10391–10422.

You, Y. (1998). Intermediate water circulation and ventilation of the Indian Ocean derived from water-mass contributions, *Journal of Marine Research* **56**: 1029–1067.

Zahn, R., Winn, K. and Sarnthein, M. (1986). Benthic foraminiferal $\delta^{13}C$ and accumulation rates of organic carbon: *Uvigerina Peregrina* group and *Cibicidoides Wuellerstorfi*, *Paleoceanography* **1**(1): 27–42.

Chapter 2

Materials & Methods

2.1 Sediment Cores

The data presented in this thesis are derived from three marine sediment piston cores 64PE304-8 (752m), 64PE303-16 (1350m) and 64PE303-15 (1985m) from offshore Tanzania in the western Indian Ocean (Figure 2.1). These cores were retrieved in 2009 using a Royal Netherlands Institute for Sea Research (NIOZ) designed piston corer onboard the *RV Pelagia* as part of the "Tropical Temperature History During Paleogene Global Warming Events" (GLOW; Kroon and Party 2010) and "Indian – Atlantic Exchange" (INATEX; Brummer and Jung 2009). The cores are composed primarily of foraminifera rich silty clay. The total length of each core is: 64PE304-8 – 6.8m; 64PE303-16 – 5.5m; 64PE303-15 – 4.5m.

2.2 Sample Preparation

Raw samples were obtained from marine sediment cores 64PE304-8, 64PE303-16 and 64PE303-15 at a spacing of 1cm. Samples were individually bagged and transferred from their storage facility at NIOZ, Texel to the Grant Institute, Edinburgh. A series of initial cleaning steps was carried out to remove the finest size fraction (<63μm) and make subsequent handling more convenient. Samples were first freeze-dried, then washed through a 63μm sieve and finally dried in an oven at

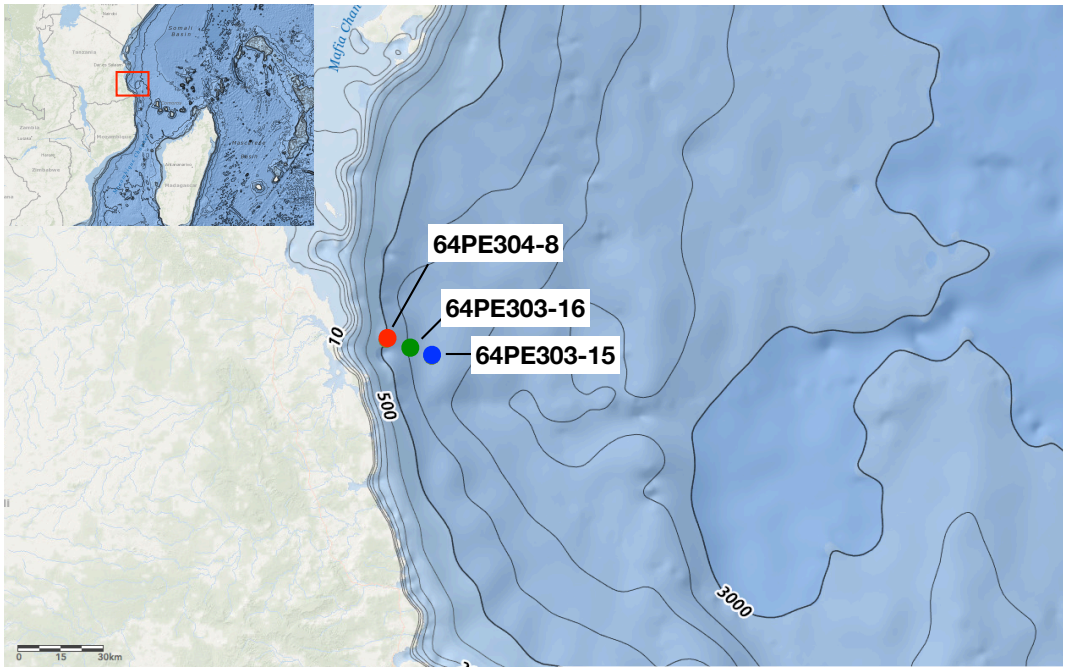

FIGURE 2.1: Map showing location of cores presented in this thesis. Water depths as follows: 64PE304-8 752m; 64PE303-16 1309m; 64PE303-15 1985m.

$\sim$ 50°C for 2-3 days. Foraminifera specimens for stable isotope analyses were handpicked using a fine brush from the 255-350μm size fraction ($\sim$20 shells of the planktonic species *G. ruber* and *N.dutertrei* and up to 15 shells of the benthic species *C.wuellerstorfi* were picked from each sample).

2.3 Carbon & Oxygen Isotope Analyses

Foraminiferal calcite samples were analysed for stable oxygen and carbon isotope ratios using a Thermo Electron Delta$^+$ Advantage stable isotope mass spectrometer coupled to a Kiel Carbonate III preparation device at the University of Edinburgh, school of GeoSciences. The planktonic specimens of individual species were homogenised (powdered) and a sub-sample used for each analysis. 2-3 benthic specimens were used for each analysis. Measured values are reported using standard δ-notation as compared to Vienna PeeDee Belemnite using laboratory standard NBS-19 (Coplen et al.; 1983). Analytical precision for both $\delta^{13}C$ and $\delta^{18}O$ was better than $\pm$0.1‰.

2.4 XRF Core Scanning

Downcore profiles of qualitative bulk sediment geochemical data were obtained by X-ray fluorescence (XRF) core scanning at 10 kV with a 1 cm resolution using an Avaatech core scanner at Royal NIOZ, Texel, Netherlands. Elements aluminium through to iron were measured. Processed data is given in counts per second (cps) for each element. In this thesis the logarithmic ratio of titanium:calcium (log(Ti/Ca)) is used to reduce potential sediment matrix effects related to variable water concentrations and grain-sizes (Weltje and Tjallingii; 2008; Hennekam and de Lange; 2012; Tjallingii et al.; 2007). For more background on the method see section 1.6.3 in chapter 1.

2.5 Radiocarbon Dates

2.5.1 Counting

The radiocarbon dates presented here were obtained from the planktonic foraminifer *G. ruber*. To help select the optimum samples to measure for radiocarbon dates, An abundance counting exercise was performed on the planktonic foraminifer *G. ruber*. This increased the likelihood that the dated material was representative of the section of core from which it was selected. Samples or sections of core with low abundance of a species have increased influence of specimens originating from older or younger section being introduced by bioturbation, sediment reworking and other post depositional processes.

First, the sections from which radiocarbon dates were desired were identified in each core. These were generally important boundaries at which age constraints are most useful. Using a sample splitter to obtain a known fraction of the sample, counts were made of total number of *G. ruber* and of total number of planktonic foraminifera in each 1cm sample. The results were factored up to the total sample and a ratio produced (for counting data see appendix C). From this counting data, the optimum samples were selected for dating.

2.5.2 Sample Preparation & Measurement

Approximately 10mg ($\sim$1000 specimens) of *G. ruber* specimens were picked from each of the samples identified by counting. These subsamples were then transferred to the Scottish Universities Environmental Research Centre (SUERC), East Kilbride where they were measured using an accelerator mass spectrometer (AMS). These dates were funded by NERC Radiocarbon Allocation Number 1796.0414. Calendar ages were computed using Calib 7.1 software (Stuiver et al.; 2006), using the marine 13 calibration curve of Reimer et al. (2013) and a ΔR of 215 $\pm$ 52 based on Southon et al. (2002). The resulting ages are given in Table 2.1.

TABLE 2.1: Details of radiocarbon dates

Core	Depth in Core (cm)	Radiocarbon Age (years)	± 1	Calibrated Age (years BP)	± 1
64PE304-8	2.5	1380	25	716	68.3
64PE304-8	61.5	6620	25	6883	68.3
64PE304-8	115.5	11416	42	12691	68.3
64PE304-8	146	17506	59	20367	68.3
64PE304-8	186	26574	144	30215	68.3
64PE304-8	216	36647	478	40644	68.3
64PE303-16	1.5	1590	25	921	68.3
64PE303-16	23.5	6445	25	6678	68.3
64PE303-16	71.5	12535	50	13790	68.3
64PE303-16	126.5	18379	61	21508	68.3
64PE303-16	291.5	32816	311	36085	68.3
64PE303-16	331	36834	495	40819	68.3
64PE303-15	0.5	1481	35	811	68.3
64PE303-15	46	9650	35	10285	68.3
64PE303-15	60	12100	44	13347	68.3
64PE303-15	90	15288	52	17852	68.3
64PE303-15	222	31157	245	34491	68.3
64PE303-15	314	42479	976	45230	68.3

2.6 Age Model Construction

The chronology of the sediment sequences used in this thesis is based on a multi-step approach. The initial age models are based on the 18 radiocarbon dates (Table 2.1) discussed above.

The next steps in the age model construction were implemented with the aim of refining the age models. The log(Ti/Ca) records were used to align between cores on the basis that the changes displayed in these records are driven by local climate factors and as such should be coeval. Based on the initial age models there was a good alignment of the log(Ti/Ca) records (Figure 2.2). Following the approach of van Der Lubbe et al. (2014), two radiocarbon dates were transposed between cores 64PE303-16 and 64PE303-15 (Figure 2.2). This approach involved visually identifying coeval events in the respective log(Ti/Ca) records and assigning the same date from the dated to the undated core. The transferred dates are indicated

in figure 2.2.

The log (Ti/Ca) records for cores 64PE303-16 and 64PE303-15 are highly similar. Within the uncertainty of the radiocarbon dates, individual events in the log (Ti/Ca) records are synchronous between both records. Comparison with $\delta^{18}O$ records from the GISP2 (Greenland) and Byrd (Antarctica) ice core (Figure 2.3) reveals that - based on the independently established age models - the log(Ti/Ca) variability of sediment cores 64PE303-16 and 64PE303-15 broadly resembles NGRIP in terms of the shape of events and timing, with only limited offsets. In contrast, the shape and timing of minima/maxima in the log(Ti/Ca) record deviate from the millennial-scale events in the oxygen isotope record of the Byrd ice core (Figure 2.3). Within the uncertainty of the radiocarbon dates, DO events 1 through 17 (Figure 2.3) in the NGRIP record co-occur with high values in the log(Ti/Ca) records of cores 64PE303-16 and 64PE303-15. We applied this relation to adjust the age models beyond the reach of the radiocarbon method, in keeping with a similar strategy adopted for sediments from the Arabian Sea (Ivanochko et al.; 2005).

The age model for the deep sections of core 64PE304-8 is based on oxygen isotope stratigraphy. The oxygen isotope record was graphically aligned with the intermediate depth Indian Ocean benthic oxygen isotope stack of Lisiecki and Stern (2016) using the minimum number of tie points (2 for 64PE304-8; Figure 2.4) required for a good visual match (Figure 2.5). Identifying termination 2 ($\sim$130ka; Jiménez-Amat and Zahn 2015) and, hence Heinrich Event 11, was possible with confidence in core 64PE304-8. The low sample density in the same section of core 64PE304-8, however, only allowed for a rough age model between 125 ka and 60 ka.

Based on our age modelling approach, 64PE304-8 provides the longest time series covering close to 150kyr of African climate change. Across the three cores the sedimentation rates vary between 0.3 and 14.6 cm/kyr, the average being 6.2

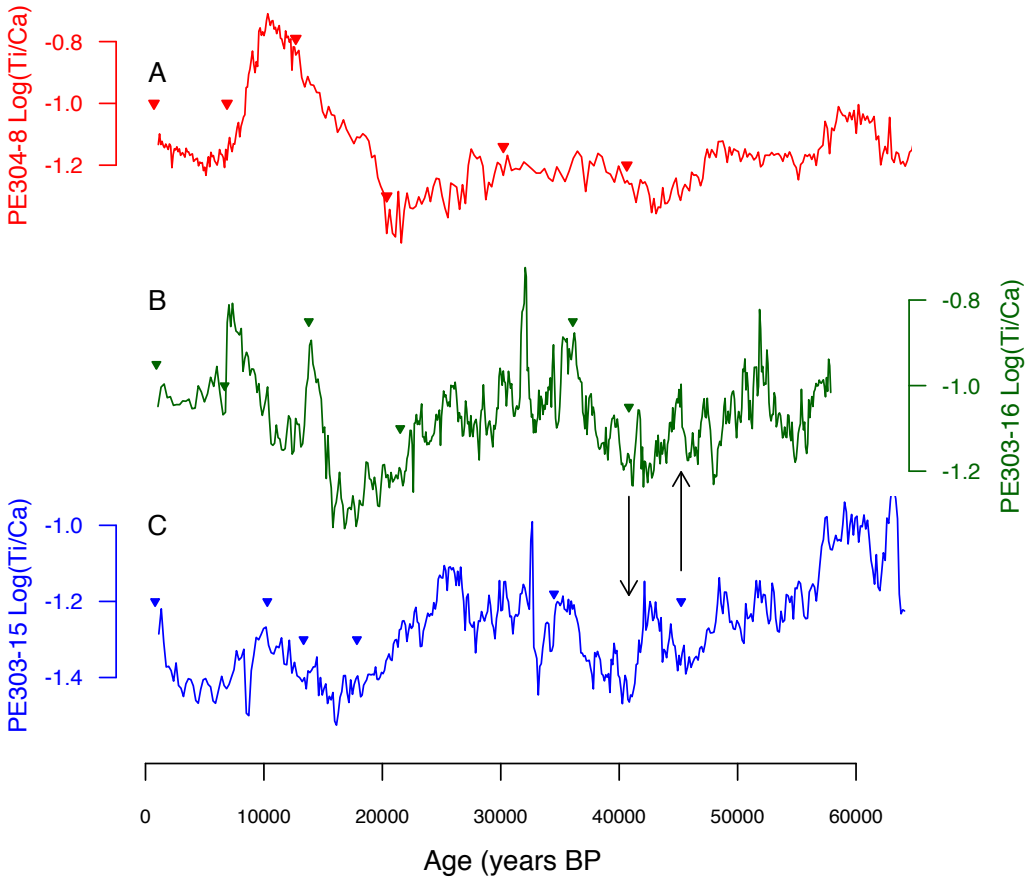

FIGURE 2.2: Log(Ti/Ca) records of (A) 64PE304-8 (B) 64PE303-16 and (C) 64PE303-15 (all this study). Radiocarbon dates indicated by solid triangles. Vertical arrows indicate radiocarbon dates transposed between cores as discussed in main text. The age models in this plot are based solely on the radiocarbon dates presented here with linear interpolation between.

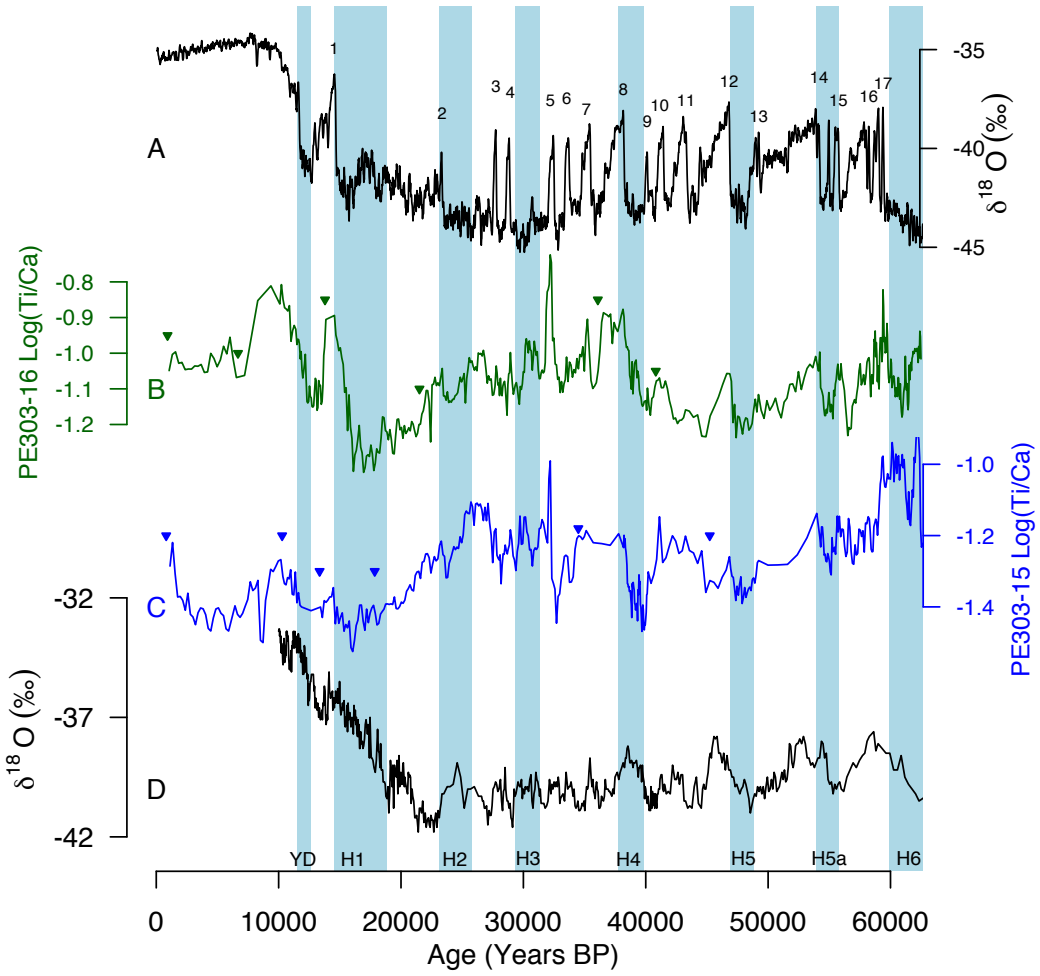

FIGURE 2.3: (A) Oxygen isotope record of Greenland ice core GISP2 (on GICC05 timescale Rasmussen et al. 2008; Grootes et al. 1993). (B) Log(Ti/Ca) record of 64PE303-16 (green). (C) Log(Ti/Ca) record of 64PE303-15 (blue). (D) Oxygen isotope record of the Byrd ice core Antarctica (Johnsen et al.; 1972).

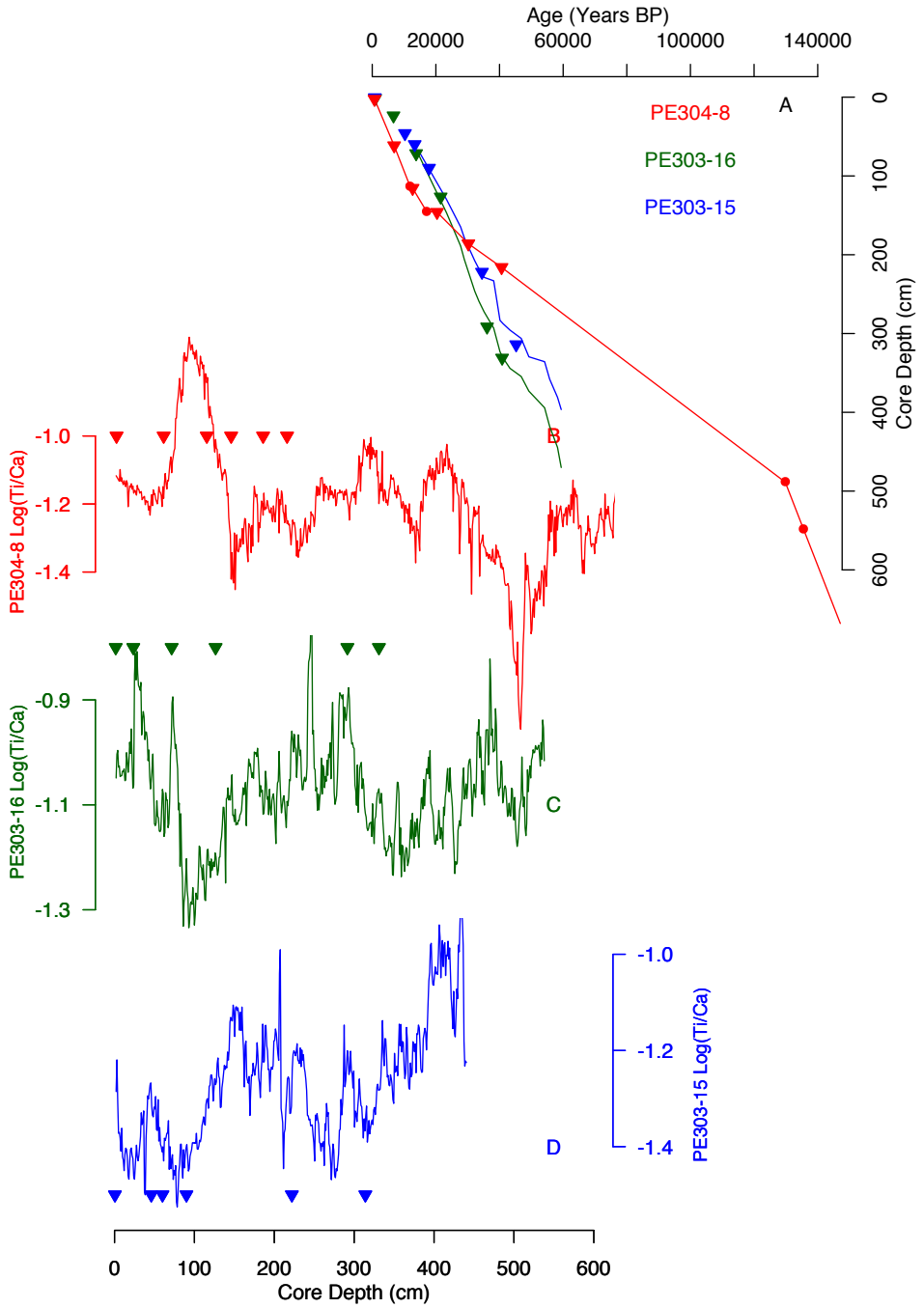

FIGURE 2.4: (A) Core depth versus Age for the three new cores presented in this thesis. Solid triangles represent radiocarbon dates. Solid circles represent extra tie points as described in section 2.6. The colour scheme adopted here is consistent throughout this chapter (and thesis) (B) Log(Ti/Ca) of core 64PE304-8 plotted against depth. (C) Log(Ti/Ca) of core 64PE303-16 plotted against depth. (D) Log(Ti/Ca) of core 64PE303-15 plotted against depth. For B, C, and D radiocarbon dates are indicated by solid triangles.

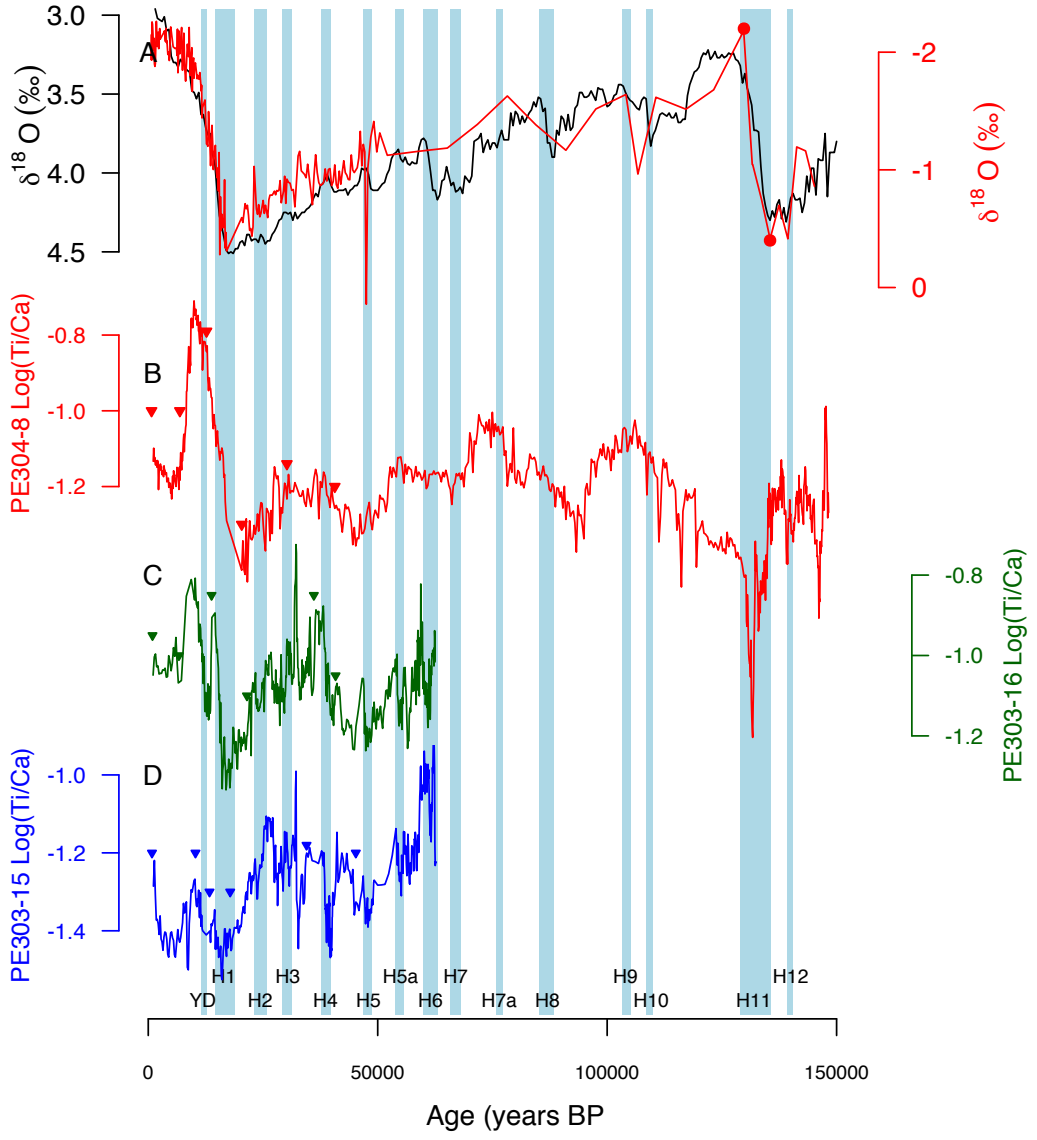

FIGURE 2.5: Plot summarizing the final age models for the three new cores presented in this study. (A) Intermediate depth Indian Ocean benthic stack of Lisiecki and Stern (2016) (black); Planktic oxygen isotope ($\delta^{18}O$) record of 64PE304-8 (this study, red) (B) Log(Ti/Ca) of core 64PE304-8 (this study, red) (C) Log(Ti/Ca) of core 64PE303-16 (1350m water depth, this study) (D) Log(Ti/Ca) of core 64PE303-15 (1985m water depth, this study).

cm/kyr (Figure 2.4). The shallowest core (64PE304-8) has a lower temporal resolution, especially in sections below two metres core depth. The likely cause for this pattern being increased sediment supply associated with sea level rise across the deglaciation. This would result in more of the continental sediment load being deposited on the shelf (i.e. core 64PE304-8), as opposed to the slope (i.e. cores 64PE303-16 and 64PE303-15). The long term sedimentation rate patterns of all three cores support this idea of changing distribution of sediment supply as a consequence of the glacial to inter-glacial transition.

Despite the rather low time resolution in certain sections, the majority of the sediment sequences used in this study allow us to address climate changes over east Africa at the millennial scale.

Bibliography

Brummer, G. and Jung, S. (2009). RV Pelagia Cruise Report : Cruise 64PE304 SE African margin ,.

Coplen, T. B., Kendall, C. and Hopple, J. (1983). Comparison of stable isotope reference samples, *Nature* **302**(5905): 236–238.

Grootes, P. M., Stuiver, M., White, J. W. C., Johnsen, S. and Jouzel, J. (1993). Comparison of oxygen isotope records from the GISP2 and GRIP Greenland ice cores, *Nature* **366**(6455): 552–554.

Hennekam, R. and de Lange, G. (2012). X-ray fluorescence core scanning of wet marine sediments: methods to improve quality and reproducibility of high-resolution paleoenvironmental records, *Limnology and Oceanography: Methods* **10**: 991–1003.

Ivanochko, T. S., Ganeshram, R. S., Brummer, G. J. A., Ganssen, G., Jung, S. J. A., Moreton, S. G. and Kroon, D. (2005). Variations in tropical convection as an amplifier of global climate change at the millennial scale, *Earth and Planetary Science Letters* **235**(1-2): 302–314.

Jiménez-Amat, P. and Zahn, R. (2015). Offset timing of climate oscillations during the last two glacial-interglacial transitions connected with large-scale freshwater perturbation, *Paleoceanography* **30**(6): 768–788.

Johnsen, S. J., Dansgaard, W., Clausen, H. B. and Langway, C. C. (1972). Oxygen Isotope Profiles through the Antarctic and Greenland Ice Sheets, *Nature* **235**(5339): 429–434.

Kroon, D. and Party, S. (2010). Tropical Temperature History during Paleogene GLObal Warming (GLOW) Events, NIOZ site survey cruise report (RV Pelagia cruise number 64PE303), *NIOZ Site* pp. 1–59.

Lisiecki, L. E. and Stern, J. V. (2016). Regional and global benthic $\delta^{18}O$ stacks for the last glacial cycle, *Paleoceanography* **31**(10): 1368–1394.

Rasmussen, S. O., Seierstad, I. K., Andersen, K. K., Bigler, M., Dahl-Jensen, D. and Johnsen, S. J. (2008). Synchronization of the NGRIP, GRIP, and GISP2 ice cores across MIS 2 and palaeoclimatic implications, *Quaternary Science Reviews* **27**(1-2): 18–28.

Reimer, P. J., Bard, E., Bayliss, A., Beck, J. W., Blackwell, P. G., Ramsey, C. B., Buck, C. E., Cheng, H., Edwards, R. L., Friedrich, M., Grootes, P. M., Guilderson, T. P., Haflidason, H., Hajdas, I., Hatté, C., Heaton, T. J., Hoffmann, D. L., Hogg, A. G., Hughen, K. A., Kaiser, K. F., Kromer, B., Manning, S. W., Niu, M., Reimer, R. W., Richards, D. A., Scott, E. M., Southon, J. R., Staff, R. A., Turney, C. S. M. and van der Plicht, J. (2013). IntCal13 and Marine13 Radiocarbon Age Calibration Curves 0–50,000 Years cal BP, *Radiocarbon* **55**(04): 1869–1887.

Southon, J., Kashgarian, M., Fontugne, M., Metivier, B. and Yim, W. W.-S. (2002). Marine reservoir corrections for the Indian Ocean and Southeast Asia, *Radiocarbon* **44**(1): 167–180.

Stuiver, M., Reimer, P. J. and Bard, E. (2006). INTCAL98 radiocarbon age calibration, 24,000-0 cal BP., **40**(3): 1041–1083.

Tjallingii, R., Röhl, U., Kölling, M. and Bickert, T. (2007). Influence of the water content on X-ray fluorescence corescanning measurements in soft marine sediments, *Geochemistry, Geophysics, Geosystems* **8**(2).

van Der Lubbe, J. H., Tjallingii, R., Prins, M. A., Brummer, G.-J. A., Jung, S. J. A., Kroon, D. and Schneider, R. R. (2014). Sedimentation patterns off the Zambezi River over the last 20,000 years, *Marine Geology* **355**: 189–201.

Weltje, G. J. and Tjallingii, R. (2008). Calibration of XRF core scanners for quantitative geochemical logging of sediment cores: Theory and application, *Earth and Planetary Science Letters* **274**(3-4): 423–438.

Chapter 3

Equatorial African climate affinity with millennial-scale northern hemisphere environmental change over the last 150 kyr

3.1 Introduction

The African continent has experienced significant climate changes over the last 150ka (deMenocal; 1995; deMenocal et al.; 2000; Trauth et al.; 2003; Prell and Kutzbach; 1987; Barker et al.; 2004). Climate along the eastern African coast is strongly controlled by changes in monsoonal rainfall due to seasonal variation in insolation. As part of the African and western Asian monsoon systems, this rainfall variability is related to shifts in the location of the Intertropical Convergence Zone (ITCZ). On orbital time-scales, precession driven variations in insolation likely affected the latitudinal range of the ITCZ and influenced the monsoon intensity. A well-documented example is the African Humid Period (AHP; Jung et al. 2004; deMenocal et al. 2000), which occurred from $\sim$15 ka to $\sim$5 ka when much of the Sahara was covered by vegetation and lakes.

Superimposed on these long-term changes, the African and Asian monsoon systems also displayed variations at millennial time-scales. Well-dated records from continental China (Cheng et al.; 2016, 2009) show that relatively short-term variations in monsoon intensity occurred in phase with the well-known millennial-scale Dansgaard-Oeschger (DO) variability in Greenland ice cores. Similarly, records from the northern and northwestern Arabian Sea region imply that variations in rainfall over eastern Africa and monsoon driven changes in the Arabian Sea also occurred in phase with millennial-scale change in Greenland (Ivanochko et al.; 2005; Altabet et al.; 2002; Schulz; 2002). The combined data suggest that large parts of the African-Asian monsoon systems varied in tune with Greenland climate change.

At a broader scale, when comparing ice core data between the poles the so-called bipolar seesaw refers to an out of phase relationship of millennial-scale temperature shifts, with the temperature variability over Antarctica leading Greenland climate change by 1-2.5 kyr (Blunier et al.; 1998; Barbante et al.; 2006; Blunier and Brook; 2001). Detailing the distribution pattern of the 'hemispheric-dominance' of this millennial-scale pattern of climate change in key areas of the Earth's climate system is important for improving our understanding the underlying controls. Current knowledge of the timing and nature of millennial-scale climate change in the western Indian Ocean region is poor due a lack of high-quality records from the region. Evidence from the limited number of records from the southern Indian Ocean provides little clarity as to whether or not they record a climate change pattern similar to that in the north or in the south. Data from the western Indian Ocean off the Zambezi river for example suggest wet conditions prevailed during Heinrich 1 (van Der Lubbe et al.; 2014) contrasting to data from the Arabian Sea (Ivanochko et al.; 2005). During the Younger Dryas, prevailing climate conditions in both regions were also contrasting. In line with earlier stadial events, dry conditions prevailed in north-eastern Africa during the Younger Dryas (Ivanochko et al.; 2005), whereas wet conditions occurred in the Zambezi catchment area (van Der

Lubbe et al.; 2014). Further south, in the Indian Ocean off southern Africa, the hemispheric dominance pattern is similarly unclear. Surface ocean data suggest a relation with Antarctic climate change whereas geochemical data confirm that the evaporation-precipitation balance in southern Africa varied in tune with northern hemisphere millennial-scale climate change (Ziegler et al.; 2013).

Here we present high-resolution data from four well dated marine sediment cores from $\sim$9°S in the western tropical Indian Ocean that reflect climate shifts in Africa at the same latitude. These cores provide an opportunity to elucidate the nature of millennial-scale change over the past 150kyr. We specifically investigate how the influence of northern versus southern hemisphere driven millennial-scale climate variability evolved in eastern Africa over the last 150kyr. A 'hinge-zone', in the sense of Tierney et al. (2010), possibly separated northern hemisphere driven millennial-scale change to the north from southern hemisphere driven change in the south. This 'hinge-zone' may be stationary, or may shift with time, both at millennial and orbital time-scales of change. We compare geochemical records of eastern African hydrological change to speleothem based monsoon records from China and Borneo to assess the impact of different insolation regimes across different longitudinal regions of equatorial latitudes as drivers of past climate change.

Our new data provide a new high-resolution set of records of eastern African climate with important implications for our understanding of the role of the tropics in orbital and millennial-scale climate change over the last 150kyr.

3.2 Continental climate recorded in deep sea sediments

This study makes use of terrestrial climate change records found in the terrigenous fraction of four marine sediment cores from offshore Tanzania. The primary sources of terrigenous material in the cores used in this study are from the Rovuma

and Rufiji and numerous smaller river catchments (Figure 3.1). Dust does not significantly contribute to the terrigenous sedimentation at our core sites. In this region, present day climate is dominated by the annual north-south movement of the ITCZ and its associated precipitation. Figure 3.1A shows the northernmost extent of the ITCZ rainfall, occurring during boreal summer (JJA) and Figure 3.1B shows the southernmost position during boreal winter (DJF). The Rovuma and Rufiji river catchments receive the majority of their annual rainfall during boreal winter (austral summer). Hence, the terrigenous materials in our cores largely reflect changes in precipitation during boreal winter when the ITCZ is in its southerly position.

3.2.1 Terrigenous versus marine sediment deposition

The titanium/calcium (Ti/Ca) ratio in marine sediments has been frequently used to reconstruct climate change in nearby continental settings (Lubbe et al.; 2011; van Der Lubbe et al.; 2014; Tjallingii et al.; 2007). Unlike other elements such as iron, the mobility of titanium is less sensitive to changing weathering conditions in continental settings. Hence, in the absence of any significant sources in the ocean, titanium concentrations in deep-sea sediments reflect climate conditions on the nearby continent. In contrast, calcium overwhelmingly stems from marine biogenic carbonates such as foraminifera and coccoliths. The Ti/Ca ratio is therefore a useful tracer of changes in terrigenous sedimentation in marine settings. The logarithmic form (log(Ti/Ca)) has been introduced to reduce potential sediment matrix effects related to variable water concentrations and grain-sizes (Weltje and Tjallingii; 2008; Hennekam and de Lange; 2012; Tjallingii et al.; 2007)

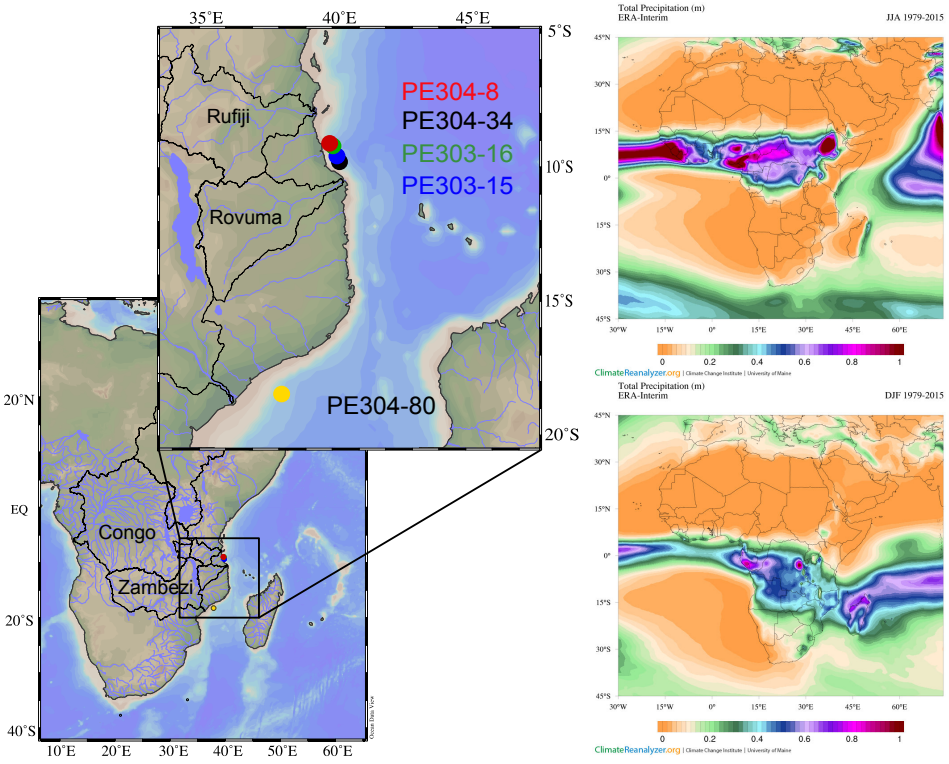

FIGURE 3.1: Left) Map detailing locations of cores presented and referred to in this chapter. Core depths below sea surface as follows: 64PE304-8 752m; 64PE304-34 1037m; 64PE303-16 1350m; 64PE303-15 1985m. Important river catchments referred to in main text are also indicated. Top Right) Map of African continent with overlay contour plot of total precipitation (m) for June, July and August. Bottom right) Same as above, this time for December, January and February.

3.3 Materials & Methods

3.3.1 Sediment Cores

The data presented here are from four marine sediment cores (64PE304-8 at 752m water depth; 64PE303-16 at 1350m water depth; 64PE303-15 at 1985m water depth; and 64PE304-34 at 1037m water depth) from offshore Tanzania in the western Indian Ocean (Figure 3.1A). These cores were retrieved in 2009 using a Royal Netherlands Institute for Sea Research (NIOZ) designed piston corer onboard the *RV Pelagia* as part of the "Tropical Temperature History During Paleogene Global Warming events" (GLOW) (Kroon and Party; 2010) and "Indian – Atlantic Exchange" (INATEX) (Brummer and Jung; 2009) cruises

3.3.2 X-Ray Fluorescence core scanning

The bulk sediment geochemical data presented in this study were obtained by X-ray fluorescence (XRF) core scanning at 10 kV with a 1 cm resolution using an Avaatech core scanner at Royal NIOZ, Texel, Netherlands. For more background on this technique, see chapter 1.

3.3.3 Oxygen isotope analyses

The oxygen isotope records presented here were produced by isotope ratio mass spectrometry. Using a sample resolution of 1-2cm, a subsample of 15-30 powdered specimens of the planktonic foraminifera species *G.ruber* and *N.dutertrei* from cores 64PE304-8, 64PE303-16 and 64PE303-15 were measured at the University of Edinburgh using a Thermo Electron Delta^{+} Advantage stable isotope mass spectrometer coupled to a Kiel Carbonate III preparation device. The stable oxygen isotope record of core 64PE304-34 is based on the planktonic foraminifera species *G.ruber* and was measured using a Thermo MAT 232 stable isotope mass spectrometer coupled to a Kiel Carbonate IV preparation device at the Royal NIOZ, Netherlands.

Data supplied for use here by Jeroen van der Lubbe. Analytical precision for both $\delta^{13}C$ and $\delta^{18}O$ was better than $\pm 0.1‰$.

3.4 Chronology and sedimentation rates

The chronology of the sediment sequences used in this study is based on a multi-step approach. The initial age models are based on 21 radiocarbon dates (Table 2.1). For cores 64PE304-8, 64PE303-16 and 64PE303-15 18 radiocarbon dates were carried out on ~10 mg samples of the planktonic foraminifera *G.ruber* at the NERC radiocarbon facility in East Kilbride, Scotland (funded by NERC Radiocarbon Allocation Number 1796.0414). Three radiocarbon dates for core 64PE304-34 have been previously measured and were supplied for use here by Jeroen van der Lubbe.

Based on the initial age models there was a good alignment of the log(Ti/Ca) records (Figure 3.2). Following the approach of van Der Lubbe et al. (2014), for clearly identifiable points in the respective log(Ti/Ca) records (Figure 3.3), two radiocarbon dates were transposed between cores 64PE303-16 and 64PE303-15 (Figure 3.2).

Based on these age models, the log(Ti/Ca) records for cores 64PE303-16 and 64PE303-15 are very similar. Within the uncertainty of radiocarbon dates, individual events in the log(Ti/Ca) records are synchronous between both records. In order to assess the influence of northern or southern hemisphere driven climate change recorded in our log(Ti/Ca) records we compared the records with $\delta^{18}O$ records from the GISP2 (Greenland) and Byrd (Antarctica) ice core (Figures 3.4 & 3.5). Based on the independently established age models, the log(Ti/Ca) variability of sediment cores 64PE303-16 and 64PE303-15 broadly resembles GISP2 in terms of the shape of events and timing, with only limited offsets. In contrast, the shape and timing of minima/maxima in the log(Ti/Ca) record deviate from the millennial-scale events in the oxygen isotope record of the Byrd ice core (Figure 3.5). Within

the uncertainty of the radiocarbon dates, DO events 1 through 17 in the GISP2 record co-occur with high values in the log(Ti/Ca) records of cores 64PE303-16 and 64PE303-15 (Figure 3.5). This close relation of the log(Ti/Ca) records with Greenland climate change supports the view that terrestrial sedimentation off Tanzania indeed varies in tune with millennial-scale climate change in the north. We applied this relation to adjust the age models exclusively beyond the reach of the radiocarbon method, in keeping with a similar strategy adopted for sediments from the Arabian Sea (Ivanochko et al.; 2005).

The age models for the deep sections of cores 64PE304-34 and 64PE304-8 are based on oxygen isotope stratigraphy. The oxygen isotope records for both sediment cores were graphically aligned with the intermediate depth Indian Ocean benthic oxygen isotope stack of Lisiecki and Stern (2016) using the minimum number of tie points (3 for 64PE304-34 and 2 for 64PE304-8, Figure 3.3) required for a good visual match (Figure 3.4). Identifying Termination 2 ($\sim$130ka; Jiménez-Amat and Zahn 2015) and, hence Heinrich event 11, was possible with confidence in both cores. Establishing a detailed chronology between $\sim$125 ka and $\sim$60 ka was possible for core 64PE304-34. The low sample density in the same section of core 64PE304-8, however, only allowed for a rough age model between $\sim$125 ka and $\sim$60 ka.

Based on our age modelling approach, 64PE304-8 and 64PE304-34 provide the longest time-series covering close to 150kyr of African climate change. Across the four cores the sedimentation rates vary between 0.3 and 14.6 cm/kyr, the average being 6.2 cm/kyr (Figure 3.3). The two shallower cores (64PE304-8 and 64E304-34; Figure 3.4) have lower temporal resolution, especially in sections below two metres core depth. Despite the rather low time resolution in certain sections (see discussion section), the majority of the sediment sequences used in this study allow us to address climate changes over eastern Africa at the millennial-scale.

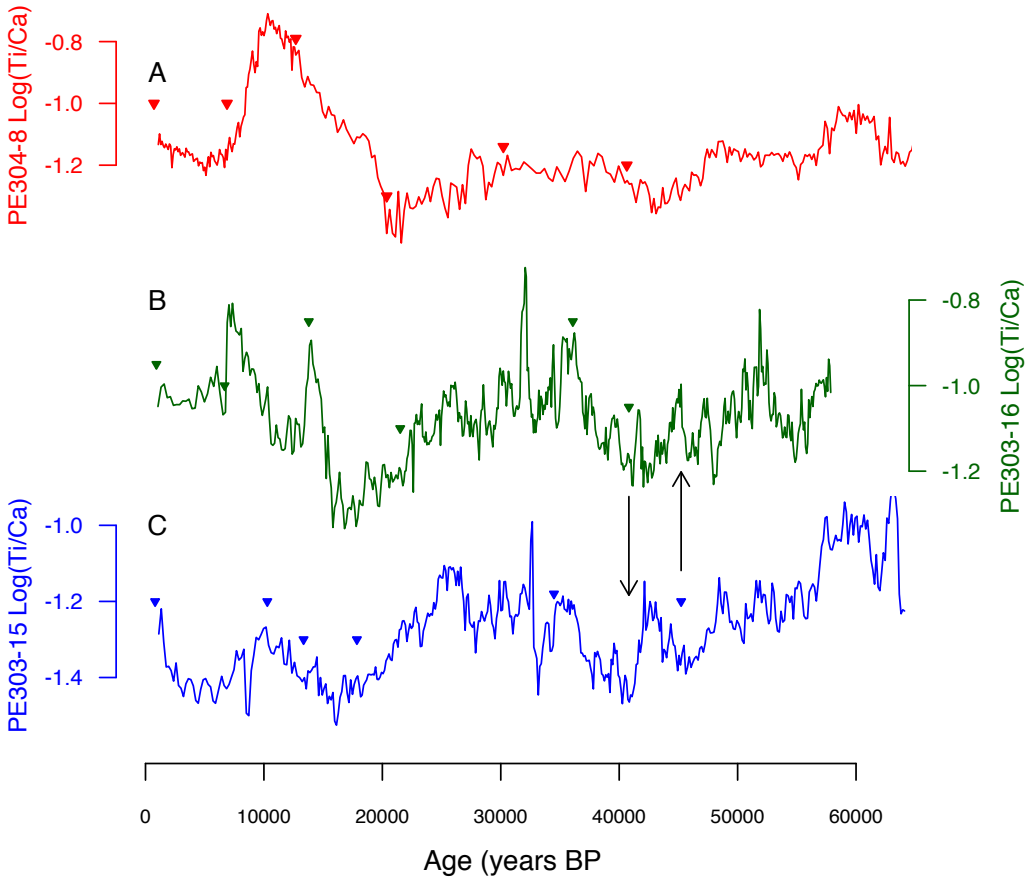

FIGURE 3.2: Log(Ti/Ca) records of (A) 64PE304-8 (B) 64PE303-16 and (C) 64PE303-15 (all this study). Radiocarbon dates indicated by solid triangles. Vertical arrows indicate radiocarbon dates transposed between cores as discussed in main text. The age models in this plot are based solely on the radiocarbon dates presented here with linear interpolation between.

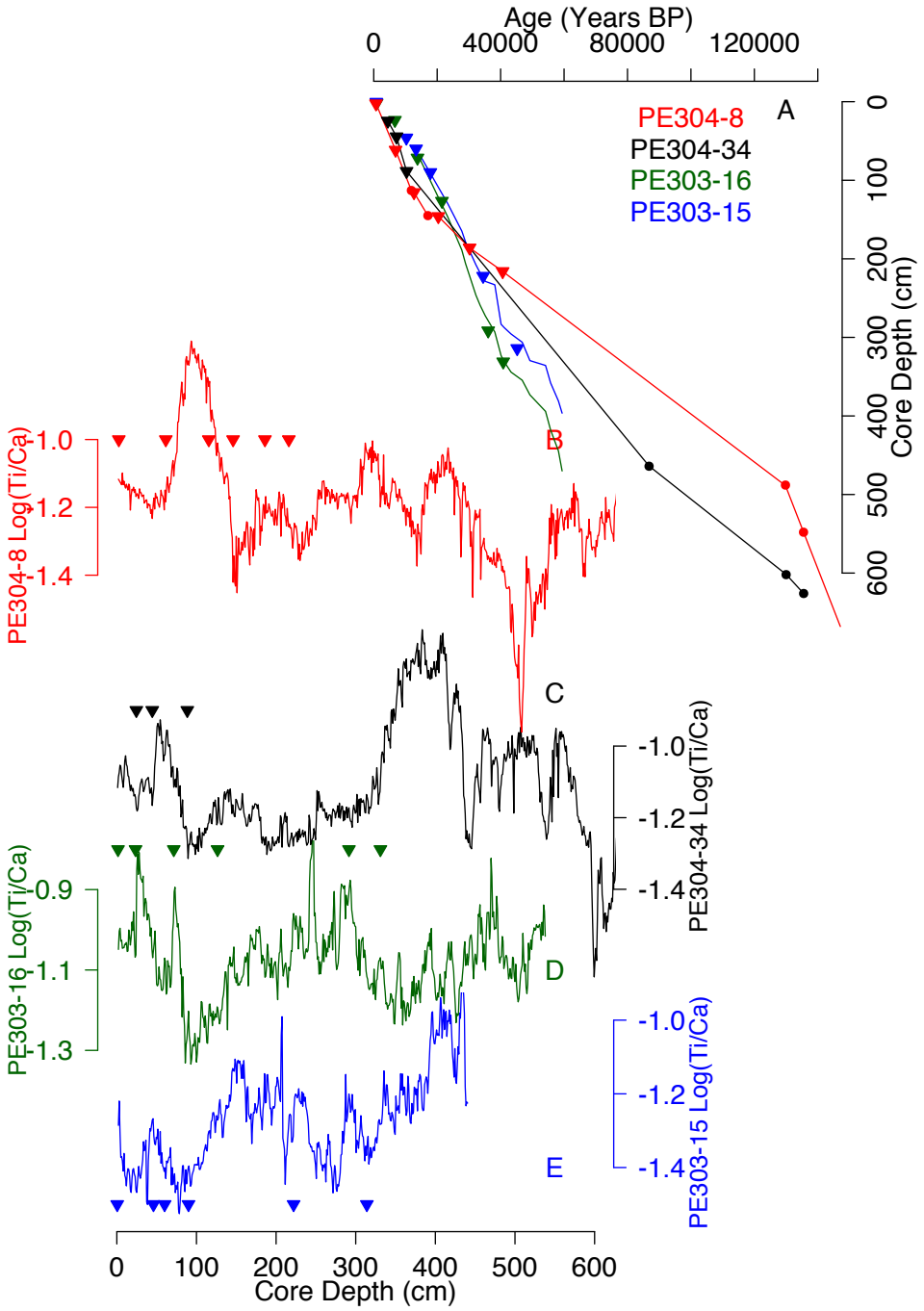

FIGURE 3.3: (A) Core depth versus age for the four new cores presented in this work. Solid triangles represent radiocarbon dates. Solid circles represent extra tie points described in text. The colour scheme adopted here is consistent throughout this chapter (and thesis) (B) Log(Ti/Ca) of core PE304-8 plotted against depth. (C) Log(Ti/Ca) of core PE304-34 plotted against depth. (D) Log(Ti/Ca) of core PE303-16 plotted against depth. (E) Log(Ti/Ca) of core PE303-15 plotted against depth. For B, C, D and E radiocarbon dates are indicated by solid triangles.

3.5 Results; XRF Data

The log(Ti/Ca) ratios vary between -1.86 and -0.67 across sediment cores 64PE303-15/16 and 64PE304-8/34. The max/min values for each core are: 64PE304-8 -0.71/-1.86; 64PE304-34 -0.67/-1.64; 64PE303-16 -0.72/-1.33; and, 64PE303-15 -0.90/-1.53. The average values across each core are around -1.3 to -1.2, except for core 64PE303-16 where an average value of around -1.1 to -1 prevails. Generally, all four log(Ti/Ca) records show two types of variability: (i) a long-term pattern with a period of ∼20kyr; and (ii) variation at the centennial to millennial-scale superimposed onto the longer-term trends. Both the long-term and the millennial-scale variations in the log(Ti/Ca) data are slightly more pronounced in the deeper cores (64PE303-15 and 64PE303-16; Figure 3.6 F&G).

The long-term trends in the log(Ti/Ca) records are broadly similar to variations in solar insolation at 4°N. Strong positive excursions occur in the early Holocene (cores 64PE303-16, 64PE304-8, weaker in core 64PE304-34, and almost absent in 64PE303-15). In addition, a broad maximum in log(Ti/Ca) values is centered around 70 ka in core 64PE304-34, the tail end of which is likely to be reflected in the high values in the lowest/oldest sections of cores 64PE303-15/16 (Figures 3.4 & 3.5). Low values in the log(Ti/Ca) records are linked to the last glacial maximum (LGM; ∼20ka) and the end of marine isotope stage 6 (MIS6; ∼135ka). Although note that MIS6 is beyond the limit of coverage of cores 64PE303-16 and 64PE303-15.

The log(Ti/Ca) variability at the millennial-scale typically ranges between 0.1 and 0.2. Most Heinrich events co-occur with low values, particularly strong at Heinrich events 1 and 11. It is interesting to note that particularly strong positive excursion occur in both deep cores (64PE303-15/16) prior to Heinrich events H5a, H5(weak), H4, H3(strong) and H2.

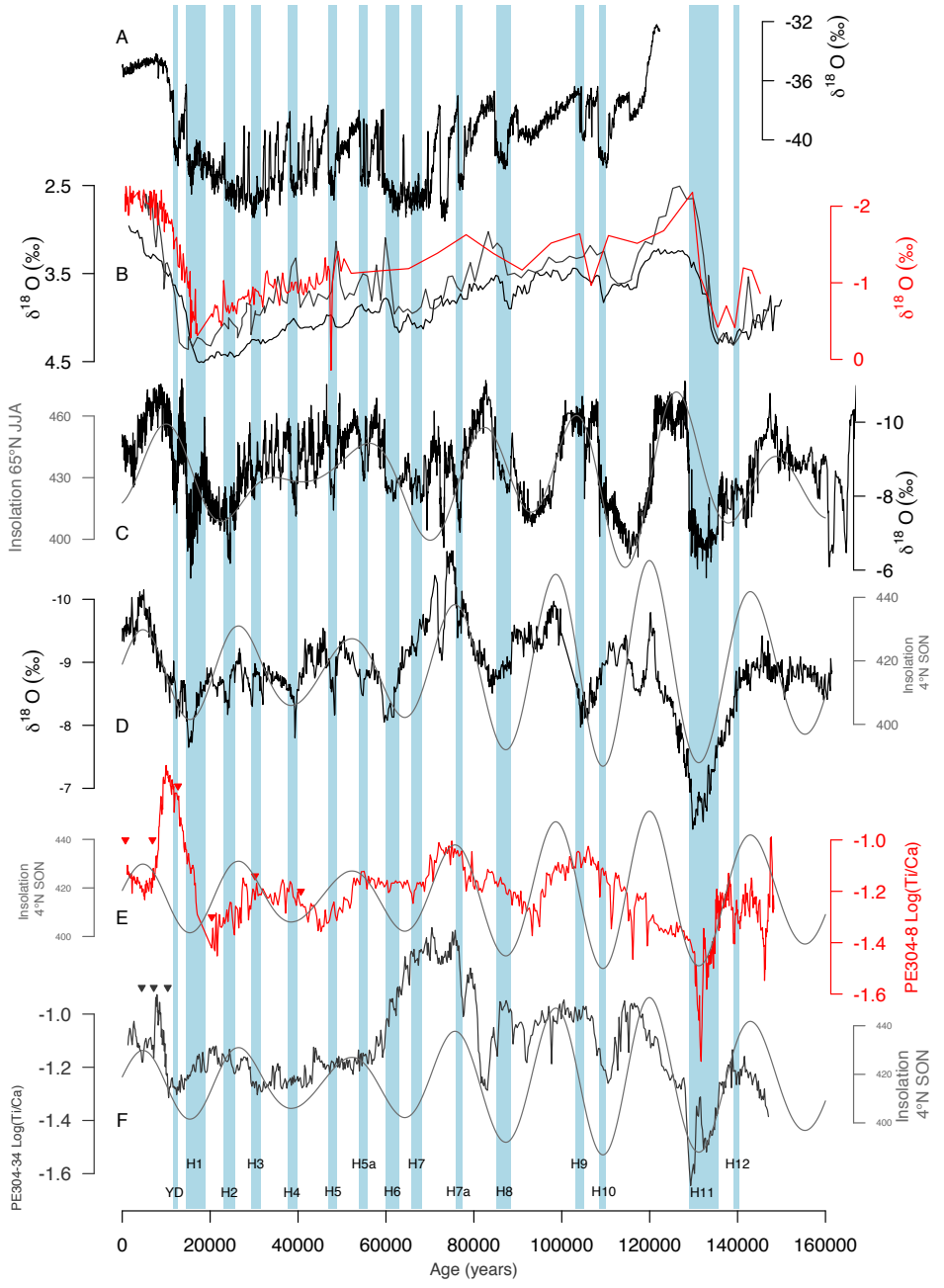

FIGURE 3.4: (A) Oxygen isotope ($\delta^{18}O$) record of Greenland ice core GISP2 (on GICC05 timescale Vinther et al. 2006; Rasmussen et al. 2008; Andersen et al. 2006; Grootes et al. 1993). A proxy for local temperature. (B) Intermediate depth Indian Ocean benthic stack of Lisiecki and Stern (2016) (black); Planktic oxygen isotope ($\delta^{18}O$) record of 64PE304-34 (this study, grey); Planktic oxygen isotope ($\delta^{18}O$) record of 64PE304-8 (this study, red)(C) Hulu-Sanbao speleothem oxygen isotope ($\delta^{18}O$) record (Cheng et al. 2016; black); with JJA insolation at 65°N (grey); (D) Mulu Stalagmite $\delta^{18}O$ from northern Borneo (4°N; Carolin et al. 2016, 2013; Partin et al. 2007; black); SON Insolation at 4°N (grey) (E) Log(Ti/Ca) of core PE304-8 (this study, red); with SON Insolation at 4°N (F) Log(Ti/Ca) of core PE304-34 (this study, grey); with SON Insolation at 4°N (black). Heinrich events indicated by vertical blue shaded lines using the nomenclature and dates adopted by Lisiecki and Stern (2016). All insolation series produced using Analyseries (Paillard et al.; 1996)

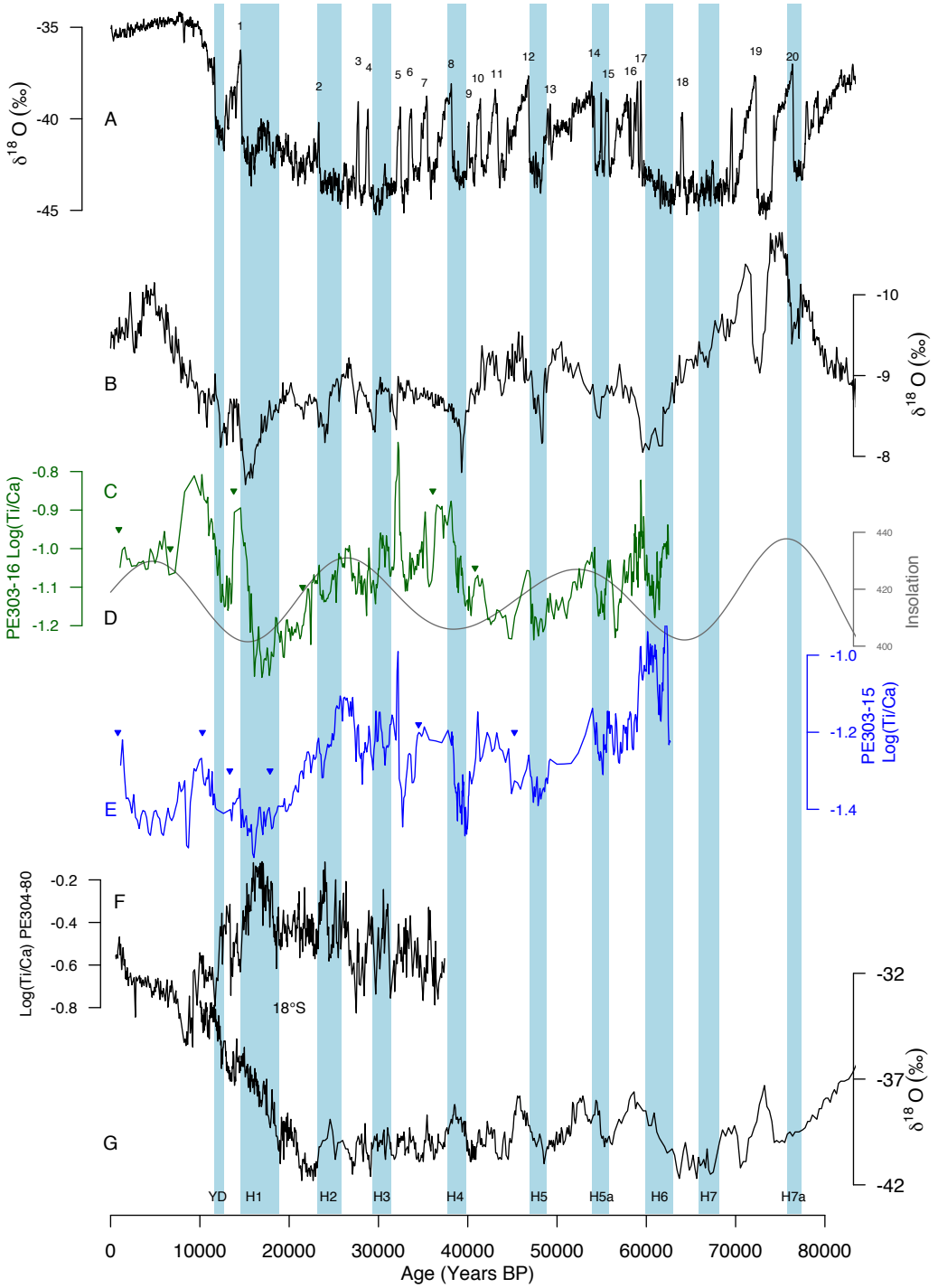

FIGURE 3.5: (A) Oxygen isotope ($\delta^{18}O$) record of Greenland ice core GISP2 (on GICC05 timescale Vinther et al. 2006; Rasmussen et al. 2008; Andersen et al. 2006; Grootes et al. 1993). A proxy for local temperature. (B) Mulu Stalagmite $\delta^{18}O$ from northern Borneo (4°N; Carolin et al. 2016, 2013; Partin et al. 2007) (C) Log(Ti/Ca) of core 64PE303-16 (this study) radiocarbon dates indicated by solid green triangles (D) Insolation at 4°N. record produced using Analyseries (Paillard et al.; 1996) (E) Log(Ti/Ca) of core 64PE303-15 (this study) (F) Log(Ti/Ca) of core 64PE304-80 (van Der Lubbe et al.; 2014) (G) Oxygen isotope ($\delta^{18}O$) record of Antarctic ice core Byrd (Johnsen et al.; 1972). Heinrich events indicated by vertical blue shaded lines using the nomenclature and dates adopted by Lisiecki and Stern (2016).

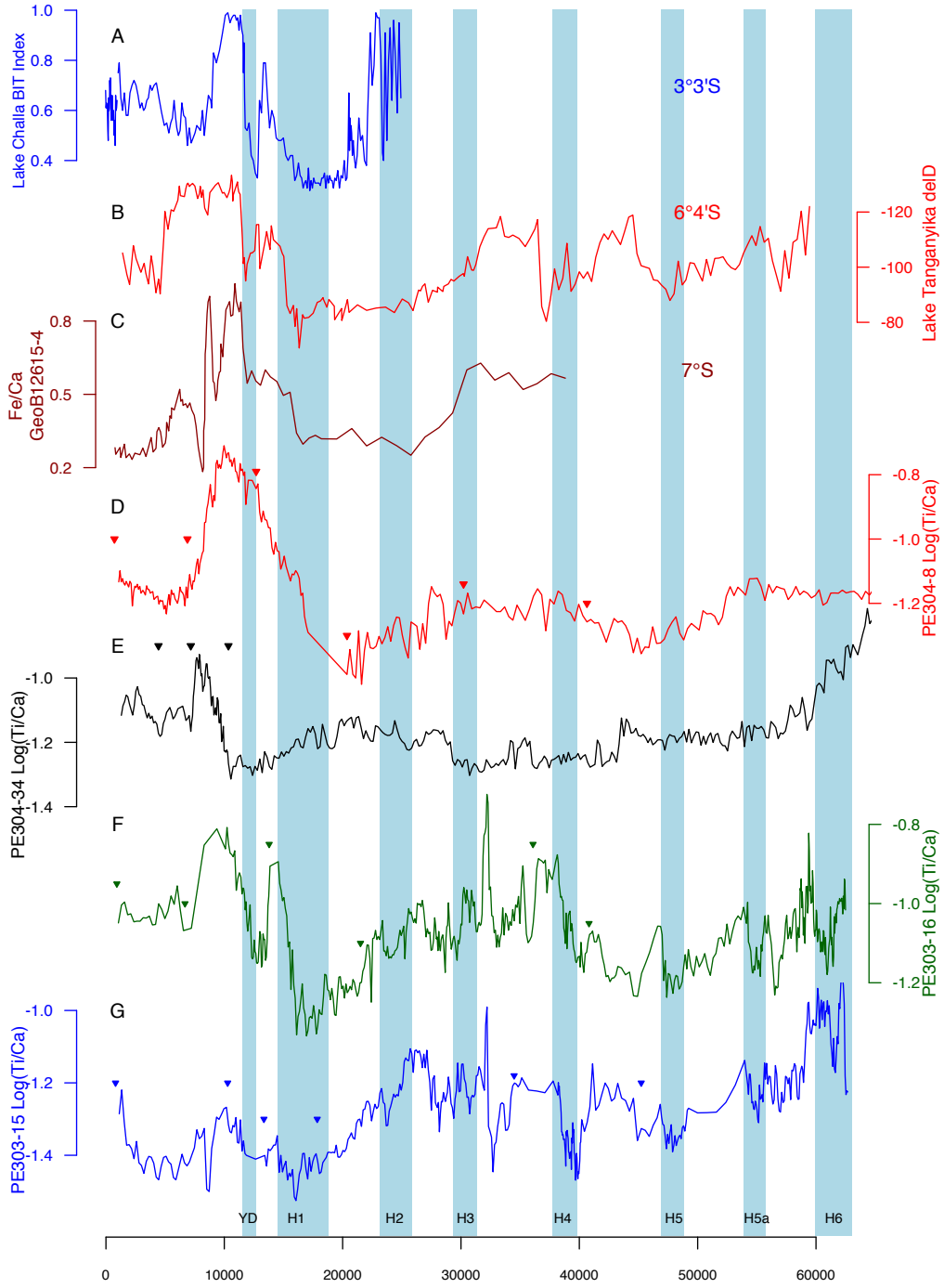

FIGURE 3.6: (A) Lake Challa BIT Index rainfall reconstruction (more positive values indicate wetter conditions; Verschuren et al. 2009) (B) Lake Tanganyika $\delta D_{(leafwax)}$ (Tierney et al.; 2008) (C) Fe/Ca of core GeoB12615-4 (446m water depth) Modified after Romahn et al. (2013) (D) Log(Ti/Ca) of core PE304-8 (this study) (E) Log(Ti/Ca) of core PE304-34 (1037m water depth, this study) (F) Log(Ti/Ca) of core PE303-16 (1350m water depth, this study)(G) Log(Ti/Ca) of core PE303-15 (1985m water depth, this study)

3.6 Discussion

3.6.1 Quality of the log(Ti/Ca) records

The variations displayed in the log(Ti/Ca) records used in this study provide a record of long- and short-term change in eastern African climate. It is not entirely clear what caused log(Ti/Ca) variability to be more pronounced in the deeper sites (cores 64PE303-15/16). In sediment sections with low sedimentation rates, bioturbation, which acts as a low-pass filter, would have had a stronger effect, leading to a smoother record. Low frequency changes would pass through with little or no change, whereas short-term variability would be dampened or removed (Trauth et al.; 1997). This is probably the case for some sections in the shallower sites. The log(Ti/Ca) data of shallower cores 64PE304-8/34 in Figure 3.4 however, show some millennial-scale change, suggesting that the effect of bioturbation was limited and did not completely remove the short-term climate signal. The presence of some millennial-scale variability also suggests that longer-term variability was not affected in the same way. Hence, applying the same rationale to differences in the long-term record does not seem appropriate. The differences in the long-term records are more likely reflecting slightly differing sedimentation regimes between the shallow and deep sites. These could for example entail shifts in sedimentation patterns due to sea level change or subsurface currents affecting local sediment accumulation. Whilst small differences between the log(Ti/Ca) time-series probably reflect subtle differences in local sedimentation pattern, the proximity of the new sites confirms that regional climate change in eastern Africa is the main driver for the variability seen in the new data presented here.

Another factor potentially affecting our interpretation is related to changes in carbonate preservation which would affect log(Ti/Ca) data (Govin et al.; 2012). The carbonate compensation depth in the Indian Ocean has been deeper (>3km) than our core sites (<2km) throughout the period covered by this study (Naidu et al.;

2014). Hence, we interpret that variations in log(Ti/Ca) are primarily influenced by changes in rainfall over eastern Africa as has been employed previously around the African margin (e.g. Ziegler et al. 2013; Revel et al. 2015).

3.6.2 Long-term changes in rainfall in eastern Africa

Our data suggest that the long-term climate variability in equatorial eastern Africa reflects precession driven changes in insolation, in line with previous studies (e.g. Tierney et al. 2008, 2010; Verschuren et al. 2009; Trauth et al. 2003). High/low log(Ti/Ca) values during precessional maximum/minimum phases in Figure 3.4 indicate strong/weak monsoons, respectively. Shifts in the position of the ITCZ, which is the main supplier of moisture to the region, are the most likely cause for this climate change pattern. Consistent with our data, modelling studies indeed show that the ITCZ will move towards the warmer hemisphere because of an increased inter-hemispheric temperature gradient (e.g. McGee et al. 2014; Broccoli et al. 2006; Chiang and Bitz 2005). Generally, long-term periods of high log(Ti/Ca) in cores 64PE303-16 and 64PE304-8 co-occur with high insolation at 4°N. Maxima in northern hemisphere insolation lead to a more northerly position of boreal summer ITCZ (Schneider et al.; 2014; Davis and Brewer; 2008). Hence, during these times the ITCZ resides further north than during modern day boreal summer. The well-known early Holocene African Humid Period (deMenocal et al. (2000) and references therein) represents the most recent occurrence of this average northerly movement of the ITCZ and is reflected in our data (Figure 3.5).

The sediments used in this study, however, do not necessarily record a (boreal) summer driven change in precipitation over equatorial eastern Africa. To date, rainfall in the catchment areas of rivers providing the terrigenous sediments to our core sites predominantly occurs during (boreal) winter (Figure 3.1). There is very limited rainfall in the catchments of the Rovuma and Rufiji rivers during (boreal)

summer. There are two possible mechanisms to explain an increase in rainfall during winter. It is possible that enhanced sea surface temperatures in the nearby Indian Ocean entailed higher evaporation, picked up by surface winds travelling the area. The increased moisture supply would have resulted in enhanced rainfall. The increased sea surface temperatures during the final stages of Termination 1 and the early Holocene in a nearby site from the equatorial western Indian Ocean (Kiefer et al.; 2006) support this model. Alternatively, the entire ITCZ related flow (winter and summer) may have shifted northward with the boreal winter position of ITCZ residing closer to our sites. In combination with a possibly prolonged positioning near the cores used in this study, rainfall would have increased in eastern Africa and the enhanced sediment supply recorded in the sediments off Tanzania. Whilst it is difficult to determine the timing of shifts in the location of the ITCZ at a seasonal scale, available data from a site off the Zambezi river indeed suggest a shift in the early Holocene positioning of the ITCZ during winter (Van Der Lubbe et al.; 2016). These data show enhanced contribution to the lithic fraction originating north of the Zambezi river, suggesting an increased runoff near the new sites used in this study. More data are required to determine the relative importance of either scenario in relation to enhanced runoff recorded in our sites.

Speleothem records from the Sanbao cave in continental China provide valuable insights about changes in the Asian monsoon system (Cheng et al.; 2016). At the millennial-scale these data demonstrate a direct relation with short-term climate change in the polar northern hemisphere. They also show variation in the Asian monsoon at the orbital time-scale. Compared to our data, there is some similarity between the log(Ti/Ca) data and the Chinese speleothem record from the Sanbao cave (Figure 3.4), but there are also important differences. For instance, we see smoother transitions between wet and dry phases in our data compared to the Chinese cave data. To better assess the importance of these differences we compare both our data and the Sanbao cave data with a recently published cave record from

Borneo at 4°N (Figure 3.4). Changes at this site reflect equatorial rainfall in the region close to the Pacific warm pool (Carolin et al.; 2016). To assess the main drivers of climate variability in the different areas, insolation changes have been added to Figure 3.4. In line with Carolin et al. (2016), we use insolation changes at 4°N for the Borneo speleothem record. Similarly, the insolation record of 65°N is added the Chinese Sanbao record following Cheng et al. (2016). In relation to our new data, we tested several scenarios using different insolation records for northern and southern hemisphere latitudes in relation to driving variations in log(Ti/Ca) time-series. The closest resemblance between insolation and elemental data emerged when using insolation changes at 4°N.

Considering the controls of equatorial climate change in the western Pacific and western Indian Oceans, the similarity between our log(Ti/Ca) data and the Borneo cave data substantiates the thought that rainfall in these regions is much more closely related to changes in near-equatorial insolation. Contrastingly, the Chinese Cave record shows a closer affinity to insolation changes further north (Wang et al.; 2001; Cheng et al.; 2016). Figure 3.4 also shows that the Borneo speleothem record of Carolin et al. (2016) and the log(Ti/Ca) data of cores 64PE304-8 and 64PE303-34 are in much better agreement (in particular in the well dated core 64PE303-34) than either record is with the Sanbao cave data from China (Figure 3.4). The relationship is less robust in the low-resolution sections of core 64PE304-8 due to the limited age control in this section of the core. The differences between the Chinese cave record and the time-series from near equatorial locations are most prominent in relation to MIS 5. Whilst the transitions towards warm intervals within MIS 5 are recorded as sharp transitions in continental China. In particular during Termination 2 and the onset of MIS 5.3, both tropical sites show much smoother transitions (Figure 3.4). The co-occurrence of a similar type of long-term climate change pattern near the equator occurring in both the equatorial western Pacific and western Indian

Oceans confirm an equatorial type climate change pattern that is distinctly different from change further north. We can only speculate why equatorial areas show smoother long-term transitions. Both equatorial sites are located near areas of trade wind driven westward transport of warm surface water. These areas were affected by long-term climate changes, but in a less dramatic fashion compared to for example more northerly areas (e.g. Cheng et al. 2016; Clark et al. 2012). This scenario entails that equatorial regions would for example not record a switch between different types of ocean currents, but rather reflect changes within the same current system. As a result, the likely smoother transitions between different climate states would have also affected the moisture supply to both equatorial sites, leading to more gradual climate change records.

3.6.3 Millennial-scale climate change in eastern Africa

In order to assess the millennial-scale variability in the new deep-sea cores, we have placed the data in the context of ice core records from both Greenland and Antarctica (Figure 3.5). In most cases the millennial-scale variability in the log(Ti/Ca) records of 64PE303-16 and 64PE303-15 are similar to the shape of millennial-scale shifts recorded in Greenland ice temperature records (Figure 3.5). Predominantly abrupt increases in log(Ti/Ca) values are followed by more gradual decreases closely resembling the succession of DO and Heinrich event variability on Greenland (Figure 3.5). A particularly striking feature of the short-term variability of log(Ti/Ca) in cores 64PE303-16 and 64PE303-15 is the relationship between the occurrence of Heinrich events in the North Atlantic and intervals of low log(Ti/Ca) values. The Younger Dryas and Heinrich events 1, 2, 4, 5 and 5a exhibit this relationship most clearly. The relationship is less clear for Heinrich events 3 and 6. There are some notable intervals of low log(Ti/Ca) values unrelated to Heinrich events, most likely affiliated with strong stadial events. In-depth assessment of the entire suite of DO

cycles requires a consistently higher resolution than that present in our sediment sequences and is therefore beyond the scope of this work.

The millennial-scale variability of the log(Ti/Ca) data show that the evaporation/precipitation balance in the Rovuma and Rufiji river catchments varied in relation to millennial-scale climate change (Figure 3.5). Low log(Ti/Ca) values during Heinrich events suggest reduced rainfall in the Rovuma and Rufiji river catchments. Findings based on sediments from the Arabian Sea off Somalia also point to dry conditions prevailing during Heinrich events (Ivanochko et al.; 2005). In order to assess the wider implications of our new data, we also compare the new findings with previously published data from core 64PE304-80 (18°S 37°E, 1329m water depth), reflecting the terrigenous input from the Zambezi river catchment (van Der Lubbe et al.; 2014). Within the accuracy of the age models the new data from cores 64PE303-16 and 64PE303-15 display opposing changes to those seen in core 64PE304-80. The low log(Ti/Ca) values generally prevailing during Heinrich events at 9°S (Figure 3.5) support the view of dry conditions in the Rovuma and Rufiji river catchments co-occurring with North Atlantic cold spells, in line with previous findings (Brown et al.; 2007; Tierney et al.; 2008). Analogous to the conclusions drawn regarding the long-term change the data support the idea of a southward shift in the boreal winter ITCZ during Heinrich events. The sites at 9°S would record dry conditions whereas in core 64PE304-80 further south, a wetting is recorded reflecting increased rainfall over the Zambezi river catchment. Hence, both sets of observations are consistent, implying large-scale southward movement of the ITCZ during Heinrich events and placing the "hinge-zone" (in the sense of Tierney et al. 2010) somewhere between ∼9°S and 18°S over eastern Africa at this time.

The new data also imply strong manifestations of more distant Heinrich events. Similar to the climate change in equatorial eastern Africa during Heinrich event 1,

Figure 3.4 shows very low log(Ti/Ca) data in cores 64PE304-8 and 64PE303-34 during Heinrich event 11, which occurred near/at the onset of Termination 2. The data suggest that a significant aridification event affected the Rovuma and Rufiji river catchments, more intense than during Heinrich event 1. This points towards a particularly strong southward shift of the ITCZ during Heinrich event 11/Termination 2 as seen in the Pacific region (Jacobel et al.; 2016). The log(Ti/Ca) data in Figure 3.4 also displays variability near/ at Heinrich events 7-10 and 12. The nature of the relation with the North Atlantic cold spells is less clear for these events. In some cases, e.g. Heinrich event 10 and Heinrich event 12, the timing of troughs in the log(Ti/Ca) data coincide with the North Atlantic climate events. With regard to the Heinrich events 7-9, either the timing of the log(Ti/Ca) change does not coincide with occurrence of its North Atlantic counterpart, or there is no change in our record (Figure 3.4). It is currently difficult to explain this mismatch. It is probably a combination of uncertainties in our age model, partly being based on very low resolution oxygen isotope time-series during this interval, and variations in sedimentation rate.

3.6.4 Interruption of long-term patterns by abrupt events

Despite uncertainties of the relationship between short-term changes in our log(Ti/Ca) data and Heinrich events in poorly dated sediment sections, the robust relation of aridification events in the Rovuma and Rufiji river catchments with North Atlantic cold spells in well dated sections of our cores allows more fundamental conclusions as to the relation of short- and long-term climate change in the region. The overall similarity in shape of the long-term change in our log(Ti/Ca) compared to the insolation forcing at 4°N (Figure 3.4) clearly suggests a rather direct response of the evaporation-precipitation balance in the region to near equatorial insolation

change. Short-term changes in the log(Ti/Ca) data related to Heinrich events appear "stamped" onto the long-term change, suggesting that the influence of precession was overridden at these times. This relationship is most pronounced when associated with glacial Terminations (Heinrich event 1 and Heinrich event 11 for Terminations 1 and 2, respectively). This is probably due a sensitivity of the location of the ITCZ to massive ice discharge events occurring at maximum ice volume sizes (McGee et al.; 2014; Broccoli et al.; 2006; Chiang and Bitz; 2005). It is interesting to note that the speleothem based oxygen isotope data from Borneo (Figure 3.4) appear to show a similar feature during Heinrich event 1 and Heinrich event 11 (Carolin et al.; 2016). The similarity of climate change pattern in the equatorial western Indian and western Pacific Oceans suggests that the aforementioned sensitivity of the location of the ITCZ to massive ice discharge events in the North Atlantic is not limited to the Indian Ocean.

3.7 Conclusions

The log(Ti/Ca) data presented for marine sediment cores 64PE304-8, 64PE303-34, 64PE303-16 and 64PE303-15 offshore Tanzania reflect changes in eastern African climate, both at the orbital and the millennial-scale. The long-term change recorded off Tanzania resembles orbitally driven climate change recorded near the Pacific warm pool (Carolin et al.; 2016). Both equatorial sites also imply a smoother transition between different climate states compared to Chinese speleothem data further north, in particular during MIS 5. These observations suggest that a dampening mechanism acts in equatorial regions, resulting in gradual records of major climate transitions.

Our data also imply a close relation of eastern African climate change with rapid variations in northern hemisphere temperatures at the millennial-scale. During Heinrich events, dry conditions prevailed in the catchments of the Rovuma and

Rufiji rivers, in line with observations from the Arabian Sea. In contrast, further south, off the Zambezi river, wetter conditions are reported, placing the "hinge zone" (in the sense of Tierney et al. 2010) somewhere between 9°S and 18°S.

Bibliography

Altabet, M. A., Higginson, M. J. and Murray, D. W. (2002). The effect of millennial-scale changes in Arabian Sea denitrification on atmospheric CO_2, *Nature* **415**(6868): 159–162.

Andersen, K. K., Svensson, A., Johnsen, S. J., Rasmussen, S. O., Bigler, M., Röthlisberger, R., Ruth, U., Siggaard-Andersen, M. L., Peder Steffensen, J., Dahl-Jensen, D., Vinther, B. M. and Clausen, H. B. (2006). The Greenland Ice Core Chronology 2005, 15-42 ka. Part 1: constructing the time scale, *Quaternary Science Reviews* **25**(23-24): 3246–3257.

Barbante, C., Barnola, J., Becagli, S., Beer, J., Bigler, M., Boutron, C., Blunier, T., Castellano, E., Cattani, O., Chappellaz, J., Dahl-Jensen, D., Debret, M., Delmonte, B., Dick, D., Falourd, S., Faria, S., Federer, U., Fischer, H., Freitag, J., Frenzel, A., Fritzsche, D., Fundel, F., Gabrielli, P., Gaspari, V., Gersonde, R., Graf, W., Grigoriev, D., Hamann, I., Hansson, M., Hoffmann, G., Hutterli, M. a., Huybrechts, P., Isaksson, E., Johnsen, S., Jouzel, J., Kaczmarska, M., Karlin, T., Kaufmann, P., Kipfstuhl, S., Kohno, M., Lambert, F., Lambrecht, A., Lambrecht, A., Landais, A., Lawer, G., Leuenberger, M., Littot, G., Loulergue, L., Lüthi, D., Maggi, V., Marino, F., Masson-Delmotte, V., Meyer, H., Miller, H., Mulvaney, R., Narcisi, B., Oerlemans, J., Oerter, H., Parrenin, F., Petit, J. R., Raisbeck, G., Raynaud, D., Röthlisberger, R., Ruth, U., Rybak, O., Severi, M., Schmitt, J., Schwander, J., Siegenthaler, U., Siggaard-Andersen, M.-L., Spahni, R., Steffensen, J., Stenni, B., Stocker, T., Tison, J.-L., Traversi, R., Udisti, R., Valero-Delgado, F., van den

Broeke, M. R., van de Wal, R. S. W., Wagenbach, D., Wegner, A., Weiler, K., Wilhelms, F., Winther, J.-G. and Wolff, E. W. (2006). One-to-one coupling of glacial climate variability in Greenland and Antarctica, *Nature* **444**(7116): 195–198.

Barker, P. A., Talbot, M. R., Street-Perrott, F. A., Marret, F., Scourse, J. and Odada, E. O. (2004). Late Quaternary climatic variability in intertropical Africa, *Past Climate Variability through Europe and Africa*, pp. 117–138.

Blunier, T. and Brook, E. J. (2001). Timing of Millennial-Scale climate change in Antartica and Greenland during the last glacial period, *Science* **291**(2001): 109–112.

Blunier, T., Chappellaz, J., Schwander, J., Clausen, H., Hammer, C. U. and Johnsen, S. (1998). Asynchrony of Antarctic and Greenland climate change during the last glacial period, *Nature* **349**: 739–743.

Broccoli, A. J., Dahl, K. A. and Stouffer, R. J. (2006). Response of the ITCZ to Northern Hemisphere cooling, *Geophysical Research Letters* **33**(1).

Brown, E. T., Johnson, T. C., Scholz, C. a., Cohen, a. S. and King, J. W. (2007). Abrupt change in tropical African climate linked to the bipolar seesaw over the past 55,000 years, *Geophysical Research Letters* **34**(20): 1–5.

Brummer, G. and Jung, S. (2009). RV Pelagia Cruise Report : Cruise 64PE304 SE African margin ,.

Carolin, S. A., Cobb, K. M., Adkins, J. F., Clark, B., Conroy, J. L., Lejau, S., Malang, J. and Tuen, A. A. (2013). Varied Response of Western Pacific Hydrology to Climate Forcings over the Last Glacial Period, *Science* **340**(6140): 1564–1566.

Carolin, S. A., Cobb, K. M., Lynch-Stieglitz, J., Moerman, J. W., Partin, J. W., Lejau, S., Malang, J., Clark, B., Tuen, A. A. and Adkins, J. F. (2016). Northern Borneo

stalagmite records reveal West Pacific hydroclimate across MIS 5 and 6, *Earth and Planetary Science Letters* **439**: 182–193.

Cheng, H., Edwards, R. L., Broecker, W. S., Denton, G. H., Kong, X., Wang, Y., Zhang, R. and Wang, X. (2009). Ice Age Terminations, *Science* **326**(5950): 248–252.

Cheng, H., Edwards, R. L., Sinha, A., Spötl, C., Yi, L., Chen, S., Kelly, M., Kathayat, G., Wang, X., Li, X., Kong, X., Wang, Y., Ning, Y. and Zhang, H. (2016). The Asian monsoon over the past 640,000 years and ice age terminations, *Nature* **534**(7609): 640–646.

Chiang, J. C. H. and Bitz, C. M. (2005). Influence of high latitude ice cover on the marine Intertropical Convergence Zone, *Climate Dynamics* **25**(5): 477–496.

Clark, P. U., Shakun, J. D., Baker, P. a., Bartlein, P. J., Brewer, S., Brook, E., Carlson, A. E., Cheng, H., Kaufman, D. S., Liu, Z., Marchitto, T. M., Mix, A. C., Morrill, C., Otto-Bliesner, B. L., Pahnke, K., Russell, J. M., Whitlock, C., Adkins, J., Blois, J. L., Clark, J., Colman, S. M., Curry, W. B., Flower, B. P., He, F., Johnson, T. C., Lynch-Stieglitz, J., Markgraf, V., McManus, J., Mitrovica, J. X., Moreno, P. I. and Williams, J. W. (2012). Global climate evolution during the last deglaciation., *Proceedings of the National Academy of Sciences of the United States of America* **109**(19): E1134—-42.

Davis, B. a. S. and Brewer, S. (2008). Orbital forcing and role of the latitudinal insolation/temperature gradient, *Climate Dynamics* **32**(2-3): 143–165.

deMenocal, P. B. (1995). Plio-pleistocene african climate, *Science* **270**(5233): 53–59.

deMenocal, P., Ortiz, J., Guilderson, T., Adkins, J., Sarnthein, M., Baker, L. and Yarusinsky, M. (2000). Abrupt onset and termination of the african humid period: rapid climate responses to gradual insolation forcing, *Quaternary Science Reviews* **19**(15): 347 – 361.

Govin, A., Holzwarth, U., Heslop, D., Ford Keeling, L., Zabel, M., Mulitza, S., Collins, J. A. and Chiessi, C. M. (2012). Distribution of major elements in Atlantic surface sediments (36°N-49°S): Imprint of terrigenous input and continental weathering, *Geochemistry, Geophysics, Geosystems* **13**(1).

Grootes, P. M., Stuiver, M., White, J. W. C., Johnsen, S. and Jouzel, J. (1993). Comparison of oxygen isotope records from the GISP2 and GRIP Greenland ice cores, *Nature* **366**(6455): 552–554.

Hennekam, R. and de Lange, G. (2012). X-ray fluorescence core scanning of wet marine sediments: methods to improve quality and reproducibility of high-resolution paleoenvironmental records, *Limnology and Oceanography: Methods* **10**: 991–1003.

Ivanochko, T. S., Ganeshram, R. S., Brummer, G. J. A., Ganssen, G., Jung, S. J. A., Moreton, S. G. and Kroon, D. (2005). Variations in tropical convection as an amplifier of global climate change at the millennial scale, *Earth and Planetary Science Letters* **235**(1-2): 302–314.

Jacobel, A. W., McManus, J. F., Anderson, R. F. and Winckler, G. (2016). Large deglacial shifts of the Pacific Intertropical Convergence Zone, *Nature Communications* **7**: 10449.

Jiménez-Amat, P. and Zahn, R. (2015). Offset timing of climate oscillations during the last two glacial-interglacial transitions connected with large-scale freshwater perturbation, *Paleoceanography* **30**(6): 768–788.

Johnsen, S. J., Dansgaard, W., Clausen, H. B. and Langway, C. C. (1972). Oxygen Isotope Profiles through the Antarctic and Greenland Ice Sheets, *Nature* **235**(5339): 429–434.

Jung, S. J. A., Davies, G. R., Ganssen, G. M. and Kroon, D. (2004). Stepwise Holocene aridification in NE Africa deduced from dust-borne radiogenic isotope records, *Earth and Planetary Science Letters* **221**(1-4): 27–37.

Kiefer, T., McCave, I. N. and Elderfield, H. (2006). Antarctic control on tropical Indian Ocean sea surface temperature and hydrography, *Geophysical Research Letters* **33**(24).

Kroon, D. and Party, S. (2010). Tropical Temperature History during Paleogene GLObal Warming (GLOW) Events, NIOZ site survey cruise report (RV Pelagia cruise number 64PE303), *NIOZ Site* pp. 1–59.

Lisiecki, L. E. and Stern, J. V. (2016). Regional and global benthic $\delta^{18}O$ stacks for the last glacial cycle, *Paleoceanography* **31**(10): 1368–1394.

Lubbe, J. V. D., Tjallingii, R., Castañeda, I. S., Brummer, G., Kroon, D. and Jung, S. (2011). Major reorganization in the transport pathway of Zambezi River sediments along and across the Mozambique Shelf during the last glacial-interglacial transition, *Geophysical Research Abstracts* **13**: 8855.

McGee, D., Donohoe, A., Marshall, J. and Ferreira, D. (2014). Changes in ITCZ location and cross-equatorial heat transport at the Last Glacial Maximum, Heinrich Stadial 1, and the mid-Holocene, *Earth and Planetary Science Letters* **390**: 69–79.

Naidu, P. D., Singh, A. D., Ganeshram, R. and Bharti, S. K. (2014). Abrupt climate-induced changes in carbonate burial in the Arabian Sea: Causes and consequences, *Geochemistry, Geophysics, Geosystems* **15**(4): 1398–1406.

Paillard, D., Labeyrie, L. and Yiou, P. (1996). Analyseries, Macintosh program performs time-series analysis, Eos Trans. AGU, 77: 379.

Partin, J. W., Cobb, K. M., Adkins, J. F., Clark, B. and Fernandez, D. P. (2007). Millennial-scale trends in west Pacific warm pool hydrology since the Last Glacial Maximum, *Nature* **449**(7161): 452–455.

Prell, W. L. and Kutzbach, J. E. (1987). Monsoon variability over the past 150,000 years, *Journal of Geophysical Research* **92**(D7): 8411.

Rasmussen, S. O., Seierstad, I. K., Andersen, K. K., Bigler, M., Dahl-Jensen, D. and Johnsen, S. J. (2008). Synchronization of the NGRIP, GRIP, and GISP2 ice cores across MIS 2 and palaeoclimatic implications, *Quaternary Science Reviews* **27**(1-2): 18–28.

Revel, M., Ducassou, E., Skonieczny, C., Colin, C., Bastian, L., Bosch, D., Migeon, S. and Mascle, J. (2015). 20,000 years of Nile River dynamics and environmental changes in the Nile catchment area as inferred from Nile upper continental slope sediments, *Quaternary Science Reviews* **130**: 200–221.

Romahn, S., Mackensen, a., Groeneveld, J. and Pätzold, J. (2013). Deglacial intermediate water reorganization: new evidence from the Indian Ocean, *Climate of the Past Discussions* **9**(4): 4035–4063.

Schneider, T., Bischoff, T. and Haug, G. H. (2014). Migrations and dynamics of the intertropical convergence zone, *Nature* **513**(7516): 45–53.

Schulz, M. (2002). On the 1470-year pacing of Dansgaard-Oeschger warm events, *Paleoceanography* **17**(2).

Tierney, J. E., Russell, J. M. and Huang, Y. (2010). A molecular perspective on Late Quaternary climate and vegetation change in the Lake Tanganyika basin, East Africa, *Quaternary Science Reviews* **29**(5): 787–800.

Tierney, J. E., Russell, J. M., Huang, Y., Damsté, J. S. S., Hopmans, E. C. and Cohen, A. S. (2008). Northern Hemisphere Controls on Tropical Southeast African Climate During the Past 60,000 Years, *Science* **322**(5899): 252 LP – 255.

Tjallingii, R., Röhl, U., Kölling, M. and Bickert, T. (2007). Influence of the water content on X-ray fluorescence corescanning measurements in soft marine sediments, *Geochemistry, Geophysics, Geosystems* **8**(2).

Trauth, M. H., Deino, A. L., Bergner, A. G. and Strecker, M. R. (2003). East Africam climate change and orbital forcing during the last 175 kyr BP, *Earth and Planetary Science Letters* **206**(3-4): 297–313.

Trauth, M. H., Sarnthein, M. and Arnold, M. (1997). Bioturbational mixing depth and carbon flux at the seafloor, *Paleoceanography* **12**(3): 517–526.

Van Der Lubbe, H. J., Frank, M., Tjallingii, R. and Schneider, R. R. (2016). Neodymium isotope constraints on provenance, dispersal, and climate-driven supply of Zambezi sediments along the Mozambique Margin during the past 45,000 years, *Geochemistry, Geophysics, Geosystems* **17**(1): 181–198.

van Der Lubbe, J. H., Tjallingii, R., Prins, M. A., Brummer, G.-J. A., Jung, S. J. A., Kroon, D. and Schneider, R. R. (2014). Sedimentation patterns off the Zambezi River over the last 20,000 years, *Marine Geology* **355**: 189–201.

Verschuren, D., Sinninghe Damsté, J. S., Moernaut, J., Kristen, I., Blaauw, M., Fagot, M. and Haug, G. H. (2009). Half-precessional dynamics of monsoon rainfall near the East African Equator., *Nature* **462**(7273): 637–641.

Vinther, B. M., Clausen, H. B., Johnsen, S. J., Rasmussen, S. O., Andersen, K. K., Buchardt, S. L., Dahl-Jensen, D., Seierstad, I. K., Siggaard-Andersen, M. L., Steffensen, J. P., Svensson, A., Olsen, J. and Heinemeier, J. (2006). A synchronized dating of three Greenland ice cores throughout the Holocene, *Journal of Geophysical Research Atmospheres* **111**(13).

Wang, Y. J., Cheng, H., Edwards, R. L., An, Z. S., Wu, J. Y., Shen, C. C. and Dorale, J. a. (2001). A high-resolution absolute-dated late Pleistocene Monsoon record from Hulu Cave, China., *Science (New York, N.Y.)* **294**(5550): 2345–2348.

Weltje, G. J. and Tjallingii, R. (2008). Calibration of XRF core scanners for quantitative geochemical logging of sediment cores: Theory and application, *Earth and Planetary Science Letters* **274**(3-4): 423–438.

Ziegler, M., Diz, P., Hall, I. R. and Zahn, R. (2013). Millennial-scale changes in atmospheric CO_2 levels linked to the Southern Ocean carbon isotope gradient and dust flux, *Nature Geoscience* **6**: 457–461.

Chapter 4

Planktonic and benthic $\delta^{18}O$ records in a depth transect offshore Tanzania show large time offsets revealing global climate linkages during the last glacial-deglaciation period

4.1 Introduction

The $\delta^{18}O$ of fossil foraminifera is a useful tool for assessing changing oceanic conditions due to its co-variance with temperature and global ice volume (Emiliani; 1955; Shackleton; 1967). This chapter describes and interprets new $\delta^{18}O$ records from three cores. The cores were retrieved from the sea bed offshore Tanzania at various depths constituting a depth transect (Kroon and Party; 2010; Brummer and Jung; 2009). The depth transect approach allows reconstruction of sea surface and

deep water conditions. The new $\delta^{18}O$ time-series based on planktonic and benthic foraminiferal species are used to quantify time offsets between $\delta^{18}O$ records within an individual core and between cores. The time offsets between $\delta^{18}O$ records serve as evidence of global climate influences on the surface and deep waters offshore Tanzania.

4.1.1 Modern Oceanography

The Indian Ocean is an important part of the global ocean circulation system. It differs from the Atlantic and Pacific in that it is completely bounded to the north by the Eurasian continental landmass. This has implications for its surface and subsurface circulation.

Surface layer circulation

The south equatorial current (SEC) arrives westwards across the Indian Ocean (Schott et al.; 2002). The SEC splits into two at the east coast of Madagascar ($\sim$15°S) to form two western boundary currents, the North-East Madagascar Current (NEMC) and the South-East Madagascar Current (SEMC). The NEMC flows into the East African Coastal Current (EACC) which is the primary surface current at the core locations used here (Figure 2.1). North of $\sim$5°S the seasonally reversing winds control surface currents and result in strong seasonal upwelling at $\sim$4°N. To the south of our cores site (9°S), surface waters advect to the Atlantic supplying heat and salt to the South Atlantic (Gordon et al.; 1992), which eventually contribute to the formation of North Atlantic Deep Water (NADW). The regional average SST is $\sim$27.6°C (Fallet et al.; 2011) with a range of 25.5 to 28.7°C (Locarnini et al.; 2013).

Sub-surface circulation

Multiple sources contribute to the intermediate waters in the region. You (1998) reported intermediate waters along the western boundary at 5°N to be composed

of 20% Antarctic Intermediate Water (AAIW), 70% Red Sea water and 10% Indonesian intermediate waters. AAIW – characterised by a salinity minimum (<34.7 psu) – flows northwards, from its formation region at the Sub-Antarctic Front (SAF; 45-55°S; Sloyan and Rintoul 2001; Hartin et al. 2011, 2014). The subduction of AAIW at the SAF is influenced by air-sea exchanges and wind strength (Ribbe; 2001). The AAIW in the study region is thought to enter the Indian Ocean in the southwest (Fine et al.; 2008). AAIW and Sub-Antarctic Mode Water (SAMW; which forms between the subantarctic and subtropical fronts by vertical convection during winter; McCartney 1982; Sarmiento et al. 2004) are upwelled in the open ocean between 5-10°S due to Ekman upwelling associated with the northern boundary of the south-east trade winds Schott and McCreary (2001). The regional bathymetry controls the deep circulation of the western Indian Ocean. The main feature of this flow is the northward flowing Circumpolar Deep Water (CDW) which penetrats north into the Somali basin (Toole and Warren; 1993; Warren; 1978; Wilson et al.; 2012). Near the northern limit of the Mascarene basin, the shallower portion of this water mass meets southwards flowing Indian deep water (IDW), which is essentially recirculated CDW (Johnson et al.; 1998) with an enriched nutrient content (You; 1997).

4.1.2 Past changes in regional oceanography

Long-term climate change in the wider Indian Ocean region correlates to global climate change associated with glacial-interglacial cyclicity forced by changes in insolation (Saraswat et al.; 2005; Kiefer et al.; 2006; Leuschner and Sirocko; 2003). Summer monsoonal circulation was weaker during the last glacial period (Sirocko et al.; 1996), although the winter monsoon may have been stronger than today (Duplessy; 1982; An et al.; 2011). The sensitivity of the monsoon to insolation changes leads to variability associated with Earth's orbital precession, with a periodicity of 19 to 23kyr.

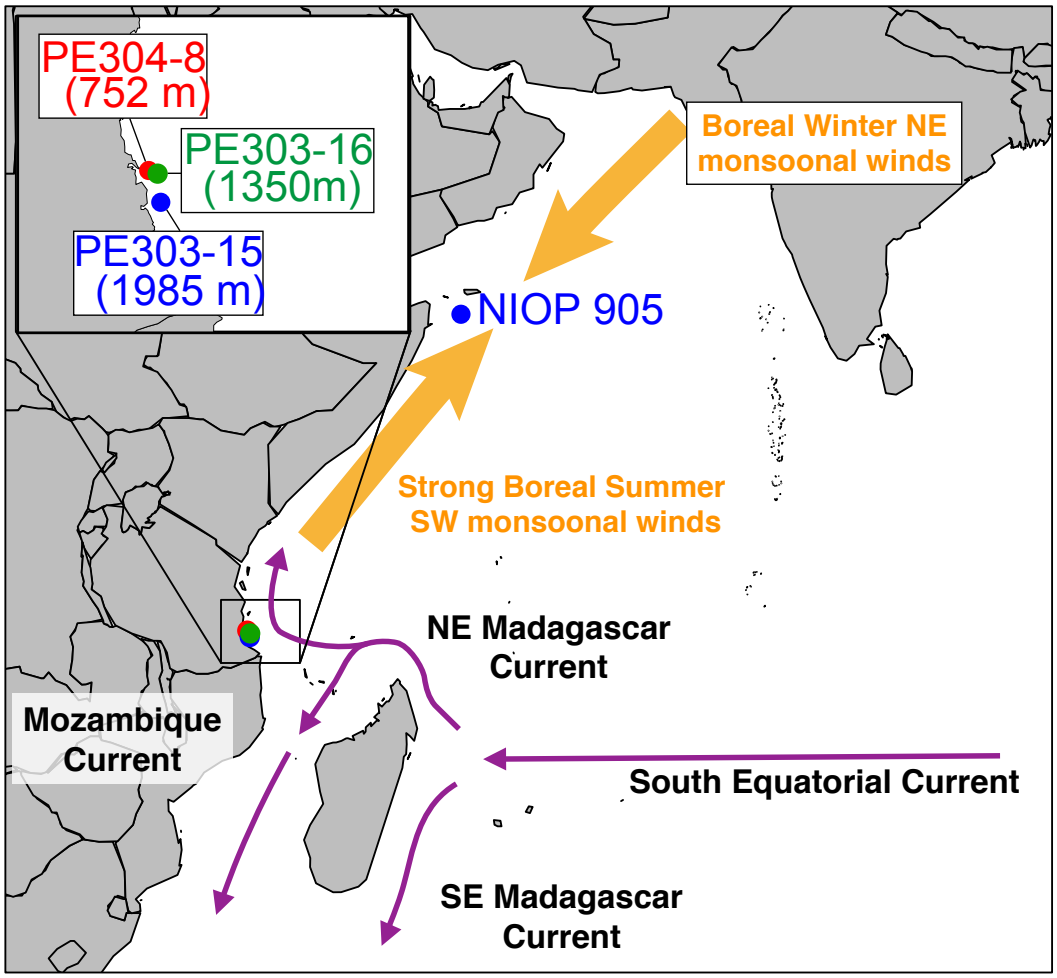

FIGURE 4.1: Map showing location of cores presented and referred to in this chapter. Also schematic representation of surface ocean currents and monsoonal wind flows.

Superimposed onto these long-term cycles, is shorter term variability on the millennial-scale that dominated climate during the last glacial period. The so called Dansgaard-Oeschger (DO) cycles represent recurrent and rapid temperature spikes over Greenland during the last glacial period (Dansgaard et al.; 1984). Embedded in this short-term variability are repeated occurrences of layers of North Atlantic sediment with increased ice-rafted debris (IRD) deposited during maximum cold conditions in the region (Heinrich; 1988; Broecker et al.; 1992). These events are termed Heinrich events. Meltwater events associated with ice-rafted debris (IRD) deposition led to reduced NADW formation (Sarnthein et al.; 1994; Jung; 1996; Elliot et al.; 2002). Given that NADW is one of the most significant water masses of the deep ocean, this variability had implications for ocean circulation and climate globally.

Sediment based records of Arabian sea surface conditions document millennial-scale changes in monsoon strength, and show strong teleconnections with Greenland's climate (Altabet et al.; 2002; Singh et al.; 2011; Schulz; 1998; Jung et al.; 2009; Ivanochko et al.; 2005; Altabet et al.; 2002; Deplazes et al.; 2014; Mohtadi et al.; 2014). South of the monsoon dominated region, surface conditions have been found to correlate with Antarctic climate change on the millennial-scale (Kiefer et al.; 2006).

In terms of intermediate ocean circulation changes in the region, sediment core records have shown changes related to southern sourced water masses, such as AAIW and SAMW, which indicate enhanced influence during the equivalent Heinrich events (Jung et al.; 2009; Romahn et al.; 2014) with some suggestion of a temperature signal carried from Antarctica i.e. warming during NH cold events (Jung and Kroon; 2011; Jung et al.; 2009). Similar evidence has also been documented in the southern Pacific Ocean (Pahnke and Zahn; 2005) and is supported by modelling work (Schmittner et al.; 2007). On the millennial time-scale, variations in intermediate water circulation may have played a crucial role in the so called bipolar seesaw (Böning and Bard; 2009; Kiefer et al.; 2006; Wang et al.; 2013; Romahn et al.; 2014;

Jung et al.; 2009).

4.2 Methods

4.2.1 Core locations

The data presented here are from three marine sediment cores 64PE304-8 (752m), 64PE303-16 (1350m) and 64PE303-15 (1985m) from offshore Tanzania in the western Indian Ocean (Figure 2.1). These cores were retrieved in 2009 using a Royal Netherlands Institute for Sea Research (NIOZ) designed piston corer onboard the *RV Pelagia* as part of the "Tropical Temperature History During Paleogene Global Warming Events" (GLOW; Kroon and Party 2010) and "Indian – Atlantic Exchange" (INATEX; Brummer and Jung 2009) cruises.

4.2.2 Sample preparation and isotope analyses

Marine sediment cores 64PE304-8, 64PE303-16 and 64PE303-15 were sampled at 1cm resolution. A series of initial cleaning steps helped remove the finest size fraction (<63μm) and make subsequent handling more convenient. Samples were first freeze-dried, then washed through a 63μm sieve and finally dried in an oven at $\sim$50°C for 2-3 days. Foraminifera specimens for stable isotope analyses were handpicked from the 255-350μm size fraction ($\sim$20 specimens of the planktonic species *G.ruber* and *N.dutertrei* and up to 15 specimens of the benthic species *C.wuellerstorfi* were picked). These species were selected to provide coverage of the water column. *G.ruber* dwells in the mixed layer, *N.dutertrei* inhabits mainly the thermocline and *C.wuellerstorfi* lives in deep water on top of the sediments (see introduction chapter for more discussion on species selection). Foraminifera samples were analysed for stable oxygen and carbon isotope ratios using a Thermo Electron Delta$^+$ Advantage stable isotope mass spectrometer coupled to a Kiel Carbonate III preparation device at the University of Edinburgh, school of Geosciences. The planktonic

specimens were powdered and a sub-sample used for each analysis. 2-3 benthic specimens were used for each analysis. Measured values are reported using standard δ-notation as compared to Vienna PeeDee Belemnite using laboratory standard NBS-19 (Coplen et al.; 1983). Analytical precision for both $\delta^{13}C$ and $\delta^{18}O$ was better than $\pm 0.1‰$.

4.2.3 Age model

The chronology of the sediment sequences used in this study is based on a multi-step approach. For full details see Methods chapter.

4.3 Results

4.3.1 Data versus depth; initial observations

The stable oxygen isotope records produced in this study are plotted against depth, in Figures 4.2, 4.3 & 4.4. The long-term pattern of all the oxygen isotope records presented here is dominated by a clear distinction between higher values during the last glacial period and lower values during the Holocene. The amplitude of change is about 1.5‰. This main transition occurs between ∼19ka (earliest onset) and ∼ 10ka when, broadly speaking, the records level out again. The exact timing and amplitude of change differs between species across this transition. Generally, the benthic $\delta^{18}O$ values are higher than the planktonic $\delta^{18}O$ values in all three cores, reflecting the deep-water temperatures and ambient $\delta^{18}O$ values of the deep water.

There are clear differences in terms of sedimentation rates between and within each core. This leads to expanded and condensed sections. This has a bearing on how well developed the short-term (millennial) scale change is in the records derived from these cores. Core 64PE304-8 (752m) displays an expanded Holocene and deglaciation throughout the uppermost 1.5m compared to the two deeper cores (64PE303-16 and 64PE303-15) where this period is represented by the uppermost

1m. However, the last glacial period is condensed into a comparatively shorter sediment section in core 64PE304-8.

4.3.2 *G.ruber* $\delta^{18}O$ during the deglaciation

The *G. ruber* $\delta^{18}O$ records of all three cores show an abrupt onset of termination at 16ka and display a single well developed plateau between 14-12ka (Figure 4.5A). Following a second abrupt step, the transition is complete by around 10ka. This pattern creates a two-step transition in the *G. ruber* $\delta^{18}O$ records of all three cores. We also see a reversal ($\sim$0.25‰) in the record of core 64PE303-16 centred on 12ka during the Younger Dryas equivalent period.

4.3.3 *N.dutertrei* $\delta^{18}O$ during the deglaciation

The *N.dutertrei* $\delta^{18}O$ records of the three cores show a less consistent pattern than *G.ruber*, although they maintain the same overall shape of the transition (fig 4.5B). The onset of termination in the *N. dutertrei* $\delta^{18}O$ record of core 64PE303-15 lags the other two cores by $\sim$1.9kyrs. The plateau/interruption of the transition at around 13ka is displayed differently in each core. It is well developed in core 64PE304-8, it shows a reversal in core 64PE303-16 and it is poorly developed in 64PE303-15. The core 64PE304-8 record shows a second plateau occurring from $\sim$10-8ka.

4.3.4 *C.wuellerstorfi* $\delta^{18}O$ during the deglaciation

Similar to the planktonic $\delta^{18}O$ records, the main observation of the benthic oxygen isotope records during the deglaciation, is the significant reduction in $\delta^{18}O$ during the deglaciation (-1.8‰ in 64PE304-8, -1.7‰ in 64PE303-16, and -2.0‰ in 64PE303-15). The onset of glacial termination occurs earliest in the benthic $\delta^{18}O$ record of core 64PE303-16, with a sharp increase at 18.4ka and subsequently shows a more gradual shift towards lighter values between 15-10ka (Figure 4.6). This pattern is

FIGURE 4.2: Data from core PE304-8 presented versus depth. A. Log(Ti/Ca). B. *G.ruber* oxygen isotope record. C. *N.dutertrei* oxygen isotope record. D. *C.wuellerstorfi* oxygen isotope record. Solid red triangles indicate depth of radiocarbon dated samples.

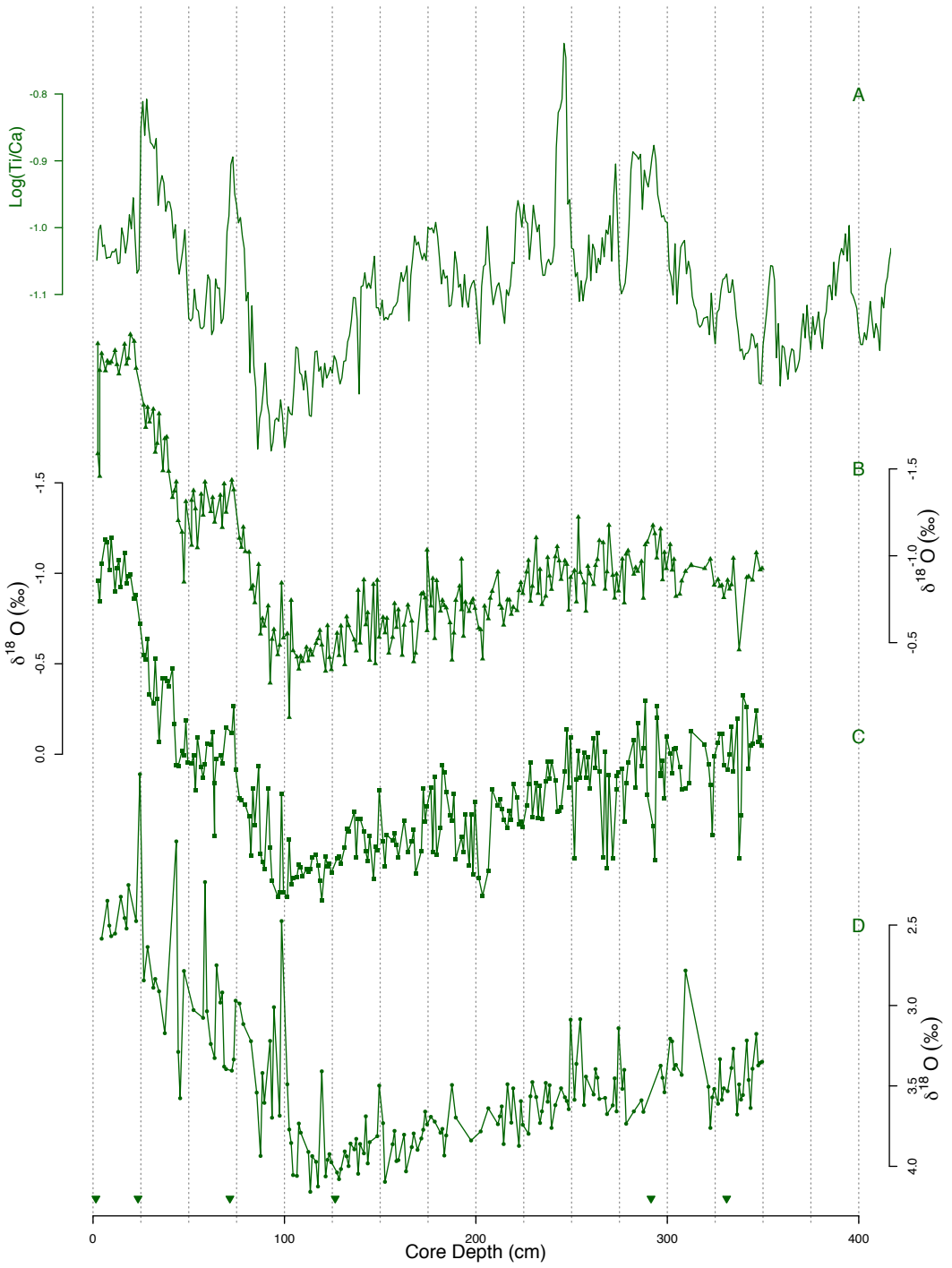

FIGURE 4.3: Data from core PE303-16 presented versus depth. A. Log(Ti/Ca). B. *G.ruber* oxygen isotope record. C. *N.dutertrei* oxygen isotope record. D. *C.wuellerstorfi* oxygen isotope record. Solid green triangles indicate depth of radiocarbon dated samples.

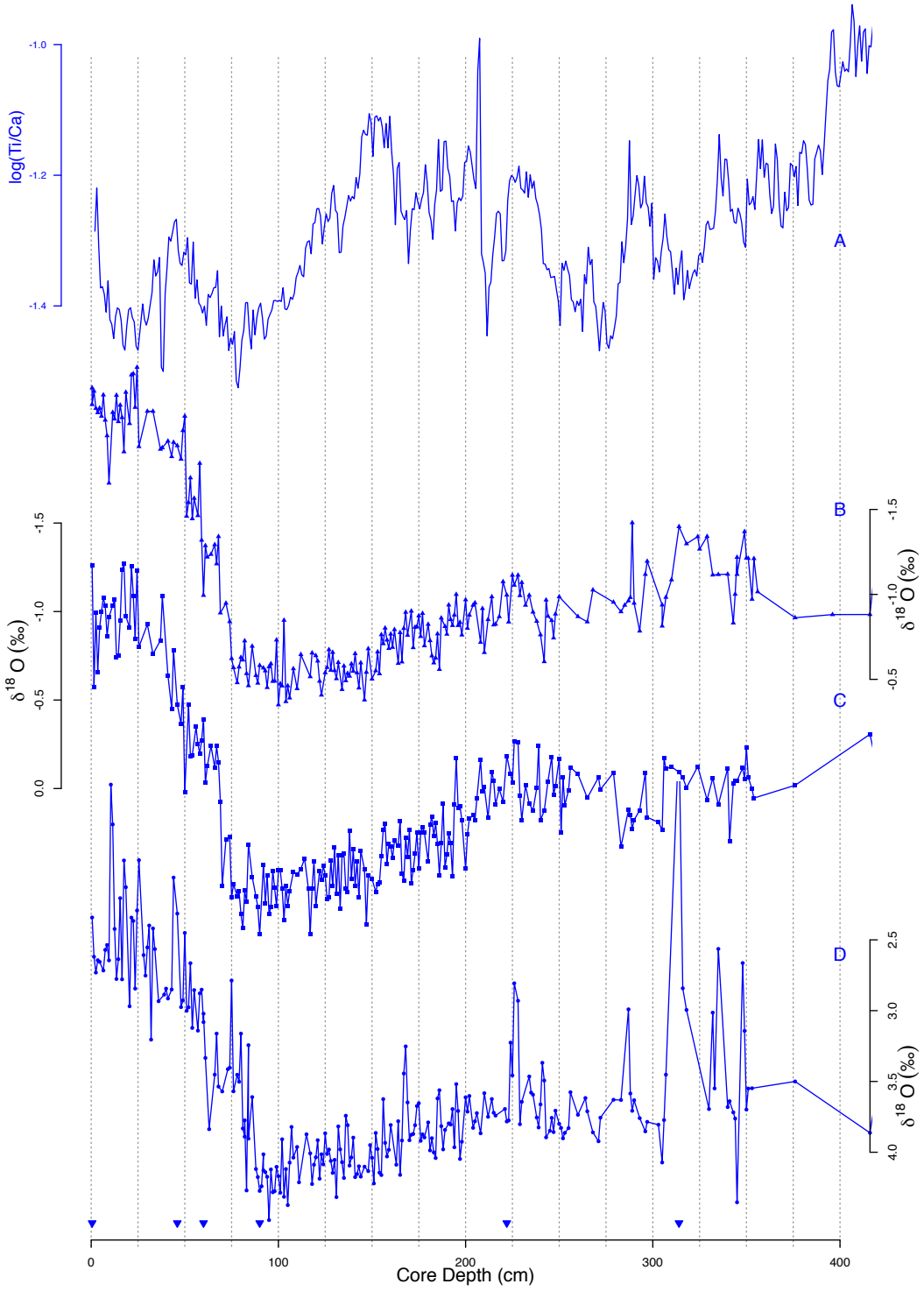

FIGURE 4.4: Data from core 64PE303-15 presented versus depth. A. Log(Ti/Ca). B. *G.ruber* oxygen isotope record. C. *N.dutertrei* oxygen isotope record. D. *C.wuellerstorfi* oxygen isotope record. Solid blue triangles indicate depth of radiocarbon dated samples.

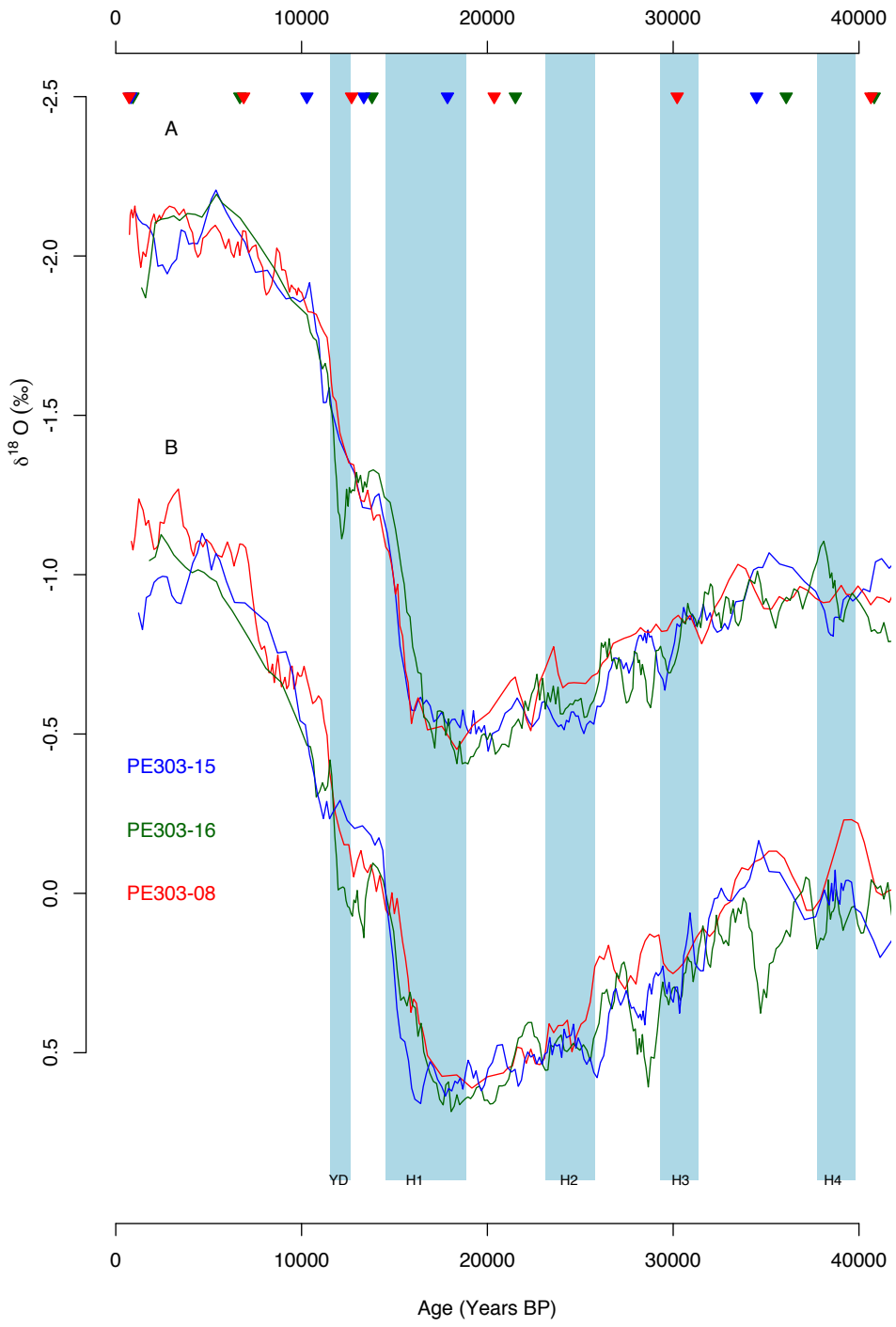

FIGURE 4.5: Oxygen isotope records of both planktonic foraminifera species used for cores 64PE304-8 (752m, red), 64PE303-16 (1350m, green) and 64PE303-15 (1985m, blue) on the same scale. A) Records of *G.ruber*, a surface dwelling species B) records of *N.dutertrei* a thermocline dwelling species. Radiocarbon dates for each core (same colour scheme) are plotted as solid triangles at top of plot. Vertical blue bars indicate the timing of North Atlantic cold events; the Younger Dryas and Heinrich events 1-5 (H1-5).

interrupted by four significant reversals at 16.2ka, 13.9ka, 11.8ka and 11.0ka. In core 64PE304-8 the transition does not begin until ∼17ka. There is also a notable reversal of ∼0.5‰ in the benthic $\delta^{18}O$ record of core 64PE304-8 centred on 14.5ka at the end of the period equivalent to Heinrich 1.

4.3.5 Millennial-scale variability during the glacial period

Millennial-scale variability in the order of 0.1-0.4‰ is displayed on all the records presented. It is worthwhile noting that in some sections (particularly the pre-termination section of core 64PE304-8) the sample resolution and sedimentation rate mean the millennial-scale variability is poorly developed. There is no obvious cyclicity in this variability. The variability shows good agreement across the three cores within each species, especially allowing for age model uncertainty. Although, there are some instances where the variability is clearly out of phase. For example at ∼36ka, where the core 64PE303-16 *N.dutertrei* record displays a clear increase whilst the cores 64PE304-8 and 64PE303-15 records show an opposing decrease (Figure 4.5B). The three records of *C. wuellerstorfi* oxygen isotope ratios show significant variability on the millennial time-scale with amplitudes of between 0.1-0.5‰ (Figure 4.6). There are some individual events of relatively greater amplitude, e.g. in the record of core 64PE303-16 during the equivalent of Heinrich event 4 and in the record of 64PE303-15 at approximately 35ka. However, there is no consistent pattern in terms of cyclicity or timing relative to the North Atlantic cold events.

4.3.6 Timing of surface versus thermocline change

Deglaciation

The shape of the transition is broadly similar between the *G.ruber* and *N.dutertrei* $\delta^{18}O$ records (Figure 4.7) . In all three cores, the termination begins earlier in the *N.dutertrei* $\delta^{18}O$ records than in the corresponding *G.ruber* $\delta^{18}O$ records (1.4kyr for

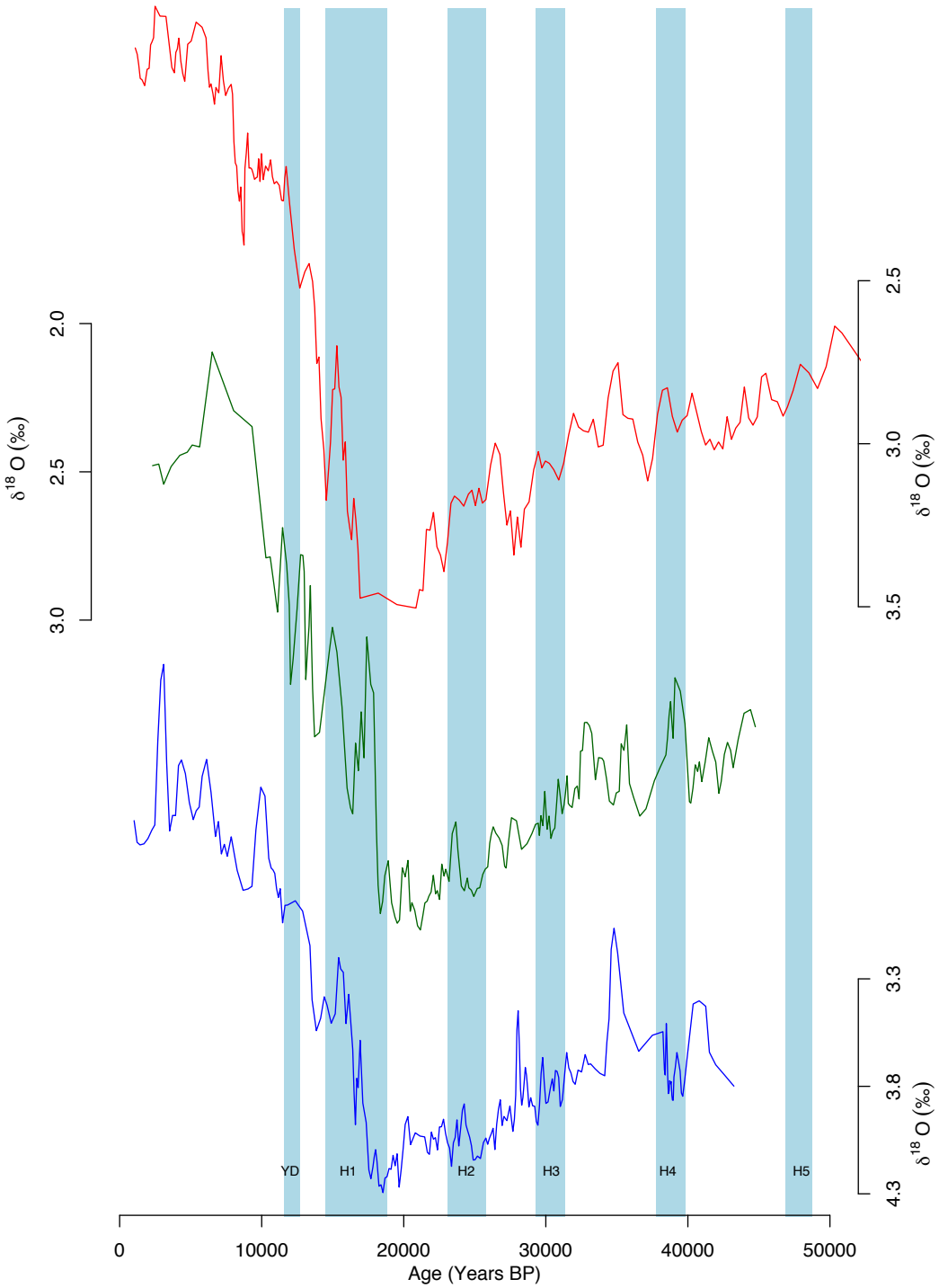

FIGURE 4.6: Oxygen isotope records of *Cibicidoides wuellerstorfi* (benthic) for each of the three cores with the same colour scheme applied as previous (PE304-8 (752m, red), PE303-16 (1350m, green) and PE303-15 (1985m, blue)). Displayed in this way, the phase relationships between these records are easier to see. Vertical blue bars indicate the timing of North Atlantic cold events; the Younger Dryas and Heinrich events 1-5 (H1-5).

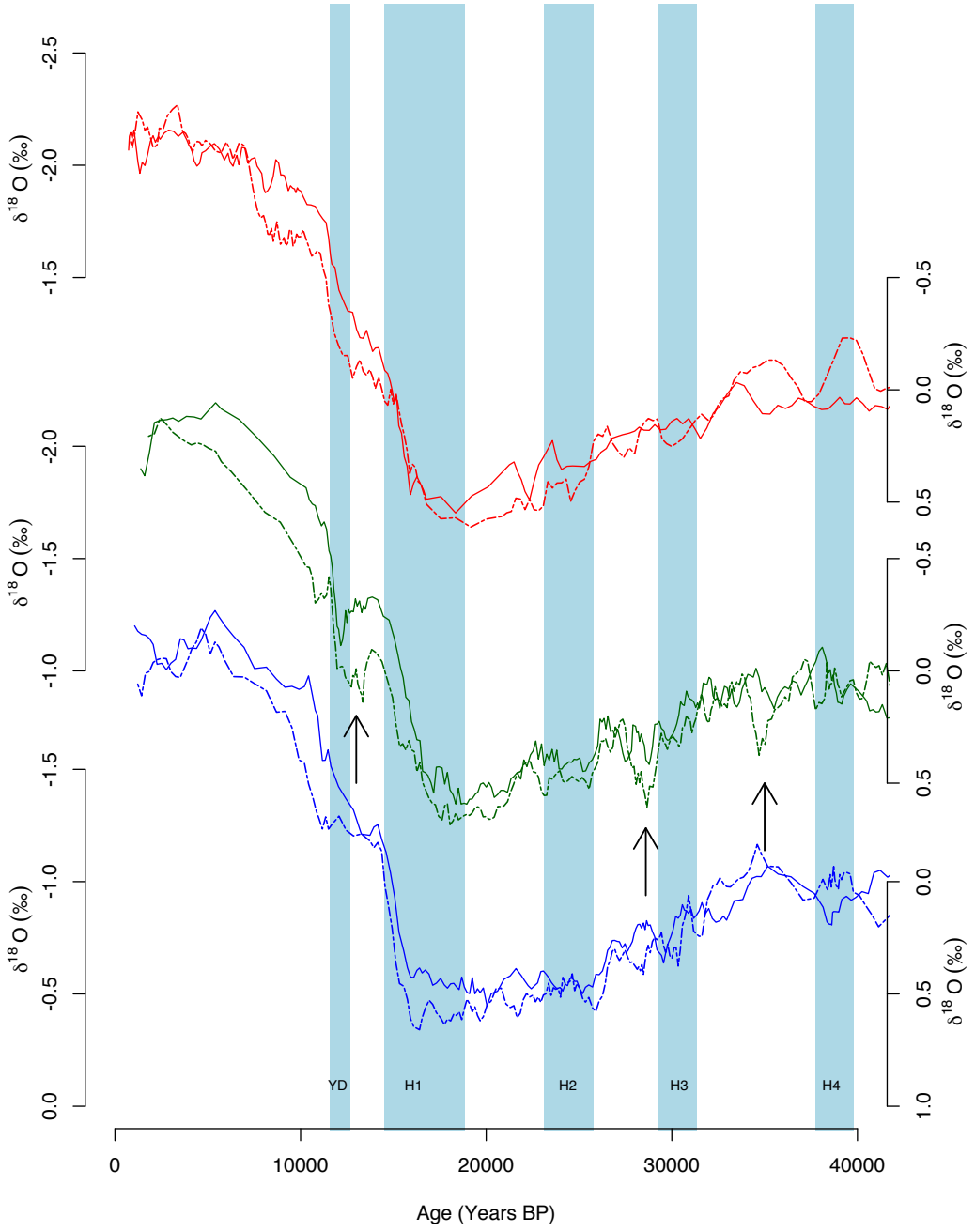

FIGURE 4.7: planktonic foraminiferal oxygen isotope records of cores PE304-8 (752m, red), PE303-16 (1350m, green) and PE303-15 (1985m, blue), this time arranged to illustrate the phasing relationships between the surface and thermocline oxygen isotope records within each core. In each case the solid line represents the oxygen isotope record of *G.ruber* and the dashed line the oxygen isotope record of *N.dutertrei*. Vertical blue bars indicate the timing of North Atlantic cold events; the Younger Dryas and Heinrich events 1-5 (H1-5). Black arrows indicate position of events referred to in text.

64PE304-8, 1.2kyr for core 64PE303-16, and 0.5kyr for core 64PE303-15). Although the initial step of the deglaciation is more sudden in the *G.ruber* $\delta^{18}O$ records. The plateau displayed in the *G.ruber* $\delta^{18}O$ records is also present in the *N.dutertrei* $\delta^{18}O$ records but it is less consistent between cores. Both *N.dutertrei* and *G.ruber* $\delta^{18}O$ records from core 64PE303-16 show a reversal at 12-14ka which is not reflected in the other two cores.

Last glacial period

Generally the $\delta^{18}O$ records of *G. ruber* and *N. dutertrei* show consistent variation within each core during the last glacial period. However, there are some notable discrepancies. Out of phase variability between surface and thermocline records occurs in core 64PE303-16 at ∼13ka, ∼28.6ka and ∼35ka (arrows in Figure 4.7). In each case the thermocline oxygen isotope conditions seem to shift towards heavier values, whilst the change is muted or absent in the corresponding record of surface oxygen isotope conditions.

4.3.7 Timing of planktonic versus benthic

Deglaciation

The nature of data presented and collated here allows investigation of the timing of deglaciation across various depths within the western Indian Ocean region. Some clear distinctions exist in the timing of deglaciation across the various records. The benthic $\delta^{18}O$ records for cores 64PE303-16 and 64PE303-15 (our two deepest cores; Figures 4.9 & 4.10) show an earlier onset (18.4ka and 17.6ka respectively), interestingly earliest in 64PE303-16 (our middle core in terms of depth; Figure 4.6). Meanwhile the surface, thermocline and benthic records of core 64PE304-8 all display a similar time of deglacial onset (∼16.9ka; Figure 4.8).

Last glacial period

At the millennial-scale, clear differences exist between the planktonic and benthic records of each core, particularly in the two deeper cores. The lesser distinction seen between planktonic and benthic in core PE304-8 is arguably a consequence of the shallower depth of this core, especially when lower glacial sea-level (∼120m lower; Siddall and Rohling 2008) is considered. This likely led to more agreement throughout the water column at this site, as suggested by our data (Figure 4.8). It should be noted that the variability between the planktonic and benthic records of 64PE304-8 is still not perfectly in phase.

Cores 64PE303-16 and 64PE303-15 show some noteworthy differences between the planktonic and benthic records within each core. The significance of these differences is due to the fact that within a single core, the relative changes are independent of their age models. Hence different modes of change can be robustly said to show different drivers acting on different levels of the water column. Generally, the records of both cores show an out of phase relationship between planktonic and benthic change. There is a large negative excursion (>0.5‰) in the benthic record of 64PE303-15 at ∼35ka which is absent from the planktonic record. A similar, but lower amplitude event occurs at ∼28ka. There are three negative excursions in the benthic record of 64PE303-16 at ∼33ka, ∼36ka and ∼39ka which are all absent from the equivalent planktonic record.

4.3.8 Relation to high latitude climate change

Deglaciation

Figures 4.8, 4.9 & 4.10 present the foraminiferal oxygen isotope records of the cores used here alongside $\delta^{18}O$ records from Greenland and Antarctica – which are used to trace temperature variability. The overall timing of the deglaciation in the planktonic $\delta^{18}O$ records of all three cores and the benthic $\delta^{18}O$ record of core 64PE304-8

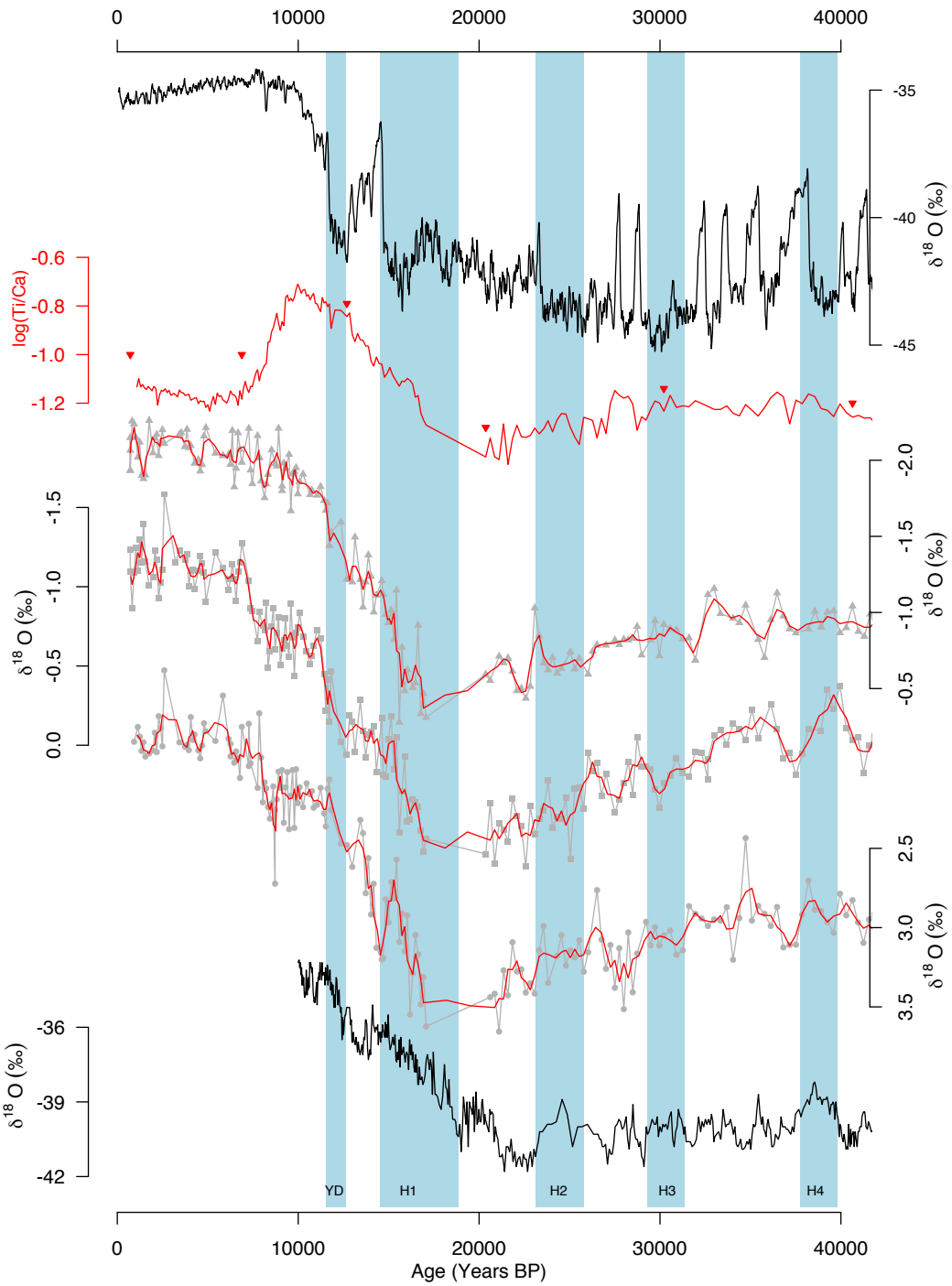

FIGURE 4.8: Presentation of data for core 64PE304-8. For each foraminiferal isotope record, original data is plotted in grey with solid triangles denoting each datum. Solid red line represents a 3-point rolling mean. A) GISP2 $\delta^{18}O$ on GICC05 timescale (Vinther et al.; 2006; Rasmussen et al.; 2008; Andersen et al.; 2006; Grootes et al.; 1993) B) Log(Ti/Ca) C) $\delta^{18}O$ *G.ruber* D) $\delta^{18}O$ of *N.dutertrei* E) $\delta^{18}O$ *C.wuellerstorfi* F) Byrd $\delta^{18}O$ (Johnsen et al.; 1972).

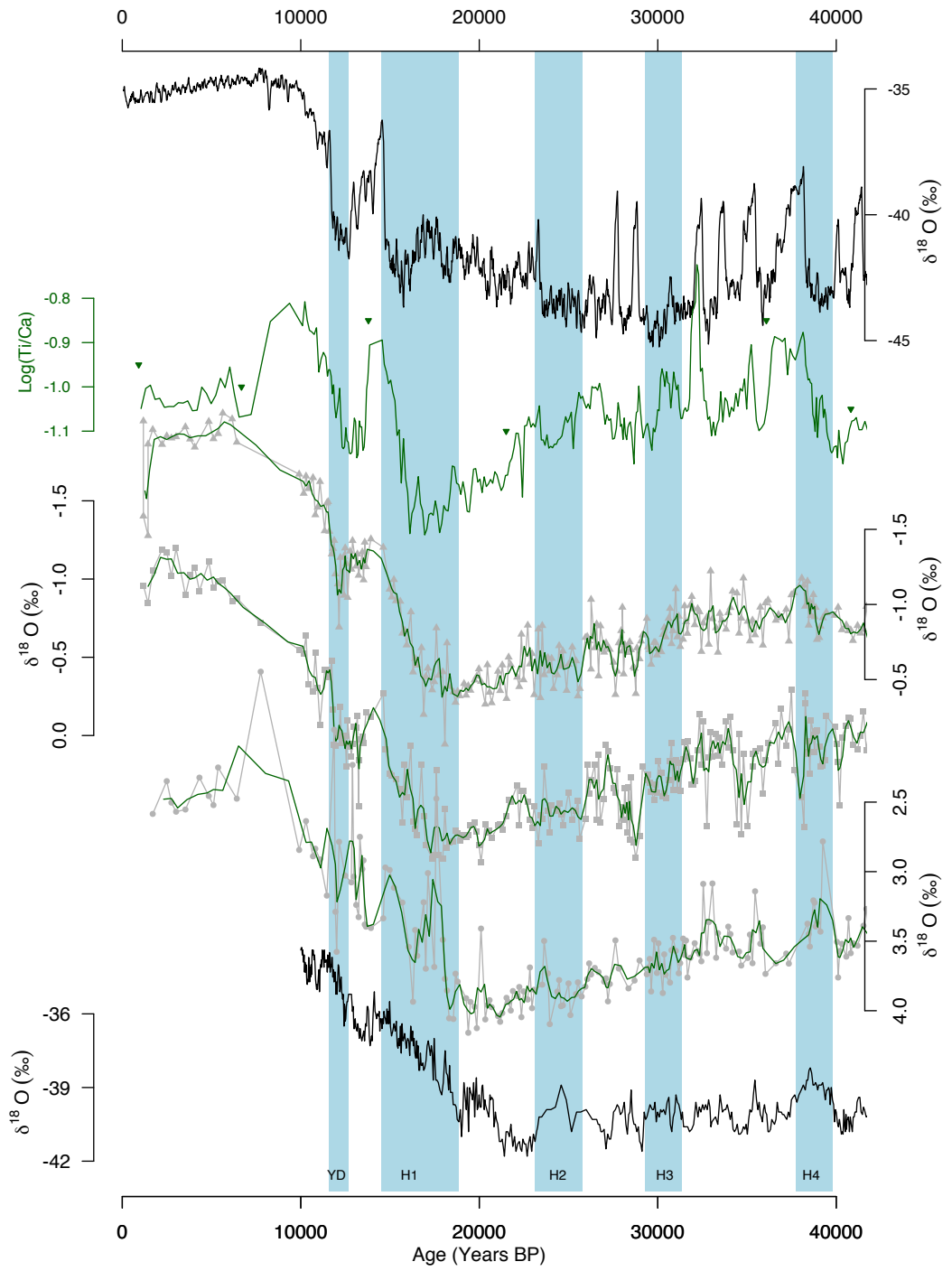

FIGURE 4.9: Presentation of data for core 64PE303-16. For each foraminiferal isotope record, original data is plotted in grey with solid triangles denoted each datum. Solid green line represents a 3 point rolling mean A) GISP2 $\delta^{18}O$ on GICC05 timescale (Vinther et al.; 2006; Rasmussen et al.; 2008; Andersen et al.; 2006; Grootes et al.; 1993) B) Log(Ti/Ca) C) $\delta^{18}O$ *G.ruber* D) $\delta^{18}O$ of *N.dutertrei* E) $\delta^{18}O$ *C.wuellerstorfi* F) Byrd $\delta^{18}O$ (Johnsen et al.; 1972).

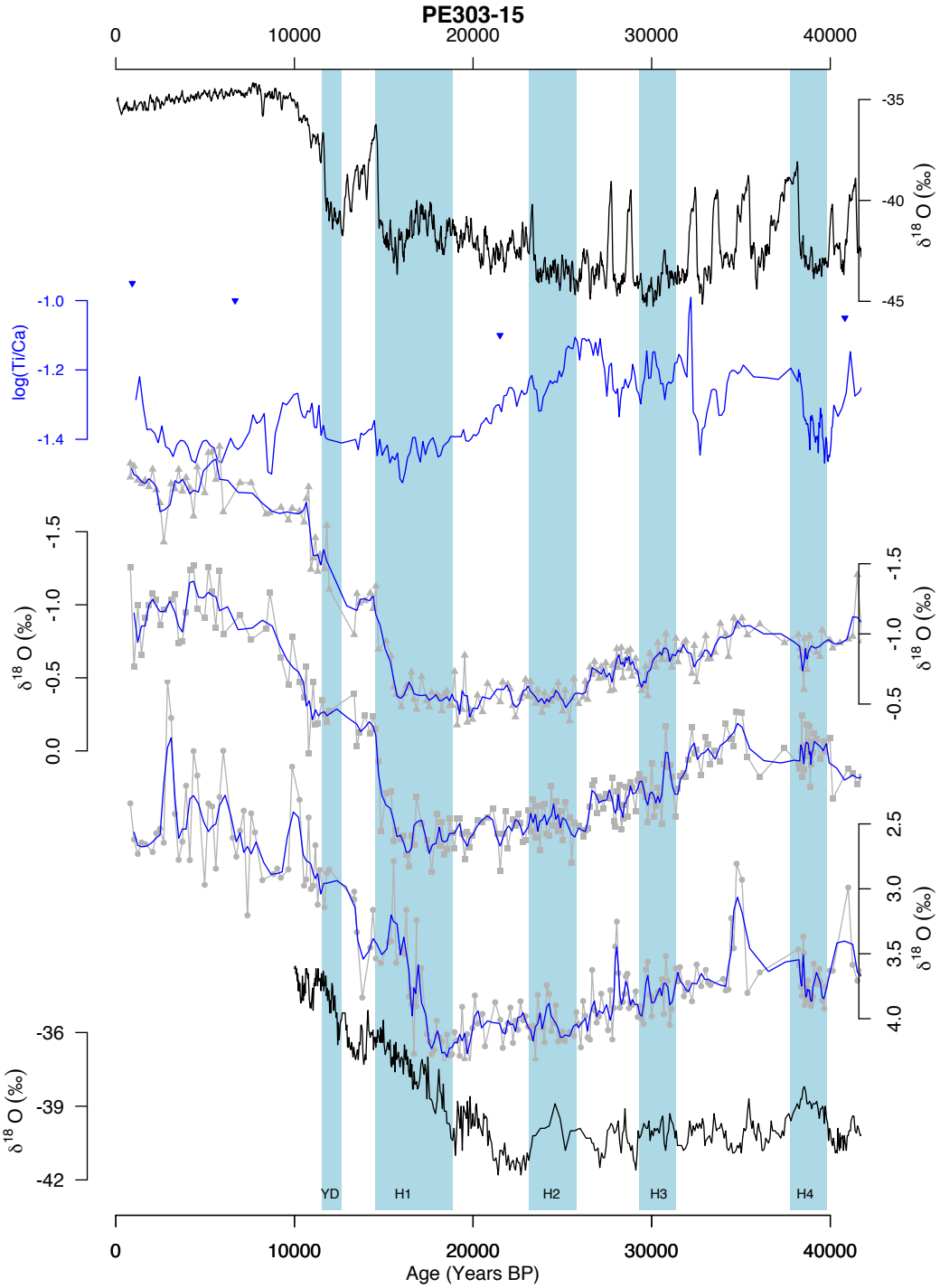

FIGURE 4.10: Presentation of data for core 64PE303-15. For each foraminiferal isotope record, original data is plotted in grey with solid triangles denoted each datum. Solid blue line represents a 3 point rolling mean A) GISP2 $\delta^{18}O$ on GICC05 timescale (Vinther et al.; 2006; Rasmussen et al.; 2008; Andersen et al.; 2006; Grootes et al.; 1993) B) Log(Ti/Ca) C) $\delta^{18}O$ *G.ruber* D) $\delta^{18}O$ of *N.dutertrei* E) $\delta^{18}O$ *C.wuellerstorfi* F) Byrd $\delta^{18}O$ (Johnsen et al.; 1972).

shows more affinities with Greenland. However, the earlier onset of deglaciation within the benthic $\delta^{18}O$ records of cores 64PE303-16 and 64PE303-15 leads to a generally greater resemblance to Antarctica in terms of timing of change. However, the shape of change throughout the deglaciation does not show such strong affinity to Antarctica during the same period.

Last glacial period

The most obvious similarity between the new $\delta^{18}O$ records and the high latitudes during the last glacial period is between the timing and nature of the millennial-scale variability in the benthic records of cores 64PE303-16 and 64PE303-15 and Antarctica. The corresponding planktonic records show a less defined similarity to Greenland.

4.4 Discussion

4.4.1 Implications for evolution of deglaciation in the region

The new $\delta^{18}O$ records presented here provide a unique opportunity to look at the timing of the last deglaciation across a range of depths within the western Indian Ocean from the surface through the thermocline to bottom water depths of 752m, 1350m and 1985m (Figure 4.11). To supplement this, we have added previously published data from nearby core GeoB12615-4 (7°S 39°E, 466m water depth; Romahn et al. 2014).

The offshore surface ocean $\delta^{18}O$ records (*G.ruber*) show good correlation in timing of deglacial onset to Greenland. This is likely due to the influence of the monsoon on the tropical western Indian Ocean, which is in turn controlled by northern hemisphere climate variability as has been previously discussed (Altabet et al.; 2002; Ivanochko et al.; 2005; Jung et al.; 2009). This may be a consequence of southward shifting ITCZ (see also discussion in chapter 3) and weaker African and Asian

monsoon systems resulting in reduced rainfall. Coherence with the GeoB12615-4 $\delta^{18}O$ record of Romahn et al. (2014) supports the notion that these records reflect the monsoon strength modulated via northern hemisphere driven atmospheric processes. Further, the deglaciation in our $\delta^{18}O$ data is punctuated by shifts towards higher values forming a plateau around the time of the Younger Dryas in cores 64PE303-16 and 64PE303-15. Although this is absent from core 64PE304-8, probably as a consequence of the shallower depth of this cores leading to influence from subsurface/bottom conditions or possibly even greater sediment reworking after deposition. This apparent similarity between our records of $\delta^{18}O$ change at 9°S and $\delta^{18}O$ change on Greenland is noteworthy in the sense that we see a northern hemisphere type signal being records as far south as 9°S in the western tropical Indian Ocean.

We have an unprecedented depth transect of $\delta^{18}O$ records that allows us to identify time offsets between the records. A significant advantage of this approach is the reduced dependence on age models; the timing of different records within each core is independent of age. Thermocline depth $\delta^{18}O$ records (*N. dutertrei*) lead the surface water $\delta^{18}O$ records (*G. ruber*) in terms of deglaciation by $\sim$1kyr (Figure 4.7). A possible explanation of this is sub-surface/intermediate depth waters of southern origin (AAIW or SAMW) carrying some signal of the earlier onset of deglaciation seen in Antarctic ice core records. By this route, the deglacial signal would be first recorded in the thermocline records, as we see in our data. The most likely option at thermocline depths being SAMW, an increased supply has previously been found – associated with Heinrich events - by Pahnke et al. (2008) & Jung et al. (2009). This is in line with the oceanic tunnel idea of Liu and Alexander (2007) and supported by Schott and McCreary (2001) who show that AAIW and SAMW are upwelled at 5-10°S by Ekman divergence at the northern limit of the South Equatorial Counter current. This provides a possible mechanism for transmitting an Antarctic type signal via the intermediate depths to the sub-tropical western

Indian Ocean that would account for the earlier deglacial signal seen in the thermocline records of our cores.

Moving focus to the four benthic $\delta^{18}O$ records, which provide details of change during the transition at water depths of 446m, 752m, 1350m and 1985m, we see that the termination occurs earliest in the 1350m core ($\sim$18.4ka). This represents the intermediate depth limb of the ocean circulation system. Based on this data, the first signs of the deglaciation reaching the subtropical Indian Ocean arrived via the intermediate ocean. This is consistent with our discussion above relating to transmission of high latitude climate signal to the sub-tropics via the intermediate depth oceans. Although at this depth (1350m) the most likely transmitter of the signal would be AAIW (Kallel et al.; 1988; Romahn et al.; 2015; You; 1998; Fine et al.; 2008).

Each new core presented here displays a decoupling of deglacial onset between surface and bottom water conditions as represented by the $\delta^{18}O$ records. The magnitude of this decoupling varies between cores (<1ka in 64PE304-8, 2.5ka in 64PE303-16 and 1.8ka in 64PE303-15). Given that the surface $\delta^{18}O$ records align well, the differences in the timing of benthic $\delta^{18}O$ records give us a strong clue as to the temporal and vertical evolution of the deglacial $\delta^{18}O$ signal in the region. The smallest planktonic-benthic offset of our three cores is seen in core 64PE304-8. The modern-day depth of 752m would have been reduced at the last glacial maximum by $\sim$120m (Siddall and Rohling; 2008) to $\sim$630m. This may be shallow enough to explain the smaller offset because of surface influence. The largest $\delta^{18}O$ offset between surface and bottom water deglaciation is seen in the intermediate depth core (64PE303-16, 1350m). This points towards an intermediate depth circulation change associated with the deglaciation in Antarctica.

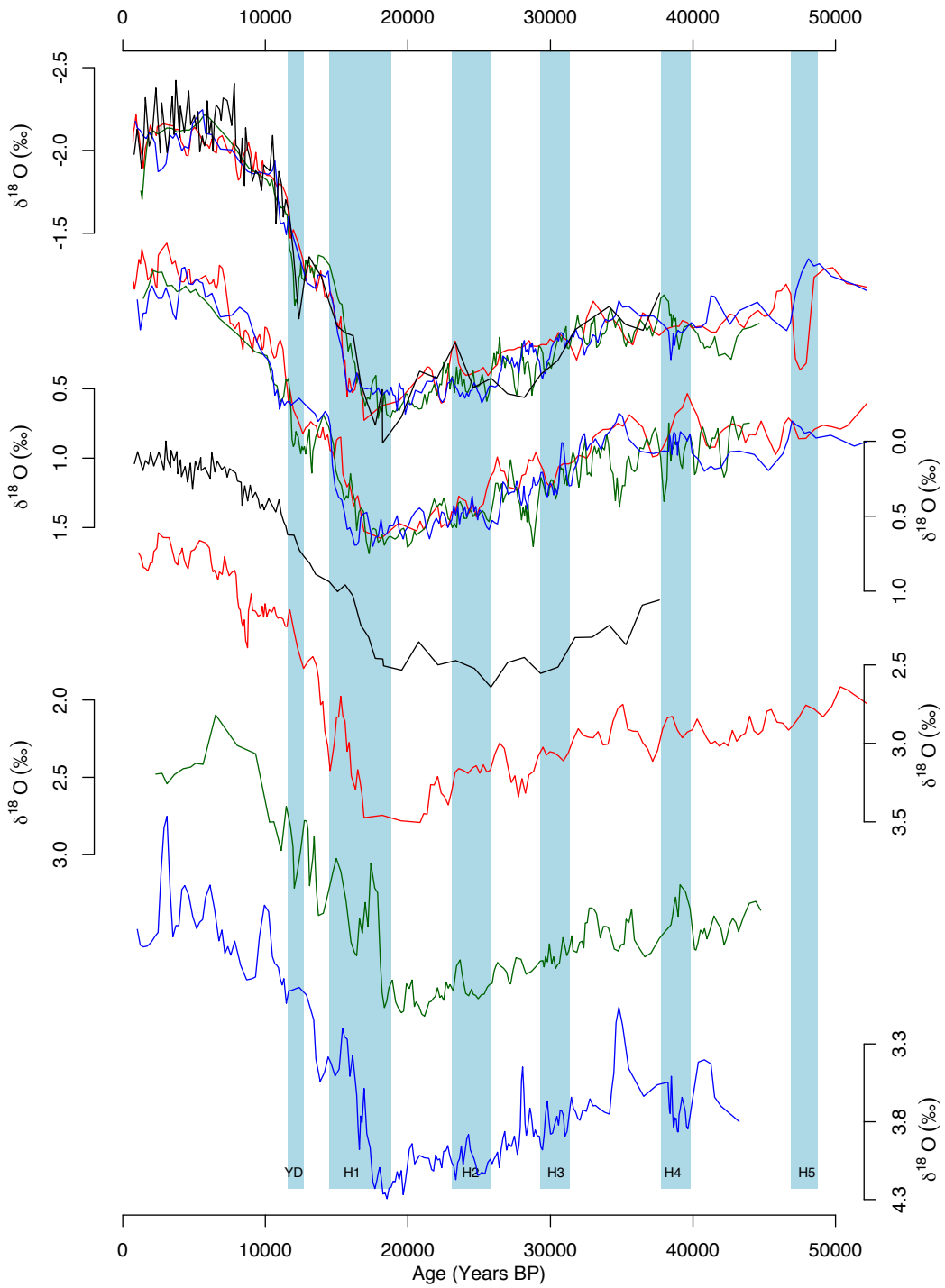

FIGURE 4.11: Overview figure of all oxygen isotope records generated in this study (PE304-8 (752m, red), PE303-16 (1350m, green) and PE303-15 (1985m, blue)) plus one external record (GeoB12615-4, 446m, Romahn et al. (2014) Plotted here in black). This figure synthesises the data presented in this chapter to help show the unique nature of the data. The combination of surface, thermocline and benthic records from an important range of depths provides a useful new data set on the changes in western Indian ocean circulation over the last 50ka. A. Oxygen isotope records of *G.ruber*. B) Oxygen isotope records of *N.dutertrei*. C) Oxygen isotope records of *C.wuellerstorfi*. Vertical blue bars indicate the timing of North Atlantic cold events; the Younger Dryas and Heinrich events 1-5 (H1-5).

4.4.2 Timing of maximum rates of change

We can further assess the sequence of change in ocean conditions during the deglaciation at the various depths covered by our cores by calculating the rate of change of oxygen isotope conditions at each site and for each species (Figure 4.12 and 4.13). This allows clearer identification of the timing of the greatest change in the oxygen isotope records at these sites. The timing of greatest change is as significant as the timing of high/low points in the records in terms of understanding the nature of change and its mechanisms. Rates of change were calculated for cores 64PE303-16 and 64PE303-15, in the manner of Jung and Kroon (2011). The same 700-year boxcar filter was applied to reduce noise and emphasize changes on the millennial-scale. The estimated rate of change is calculated by dividing the difference in isotope values between successive neighboring samples by the age difference between the same two samples. We have also used the same method to calculate rate of change data for the oxygen isotope records of the North Greenland Ice-coring Project (NGRIP; Vinther et al. 2006; Rasmussen et al. 2008; Andersen et al. 2006; Grootes et al. 1993) and European Project for Ice Coring in Antarctica (EPICA) Dronning Maud Land (EDML; Bazin et al. 2013; Barbante et al. 2006) ice cores (Figure 4.12 and 4.13).

This exercise produced some striking results and strengthens our earlier discussion of the oxygen isotope data. Figures 4.12 and 4.13 make clear the nature of the timing relationships - in terms of rates of change – between our two deepest cores (64PE303-16 and 64PE303-15) and the two high latitude ice cores.

Looking at our data alone (Figures 4.12 B,C & D and 4.13 B,C & D) we can see good agreement of the rate of change in oxygen isotope records between cores (for the same species). Notable discrepancy at the end of the Younger Dryas period when the peak rate of change in the *G. ruber* record of 64PE303-15 is delayed relative to that of 64PE303-16. This in anomalous as these records should reflect the

same surface ocean condition changes. The difference is possibly related to post depositional processes. Most likely bioturbation causing a smoothing of the variability, manifest here as a slower change.

There are also some events which show significant time off-sets between cores in the older/deeper sediment sections. For example between the *N.dutertrei* records of the two cores at ∼35ka (Figures 4.12 C and 4.13 C). In this time period the age model uncertainty will play a significant role.

When comparing the data from our own cores to the data of the ice cores (Figure 4.12 & 4.13), very interesting patterns emerge. The rate of change records of the two shallower foraminifera species (*G.ruber* and *N.dutertrei*) records show a very consistent relationship to the timing of change in Greenland. This connection has been previously discussed here and elsewhere (Jung and Kroon; 2011). The causal mechanisms behind this relationship may not be unanimously agreed but have been well discussed (e.g. Ivanochko et al. 2005; Deplazes et al. 2014.

Less clear is the meaning of the patterns seen in the rate of change data of the benthic (*C. wuellerstorfi*) records (Figure 4.12D) in the context of high latitude change. There are some similarities between the benthic record and Antarctica ice core, however the consistency of relationship is low and suggests a much weaker link than that displayed between the planktonic records and Greenland ice. In some sections (particularly during the Holocene) the rate of change of the $\delta^{18}O$ is almost erratic. If this signal is indeed real, it is very difficult to explain.

4.4.3 Comparison to deglacial timing in the Arabian Sea

The idea that intermediate depth Indian Ocean/Arabian Sea circulation changes are southern sourced has been previously suggested to explain the benthic stable isotope records of core NIOP-905 (10°N, 51°E, 1580m water depth; Jung et al. 2009). We can test this theory by comparing our records to the previously published records of NIOP-905 which lies further north of our cores north in the Indian

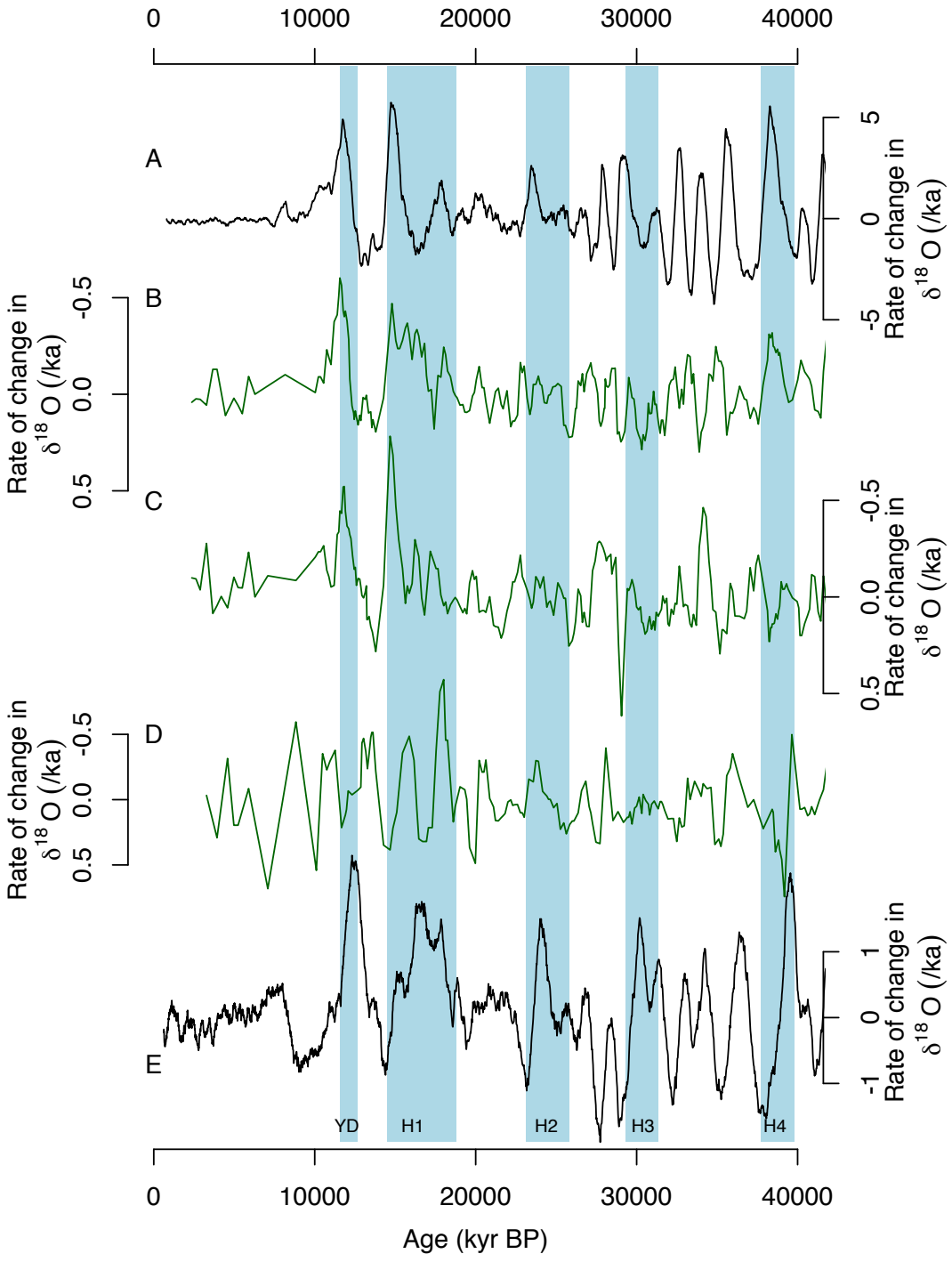

FIGURE 4.12: Rate of change in oxygen isotope conditions for (A) NGRIP ice core (Adapted from Vinther et al. (2006); Rasmussen et al. (2008); Andersen et al. (2006); Grootes et al. (1993)) (B) 64PE303-16 *G.ruber* (C) 64PE303-16 *N.dutertrei* (D) 64PE303-16 *C.wuellerstorfi* and (D) EDML ice core (adapted from Bazin et al. (2013); Barbante et al. (2006)). For details on calculation of this data see text in discussion.

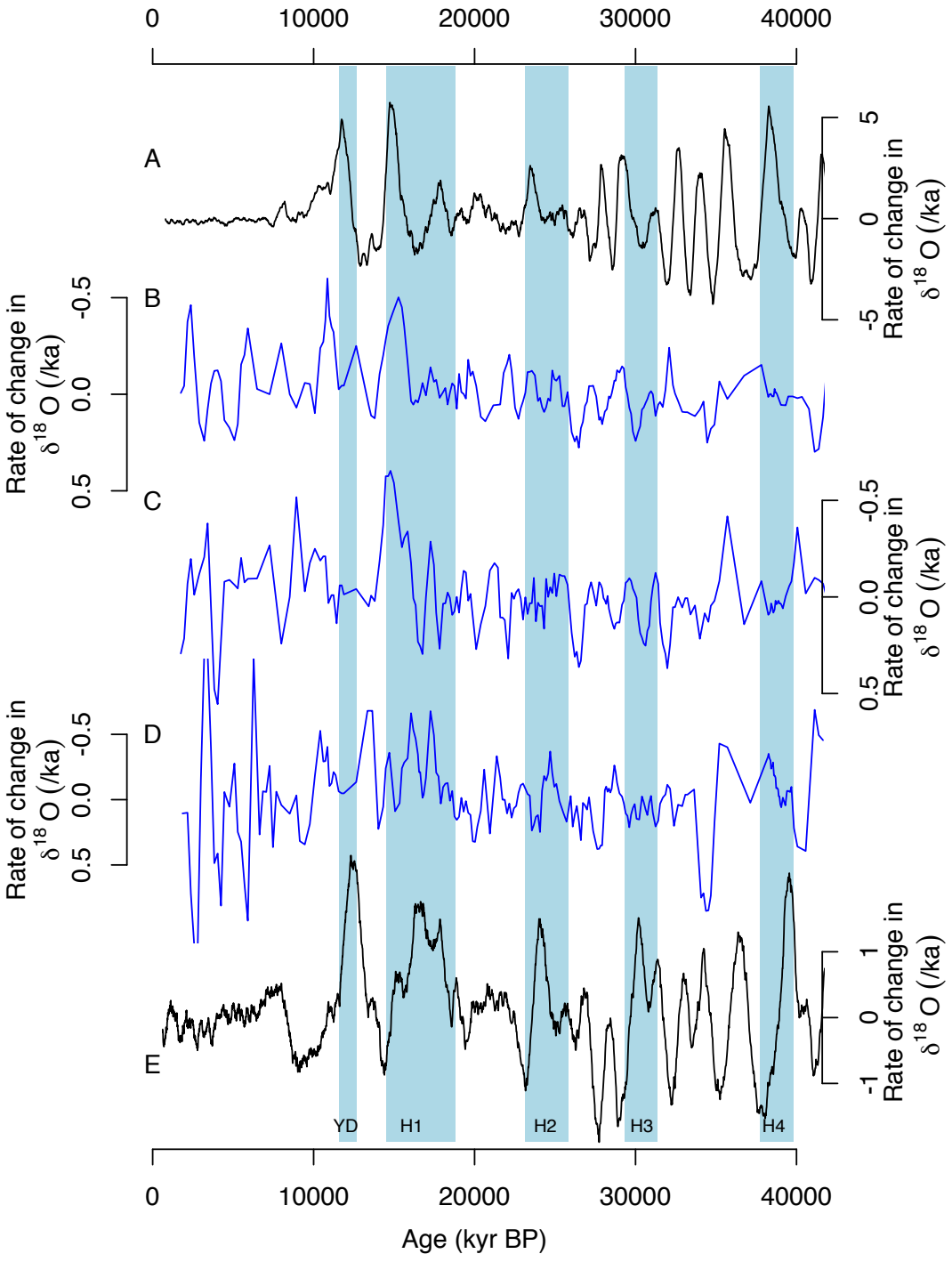

FIGURE 4.13: Rate of change in oxygen isotope conditions for (A) NGRIP ice core (Adapted from Vinther et al. (2006); Rasmussen et al. (2008); Andersen et al. (2006); Grootes et al. (1993)) (B) 64PE303-15 *G.ruber* (C) 64PE303-15 *N.dutertrei* (D) 64PE303-15 *C.wuellerstorfi* and (D) EDML ice core (adapted from Bazin et al. (2013); Barbante et al. (2006)). For details on calculation of this data see text in discussion

Ocean. This theory places the cores presented here 'upstream' of the changes seen in NIOP-905. Additionally, our cores form a depth transect which allows us to also constrain the vertical extent of any changes seen. This is an extra step in testing the idea that the intermediate depth western Indian Ocean displays a ventilation signal associated with southern sourced water masses around the time of the Heinrich events of the last glacial period and deglaciation. For this we have added the planktonic and benthic oxygen isotope records of NIOP-905 to plot 4.14.

The previously published stable isotope records of Arabian Sea intermediate depth core NIOP-905 (Jung et al.; 2009) form an important starting point to this project. A strong contrast is seen between the surface and bottom water records of NIOP-905. The benthic oxygen isotope record seems to lead the surface records by 1-3 kyr in terms of millennial-scale variability. Further, this benthic record shows a good match with the oxygen isotope record of the Byrd ice core (Antarctica). This suggests a connection between high and low southern latitude climate change, apparently mediated by intermediate depth ocean circulation. The benthic carbon isotope record of NIOP-905 also shows an anti-phase signal to the ventilation state of the deep Atlantic (See Jung et al. 2009 Figure 3 for more detail). That is, during Heinrich events when North Atlantic ventilation is minimal, the intermediate depth Indian Ocean shows a maximum in ventilation state; a promising link between ocean circulation and the bipolar seesaw (Jung and Kroon; 2011; Shackleton et al.; 2000).

The deglacial timing of $\delta^{18}O$ in NIOP-905 ($\sim$17.1ka) strongly resembles that of core 64PE303-15 ($\sim$17.6ka; 1985m, this study), both of which lag the deglacial onset of core 64PE303-16 ($\sim$18.4ka; 1350m, this study). This sequence fits the idea that the deglacial signal is transmitted from the south by intermediate waters. And in fact, suggests that the signal spread vertically and horizontally to reach the Arabian sea and the deep ($\sim$2km) western Indian Ocean at around the same time. Given that the oxygen isotope ratio variability reflects a combination of temperature and

isotope ratio of ambient seawater, this signal fairly robustly indicates an influence of the wider global deglaciation at these core sites. This finding is significant in the context of previous work (Romahn et al.; 2014; Jung et al.; 2009) as it provides evidence of a western Indian Ocean wide change in circulation associated with millennial-scale events as opposed to the possibility of localised changes in circulation/ventilation based on NIOP-905 data alone (Jung et al.; 2009). This idea is also supported by modeling work (Schmittner et al.; 2007). The oxygen isotope ratio is useful for assessing the timing of changes but is limited in its ability to distinguish circulation changes at the level of specific water masses. A more in-depth assessment of this theory is given in chapter 5 where the addition of a ventilation proxy strengthens our discussion.

4.5 Conclusions

The new planktonic and benthic $\delta^{18}O$ records presented here show important time offsets across the water column offshore Tanzania. This reveals global climate linkages during the last glacial-deglaciation period. The combination of oxygen isotope records and rate of change records have enabled discussion of the timing and succession of change in the water column at our sites.

Our new data highlight significant differences across the water column - within each core - in the timing of deglaciation. These differences are important as a consequence of the lack of age model dependency when assessing records from an individual core.

The rate of change records calculated further highlight these offsets and strengthen the apparent relationship between our surface records and Greenland in terms of timing of change. They also highlight that the benthic records do not appear to be so strongly related to change in either Greenland or Antarctica.

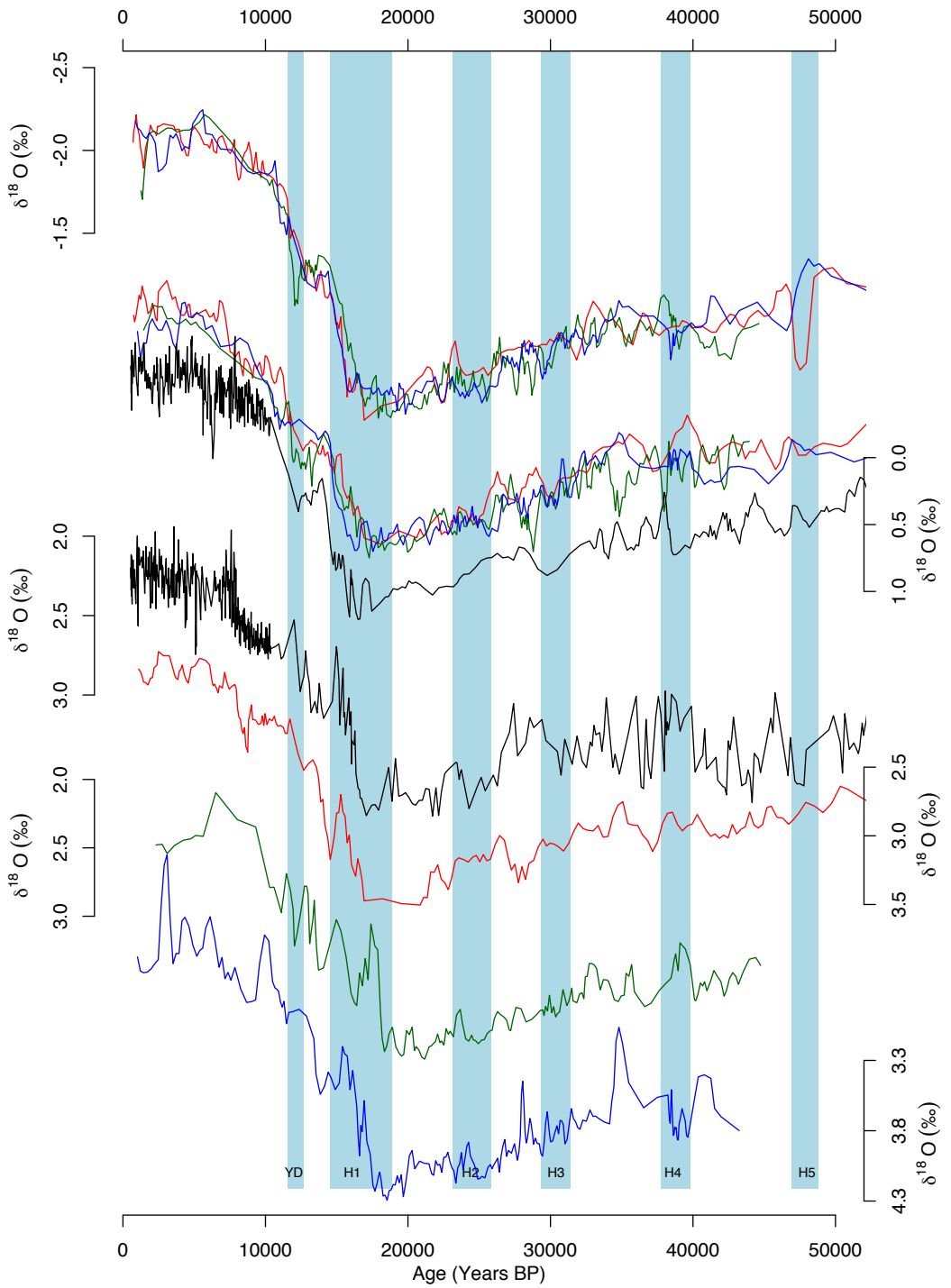

FIGURE 4.14: Data from cores presented here plus planktonic and benthic oxygen isotope records of core NIOP-905 (Jung et al.; 2009). A. *G.ruber* records. B. *N.dutertrei* records. D. C.kullenbergi record of NIOP-905 E,F,G *C.wuellerstorfi* records of PE304-8, PE303-16 and PE303-15 respectively.

When placed in a broader Indian Ocean/Arabian sea context the new data begin to test the idea that the intermediate depths of the Indian Ocean play a role in millennial-scale change, particularly during Heinrich events. The oxygen isotope data provides support for the idea of a southern sourced intermediate ocean signal associated with rapid/millennial-scale climate change. However, the main discussion of this is reserved for chapter 5.

Overall this chapter provides important evidence of subsurface and surface ocean change during the deglaciation and last glacial period that suggest large time off-sets across the water column during the deglaciation and millennial-scale climate change events within the region. The planktonic and benthic $\delta^{18}O$ records presented in this chapter provides a basis for the next chapter – using the equivalent carbon records – to further investigate and test the proposed surface and subsurface changes over the last 40kyrs.

Bibliography

Altabet, M. A., Higginson, M. J. and Murray, D. W. (2002). The effect of millennial-scale changes in Arabian Sea denitrification on atmospheric CO_2, *Nature* **415**(6868): 159–162.

An, Z. S., Clemens, S., Shen, J., Qiang, X., Jin, Z., Sun, Y., Prell, W. L., Luo, J., Wang, S., Xu, H., Cai, Y., Zhou, W., Liu, X., Liu, W., Shi, Z., Yan, L., Xiao, X., Chang, H., Wu, F., Ai, L. and Lu, F. (2011). Glacial-interglacial Indian summer monsoon dynamics., *Science (New York, N.Y.)* **333**(6043): 719–723.

Andersen, K. K., Svensson, A., Johnsen, S. J., Rasmussen, S. O., Bigler, M., Röthlisberger, R., Ruth, U., Siggaard-Andersen, M. L., Peder Steffensen, J., Dahl-Jensen, D., Vinther, B. M. and Clausen, H. B. (2006). The Greenland Ice Core Chronology 2005, 15-42 ka. Part 1: constructing the time scale, *Quaternary Science Reviews*

25(23-24): 3246–3257.

Barbante, C., Barnola, J., Becagli, S., Beer, J., Bigler, M., Boutron, C., Blunier, T., Castellano, E., Cattani, O., Chappellaz, J., Dahl-Jensen, D., Debret, M., Delmonte, B., Dick, D., Falourd, S., Faria, S., Federer, U., Fischer, H., Freitag, J., Frenzel, A., Fritzsche, D., Fundel, F., Gabrielli, P., Gaspari, V., Gersonde, R., Graf, W., Grigoriev, D., Hamann, I., Hansson, M., Hoffmann, G., Hutterli, M. a., Huybrechts, P., Isaksson, E., Johnsen, S., Jouzel, J., Kaczmarska, M., Karlin, T., Kaufmann, P., Kipfstuhl, S., Kohno, M., Lambert, F., Lambrecht, A., Lambrecht, A., Landais, A., Lawer, G., Leuenberger, M., Littot, G., Loulergue, L., Lüthi, D., Maggi, V., Marino, F., Masson-Delmotte, V., Meyer, H., Miller, H., Mulvaney, R., Narcisi, B., Oerlemans, J., Oerter, H., Parrenin, F., Petit, J. R., Raisbeck, G., Raynaud, D., Röthlisberger, R., Ruth, U., Rybak, O., Severi, M., Schmitt, J., Schwander, J., Siegenthaler, U., Siggaard-Andersen, M.-L., Spahni, R., Steffensen, J., Stenni, B., Stocker, T., Tison, J.-L., Traversi, R., Udisti, R., Valero-Delgado, F., van den Broeke, M. R., van de Wal, R. S. W., Wagenbach, D., Wegner, A., Weiler, K., Wilhelms, F., Winther, J.-G. and Wolff, E. W. (2006). One-to-one coupling of glacial climate variability in Greenland and Antarctica, *Nature* **444**(7116): 195–198.

Bazin, L., Landais, A., Lemieux-Dudon, B., Toyé Mahamadou Kele, H., Veres, D., Parrenin, F., Martinerie, P., Ritz, C., Capron, E., Lipenkov, V., Loutre, M. F., Raynaud, D., Vinther, B., Svensson, A., Rasmussen, S. O., Severi, M., Blunier, T., Leuenberger, M., Fischer, H., Masson-Delmotte, V., Chappellaz, J. and Wolff, E. (2013). An optimized multi-proxy, multi-site Antarctic ice and gas orbital chronology (AICC2012): 120-800 ka, *Climate of the Past* **9**(4): 1715–1731.

Böning, P. and Bard, E. (2009). Millennial/centennial-scale thermocline ventilation changes in the Indian Ocean as reflected by aragonite preservation and geochemical variations in Arabian Sea sediments, *Geochimica et Cosmochimica Acta* **73**(22): 6771–6788.

Broecker, W., Bond, G., Klas, M., Clark, E. and McManus, J. (1992). Origin of the northern Atlantic 's Heinrich events, *Climate Dynamics* **6**: 265–273.

Brummer, G. and Jung, S. (2009). RV Pelagia Cruise Report : Cruise 64PE304 SE African margin ,.

Coplen, T. B., Kendall, C. and Hopple, J. (1983). Comparison of stable isotope reference samples, *Nature* **302**(5905): 236–238.

Dansgaard, W., Johnsen, S., Clausen, H., Dahl-Jensen, D., Gundestrup, N., Hammer, C. U. and Oeschger, H. (1984). h, *in* J. E. Hansen and T. Takahashi (eds), *Climate Processes and Climate Sensitivity, Geophys. Monogr. Ser., vol. 29*, AGU, pp. 288–298.

Deplazes, G., Lückge, A., Stuut, J.-B. W., Pätzold, J., Kuhlmann, H., Husson, D., Fant, M. and Haug, G. H. (2014). Weakening and strengthening of the indian monsoon during heinrich events and dansgaard-oeschger oscillations, *Paleoceanography* **29**(2): 99–114. 2013PA002509.

Duplessy, J. (1982). Glacial to interglacial contrasts in the northern Indian Ocean.

Elliot, M., Labeyrie, L. and Duplessy, J. (2002). Changes in North Atlantic deep-water formation associated with the Dansgaard – Oeschger temperature oscillations (60 – 10 ka), *Quaternary Science Reviews* **21**: 1153–1165.

Emiliani, C. (1955). Pleistocene Temperatures, *The Journal of Geology* .

Fallet, U., Ullgren, J. E., Casta??eda, I. S., van Aken, H. M., Schouten, S., Ridderinkhof, H. and Brummer, G. J. A. (2011). Contrasting variability in foraminiferal and organic paleotemperature proxies in sedimenting particles of the Mozambique Channel (SW Indian Ocean), *Geochimica et Cosmochimica Acta* **75**(20): 5834–5848.

Fine, R. A., Smethie, W. M., Bullister, J. L., Rhein, M., Min, D. H., Warner, M. J., Poisson, A. and Weiss, R. F. (2008). Decadal ventilation and mixing of Indian Ocean waters, *Deep-Sea Research Part I: Oceanographic Research Papers* **55**(1): 20–37.

Gordon, A. L., Weiss, R. F., Smethie, W. M. and Warner, M. J. (1992). Thermocline and intermediate water communication between the South Atlantic and Indian Oceans, *Journal of Geophysical Research* **97**(C5): 7223.

Grootes, P. M., Stuiver, M., White, J. W. C., Johnsen, S. and Jouzel, J. (1993). Comparison of oxygen isotope records from the GISP2 and GRIP Greenland ice cores, *Nature* **366**(6455): 552–554.

Hartin, C. A., Fine, R. A., Kamenkovich, I. and Sloyan, B. M. (2014). Comparison of Subantarctic Mode Water and Antarctic Intermediate Water formation rates in the South Pacific between NCAR-CCSM4 and observations, *Geophysical Research Letters* **41**(2): 519–526.

Hartin, C. A., Fine, R. A., Sloyan, B. M., Talley, L. D., Chereskin, T. K. and Happell, J. (2011). Formation rates of Subantarctic mode water and Antarctic intermediate water within the South Pacific, *Deep-Sea Research Part I: Oceanographic Research Papers* **58**(5): 524–534.

Heinrich, H. (1988). Origin and consequences of cyclic ice rafting in the Northeast Atlantic Ocean during the past 13,000 years, *Quaternary Research* **29**: 142–152.

Ivanochko, T. S., Ganeshram, R. S., Brummer, G. J. A., Ganssen, G., Jung, S. J. A., Moreton, S. G. and Kroon, D. (2005). Variations in tropical convection as an amplifier of global climate change at the millennial scale, *Earth and Planetary Science Letters* **235**(1-2): 302–314.

Johnsen, S. J., Dansgaard, W., Clausen, H. B. and Langway, C. C. (1972). Oxygen Isotope Profiles through the Antarctic and Greenland Ice Sheets, *Nature* **235**(5339): 429–434.

Johnson, G. C., Musgrave, D. L., Warren, B. A., Ffield, A. and Olson, D. B. (1998). Flow of bottom and deep water in the Amirante Passage and Mascarene Basin, *Journal of Geophysical Research: Oceans* **103**(13): 30973–30984.

Jung, S. (1996). *Wassermassenaustausch zwischen NE-Atlantik und Nordmeer wahrend der letzten 300 000/80 000 Jahre im Abbild stabiler O- und C-Isotope*, PhD thesis, Christian-Albrechts-Universitat Kiel.

Jung, S. J. A., Kroon, D., Ganssen, G., Peeters, F. and Ganeshram, R. (2009). Enhanced Arabian Sea intermediate water flow during glacial North Atlantic cold phases, *Earth and Planetary Science Letters* **280**(1-4): 220–228.

Jung, S. and Kroon, D. (2011). Quantifying rates of change in ocean conditions with implications for timing of sea level change, *Global and Planetary Change* **79**(3): 204–213.

Kallel, N., Labeyrie, L. and Juillet-Leclerc, A. (1988). A deep hydrological front between intermediate and deep-water masses in the glacial Indian Ocean, *Nature* **333**: 651–655.

Kiefer, T., McCave, I. N. and Elderfield, H. (2006). Antarctic control on tropical Indian Ocean sea surface temperature and hydrography, *Geophysical Research Letters* **33**(24).

Kroon, D. and Party, S. (2010). Tropical Temperature History during Paleogene GLObal Warming (GLOW) Events, NIOZ site survey cruise report (RV Pelagia cruise number 64PE303), *NIOZ Site* pp. 1–59.

Leuschner, D. C. and Sirocko, F. (2003). Orbital insolation forcing of the Indian Monsoon - a motor for global climate changes ?, *Palaeogeography, Palaeoclimatology*, **197**: 83–95.

Liu, Z. and Alexander, M. (2007). Atmospheric bridge, oceanic tunnel, and global climatic teleconnections, *Reviews of Geophysics* (2005): 1–34.

Locarnini, R. A., Mishonov, A. V., Antonov, J. I., Boyer, T. P., Garcia, H. E., Baranova, O. K., Zweng, M. M., Paver, C. R., Reagan, J. R., Johnson, D. R., Hamilton, M. and Seidov, D. (2013). World Ocean Atlas 2013. Vol. 1: Temperature., *Technical Report September*.

McCartney, M. S. (1982). The subtropical recirculation of mode waters, *J. Mar. Res* **40**: 427–464.

Mohtadi, M., Prange, M., Oppo, D. W., De Pol-Holz, R., Merkel, U., Zhang, X., Steinke, S. and Lückge, A. (2014). North Atlantic forcing of tropical Indian Ocean climate., *Nature* **509**(7498): 76–80.

Pahnke, K., Goldstein, S. L. and Hemming, S. R. (2008). Abrupt changes in Antarctic Intermediate Water circulation over the past 25,000 years, *Nature Geosci* **1**(12): 870–874.

Pahnke, K. and Zahn, R. (2005). Southern Hemisphere water mass conversion linked with North Atlantic climate variability, *Science* **307**(5716): 1741–1746.

Rasmussen, S. O., Seierstad, I. K., Andersen, K. K., Bigler, M., Dahl-Jensen, D. and Johnsen, S. J. (2008). Synchronization of the NGRIP, GRIP, and GISP2 ice cores across MIS 2 and palaeoclimatic implications, *Quaternary Science Reviews* **27**(1-2): 18–28.

Ribbe, J. (2001). Intermediate water mass production controlled by southern hemisphere winds, *Geophysical Research Letters* **28**(3): 535–538.

Romahn, S., MacKensen, A., Groeneveld, J. and Pätzold, J. (2014). Deglacial intermediate water reorganization: New evidence from the Indian Ocean, *Climate of the Past* **10**(1): 293–303.

Romahn, S., Mackensen, A., Kuhlmann, H. and Pätzold, J. (2015). Benthic foraminiferal response to Late Glacial and Holocene sea level rise and rainfall variability off East Africa, *Marine Micropaleontology* **119**: 34–48.

Saraswat, R., Nigam, R., Weldeab, S., Mackensen, A. and Naidu, P. D. (2005). A first look at past sea surface temperatures in the equatorial Indian Ocean from Mg/Ca in foraminifera, *Geophysical research Letters* **32**: 2–5.

Sarmiento, J. L., Gruber, N., Brzezinski, M. A. and Dunne, J. P. (2004). High-latitude controls of thermocline nutrients and low latitude biological productivity, *Nature* **427**: 56–60.

Sarnthein, M., Winn, K., Jung, S., Duplessy, J., Labeyrie, L., Erlenkeuser, H. and Ganssen, G. (1994). Changes in east Atlantic deepwater circulation over the last 30 , 000 years : Eight time slice reconstructions, *Paleoceanography* **9**(2): 209–267.

Schmittner, A., Galbraith, E. D., Hostetler, S. W., Pedersen, T. F. and Zhang, R. (2007). Large fluctuations of dissolved oxygen in the Indian and Pacific oceans during Dansgaard-Oeschger oscillations caused by variations of North Atlantic Deep Water subduction, *Paleoceanography* **22**.

Schott, F. A., Dengler, M. and Schoenefeldt, R. (2002). The shallow overturning circulation of the Indian Ocean, *Progress in Oceanography* **53**(1): 57–103.

Schott, F. A. and McCreary, J. P. (2001). The monsoon circulation of the Indian Ocean, *Progress in Oceanography* **51**(1): 1–123.

Schulz, H. (1998). Correlation between Arabian Sea and Greenland climate oscillations of the past 110,000 years, *Nature* **393**(May): 23–25.

Shackleton, N. J. (1967). Oxygen isotope analyses and pleistocene temperatures re-assessed, *Nature* **215**: 15–17.

Shackleton, N. J., Hall, M. A. and Vincent, E. (2000). Phase relationships between millennial-scale events 64,000-24,000 years ago, *Paleoceanography* **15**(6): 565–569.

Siddall, M. and Rohling, E. J. (2008). Marine isotope stage 3 sea level fluctuations: data synthesis and new outlook, *Reviews of Geophysics* **46**(4): 1–29.

Singh, A., Jung, S., Darling, K., Ganeshram, R., Ivanochko, T. and Kroon, D. (2011). Productivity collapses in the Arabian Sea during glacial cold phases, *Paleoceanography* **26**(3): 1–10.

Sirocko, F., Garbe-Schönberg, D., McIntyre, A. and Molfino, B. (1996). Teleconnections between the subtropical monsoons and high-latitude climates during the last deglaciation, *Science* **272**(April): 2–5.

Sloyan, B. M. and Rintoul, S. R. (2001). Circulation, Renewal, and Modification of Antarctic Mode and Intermediate Water, *Journal of Physical Oceanography* **31**(4): 1005–1030.

Toole, J. M. and Warren, B. A. (1993). A hydrographic section across the subtropical South Indian Ocean, *Deep-Sea Research Part I* **40**(10): 1973–2019.

Vinther, B. M., Clausen, H. B., Johnsen, S. J., Rasmussen, S. O., Andersen, K. K., Buchardt, S. L., Dahl-Jensen, D., Seierstad, I. K., Siggaard-Andersen, M. L., Steffensen, J. P., Svensson, A., Olsen, J. and Heinemeier, J. (2006). A synchronized dating of three Greenland ice cores throughout the Holocene, *Journal of Geophysical Research Atmospheres* **111**(13).

Wang, Y. V., Leduc, G., Regenberg, M., Andersen, N., Larsen, T., Blanz, T. and Schneider, R. R. (2013). Northern and southern hemisphere controls on seasonal sea surface temperatures in the Indian Ocean during the last deglaciation, *Paleoceanography* **28**(4): 619–632.

Warren, B. A. (1978). Bottom water transport through the Southwest Indian Ridge, *Deep Sea Research* **25**(3): 315–321.

Wilson, D. J., Piotrowski, A. M., Galy, A. and McCave, I. N. (2012). A boundary exchange influence on deglacial neodymium isotope records from the deep western Indian Ocean, *Earth and Planetary Science Letters* **341-344**: 35–47.

You, Y. (1997). Seasonal variations of thermocline circulation and ventilation in the Indian Ocean, *Journal of Geophysical Research: Oceans* **102**(C5): 10391–10422.

You, Y. (1998). Intermediate water circulation and ventilation of the Indian Ocean derived from water-mass contributions, *Journal of Marine Research* **56**: 1029–1067.

Chapter 5

Regional and temporal water mass variability in the Indian Ocean over the last 40kyr

5.1 Introduction

Circulation in the world ocean is crucial for Earth's climate because it facilitates energy redistribution around the globe. Surface and subsurface circulation in the ocean is part of the so-called global thermohaline circulation (Broeker; 1991), linking seawater flow between ocean basins on a global scale (Figure 5.1). Through time, significant changes in surface and subsurface circulation have occurred along with changes in the Earth's climate system. The majority of paleoceanographic work has been carried out in the Atlantic sector of the world ocean. Here, two main deep/bottom water masses prevail in the modern ocean that are relevant with regard to circulation in the abyssal Indian Ocean. North Atlantic deep water (NADW) is formed in the Labrador Sea and the Greenland-Iceland-Norwegian (GIN) Sea whereas Antarctic Bottom Water (AABW) is predominantly formed in the Weddell Sea. At intermediate water depth, Antarctic Intermediate Water (AAIW), sourced in the southern hemisphere occupies large parts of the intermediate depth

South Atlantic Ocean. AAIW does not penetrate far into the North Atlantic.

In tune with long- and short-term changes in Earth's climate, substantial water mass reorganizations occurred in the deep Atlantic Ocean on glacial to interglacial time-scales (Bickert and Mackensen; 2004; Duplessy et al.; 1988; Lynch-Stieglitz; 2017; Sarnthein et al.; 1994) with AABW being generally more dominant during glacial periods. The unearthing of the so-called Dansgaard-Oeschger (DO) events from ice core data (Dansgaard et al. 1984; short lived millennial-scale warmings occurring during the last glacial period) stimulated new research based on deep sea sediments. This initiative gained further momentum from the subsequent discovery of an out of phase occurrence of these millennial-scale climate oscillations between the poles (bipolar seesaw; Blunier et al. 1998; Barbante et al. 2006). Sediment-based work established that deep and intermediate water flow in the Atlantic Sector varied substantially at the millennial-scale, suggesting a crucial role of seawater flow at depth in millennial-scale climate change. Significant change occurred in the North Atlantic where NADW formation appears to have fluctuated at the millennial-scale, with cold periods generally showing a slowdown of the overturning circulation (Jung; 1996; Lynch-Stieglitz; 2017; Sarnthein et al.; 1994). During maximum cold conditions in the North Atlantic, when iceberg armadas travelled the North Atlantic Ocean (known as Heinrich events), NADW formation largely ceased (Jung; 1996; Lynch-Stieglitz; 2017; McManus et al.; 2004; Sarnthein et al.; 1994; Vidal et al.; 1997).

In contrast to the wealth of data available for the Atlantic Sector, the role of variations in intermediate and deep water flow in the Indian Ocean in relation to changes in Earth's climate has received little attention. The limited number of available studies document changes in deep water flow on glacial-interglacial time scales (Curry et al.; 1988; McCave et al.; 2005; McCorkle et al.; 1998) that are to some degree in line with Atlantic Ocean data suggesting more advection of southern hemisphere sourced water. This change being more dominant in the western

Indian Ocean. This change does not seem to have been uniform across the Indian Ocean, but details of this distribution pattern are unclear (McCorkle et al.; 1998).

With regard to changes in the intermediate depth water column, a recent study suggested that glacial AAIW repeatedly penetrated across the Indian Ocean, recorded as short periods of increased intermediate water oxygenation in the Arabian Sea (Jung and Kroon; 2011; Jung et al.; 2009). These periods coincided with Heinrich events in the North Atlantic. This finding is in line with the earlier discovery that AAIW in the southwestern Pacific Ocean varied in a similar fashion (Pahnke and Zahn; 2005), with enhanced AAIW flow during Heinrich events. With regard to the Arabian Sea, new data from off-shore Tanzania have been used to question the proposed expanded glacial AAIW scenario for the Arabian Sea and a southern sourced deep water has been envisaged to have affected the Arabian Sea record (Romahn et al.; 2014).

The main aim of this study is to further evaluate the findings from the Arabian Sea in the wider context of subsurface changes in the Indian Ocean. Based on high-resolution stable oxygen and carbon isotope data from a set of new sediment cores retrieved from the sea bed off Tanzania, our data enable a better assessment of the origin of the oxygenation pulses in the Arabian Sea, that either reflect local changes in intermediate water properties, or indeed bear evidence of a larger, Indian Ocean wide expansion of glacial AAIW. The new data will be combined with published data to assess modes of ocean circulation in the Indian Ocean over the past 40kyr.

Specifically this study will address two issues: the spread and vertical extent of glacial AAIW during Hienrich events, and; changes in Indian and Southern Ocean ventialation across the deglacial period and possible teleconnection pathways to explain the observed δ^{13}C patterns in the Indian Ocean.

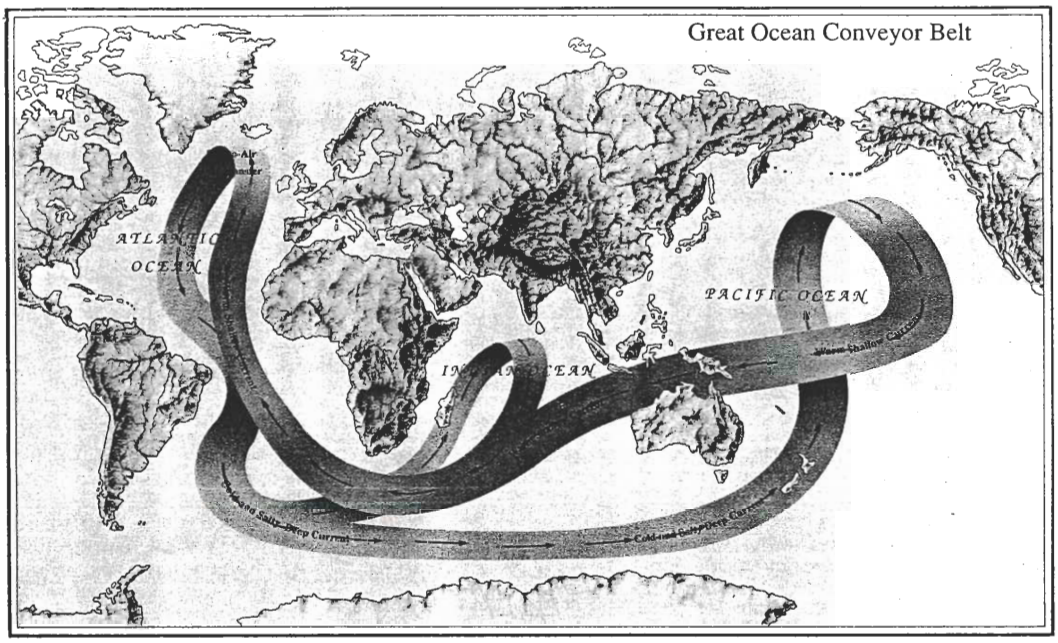

FIGURE 5.1: Great Ocean Conveyor logo (taken from Broeker 1991)

5.2 Modern intermediate to bottom water flow in the Indian Ocean

Due to the absence of deep overturning circulation in the northern Indian Ocean, intermediate to bottom water mass renewal in the Indian Ocean is facilitated by advection from the south. The flow of bottom and deep water in the Indian Ocean is guided by the bottom topography (compare Figure 5.2 & 5.3). With the exception of the southeastern part, deep and bottom water in the Indian Ocean originate from Circumpolar Deep Water (CDW), itself comprising Lower CDW (LCDW) and Upper (UCDW). In general, CDW circling Antarctica represents a mixture of waters of Atlantic, Indian, Pacific and off-Antarctic origin (see summaries in Mantyla and Reid 1995 & Srinivasan 1999). NADW and AABW are the main contributors to LCDW, whereas UCDW is a mix of Indian and Pacific common waters (for a summary see Srinivasan 1999). Salinities and temperatures are generally slightly

higher in UCDW compared to LCDW, whereas oxygen concentrations are slightly higher in LCDW. These property differences are reflected in the temperature, salinity and oxygen profiles in Figures 5.4, 5.5 & 5.6, in particular at the southern end of all north-south oriented sections. Albeit somewhat less obvious due to the lower sample density, the distribution of carbon isotope data supports this distribution pattern in the modern ocean. In areas of higher/lower oxygen concentrations close to Antarctica, a similar distribution pattern of higher/lower carbon isotope values is shown in Figure 5.7.

CDW propagates northward in the Indian Ocean via two main passages (Figure 5.3). In the west, CDW travels northward through the Crozet Basin and passes via cracks in the South Indian Ridge into the Madagascar Basin (Srinivasan; 1999). Passing on the eastern side of Madagascar into the Mascarene Basin, CDW spills into the Somali Basin via the Amirante Passage. Parts of CDW cross the Carlsberg Ridge and enter the Arabian Basin (Figure 5.3). The second main pathway for deep and bottom water resides in the eastern Indian Ocean. CDW spreads northward east of the Southeast Indian Ridge (Figure 5.3). Subsequently, generally flowing in a northwesterly direction, CDW splits in two branches near the southwestern end of Broken Plateau (Figure 5.2). As part of the western branch, CDW flows along the Central Indian Ocean Ridge until it reaches the southern tip of the Chagos-Laccadive Ridge where it splits into three parts (see Srinivasan (1999) for summary). Parts of the CDW travel into the Somali basin, another part ventures northward between the Carlsberg and the Chagos-Laccadive Ridges to end up in the Arabian Basin, where it mixes with CDW having initially travelled northward via the Crozet Basin. In particular within the UCDW layer, due to en-route mixing with other water masses and interaction with sediments, seawater properties change. In the northern Indian Ocean, this continued change in properties gives rise to the Northern Indian Ocean deep water (NIDW), having substantially lower oxygen concentrations than both, LCDW and UCDW (McCave et al.; 2005;

Srinivasan; 1999). This general lowering in oxygen concentrations is reflected in all transects in Figure 5.6, showing lowest values in deep and bottom waters prevailing in the northern Indian Ocean. NIDW flows southward via the Amirante Passage (McCave et al.; 2005) leading to recirculation in the Mascarene Basin (yellow arrows in Figure 5.3).

CDW flowing along the third branch, after splitting near the southern tip of the Chagos-Laccadive Ridge, continues to travel northward in the Central Indian Basin en-route to the Bay of Bengal. The eastern branch of the initial split off, flows around Broken Plateau, and most of this water continues to flow northward eastward of 90 East Ridge (Figure 5.3; Mantyla and Reid 1995; Srinivasan 1999). Small amounts of this water spill over into the Central Indian Ocean near the northern end of Broken Plateau and further to the North, via cracks in the 90 East Ridge.

Whilst bottom and deep water in most parts of the Indian Ocean is a mixture of multiple water masses, close to South Africa NADW proper prevails at a core depth of 2500m (Mantyla and Reid; 1995; Reid and Lynn; 1971). NADW enters the Indian Ocean close to the South African coast, heading northward through the Mozambique Channel. Here, it is trapped by the relatively shallow Davie Ridge blocking the northward flow of most of the NADW (Grundlingh et al.; 1991; Srinivasan; 1999). Recent studies have, however, suggested that a portion of modern NADW might cross the Davie Ridge northward (van Aken et al.; 2004).

Above the deep water layer, there are two principle southern hemisphere sourced intermediate water masses. AAIW and Sub Antarctic Mode Water (SAMW) enter the Indian Ocean at several locations in an intermediate water depth. AAIW-formation in the modern ocean primarily occurs in the southeastern Pacific and the southwestern Atlantic Oceans (Sloyan and Rintoul; 2001) and involves mixing of cold and fresh Antarctic surface waters with NADW shoaling off Antarctica. SAMW is formed during winter north of the Antarctic Circumpolar Current (ACC). Both AAIW and SAMW, entrained in the ACC, reach the Indian Ocean where they

flow northward. SAMW and AAIW entering the Indian Ocean in the west is entrained in the intense recirculation related to the Agulhas retroflection (Sloyan and Rintoul; 2001). SAMW and AAIW travelling northward in the Perth Basin become involved in the subtropical gyre circulation. In both regions SAMW and AAIW increasingly become warmer and saltier. In general, AAIW and SAMW are characterised by a large range of T and S properties (δTemp AAIW: <3-<6°C, δTemp SAMW: ∼6-12°C; δSal AAIW: 34.2-34.5 PSU, δSal SAMW: 34.25-35 PSU; Sloyan and Rintoul 2001). In comparison with the underlying NADW or UCDW, AAIW and SAMW are less saline. With regard to temperature differences the lowest temperatures in AAIW are similar to those found in NADW or UCDW, whereas temperatures in SAMW are slightly higher. Both, AAIW and SAMW are characterised by higher oxygen concentrations than the underlying UCDW, but have lower oxygen concentrations than the NADW prevailing in the deep southeastern Indian Ocean (Figure 5.6). Currently, neither SAMW nor AAIW occurs in the Arabian Sea (McCarthy and Talley; 1999).

In addition to the southern sourced intermediate waters, regionally important intermediate water formed in the Red Sea can be traced along the coast of Africa down into the Mozambique Channel (Beal et al.; 2000). In the light of a lowered glacial sea level it is unlikely that Red Sea Water contributed significant amounts of water to the intermediate water layer in the Indian Ocean between 60-15ka. As a consequence of the rising sea level during Termination 1, however, when climate transitioned toward the modern warm period, an increasing influence at the sites of the new sediment cores used in this study is possible.

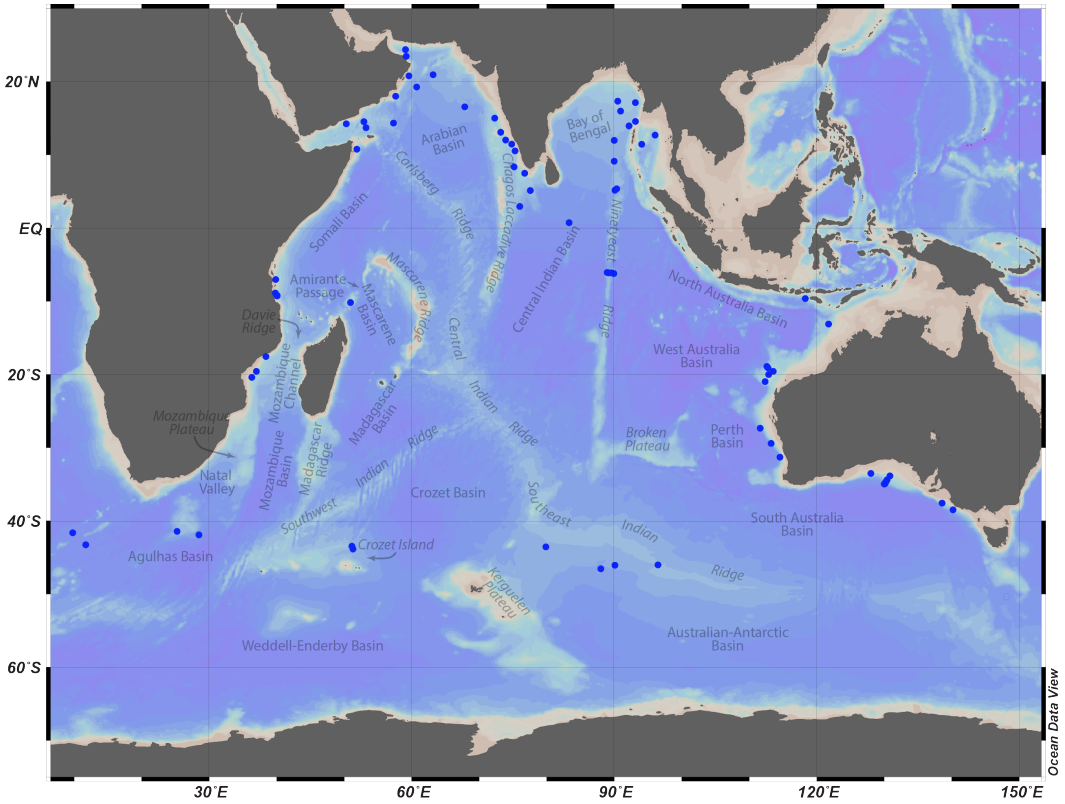

FIGURE 5.2: Map of the Indian Ocean and adjacent areas showing bathymetry features referred to in the text

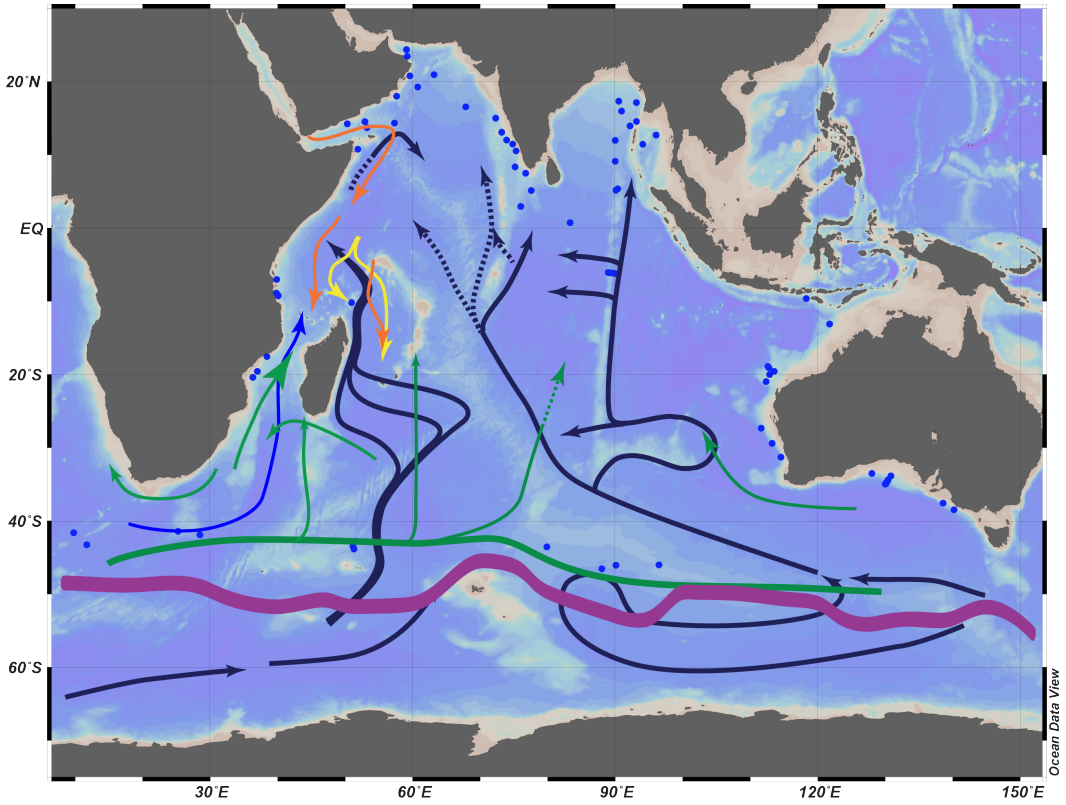

FIGURE 5.3: Map of the Indian Ocean and adjacent areas showing main modern subsurface currents (black = CDW, blue = NADW, green = SAMW/AAIW, red = RSW, yellow = IODW, purple = ACC)

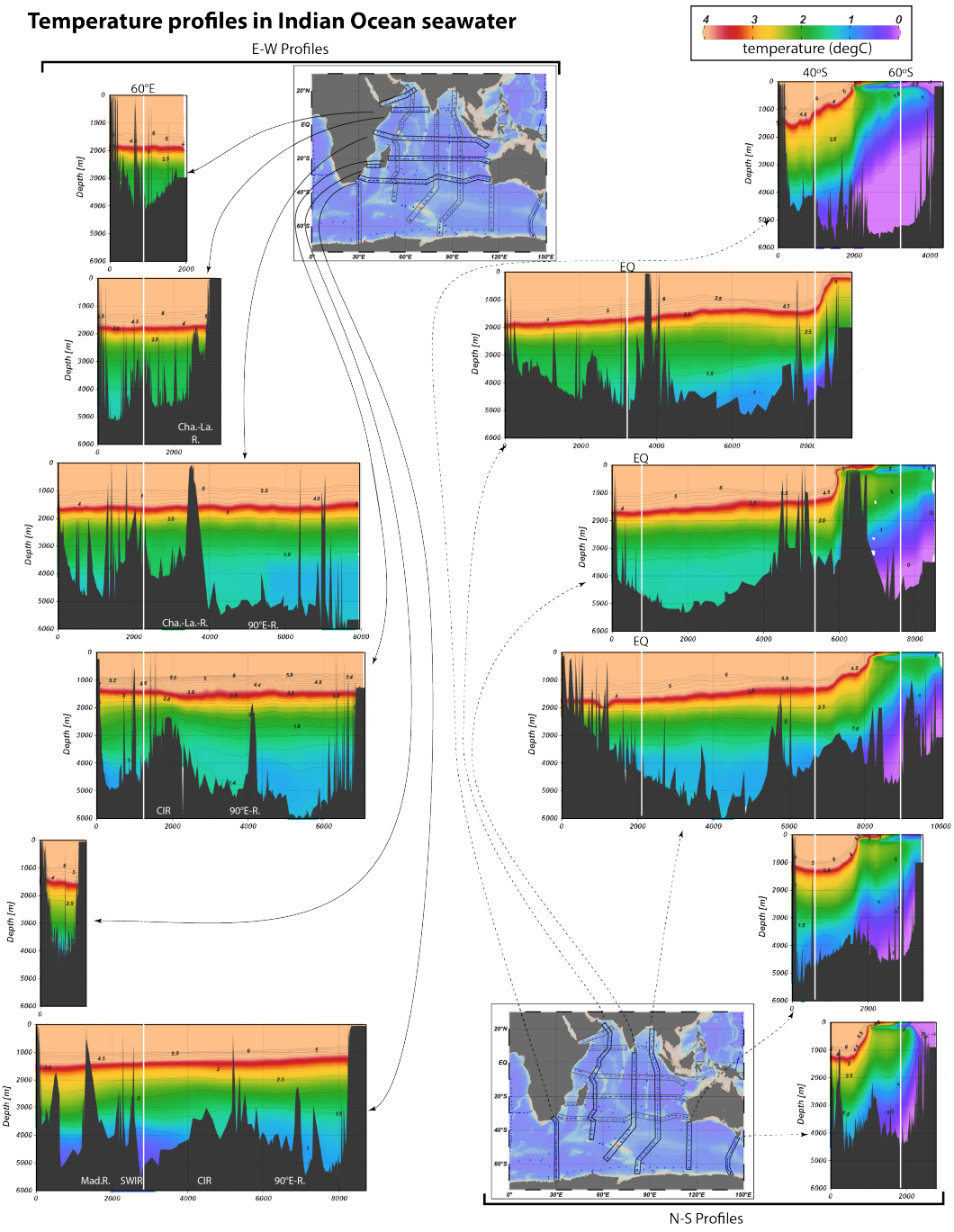

FIGURE 5.4: Overview of seawater temperature in the Indian Ocean. The world ocean data atlas 2013 was used. The data were plotted with the Oceandataview software (version 4).

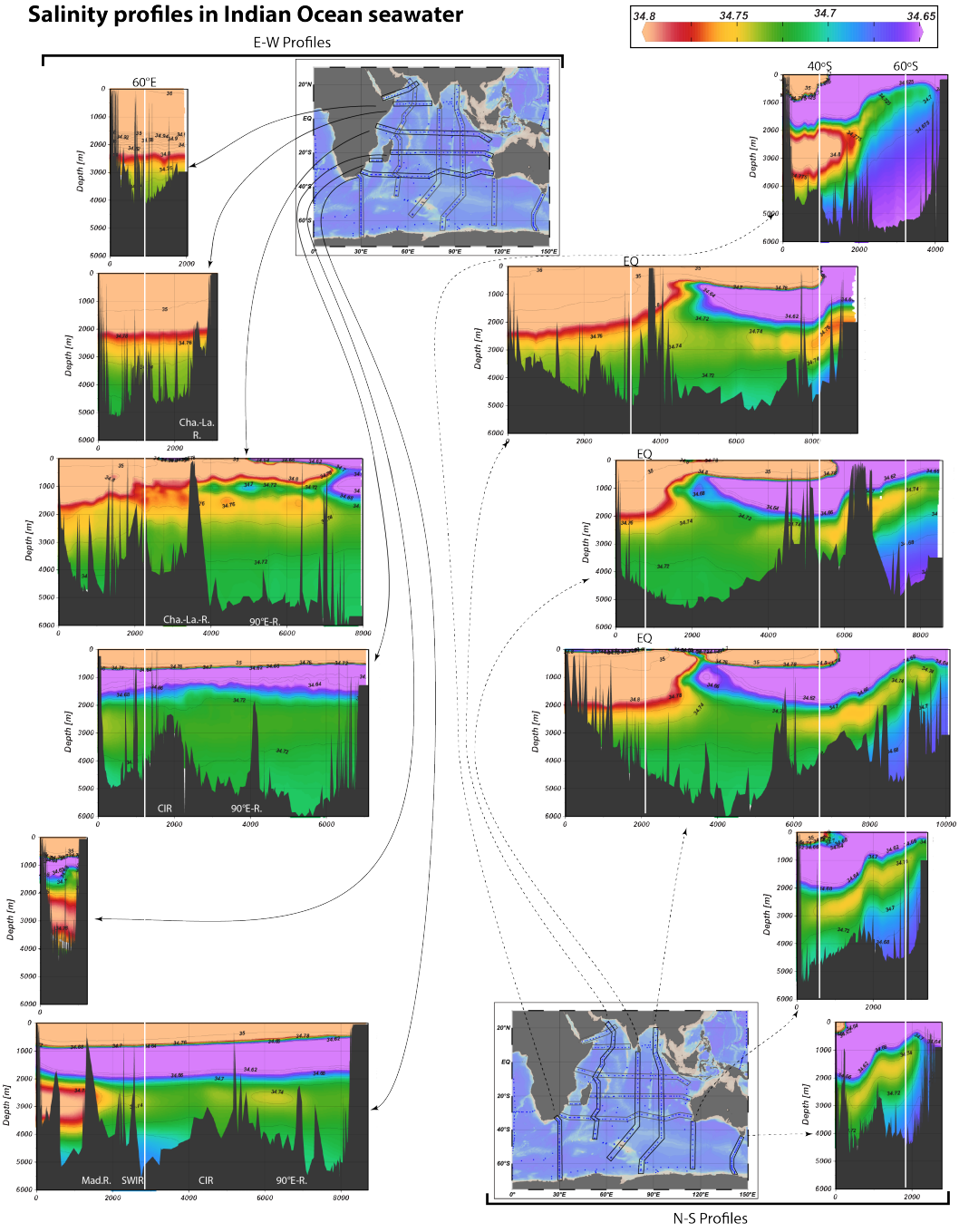

FIGURE 5.5: Overview of seawater salinity in the Indian Ocean. The world ocean data atlas 2013 was used. The data were plotted with the Oceandataview software (version 4).

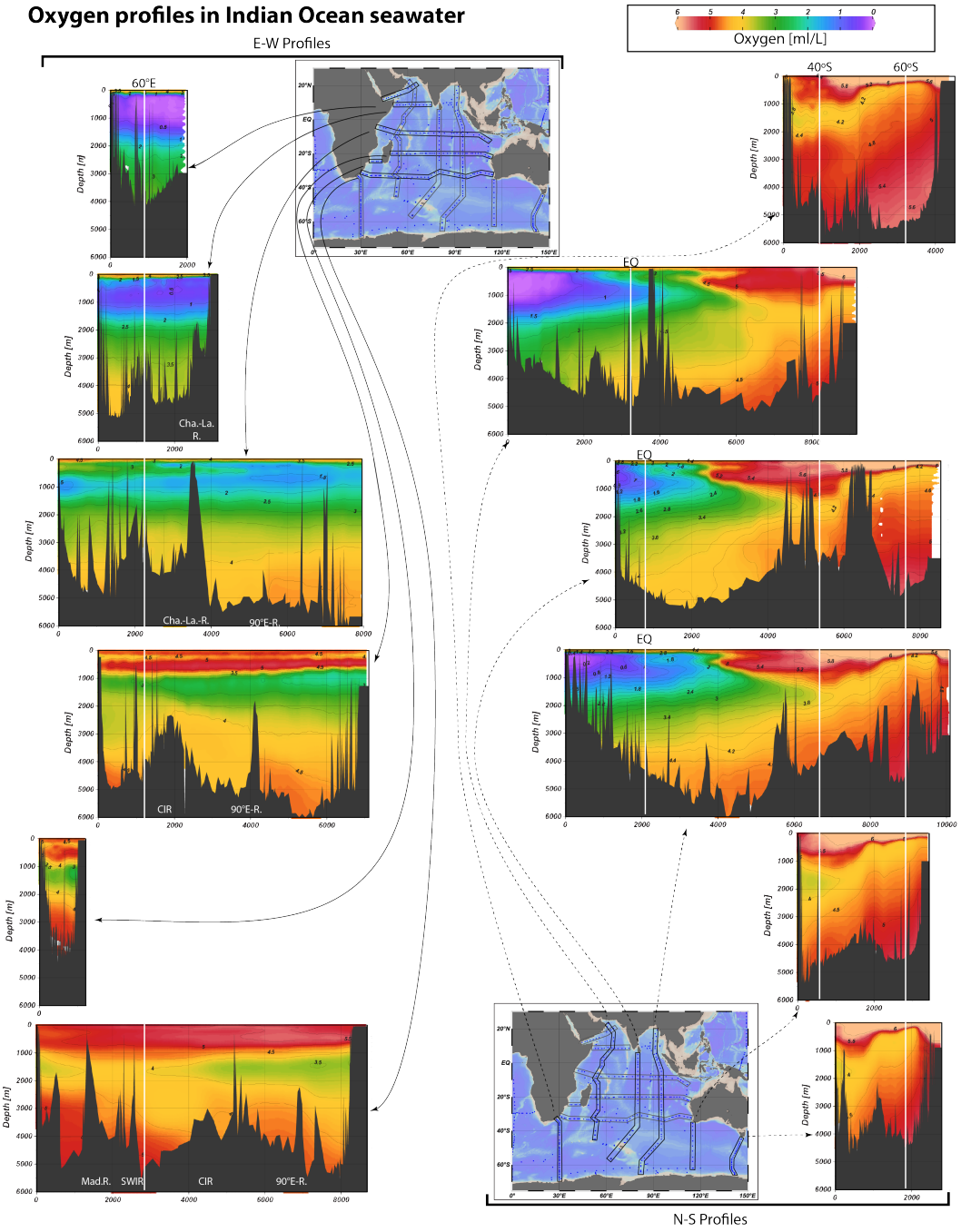

FIGURE 5.6: Overview of seawater oxygen concentration in the Indian Ocean. The world ocean data atlas 2013 was used. The data were plotted with the Oceandataview software (version 4).

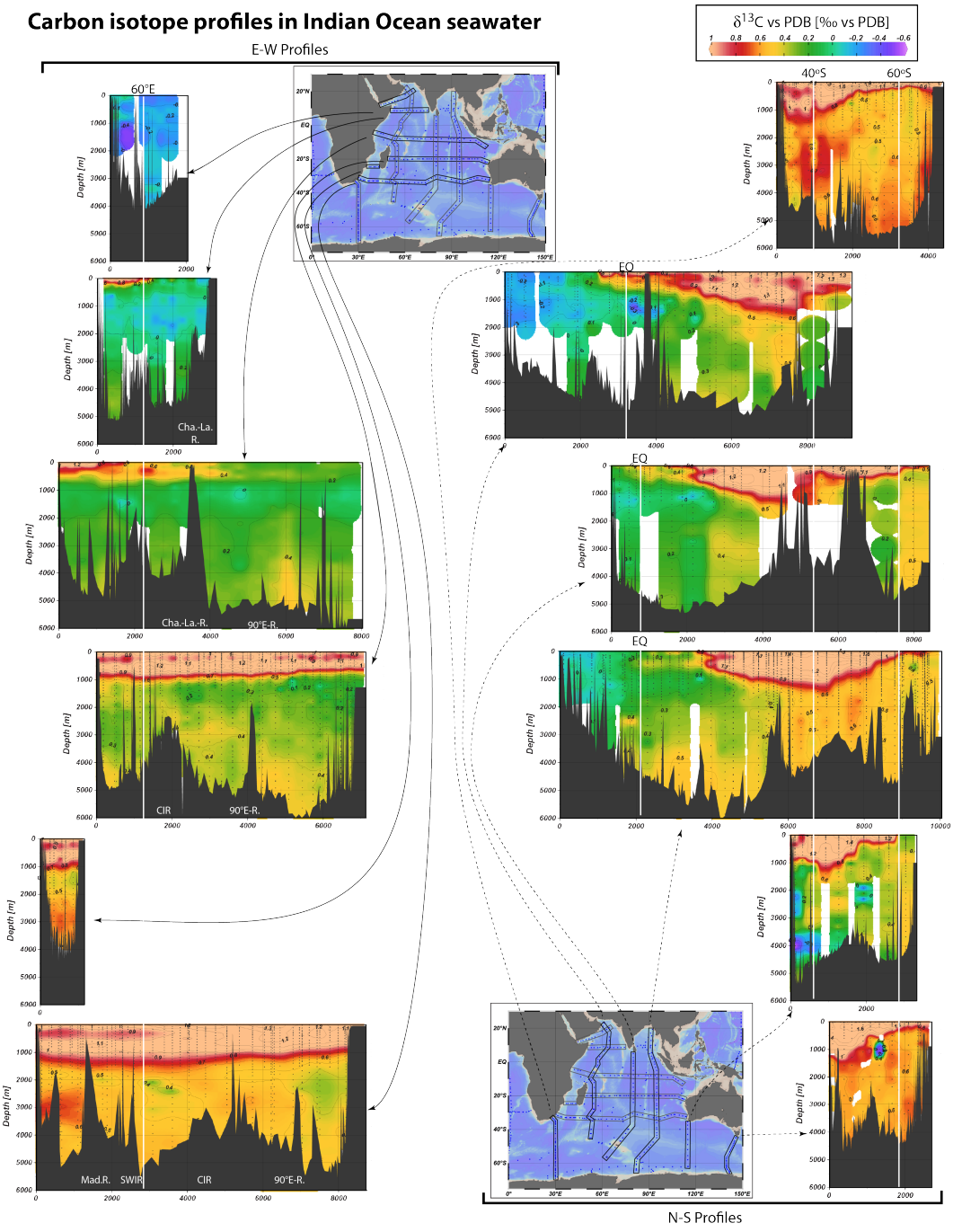

FIGURE 5.7: Overview of seawater carbon concentration in the Indian Ocean. The world ocean data atlas 2013 was used. The data were plotted with the Oceandataview software (version 4).

5.3 Methods

5.3.1 Epibenthic stable isotope data

In order to reconstruct seawater properties through the water column we exclusively rely on stable oxygen and carbon isotope data of epibenthic foraminifera, in line with Zahn et al. (1986). This approach utilizes the fact that epibenthic foraminifera live above the sediment surface (Lutze and Thiel; 1989), in contrast to endobenthic foraminifera living in the sediment. Due to their habitat, stable isotope data of endobenthic foraminifera primarily reflect properties of the ambient pore waters in deep sea sediments, not allowing a reconstruction of bottom water conditions. Only under specific circumstances, triggered by excess oxidation of increased flux of organic material raining down from the surface ocean, may epibenthic foraminifera record bottom water properties in a similarly unfaithful fashion (Gottschalk et al.; 2016; Mackensen et al.; 1993). Generally, epibenthic foraminifera reflect properties of the prevailing seawater above the sediment surface and are therefore widely used for reconstructions of water properties in deep and bottom waters.

5.3.2 New sediment cores from the sea bed off Tanzania

Sediment cores 64PE303-15, 64PE303-16 and 64PE304-8 were retrieved along a water column transect off Tanzania. Details on the location and water depth are in Table 5.1. All sediment cores were sampled in 1cm steps. For this study, the top sections of all three cores, covering 40-50ka, were analyzed in detail by measuring stable isotopes at 1-2cm sample spacing. Deeper sections of each core were analyzed at greater sample spacing. The samples were wet-washed over a 63μm screen and the coarse fraction used for picking foraminifera. For this study 2-3 specimens of the epibenthic foraminifera *C. wuellerstorfi* were extracted for stable oxygen and

carbon isotope analysis. Subsequent sample preparation followed standard techniques. Measurements were carried out on a Thermo Delta$^+$ Advantage mass spectrometer linked to a Kiel Carbonate III automated extraction line. The resulting stable isotope data are reported relative to the Vienna Pee Dee Belemnite with calibration being based on in-house standards that are correlated to the international standard NBS-19. For both $\delta^{18}O$ and $\delta^{13}C$-measurements, the analytical precision is better than $\pm 0.1‰$. The age models for all three cores are based on radiocarbon dates (details are provided in chapter 2).

TABLE 5.1: Location and depth's of sediment cores used in this study

Sediment Core	**Longitude**	**Latitude**	**Water depth**	**Data source**
64PE303-15	39.8220	-9.0125	1987	this study
64PE303-16	39.7295	-8.9703	1309	this study
64PE304-8	39.6655	-8.9505	752	this study
GeoB12615	39.8408	-7.1383	446	Romahn et al. (2014)

5.4 Results

5.4.1 Time series results for cores 64PE304-8, 64PE303-16 and 64PE303-15

The stable isotope data for core 64PE303-15, 64PE303-16 and 64PE304-8 are presented in Figure 5.8. The oxygen isotope records of all three cores show the ice volume driven increase in values towards the end of the LGM. It is interesting to note that the two deeper sites 64PE303-15/16 show a decrease in oxygen isotopes prior to Heinrich event 1, whilst the timing of the onset of Termination 1 in core 64PE304-8 appears to roughly coincide with Heinrich event 1. A firm statement is unfortunately hampered by the lack of the data in this core for most of the LGM. Superimposed on these long-term changes, there are numerous minimum spikes in

all three records. Generally, pronounced minimum spikes occur along with maximum cold conditions in the North Atlantic in core 64PE303-16 (Heinrich event 1,2,4 and less pronounced at Heinrich event 3). These Heinrich events are reflected by generally smaller minimum spikes in deeper core 64PE303-15, which does, however, show a strong oxygen isotope minimum related to Heinrich event 5. The record of the shallowest site 64PE304-8, shows a mixed signal. Heinrich events 1, 3 & 5 appear to be linked to small oxygen isotope minima, whereas Heinrich events 2 & 4 occur alongside small increases in oxygen isotope values.

With regard to the carbon isotope time series, both deeper cores (64PE303-15/16) differ substantially from the record of shallowest site 64PE304-8 (Figure 5.8). Long term minima in carbon isotope values broadly center around 24ka, around 35ka and around 44-46ka (core 64PE303-15). Long-term maximum spikes occur in both cores around 16-18ka and around 28-30ka (Figure 5.8). In addition, generally high values occur in both cores during the Holocene. Superimposed on these long-term trends, millennial-scale variability is documented in both records. Maximum spikes occur in cores 64PE303-15/16 during Heinrich events 1-3. There are also carbon isotope maximum spikes in both cores at Heinrich event 4. In core 64PE303-16, however, this event appears as a double spike, with a central carbon isotope minimum. It is interesting to note generally more pronounced carbon isotope maxima residing with intermediate water site 64PE303-16.

The carbon isotope data for shallow site 64PE304-8 substantially differs from those for the two deeper sites. Long-term maxima broadly center around 28-32ka, 35-36ka. Following a substantial drop in carbon isotope values of $\sim$0.7‰, carbon isotope values increase between 12-13ka and the topmost section of this core, a trend broadly in line with the change in deeper sites 64PE303-15 and 64PE303-16. Long-term minima in core 64PE304-8 center around 24-26ka, around 37-39ka and around 50-52ka. In contrast to both deeper sites the superimposed millennial-scale change in core 64PE304-8 generally manifests as minimum spikes occurring during

Heinrich events. A possible exception is a one data point based maximum spike at Heinrich event 1.

5.5 Discussion

The main findings in this work allow an evaluation of rapid changes in the water column structure off Tanzania.

5.5.1 Changes in water mass prevalence off Tanzania during MIS 3, 2 and the Holocene

Whilst changes in NADW and AABW - being the major water masses prevailing in abyssal regions of the world ocean - have been intensely studied, changes in the intermediate to upper deep water layer have received little attention. Since the discovery of an unexpected rapid change in AAIW propagating in the southeastern Pacific ocean (Bostock et al.; 2013; Pahnke and Zahn; 2005), more attention has been given to a better understanding of changes at this water level in relation to short and long term climate change. In line with the Pacific data, benthic carbon isotope data from the intermediate water/upper deep water boundary indicate short periods of enhanced glacial AAIW propagation into the Arabian Sea (Jung and Kroon; 2011; Jung et al.; 2009). The respective oxygen isotope records aid the view of a relatively warm and expanded AAIW that may temporarily store energy, as part of the inter-hemispheric temperature imbalance associated with the bipolar seesaw (Jung et al.; 2009). This view was criticized in recent work by Romahn et al. (2014) proposing an alternative interpretation of the intermediate water benthic records for both the Arabian Sea and the Pacific Ocean. Rather than expanded glacial AAIW being record in those sediment cores, a form of CDW is advocated as the likely cause for the stable isotope records in both areas. Based on the new data presented for cores

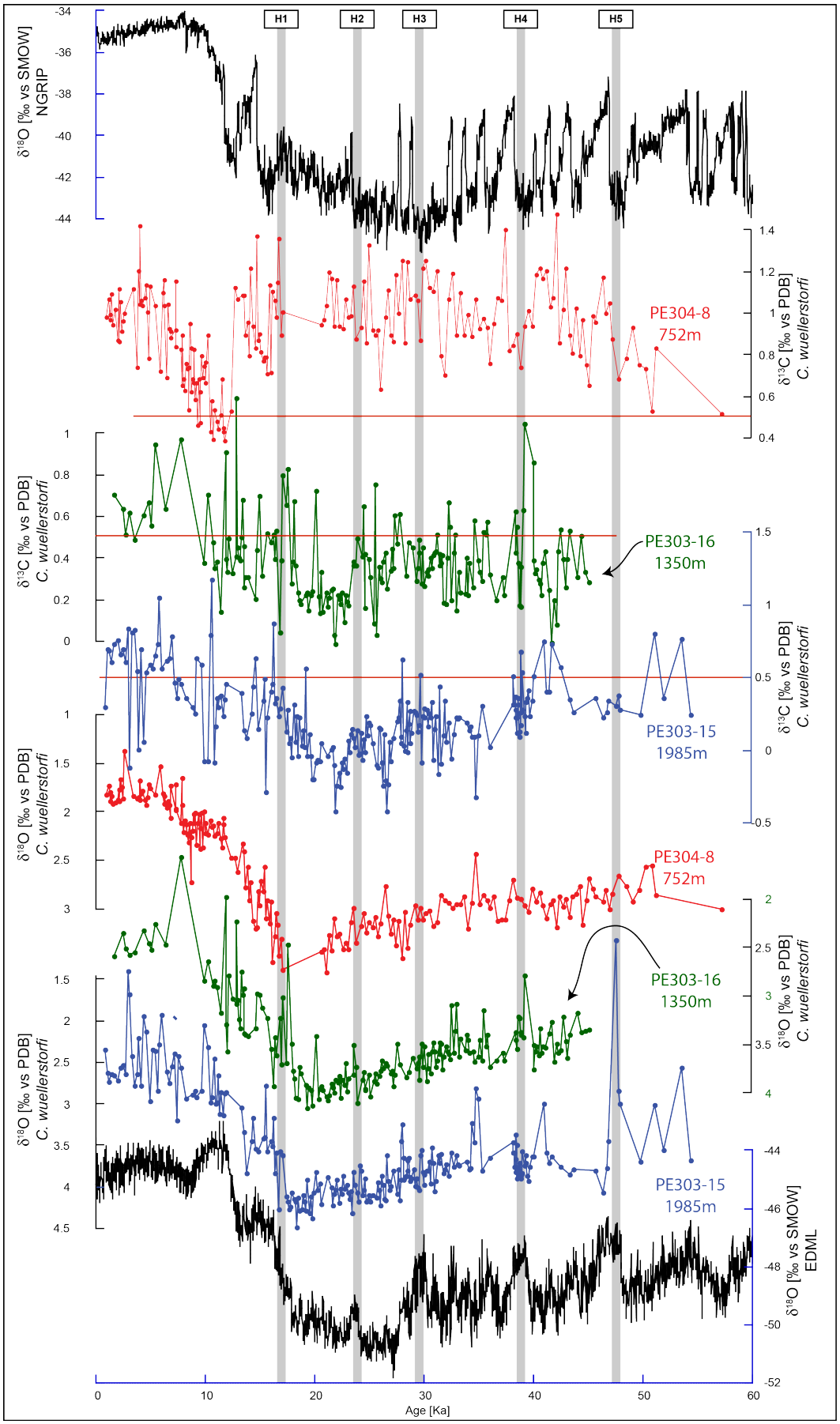

FIGURE 5.8: Stable oxygen and carbon isotopes from epibenthic foraminifera for cores 64PE303-15, 64PE303-16 and 64PE304-8. Stable oxygen isotope records for the Greenland NGRIP and the Antarctic EDML ice cores are plotted for comparison (see Vinther et al. 2006; Rasmussen et al. 2006; Andersen et al. 2006; Wolff et al. 2010 for details).

64PE303-15/16 and 64PE304-8 a new assessment of changes in the water mass distribution through time is possible. We find evidence that broadly supports the data of Jung et al. (2009) that suggests expanded glacial AAIW during Heinrich events.

In order to better visualize changes in carbon isotope distribution patterns off Tanzania, we use a water column-time transect (Figure 5.9) that includes the carbon isotope data from the new cores presented in this study, the benthic carbon isotope data from Romahn et al. (2014) and the respective data from nearby core WIND28k (McCave et al.; 2005). Figure 5.9 was constructed using the Ocean data view gridding software. The carbon isotope data of the cores used in Figure 5.9 are positioned on the ordinate according to the retrieval depth of the sediment cores. Using these cores in this transect is straightforward for the new cores presented in this study as well as for core GeoB12615-4 (Romahn et al.; 2014) given their proximity. Core WIND28k has been retrieved from the Amirante passage, where deep and bottom water are exchanged between the Somali and the Mascarene Basin (see earlier description). Given the relatively small distance between the continental margin off Tanzania and the location of core WIND28k it is likely that no large chemical or physical gradient occurred across the deepest part of the Somali basin. Small to absent gradients in the modern water mass profiles in figures 5.5, 5.6 & 5.7 support this view. Hence, it is a justifiable assumption that the change recorded in core WIND28k is a reflection of changes in water properties near the base of the continental margin off Tanzania.

Figure 5.9 reveals a number of notable changes in the distribution pattern of carbon isotopes over the last 60ka. It is important to note that for most of the time covered, the carbon isotope values in both shallow cores (64PE304-8 and GeoB12615-4) are fundamentally different than the values deeper in the water column, implying that both cores largely record near surface water signal rather than intermediate to deep-water signal. The only notable exception is recorded around 10-12ka, where values closer to those recorded at depth are displayed for both shallow cores in

Figure 5.9. The cause of this anomaly will be discussed below.

The changes in the intermediate to deep water sections in Figure 5.9 reflect changes in the mix of waters traveling as LCDW/UCDW/NIDW or, assuming that some portions can cross the Davie Ridge, a direct recording of NADW (sensu van Aken 2007). Overall, there is a long-term change in the carbon isotope gradient between cores 64PE303-15/16 and WIND28k. During early MIS3, carbon isotope values in core WIND28k are generally slightly lower than in cores 64PE303-15/16. Superimposed on this long-term difference, sporadic carbon isotope maxima in cores 64PE303-15/16 result in enhanced $\delta^{13}C$ gradients between mid-depth and abyssal parts of the water column off Tanzania, indicating a reversed carbon isotope gradient compared to today. Towards the end of MIS3 and culminating in MIS2, there is a general decrease in carbon isotope values in both, core 64PE303-15/16 and core WIND28k. Occasionally, there are periods when the water column was homogenized from intermediate to bottom depths. Periods of low carbon isotopes prevailing are centered at (weakly defined) 32-33 ka, 26-27 ka and 20 ka. Periods with high carbon isotopes prevailing occurred at 28 ka and 34 ka. There are also short periods with low carbon isotope values only occurring in core WIND28k at 29 ka, 23 ka and in pulses between 19 ka and 14 ka.

The Holocene is divided into two sections. During the early Holocene, short pulses of high carbon isotope values are recorded in core WIND28k, whereas lower values are shown in cores 64PE303-15/16. Subsequently, higher values are found in both mid-depth cores, roughly matching the values in core WIND28k during the time period of overlap. Superimposed on this long-term change are changes in carbon isotopes at the millennial scale (figure 5.9).

Assuming that modern water mass distributions prevailed throughout MIS 3, the higher oxygen concentrations and higher carbon isotope values in LCDW (Figures 5.6 & 5.7), compared to UCDW, are at odds with the carbon isotope distribution for a number of time periods covered in figure 5.9 (centered around 41-42ka,

52ka and 54ka). The generally lower carbon isotope values during MIS 3 in core WIND28K (reflecting LCDW) for example imply a less ventilated water mass prevailing in the abyssal Somali basin, compared to the overlying water. Using a scenario where all three cores (64PE303-15/16 and WIND28k) reflect either LCDW or UCDW/IODW it is difficult to explain the differences between the shallower cores and core WIND28K for the time periods given above. Some form of water mass aging, driven by oxidization of organic matter raining down from sea surface may explain the lower carbon isotope values found in core WIND28k. There is, however, no area of high primary productivity in the region that could lead to a change in bottom water carbon isotopes at site WIND28k, nor is the distance between the cores sufficiently large to allow any significant water aging to occur.

The increasing awareness that NADW might affect water mass properties north of the Davie Ridge in the modern ocean (sensu van Aken 2004) may offer an explanation for the carbon isotope distribution in figure 5.9. In a scenario of generally decreasing overturning circulation in the North Atlantic during MIS 3 (and MIS 2) along with a shoaling of glacial NADW (Jung; 1996; Sarnthein et al.; 2001), it is possible that this shoaling entailed a shallower depth of glacial NADW when approaching the Davie Ridge. In such a scenario, depending on the duration of the shoaling events in the North Atlantic, during periods with an inverted carbon isotope gradient during MIS 3, enhanced NADW would have been recorded as incursions of higher carbon isotope water masses at mid depth off Tanzania in cores 64PE303-15/16. Core Wind28k would be unaffected by glacial NADW and record LCDW.

Whilst most of the carbon isotope gradient inversions in figure 5.9 during MIS 3 may be explained by the above mechanism, MIS 2 requires a different explanation. During MIS 2, aside from during Heinrich events, NADW formed at its lowest rate (Duplessy et al.; 1988; Jung; 1996; Lynch-Stieglitz; 2017; Sarnthein et al.; 2001) with lower carbon isotopes prevailing in this water in the south Atlantic. The reduced

advection resulted in a reduced contribution of glacial NADW to LCDW (Ahmad et al.; 2008). It is therefore likely that the mixing ratio of glacial NADW and AABW changed accordingly. In addition, carbon isotope ratios in glacial AABW were also lower than in the modern ocean (Sarnthein et al.; 2001). Hence, with lowered glacial carbon isotope values occurring in two major water mass contributors it is likely that in the resulting LCDW mix lowered carbon isotope values prevailed during MIS 2. This would explain the observation of LCDW and UCDW being characterized by similar carbon isotope values, rendering a differentiation based on this proxy impossible. The carbon isotope minimum pulses during MIS 2 covering large parts of the water column may reflect such a scenario.

The generally higher carbon isotope values in prevailing in cores 64PE303-15/16 and core Wind28k during the Holocene, reflect a general change in deep ocean circulation overall similar to the modern. Superimposed onto this general change, figure 5.9 displays a subtle division with lower carbon isotope values prevailing during the early Holocene in cores 64PE303-15/16 compared to the higher values found thereafter. It is interesting to note that Jung (1996) and Sarnthein et al. (2001) found a similar subdivision during the Holocene in the North Atlantic. During the early Holocene, NADW formation peaked and likely settled deeper in the water column compared with modern type NADW formation prevailing thereafter. In a scenario of a deepened early Holocene NADW it is conceivable that this water mass also traveled at greater depth further downstream. Hence, it is likely that at that time the Davie Ridge inhibited the flow of NADW into the Somali basin. This would mean that mostly LCDW, being a mix of NADW and AABW, would record this early Holocene peak in NADW formation. This is consistent with the high carbon isotope spikes in the abyssal Indian Ocean off Tanzania in core WIND28k at this time. At mid depth, UCDW would prevail, not being affected by NADW. During the later part of the Holocene, NADW formation was less intense than during

the early Holocene (Jung; 1996; Sarnthein et al.; 2001). During this time, carbon isotope values are consistently high in cores 64PE303-15/16. Assuming the modern water masses prevailed during the late Holocene, the low carbon isotope values in the modern Indian Ocean support the notion of UCDW/NIDW being recorded in core 64PE303-15/16, probably as small proportions of shoaled NADW crossing the Davie Ridge and affected water proper- ties north of Davie Ridge.

Our findings in cores 64PE303-15/16 (particularly the latter) reflecting the intermediate to deep water section of the water column off Tanzania at the millennial scale, in line with the findings from core NIOP-905, show positive carbon isotope spikes during most Heinrich events (Figures 5.8 & 5.9). Our new shallower record 64PE304-8 does not show such a relation. Also, the carbon isotope values documented in both shallow water cores (64PE304-8 and GeoB12615-4), are substantially higher, than those found in the deeper sites for most of MIS 2 and MIS 3. This finding demonstrates that the water mass being recorded in core 64PE304-8 and above (core GeoB12615-4) is independent of water below. It is likely that both sites record changes in surface water advecting via the SEC, given that this water, near the African coast reaches a depth of roughly 1km (Chen and Wu; 2015; Schott and McCreary; 2001). In cores 64PE303-15/16 however, short periods of enhanced southern sourced intermediate to upper deep water are recorded.

Support for expanded glacial AAIW during Heinrich events recorded as positive carbon isotope spikes as originally proposed for the Arabian Sea (Jung et al.; 2009) has recently been reported for an intermediate water site in the Bay of Bengal (Delong; 2015).The collection of records in figure 5.9 enables a better assessment of the vertical extension of the carbon isotope heavy water mass. In the Arabian Sea, the Heinrich event related positive carbon isotope excursions were recorded at 1580m water depth (Jung et al.; 2009). Finding a convincing similar carbon isotope signal, compared to Arabian Sea core NIOP 905, in core in core 64PE303-16 (1350m water depth) indeed supports the notion of southern sourced water mass traveling

northwards at Heinrich events. The occurrence of carbon isotope maxima at Heinrich events in deeper site 64PE303-15 (1985 m water depth), however, implies that glacial AAIW extended downward into the upper deep water section of the glacial Indian Ocean. Estimating the vertical extension of this high carbon isotope water mass downward beyond the retrieval depth of core 64PE303-15 is difficult because there is a gap, with more than 2000m of the water column not being covered by any sediment record (figure 5.9). It is likely, however, that the vertical extension of the glacial AAIW propagating northward (sensu Jung et al. 2009), extended into the upper deep water layer beyond the retrieval depth of core PE303-15. There are differences in the expressions of Heinrich event carbon isotope maxima when comparing the records of 64PE303-15 and 64PE-303-16. Weaker carbon isotope maxima in core 64PE303-15 suggest this core being close to the boundary of the deepened glacial AAIW for example at Heinrich events 2 and 5, whereas pronounced carbon isotope maxima (e.g. Heinrich events 3 and 4) may have been recorded when glacial AAIW might have extended well below the retrieval depth of core PE303-15 (compare figures 5.8 and 5.9). Without additional cores covering the western Indian Ocean off Tanzania between 2 and 4 km water depth, a proper estimate of the extension of glacial AAIW is not possible.

With regard to the peaks in glacial AAIW formation, evidence from the early part of the deglaciation may provide clues to the processes involved. Sea surface temperatures in the Southern Ocean sites lead oxygen isotope change along with peaks in salinity during the early part of the temperature decrease (Labeyrie et al.; 1996). Whilst these findings sensu stricto reflect the changes in relation to Termination 1, they do allow some conclusion with regard to millennial-scale change, given that Termination 1 involves Heinrich event 1. Salinity peaks during southern hemisphere warm periods, as recorded in Antarctic ice core records (Barbante et al.; 2006), supports the idea of repeated periods of increased surface water densities in the sub polar Antarctic, leading to enhanced intermediate water formation. Given

the similar properties in SAMW and AAIW it is difficult to distinguish which was the main driver in the expansions of glacial southern hemisphere sourced intermediate water.

5.5.2 Indian and Southern Ocean ventilation changes across the last deglaciation

For the majority of the time period covered in Figure 5.9, the carbon isotope values shown in both shallow water cores (64PE304-8 and GeoB12615-4) are substantially higher than those found in the deeper sites. There are short spells, however, when this isotope gradient is weakened, the most notable occurring in the final part of the deglaciation around 10-12ka. There is no straightforward explanation for this change. Studies assessing the changes in ocean circulation across the last deglaciation have shown major water mass/current reorganizations in the ocean occurring in the earlier part of the deglaciation, mostly leveling off near the end of the Younger Dryas (Jung; 1996; Lynch-Stieglitz; 2017; McManus et al.; 2004; Sarnthein et al.; 1994; Vidal et al.; 1997). The carbon isotope minimum pulse in Figure 5.9 largely postdates the Younger Dryas. Hence, a straightforward explanation involving a water mass reorganization in relation to major steps in the deglacial sequence is unlikely. Recent work in relation to oxygenation in intermediate waters in the Arabian Sea offers potential clues as to the origin of the carbon isotope minimum pulse in shallow waters off Tanzania. The data imply repeated periods when old carbon dominated in the relatively shallow Arabian Sea (Bryan et al.; 2010). The latest of these events coincides with the shallow water carbon isotope minimum off Tanzania.

Three possible mechanisms are discussed in order to explain the Arabian Sea data (Bryan et al.; 2010), two of which in our view are rather unlikely when searching for an explanation that would apply to both the Arabian Sea and southeast

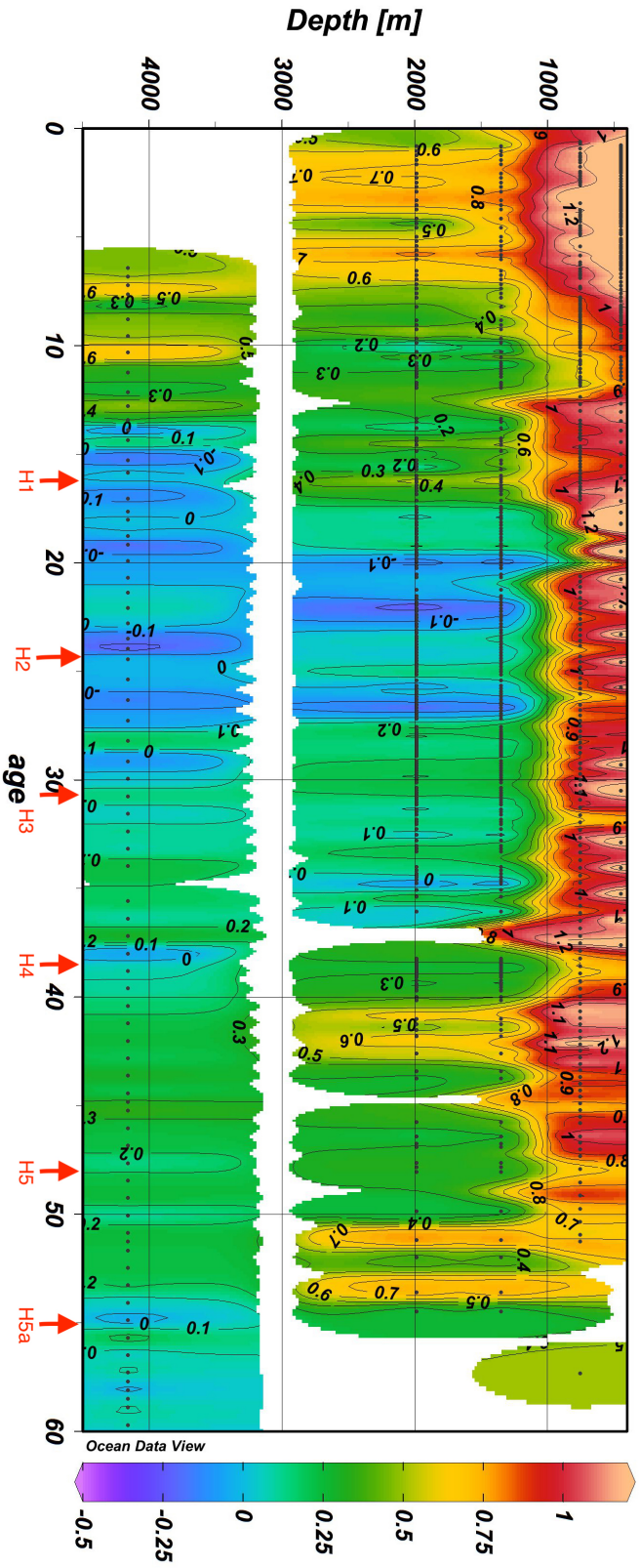

FIGURE 5.9: Water column depth/time transect of stable carbon isotope data from epibenthic foraminifera extracted from sediment cores 64PE303-15, 64PE303-16 and 64PE304-8, GeoB12615-4 and WIND28k. For data source see Table 5.1. The data were plotted using the Oceandataview software (version 4).

Africa off Tanzania. One mechanism would involve in-situ water mass aging. Water mass aging requires substantial amount of primary production driven organic matter raining down onto the seafloor. Subsequent oxidation would lead to release of CO_2 with a low carbon isotope signature that in turn would be recorded in carbon isotope minimum spikes in benthic foraminifera. Whilst the high, monsoon driven, primary production may explain the Arabian Sea data, off Tanzania relatively low primary productivity levels prevail, rendering this explanation unlikely. A second scenario involves old carbon to be released by a "geologic" event in the abyssal ocean. This carbon would subsequently invade shallow parts of the water column and be recorded as carbon isotope minimum spikes. This scenario requires deeper sites to show a stronger depletion in carbon isotope data, compared to shallower sites. The relatively high and homogenous carbon isotope data below roughly 1300m water depth, refute such a scenario.

The most likely scenario explaining the carbon isotope minimum pulse in the shallow waters off Tanzania involves advection of an "old carbon" spiked water via ocean currents. Figure 5.9 shows that across the final part of the deglaciation (<13ka), carbon isotope values in below roughly 1300m were rather homogenous. A substantial drop in carbon isotope values around 10-12ka is not recorded. Hence, the carbon isotope minimum pulse is limited to both shallow sites, reflecting the upper $\sim$750m of the water column. In addition, previous studies from the Pacific Ocean have demonstrated the repeated occurrences of old carbon-spiked waters above roughly 1100m water depth (e.g. Marchitto et al. 2007; Stott et al. 2007, 2009). Supporting evidence has also been published for the Southern Ocean ventilation during the deglaciation (Anderson et al. 2009; Figure 5.10). Periods of enhanced opal flux co-occurred with rises in CO_2 during the last deglaciation (Anderson et al.; 2009), the most recent period roughly coinciding with the shallow water carbon isotope minimum spike in figure 5.9 (cores GeoB12614-15 and 64PE304-8). Enhanced opal flux in the Southern Ocean entails the presence of chemically old

water at or near the sea surface (Anderson et al.; 2009), in principle in line with the carbon isotope minimum spikes in figure 5.9 . More recently, Siani et al. (2013) also reported periods of upwelling involving chemically old water in the South Pacific, the last of those periods being roughly synchronous with the carbon minimum spike in shallow water around 10-12ka in figure 5.9 . These combined findings demonstrate the presence of low carbon isotope water at or near the sea surface in a number of areas of the world ocean.

As argued above, the shallow water sites off Tanzania require a distant source of the low carbon isotope water. Whilst a definitive answer is not possible without better knowledge of the sub/surface flow in the western Indian Ocean, using the modern circulation patterns in the Indian Ocean as a starting point, some conclusions are possible. Water renewal at the sub/surface in the western Indian Ocean is largely driven by the SEC reaching a depth of roughly 1km in the western Indian Ocean (Chen and Wu; 2015; Schott and McCreary; 2001). Hence, both shallow sites off Tanzania reflect changes in the SEC, involving a generally southward flow near the cores used in this this study. If this flow pattern also persisted along with the recording of the carbon isotope minimum around 10-12 ka it is difficult to envisage a scenario where this carbon isotope signal traveled northward in the western Indian Ocean, against the general flow direction of subsurface water in the region. Advection of low carbon isotope water via the SEC is far more likely. If so, it suggests that the source of the old carbon events is located in the Pacific Ocean. It is conceivable that the low carbon isotope waters found in the Pacific Ocean (Marchitto et al.; 2007; Stott et al.; 2009) were entrained in the basin wide upper circulation in the Pacific Ocean, eventually contributing to ITW feeding into the SEC. This would ultimately drive the mobilization of chemically aged water masses within the Pacific Ocean, through the Indonesian through-flow and into the SEC.

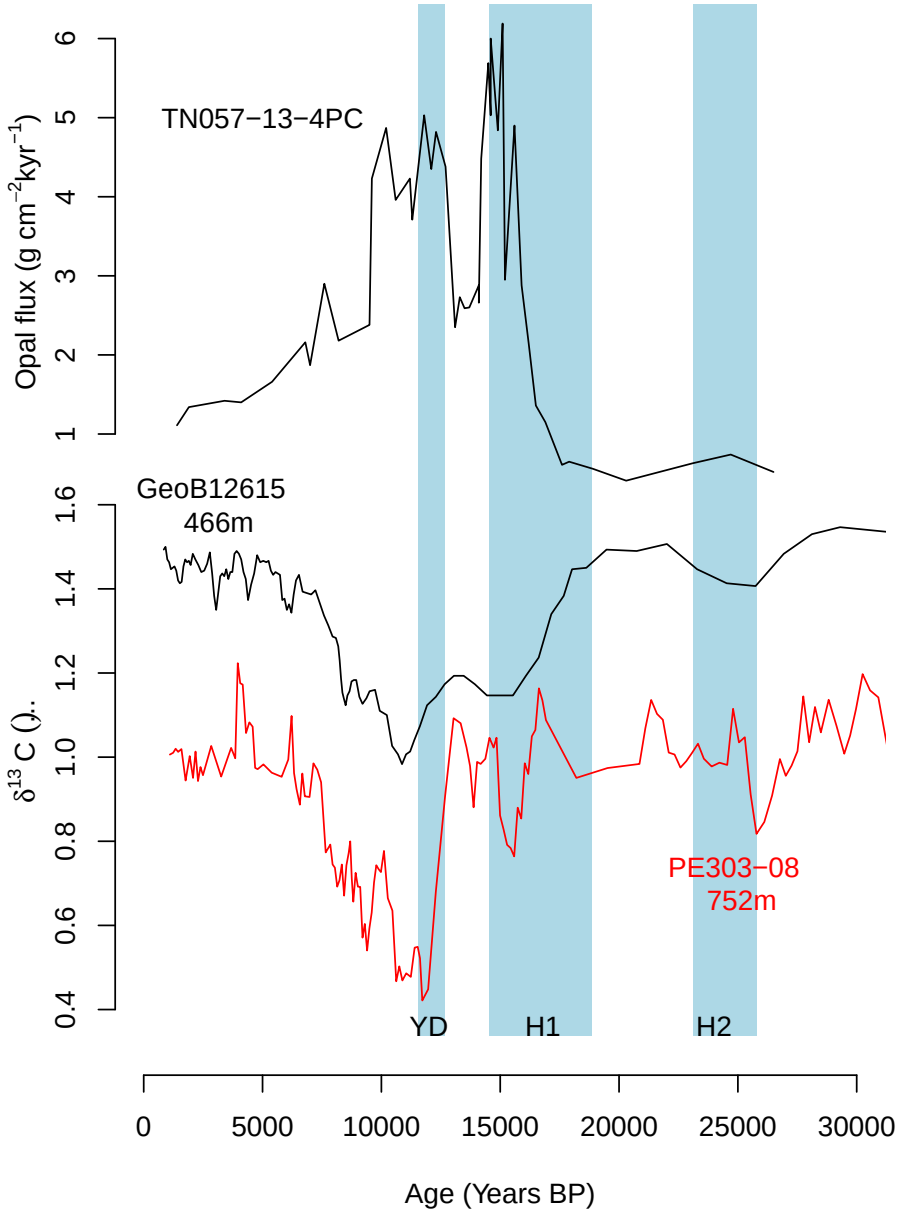

FIGURE 5.10: Comparison with opal flux record from core TN057-13-4PC, a proxy for Southern Ocean ventilation (Anderson et al. 2009; top) and the benthic carbon isotope records of cores 64PE304-8 and GeoB12615 (Romahn et al.; 2014).

5.6 Conclusions

This study provides valuable new insights into past changes in ocean circulation in the western Indian Ocean with important implications for our understanding of the role of ocean circulation in millennial scale and deglacial climate shifts. First, we see evidence of a deglacial reorganistaion of the ventilation pattern in the region across the deglaciation. This involves a chemically aged water mass reaching the western Indian Ocean via the Indonesian Through-flow and the SEC. Second, our new data supports the notion of expanded glacial AAIW at intermediate depths within the Indian Ocean during Heinrich events. Third, in the upper deep water reaches of the water column we see evidence of pulses of glacial NADW crossing the Davie ridge into the Somali basin as a result of shoaling formation depth during MIS 3 and 2.

The lack of suitable data for wide areas from the Indian Ocean is currently the biggest problem hampering a comprehensive reconstruction of long- and short-term changes in circulation and their role in global climate change. Future studies will help test the findings presented here.

Bibliography

Ahmad, S. M., Babu, G. A., Padmakumari, V. M. and Raza, W. (2008). Surface and deep water changes in the northeast Indian Ocean during the last 60 ka inferred from carbon and oxygen isotopes of planktonic and benthic foraminifera, *Palaeogeography, Palaeoclimatology, Palaeoecology* **262**(3-4): 182–188.

Andersen, K. K., Svensson, A., Johnsen, S. J., Rasmussen, S. O., Bigler, M., Röthlisberger, R., Ruth, U., Siggaard-Andersen, M. L., Peder Steffensen, J., Dahl-Jensen, D., Vinther, B. M. and Clausen, H. B. (2006). The Greenland Ice Core Chronology 2005, 15-42 ka. Part 1: constructing the time scale, *Quaternary Science Reviews*

25(23-24): 3246–3257.

Anderson, R. F., Ali, S., Bradtmiller, L. I., Nielsen, S. H. H., Fleisher, M. Q., Anderson, B. E. and Burckle, L. H. (2009). Wind-driven upwelling in the Southern Ocean and the deglacial rise in atmospheric CO2., *Science (New York, N.Y.)* **323**(5920): 1443–1448.

Barbante, C., Barnola, J., Becagli, S., Beer, J., Bigler, M., Boutron, C., Blunier, T., Castellano, E., Cattani, O., Chappellaz, J., Dahl-Jensen, D., Debret, M., Delmonte, B., Dick, D., Falourd, S., Faria, S., Federer, U., Fischer, H., Freitag, J., Frenzel, A., Fritzsche, D., Fundel, F., Gabrielli, P., Gaspari, V., Gersonde, R., Graf, W., Grigoriev, D., Hamann, I., Hansson, M., Hoffmann, G., Hutterli, M. a., Huybrechts, P., Isaksson, E., Johnsen, S., Jouzel, J., Kaczmarska, M., Karlin, T., Kaufmann, P., Kipfstuhl, S., Kohno, M., Lambert, F., Lambrecht, A., Lambrecht, A., Landais, A., Lawer, G., Leuenberger, M., Littot, G., Loulergue, L., Lüthi, D., Maggi, V., Marino, F., Masson-Delmotte, V., Meyer, H., Miller, H., Mulvaney, R., Narcisi, B., Oerlemans, J., Oerter, H., Parrenin, F., Petit, J. R., Raisbeck, G., Raynaud, D., Röthlisberger, R., Ruth, U., Rybak, O., Severi, M., Schmitt, J., Schwander, J., Siegenthaler, U., Siggaard-Andersen, M.-L., Spahni, R., Steffensen, J., Stenni, B., Stocker, T., Tison, J.-L., Traversi, R., Udisti, R., Valero-Delgado, F., van den Broeke, M. R., van de Wal, R. S. W., Wagenbach, D., Wegner, A., Weiler, K., Wilhelms, F., Winther, J.-G. and Wolff, E. W. (2006). One-to-one coupling of glacial climate variability in Greenland and Antarctica, *Nature* **444**(7116): 195–198.

Beal, L., Ffield, A. and Gordon, A. L. (2000). Spreading of Red Sea overflow waters in the Indian Ocean, *Journal of Geophysical Research* **105**(February 1995): 8549–8564.

Bickert, T. and Mackensen, A. (2004). Last Glacial to Holocene Changes in South Atlantic Deep Water Circulation BT - The South Atlantic in the Late Quaternary:

Reconstruction of Material Budgets and Current Systems, Springer Berlin Heidelberg, Berlin, Heidelberg, pp. 671–693.

Blunier, T., Chappellaz, J., Schwander, J., Clausen, H., Hammer, C. U. and Johnsen, S. (1998). Asynchrony of Antarctic and Greenland climate change during the last glacial period, *Nature* **349**: 739–743.

Bostock, H. C., Barrows, T. T., Carter, L., Chase, Z., Cortese, G., Dunbar, G. B., Ellwood, M., Hayward, B., Howard, W., Neil, H. L., Noble, T. L., Mackintosh, A., Moss, P. T., Moy, A. D., White, D., Williams, M. J. and Armand, L. K. (2013). A review of the Australian-New Zealand sector of the Southern Ocean over the last 30ka (Aus-INTIMATE project), *Quaternary Science Reviews* **74**: 35–57.

Broeker, W. (1991). The Great Ocean Conveyor, *Oceanography* **4**(2): 79–89.

Bryan, S., Marchitto, T. and Lehman, S. (2010). The release of 14C-depleted carbon from the deep ocean during the last deglaciation: Evidence from the Arabian Sea, *Earth and Planetary Science Letters* **298**(1-2): 244–254.

Chen, Z. and Wu, L. (2015). Seasonal Variation of the Pacific South Equatorial Current Bifurcation, *Journal of Physical Oceanography* **45**(6): 1757–1770.

Curry, W., Duplessy, J., Labeyrie, L. and Shackleton, N. (1988). Changes in the Distribution of $\delta^{13}C$ of Deep Water ΣCO_2 between the Last Glaciation and the Holocene, *Paleoceanography* **3**(3): 317–341.

Dansgaard, W., Johnsen, S., Clausen, H., Dahl-Jensen, D., Gundestrup, N., Hammer, C. U. and Oeschger, H. (1984). h, *in* J. E. Hansen and T. Takahashi (eds), *Climate Processes and Climate Sensitivity, Geophys. Monogr. Ser., vol. 29*, AGU, pp. 288–298.

Delong, K. (2015). *Millennial-scale variability in the Indian monsoon and links to ocean circulation*, Masters thesis.

Duplessy, J. C., Shackleton, N. J., Fairbanks, R. G., Labeyrie, L., Oppo, D. and Kallel, N. (1988). Deepwater source variations during the last climatic cycle and their impact on the global deepwater circulation, *Paleoceanography* **3**(3): 343–360.

Gottschalk, J., Vázquez Riveiros, N., Waelbroeck, C., Skinner, L. C., Michel, E., Duplessy, J. C., Hodell, D. and Mackensen, A. (2016). Carbon isotope offsets between benthic foraminifer species of the genus *Cibicides* (*Cibicidoides*) in the glacial sub-Antarctic Atlantic, *Paleoceanography* **31**(12): 1583–1602.

Grundlingh, M., Carter, R. and Stanton, R. (1991). Circulation and water properties of the southwest indian ocean, spring 1987, *Progress in Oceanography* **28**(4): 305 – 342.

Jung, S. (1996). *Wassermassenaustausch zwischen NE-Atlantik und Nordmeer wahrend der letzten 300 000/80 000 Jahre im Abbild stabiler O- und C-Isotope*, PhD thesis, Christian-Albrechts-Universitat Kiel.

Jung, S. J. A., Kroon, D., Ganssen, G., Peeters, F. and Ganeshram, R. (2009). Enhanced Arabian Sea intermediate water flow during glacial North Atlantic cold phases, *Earth and Planetary Science Letters* **280**(1-4): 220–228.

Jung, S. and Kroon, D. (2011). Quantifying rates of change in ocean conditions with implications for timing of sea level change, *Global and Planetary Change* **79**(3): 204–213.

Labeyrie, L., Labracherie, M., Gorfti, N., Pichon, J. J., Vautravers, M., Arnold, M., Duplessy, J. C., Paterne, M., Michel, E., Duprat, J., Caralp, M. and Turon, J. L. (1996). Hydrographic changes of the Southern Ocean (southeast Indian sector) over the last 230 kyr, *Paleoceanography* **11**(1): 57–76.

Lutze, G. F. and Thiel, H. (1989). Epibenthic foraminifera from elevated microhabitats; *Cibicidoides wuellerstorfi* and *Planulina ariminensis*, *The Journal of Foraminiferal Research* (2): 153–158.

Lynch-Stieglitz, J. (2017). The Atlantic Meridional Overturning Circulation and Abrupt Climate Change, *Annual Review of Marine Science* **9**(1): 83–104.

Mackensen, A., Hubberten, H. W., Bickert, T., Fischer, G. and Fütterer, D. K. (1993). The $\delta^{13}C$ in benthic foraminiferal tests of *Fontbotia wuellerstorfi* (Schwager) Relative to the $\delta^{13}C$ of dissolved inorganic carbon in Southern Ocean Deep Water: Implications for glacial ocean circulation models, *Paleoceanography* **8**(5): 587–610.

Mantyla, A. W. and Reid, J. L. (1995). On the origins of deep and bottom waters of the indian ocean, *Journal of Geophysical Research: Oceans* **100**(C2): 2417–2439.

Marchitto, T. M., Lehman, S. J., Ortiz, J. D., Fluckiger, J. and van Geen, A. (2007). Marine Radiocarbon Evidence for the Mechanism of Deglacial Atmospheric CO_2 Rise, *Science* **316**(5830): 1456–1459.

McCarthy, M. C. and Talley, L. D. (1999). Three-dimensional isoneutral potential vorticity structure in the Indian Ocean, *Journal of geophysical research* **104**.

McCave, I. N., Kiefer, T., Thornalley, D. J. R. and Elderfield, H. (2005). Deep flow in the Madagascar-Mascarene Basin over the last 150000 years, *Philosophical Transactions of the Royal Society A: Mathematical, Physical and Engineering Sciences* **363**(1826): 81–99.

McCorkle, D. C., Heggie, D. T. and Veeh, H. H. (1998). Glacial and holocene stable isotope distributions in the southeastern Indian Ocean, *Paleoceanography* **13**(1): 20–34.

McManus, J. F., Francois, R., Gherardi, J.-M., Keigwin, L. D. and Brown-Leger, S. (2004). Collapse and rapid resumption of Atlantic meridional circulation linked to deglacial climate changes., *Nature* **428**(6985): 834–837.

Pahnke, K. and Zahn, R. (2005). Southern Hemisphere water mass conversion linked with North Atlantic climate variability, *Science* **307**(5716): 1741–1746.

Rasmussen, S. O., Andersen, K. K., Svensson, A. M., Steffensen, J. P., Vinther, B. M., Clausen, H. B., Siggaard-Andersen, M. L., Johnsen, S. J., Larsen, L. B., Dahl-Jensen, D., Bigler, M., Röthlisberger, R., Fischer, H., Goto-Azuma, K., Hansson, M. E. and Ruth, U. (2006). A new Greenland ice core chronology for the last glacial termination, *Journal of Geophysical Research Atmospheres* **111**(6).

Reid, J. L. and Lynn, R. J. (1971). On the influence of the Norwegian-Greenland and Weddell seas upon the bottom waters of the Indian and Pacific oceans, *Deep-Sea Research and Oceanographic Abstracts* **18**(11).

Romahn, S., MacKensen, A., Groeneveld, J. and Pätzold, J. (2014). Deglacial intermediate water reorganization: New evidence from the Indian Ocean, *Climate of the Past* **10**(1): 293–303.

Sarnthein, M., Stattegger, K., Dreger, D., Erlenkeuser, H., Grootes, P., Haupt, B., Jung, S., Kiefer, T., Kuhnt, W., Pflaumann, U., Schafer-Neth, C., Schulz, H., Schulz, M., Seivdov, D., Simstisch, J., van Kreveld, S., Vogelsang, E., Volker, A. and Weinelt, M. (2001). Fundamental modes and abrupt changes in North Atlantic circulation and climate over the last 60 kyr concepts, reconstructions and numerical modeling., *in* P. Schafer, W. Ritzrau, M. Schluter and J. Thiede (eds), *The Northern North Atlantic*, Springer, pp. 365–410.

Sarnthein, M., Winn, K., Jung, S., Duplessy, J., Labeyrie, L., Erlenkeuser, H. and Ganssen, G. (1994). Changes in east Atlantic deepwater circulation over the last 30 , 000 years : Eight time slice reconstructions, *Paleoceanography* **9**(2): 209–267.

Schott, F. A. and McCreary, J. P. (2001). The monsoon circulation of the Indian Ocean, *Progress in Oceanography* **51**(1): 1–123.

Siani, G., Michel, E., De Pol-Holz, R., Devries, T., Lamy, F., Carel, M., Isguder, G., Dewilde, F. and Lourantou, A. (2013). Carbon isotope records reveal precise timing of enhanced Southern Ocean upwelling during the last deglaciation, *Nature*

Communications .

Sloyan, B. M. and Rintoul, S. R. (2001). Circulation, Renewal, and Modification of Antarctic Mode and Intermediate Water, *Journal of Physical Oceanography* **31**(4): 1005–1030.

Srinivasan, A. (1999). *Deep circulation in the Indian Ocean: Tracer diagnostics*, PhD thesis, ProQuest Dissertations Publishing.

Stott, L., Southon, J., Timmermann, A. and Koutavas, A. (2009). Radiocarbon age anomaly at intermediate water depth in the Pacific Ocean during the last deglaciation, *Paleoceanography* **24**(2).

Stott, L., Timmermann, A. and Thunell, R. (2007). Southern Hemisphere and deep-sea warming led deglacial atmospheric CO2 rise and tropical warming., *Science (New York, N.Y.)* **318**(5849): 435–438.

van Aken, H. M. (2007). *The Oceanic Thermohaline Circulation; An Introduction*, Springer, New York.

van Aken, H. M., Ridderinkhof, H. and de Ruijter, W. P. M. (2004). North Atlantic deep water in the south-western Indian Ocean, *Deep Sea Research Part I: Oceanographic Research Papers* **51**(6): 755–776.

Vidal, L., Labeyrie, L. and Cortijo, E. (1997). Evidence for changes in the North Atlantic Deep Water linked to meltwater surges during the Heinrich events, *Earth and Planetary* **146**: 13–27.

Vinther, B. M., Clausen, H. B., Johnsen, S. J., Rasmussen, S. O., Andersen, K. K., Buchardt, S. L., Dahl-Jensen, D., Seierstad, I. K., Siggaard-Andersen, M. L., Steffensen, J. P., Svensson, A., Olsen, J. and Heinemeier, J. (2006). A synchronized dating of three Greenland ice cores throughout the Holocene, *Journal of Geophysical Research Atmospheres* **111**(13).

Wolff, E. W., Chappellaz, J., Blunier, T., Rasmussen, S. and Svensson, A. (2010). Millennial-scale variability during the last glacial: The ice core record, *Quaternary Science Reviews* **29**(21-22): 2828–2838.

Zahn, R., Winn, K. and Sarnthein, M. (1986). Benthic foraminiferal $\delta^{13}C$ and accumulation rates of organic carbon: *Uvigerina Peregrina* group and *Cibicidoides Wuellerstorfi*, *Paleoceanography* **1**(1): 27–42.

Chapter 6

Conclusions & wider outlook

The main thrust of this thesis was to assess variability in the western Indian Ocean over the last 60kyrs, with a particular focus on the timing and relation of surface and intermediate deep water change at the millennial scale. The main scientific incentive for this research was to better understand the relation of surface to deep water variability in the context of the so-called bipolar seesaw (Blunier et al.; 1998; Barbante et al.; 2006). The bipolar seesaw involves an out of phase climate change between the poles at the millennial scale. Some progress has been made in mapping areas around the globe either displaying a change similar in timing and shape compared to the north or to the south. Some studies exist for the Indian Ocean, mostly focused on the Arabian Sea and the Bay of Bengal (Delong; 2015). With regard the Arabian Sea, monsoonal driven surface ocean variability shows a clear affinity with northern hemisphere climate change (Ivanochko et al.; 2005; Singh et al.; 2011; Altabet et al.; 2002; Schulz; 1998). Interestingly, changes at intermediate water depth suggest repeated incursions of southern sourced intermediate water, possibly entailing an important role of the intermediate water layer for the bipolar seesaw (Jung et al.; 2009; Pahnke et al.; 2008). Further south in the western Indian Ocean, records allowing a combined study of surface to deep ocean change are scarce. My thesis, based on a three new sediment cores from the western Indian Ocean off Tanzania, helps close this knowledge gap. These sediment cores form

a sea floor depth transect in the western Indian Ocean. The water column coverage provided by this transect of cores facilitates reconstruction of surface and deep ocean change through time, using a variety of paleoceanographic proxies. By including proxies reflecting climate change on the nearby African continent the new data also provides an opportunity to assess the coupled evolution of climate related changes over Africa and variations in the western Indian Ocean. The terrigenous proxies used in this project (based on bulk sediment geochemistry, specifically log (Ti/Ca)), provide insights into changes in east African monsoonal rainfall. This is particularly relevant in the context of latitudinal shifts of areas of Africa reflecting a northern or southern hemisphere influence over long and short term time scales over the last 150kyr. Such knowledge is pertinent in context of the bipolar seesaw phenomenon and the processes controlling this phenomenon. Establishing stable isotope analysis based on planktic and benthic foraminifera for the cores used in this study provides an opportunity to document surface ocean changes and compare them with circulation variations at intermediate to deep water depth in the western Indian ocean. The use of paired planktic-benthic analyses (from the same samples) allows more robust analysis of the phasing of surface ocean changes compared to changes deeper in the water column. Given its strategic location, this new suite of data specifically allows better assessment of the role northward advection of southern sourced water at depth, recorded as periods of enhanced intermediate depth ventilation during northern hemisphere Heinrich events (Jung et al. 2009).

6.1 Regional dominance of millennial scale climate change

With regard to the coupled continent-ocean changes a number of important conclusions are possible. At the millennial-scale, the new data imply a close relation of eastern African climate change with rapid variations in northern hemisphere temperatures (see figure 6.1). During Heinrich events, dry conditions prevailed in

the catchments of the Rovuma and Rufiji rivers, in line with observations from the Arabian Sea. Further south, off the Zambezi river, wetter conditions are reported, placing the "hinge zone" (in the sense of Tierney et al. 2010) somewhere between 9°S and 18°S.

Interestingly, a comparison of the new western Indian Ocean data with a recently published speleothem record from Borneo (Carolin et al.; 2016), adds another angle to the discussion surrounding the dominance of northern or southern hemisphere type climate change across the globe. In particular during MIS 5, both our records and the Borneo cave data display a rather smooth transition across termination 2. In contrast, Chinese speleothem data further north imply a much more rapid climate transition (see Figure 6.1, Cheng et al. 2016). This finding lends support to the idea that Antarctic type of climate change affected both the tropical western Pacific and the tropical western Indian Ocean more than it affected climate change on mainland China. During termination 1, however, our data display a stronger affinity with northern hemisphere climate change, implying that the processes controlling terminations differ between different terminations. This conclusion highlights the need for detailed information about the timing and shape of climate change in key areas across major climate transitions.

Variations in regional dominance of southern or northern hemisphere type climate change, when comparing Pacific and Indian Ocean climate change, also entail that a simple black and white approach in mapping these distribution patterns is too simplistic. This conclusion gives support to a recently published assessment of the hemispheric controls being reflected in the well-known Chinese cave records (Rohling et al.; 2009), suggesting a much stronger southern hemisphere influence on millennial scale events during glacial periods. A stronger northern hemisphere control would occur during interglacials and deglacial periods. Such a generic statement, however, implying a similar type of climate change to dominate during comparable time periods is at odds with our finding when comparing termination

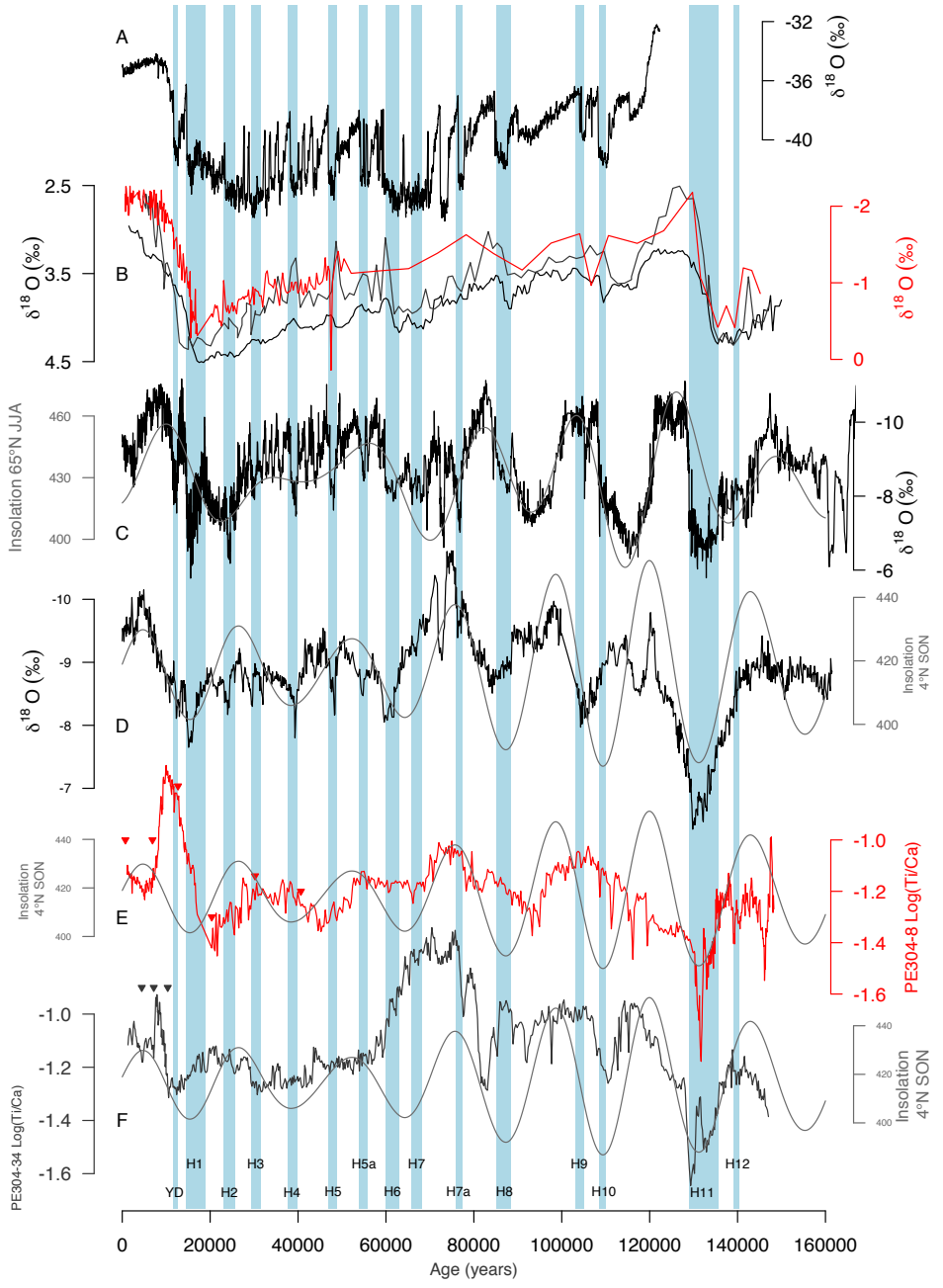

FIGURE 6.1: (A) Oxygen isotope ($\delta^{18}O$) record of Greenland ice core GISP2 (on GICC05 timescale Vinther et al. 2006; Rasmussen et al. 2008; Andersen et al. 2006; Grootes et al. 1993). A proxy for local temperature. (B) Intermediate depth Indian Ocean benthic stack of Lisiecki and Stern (2016) (black); Planktic oxygen isotope ($\delta^{18}O$) record of 64PE304-34 (this study, grey); Planktic oxygen isotope ($\delta^{18}O$) record of 64PE304-8 (this study, red)(C) Hulu-Sanbao speleothem oxygen isotope ($\delta^{18}O$) record (Cheng et al. 2016; black); with JJA insolation at 65°N (grey); (D) Mulu Stalagmite $\delta^{18}O$ from northern Borneo (4°N; Carolin et al. 2016, 2013; Partin et al. 2007; black); SON Insolation at 4°N (grey) (E) Log(Ti/Ca) of core PE304-8 (this study, red); with SON Insolation at 4°N (F) Log(Ti/Ca) of core PE304-34 (this study, grey); with SON Insolation at 4°N (black). Heinrich events indicated by vertical blue shaded lines using the nomenclature and dates adopted by Lisiecki and Stern (2016).

All insolation series produced using Analyseries (Paillard et al.; 1996)

1 and 2. Whilst speculation, it seems conceivable that such differences in hemispheric climate dominance not only occurred along with major transitions, but also along with individual millennial-scale events.

6.2 Surface to deep ocean changes off Tanzania

The new data support a number of important conclusions regarding surface to deep ocean change in the western Indian Ocean, involving changes of the importance of glacial NADW for deep water circulation, periods of enhanced glacial AAIW formation and a distant origin of chemically old sub/surface water prevailing off Tanzania near the end of the last deglaciation. With regard to periods of increased influence of deep water originating in the Atlantic Ocean, inversions in carbon isotope records during MIS3 (figure 6.2) suggest occasional stronger influence of a glacially shoaled NADW, probably leaking across the Davie Ridge and being recorded in deep water records off Tanzania (64PE303-15 and WIND28k, McCave et al. 2005). During MIS 2, with the exception of short term periods when $\delta^{13}C$-maxima occurred in the upper deep water to intermediate water layer, carbon isotope gradients below roughly 1400m are small. The most likely scenario entails a reduced contribution of glacial NADW. In addition carbon isotopes in glacial NADW and AABW were lower (Sarnthein et al.; 2001; Hoogakker et al.; 2006; Köhler et al.; 2010) . It is likely that lowered carbon isotope ratios alongside a lowered contribution of glacial NADW to the LCDW mix led to similar $\delta^{13}C$ values occurring in LCDW and UCDW, rendering it impossible to distinguish both water based on carbon isotopes during parts of MIS 2.

At the millennial scale and in the light of recent contrasting work by Jung et al. (2009) and Romahn et al. (2013), a significant motivation behind this thesis was to further investigate the nature of millennial scale changes in ocean circulation in western Indian Ocean. The conflicting theories presented by these authors have

been discussed in chapter 5. However a revisiting of the issue is worthwhile. Both shallower cores (64PE304-8; this study and GeoB12615-4; Romahn et al. 2013) largely record near surface water signal rather than intermediate to deep-water signal, implying that neither time series reflects repeated incursions of glacial AAIW. In addition, the deeper cores (64PE303-15/16) in Figure 6.1, confirm periods of enhanced glacial AAIW which are recorded as carbon isotope maxima at intermediate depth off eastern Africa during Heinrich events. This finding is also in line with the phase offset between planktic and benthic $\delta^{18}O$ records along with termination 1, suggesting a southern hemisphere driven change at depth compared to that at the surface ocean being linked to northern hemisphere climate change. This combined set of findings lends support to conclusions drawn based on data from the Arabian Sea (Jung et al.; 2009) and the Bay of Bengal (Delong; 2015), indeed placing the importance of periods of enhanced glacial AAIW formation on a Indo-Pacific scale (this work, Pahnke et al. 2003), probably with a crucial role in the bipolar seesaw (sensu Jung et al. 2009).

With respect to the final stages of the last deglaciation, our data show a carbon isotope minimum spike prevailing in the two shallow most cores (64PE304-8 and 64PE303-16) around 10-12Ka. Similar findings have been previously reported from the Arabian Sea (Bryan et al.; 2010). In the absence of any probable mechanism explaining this incursion of chemically old sub/surface water locally, a distant origin of this water is required. The by far most likely scenario involves advection of carbon 12 spiked water via the Indonesian throughflow and the SEC, eventually being recorded off Tanzania and in the Arabian Sea, the latter signal being entrained in the Somali current.

6.3 Concluding remarks

In conclusion, this work provides new insights into the local water mass changes at various depth, their relationship with distal events and the link of regional climate change over Africa with far-field changes in the Pacific warm pool area. The findings in this work emphasize the importance of better understanding changes in the atmosphere and in the ocean in the Indian Ocean region and their role in long and short term climate change. This work, however, only adds the "Tanzanian" perspective to our knowledge. More research from other, to date largely unstudied, areas is required to arrive at a more comprehensive assessment of the processes driving climate change on Earth.

6.4 Limitations of work and outlook

Although this project has presented a significant new contribution in the form of a large data set, there are some areas where further data would help test the theories and understanding discussed here. In many cases the limitations were imposed by the time and financial constraints of the project.

In particular an extra core deeper in transect, within the same basin as cores 64PE303-16/15, would provide better coverage of the entire water column. This would strengthen our discussion of change across the water column by making clearer the position of water mass boundaries.

A paleothermometer, such as the Mg/Ca ratio of foraminiferal calcite, would also prove a very useful addition to the data presented here. This would allow separation of the temperature component of changes in the oxygen isotope ratio of foraminifera. In the surface records, this would allow more in-depth assessment of the tie between surface ocean change and hydrological change on nearby climate. In subsurface records this would allow quantification of possible changes in heat storage by intermediate depth water masses on millennial timescales.

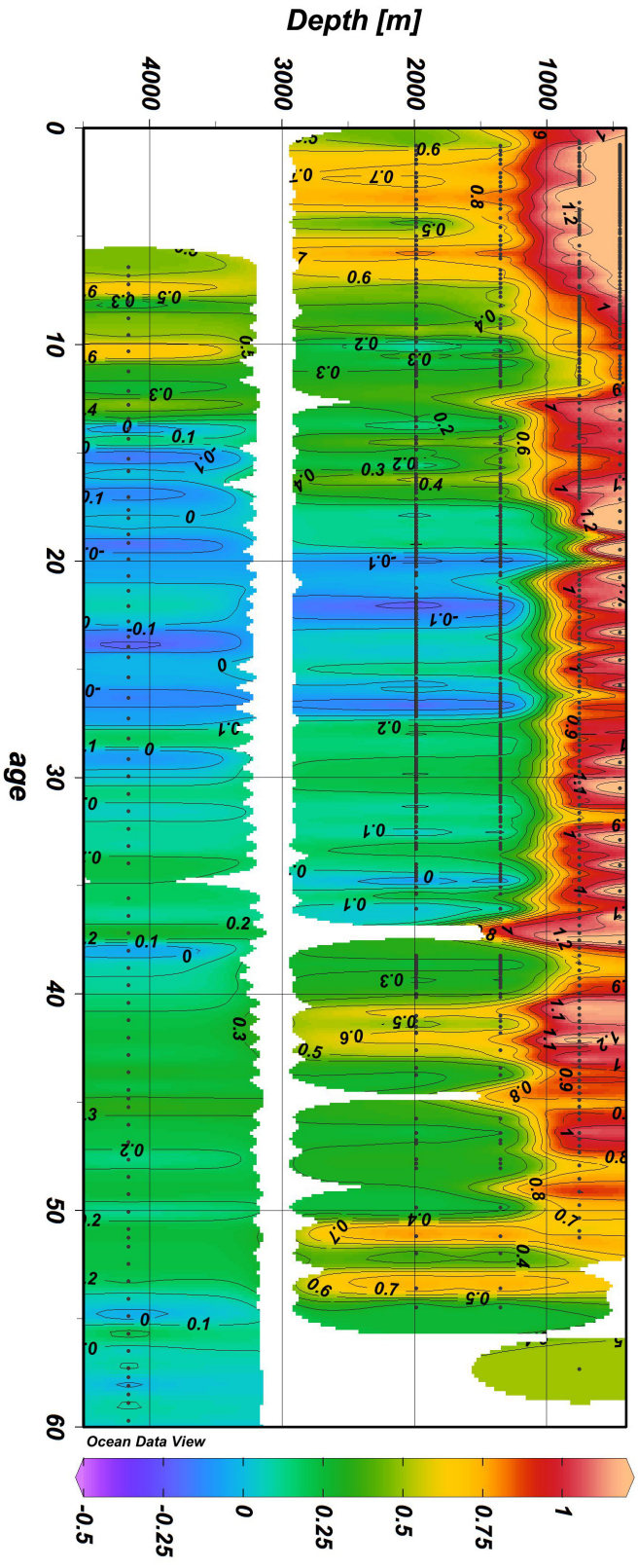

FIGURE 6.2: Water column depth/time transect of stable carbon isotope data from epibenthic foraminifera extracted from sediment cores 64PE303-15, 64PE303-16 and 64PE304-8, GeoB12615-4 and WIND28k. For data source see Table 5.1 (Chapter 5). The data were plotted using the Oceandataview software (version 4).

Finally, longer sediment cores retrieved from the same region would allow investigation of changes in previous glacial cycles.

Bibliography

Altabet, M. A., Higginson, M. J. and Murray, D. W. (2002). The effect of millennial-scale changes in Arabian Sea denitrification on atmospheric CO_2, *Nature* **415**(6868): 159–162.

Andersen, K. K., Svensson, A., Johnsen, S. J., Rasmussen, S. O., Bigler, M., Röthlisberger, R., Ruth, U., Siggaard-Andersen, M. L., Peder Steffensen, J., Dahl-Jensen, D., Vinther, B. M. and Clausen, H. B. (2006). The Greenland Ice Core Chronology 2005, 15-42 ka. Part 1: constructing the time scale, *Quaternary Science Reviews* **25**(23-24): 3246–3257.

Barbante, C., Barnola, J., Becagli, S., Beer, J., Bigler, M., Boutron, C., Blunier, T., Castellano, E., Cattani, O., Chappellaz, J., Dahl-Jensen, D., Debret, M., Delmonte, B., Dick, D., Falourd, S., Faria, S., Federer, U., Fischer, H., Freitag, J., Frenzel, A., Fritzsche, D., Fundel, F., Gabrielli, P., Gaspari, V., Gersonde, R., Graf, W., Grigoriev, D., Hamann, I., Hansson, M., Hoffmann, G., Hutterli, M. a., Huybrechts, P., Isaksson, E., Johnsen, S., Jouzel, J., Kaczmarska, M., Karlin, T., Kaufmann, P., Kipfstuhl, S., Kohno, M., Lambert, F., Lambrecht, A., Lambrecht, A., Landais, A., Lawer, G., Leuenberger, M., Littot, G., Loulergue, L., Lüthi, D., Maggi, V., Marino, F., Masson-Delmotte, V., Meyer, H., Miller, H., Mulvaney, R., Narcisi, B., Oerlemans, J., Oerter, H., Parrenin, F., Petit, J. R., Raisbeck, G., Raynaud, D., Röthlisberger, R., Ruth, U., Rybak, O., Severi, M., Schmitt, J., Schwander, J., Siegenthaler, U., Siggaard-Andersen, M.-L., Spahni, R., Steffensen, J., Stenni, B., Stocker, T., Tison, J.-L., Traversi, R., Udisti, R., Valero-Delgado, F., van den

Broeke, M. R., van de Wal, R. S. W., Wagenbach, D., Wegner, A., Weiler, K., Wilhelms, F., Winther, J.-G. and Wolff, E. W. (2006). One-to-one coupling of glacial climate variability in Greenland and Antarctica, *Nature* **444**(7116): 195–198.

Blunier, T., Chappellaz, J., Schwander, J., Clausen, H., Hammer, C. U. and Johnsen, S. (1998). Asynchrony of Antarctic and Greenland climate change during the last glacial period, *Nature* **349**: 739–743.

Bryan, S., Marchitto, T. and Lehman, S. (2010). The release of 14C-depleted carbon from the deep ocean during the last deglaciation: Evidence from the Arabian Sea, *Earth and Planetary Science Letters* **298**(1-2): 244–254.

Carolin, S. A., Cobb, K. M., Adkins, J. F., Clark, B., Conroy, J. L., Lejau, S., Malang, J. and Tuen, A. A. (2013). Varied Response of Western Pacific Hydrology to Climate Forcings over the Last Glacial Period, *Science* **340**(6140): 1564–1566.

Carolin, S. A., Cobb, K. M., Lynch-Stieglitz, J., Moerman, J. W., Partin, J. W., Lejau, S., Malang, J., Clark, B., Tuen, A. A. and Adkins, J. F. (2016). Northern Borneo stalagmite records reveal West Pacific hydroclimate across MIS 5 and 6, *Earth and Planetary Science Letters* **439**: 182–193.

Cheng, H., Edwards, R. L., Sinha, A., Spötl, C., Yi, L., Chen, S., Kelly, M., Kathayat, G., Wang, X., Li, X., Kong, X., Wang, Y., Ning, Y. and Zhang, H. (2016). The Asian monsoon over the past 640,000 years and ice age terminations, *Nature* **534**(7609): 640–646.

Delong, K. (2015). *Millennial-scale variability in the Indian monsoon and links to ocean circulation*, Masters thesis.

Grootes, P. M., Stuiver, M., White, J. W. C., Johnsen, S. and Jouzel, J. (1993). Comparison of oxygen isotope records from the GISP2 and GRIP Greenland ice cores, *Nature* **366**(6455): 552–554.

Hoogakker, B. A., Rohling, E. J., Palmer, M. R., Tyrrell, T. and Rothwell, R. G. (2006). Underlying causes for long-term global ocean delta13C fluctuations over the last 1.20Myr, *Earth and Planetary Science Letters* .

Ivanochko, T. S., Ganeshram, R. S., Brummer, G. J. A., Ganssen, G., Jung, S. J. A., Moreton, S. G. and Kroon, D. (2005). Variations in tropical convection as an amplifier of global climate change at the millennial scale, *Earth and Planetary Science Letters* **235**(1-2): 302–314.

Jung, S. J. A., Kroon, D., Ganssen, G., Peeters, F. and Ganeshram, R. (2009). Enhanced Arabian Sea intermediate water flow during glacial North Atlantic cold phases, *Earth and Planetary Science Letters* **280**(1-4): 220–228.

Köhler, P., Fischer, H. and Schmitt, J. (2010). Atmospheric delta ^{13} CO 2 and its relation to p CO 2 and deep ocean δ 13 C during the late Pleistocene, *Paleoceanography* **25**(1): 1–16.

Lisiecki, L. E. and Stern, J. V. (2016). Regional and global benthic $\delta^{18}O$ stacks for the last glacial cycle, *Paleoceanography* **31**(10): 1368–1394.

McCave, I. N., Kiefer, T., Thornalley, D. J. R. and Elderfield, H. (2005). Deep flow in the Madagascar-Mascarene Basin over the last 150000 years, *Philosophical Transactions of the Royal Society A: Mathematical, Physical and Engineering Sciences* **363**(1826): 81–99.

Pahnke, K., Goldstein, S. L. and Hemming, S. R. (2008). Abrupt changes in Antarctic Intermediate Water circulation over the past 25,000 years, *Nature Geosci* **1**(12): 870–874.

Pahnke, K., Zahn, R., Elderfield, H. and Schulz, M. (2003). 340,000-Year Centennial-Scale Marine Record of Southern Hemisphere Climatic Oscillation, *Science* **301**: 948–952.

Paillard, D., Labeyrie, L. and Yiou, P. (1996). Analyseries, Macintosh program performs time-series analysis, Eos Trans. AGU, 77: 379.

Partin, J. W., Cobb, K. M., Adkins, J. F., Clark, B. and Fernandez, D. P. (2007). Millennial-scale trends in west Pacific warm pool hydrology since the Last Glacial Maximum, *Nature* **449**(7161): 452–455.

Rasmussen, S. O., Seierstad, I. K., Andersen, K. K., Bigler, M., Dahl-Jensen, D. and Johnsen, S. J. (2008). Synchronization of the NGRIP, GRIP, and GISP2 ice cores across MIS 2 and palaeoclimatic implications, *Quaternary Science Reviews* **27**(1-2): 18–28.

Rohling, E., Liu, Q. S., a.P. Roberts, Stanford, J. D., Rasmussen, S., Langen, P. L. and Siddall, M. (2009). Controls on the East Asian monsoon during the last glacial cycle, based on comparison between Hulu Cave and polar ice-core records, *Quaternary Science Reviews* **28**(27-28): 3291–3302.

Romahn, S., Mackensen, a., Groeneveld, J. and Pätzold, J. (2013). Deglacial intermediate water reorganization: new evidence from the Indian Ocean, *Climate of the Past Discussions* **9**(4): 4035–4063.

Sarnthein, M., Stattegger, K., Dreger, D., Erlenkeuser, H., Grootes, P., Haupt, B., Jung, S., Kiefer, T., Kuhnt, W., Pflaumann, U., Schafer-Neth, C., Schulz, H., Schulz, M., Seivdov, D., Simstisch, J., van Kreveld, S., Vogelsang, E., Volker, A. and Weinelt, M. (2001). Fundamental modes and abrupt changes in North Atlantic circulation and climate over the last 60 kyr concepts, reconstructions and numerical modeling., *in* P. Schafer, W. Ritzrau, M. Schluter and J. Thiede (eds), *The Northern North Atlantic*, Springer, pp. 365–410.

Schulz, H. (1998). Correlation between Arabian Sea and Greenland climate oscillations of the past 110,000 years, *Nature* **393**(May): 23–25.

Singh, A., Jung, S., Darling, K., Ganeshram, R., Ivanochko, T. and Kroon, D. (2011). Productivity collapses in the Arabian Sea during glacial cold phases, *Paleoceanography* **26**(3): 1–10.

Tierney, J. E., Russell, J. M. and Huang, Y. (2010). A molecular perspective on Late Quaternary climate and vegetation change in the Lake Tanganyika basin, East Africa, *Quaternary Science Reviews* **29**(5): 787–800.

Vinther, B. M., Clausen, H. B., Johnsen, S. J., Rasmussen, S. O., Andersen, K. K., Buchardt, S. L., Dahl-Jensen, D., Seierstad, I. K., Siggaard-Andersen, M. L., Steffensen, J. P., Svensson, A., Olsen, J. and Heinemeier, J. (2006). A synchronized dating of three Greenland ice cores throughout the Holocene, *Journal of Geophysical Research Atmospheres* **111**(13).

Appendix A

Bulk Sediment Geochemical Data

TABLE A.1: Bulk sediment geochemical data presented in this thesis. Derived from XRF core-scanning

64PE304-8		64PE304-34		64PE303-16		64PE303-15	
depth (cm)	Log (Ca/Ti)	depth (cm)	Log(Ti/Ca)	depth (cm)	Log Ti/Ca	depth (cm)	log Ti/Ca
2	-1.12	1	-1.12	1		0	
6	-1.13	2	-1.09	2	-1.05	1	
7	-1.10	3	-1.07	3	-1.00	2	-1.29
8	-1.13	4	-1.05	4	-1.00	3	-1.22
9	-1.12	5	-1.06	5	-1.03	4	-1.31
10	-1.14	6	-1.08	6	-1.03	5	-1.37
11	-1.14	7	-1.10	7	-1.05	6	-1.37
12	-1.13	8	-1.12	8	-1.04	7	-1.38
13	-1.14	9	-1.09	9	-1.04	8	-1.41
14	-1.15	10	-1.04	10	-1.04	9	-1.36
15	-1.13	11	-1.03	11	-1.04	10	-1.42
16	-1.14	12	-1.05	12	-1.03	11	-1.43
17	-1.21	13	-1.06	13	-1.05	12	-1.45
18	-1.17	14	-1.08	14	-1.05	13	-1.42
19	-1.15	15	-1.09	15	-1.00	14	-1.40

Table A.1 continued from previous page

64PE304-8		64PE304-34		64PE303-16		64PE303-15	
depth (cm)	Log (Ca/Ti)	depth (cm)	Log(Ti/Ca)	depth (cm)	Log Ti/Ca	depth (cm)	log Ti/Ca
20	-1.15	16	-1.11	16	-1.01	15	-1.41
21	-1.14	17	-1.12	17	-1.04	16	-1.42
22	-1.16	18	-1.11	18	-1.02	17	-1.46
23	-1.15	19.5	-1.13	19	-0.98	18	-1.47
24	-1.17	20.5	-1.12	20	-1.00	19	-1.43
25.5	-1.16	21.5	-1.14	21	-0.96	20	-1.41
26.5	-1.17	22.5	-1.14	22	-1.02	21	-1.40
27.5	-1.17	23.5	-1.14	23	-1.07	22	-1.42
28.5	-1.15	24.5	-1.17	24	-1.06	23	-1.42
29.5	-1.16	25.5	-1.18	25	-0.85	24	-1.46
30.5	-1.16	26.5	-1.18	26	-0.81	25	-1.47
31.5	-1.17	27.5	-1.14	27	-0.86	27.5	-1.40
32.5	-1.17	28.5	-1.13	28	-0.81	28.5	-1.42
33.5	-1.16	29.5	-1.11	29	-0.85	29.5	-1.43
34.5	-1.19	30.5	-1.10	30	-0.87	30.5	-1.42

Table A.1 continued from previous page

64PE304-8		64PE304-34		64PE303-16		64PE303-15	
depth (cm)	Log (Ca/Ti)	depth (cm)	Log(Ti/Ca)	depth (cm)	Log Ti/Ca	depth (cm)	log Ti/Ca
35.5	-1.18	31.5	-1.09	31	-0.88	31.5	-1.40
36.5	-1.18	32.5	-1.11	32	-0.88	32.5	-1.38
37.5	-1.18	33.5	-1.13	33	-0.87	33.5	-1.33
38.5	-1.20	34.5	-1.12	34	-0.97	34.5	-1.35
39.5	-1.19	35.5	-1.11	35	-0.94	35.5	-1.35
40.5	-1.19	36.5	-1.10	36	-0.92	36.5	-1.33
41.5	-1.19	39.5	-1.09	37	-0.93	37.5	-1.49
42.5	-1.22	40.5	-1.11	38	-0.98	38.5	-1.50
43.5	-1.21	41.5	-1.13	39	-0.96	39.5	-1.38
44.5	-1.23	42.5	-1.13	40	-0.96	40.5	-1.34
45.5	-1.20	43.5	-1.12	41	-0.98	41.5	-1.29
46.5	-1.17	44.5	-1.17	42	-1.02	42.5	-1.30
47.5	-1.20	45.5	-1.14	43	-1.00	43.5	-1.29
48.5	-1.16	46.5	-1.12	44	-1.05	44.5	-1.27
49.5	-1.17	47.5	-1.06	45	-1.07	45.5	-1.27

Table A.1 continued from previous page

64PE304-8		64PE304-34		64PE303-16		64PE303-15	
depth (cm)	Log (Ca/Ti)	depth (cm)	Log(Ti/Ca)	depth (cm)	Log Ti/Ca	depth (cm)	log Ti/Ca
50.5	-1.17	48.5	-1.03	46	-1.05	46.5	-1.32
51.5	-1.19	49.5	-0.99	47	-1.03	47.5	-1.33
52.5	-1.19	50.5	-0.95	48	-1.00	48.5	-1.34
53.5	-1.20	51.5	-0.94	49	-1.07	49.5	-1.32
54.5	-1.18	52.5	-0.95	50	-1.14	50.5	-1.32
55.5	-1.15	53.5	-0.97	51	-1.14	51.5	-1.30
56.5	-1.16	54.5	-0.93	52	-1.13	52.5	-1.36
57.5	-1.17	55.5	-0.95	53	-1.09	53.5	-1.37
58.5	-1.18	56.5	-0.99	54	-1.12	54.5	-1.30
59.5	-1.21	57.5	-0.99	55	-1.12	55.5	-1.39
60.5	-1.15	58.5	-1.04	56	-1.15	56.5	-1.36
61.5	-1.18	59.5	-1.03	57	-1.15	57.5	-1.40
62.5	-1.14	60.5	-1.02	58	-1.15	58.5	-1.40
63.5	-1.11	61.5	-0.98	59	-1.11	59.5	-1.41
64.5	-1.14	62.5	-0.96	60	-1.07	60.5	-1.40

Table A.1 continued from previous page

64PE304-8		64PE304-34		64PE303-16		64PE303-15	
depth (cm)	Log (Ca/Ti)	depth (cm)	Log(Ti/Ca)	depth (cm)	Log Ti/Ca	depth (cm)	log Ti/Ca
65.5	-1.16	63.5	-0.96	61	-1.08	61.5	-1.43
66.5	-1.13	64.5	-1.00	62	-1.16	62.5	-1.38
67.5	-1.13	65.5	-1.00	63	-1.15	63.5	-1.39
68.5	-1.10	66.5	-1.00	64	-1.08	64.5	-1.38
69.5	-1.08	67.5	-1.03	65	-1.09	65.5	-1.37
70.5	-1.06	68.5	-1.09	66	-1.09	66.5	-1.37
71.5	-1.11	69.5	-1.06	67	-1.14	67.5	-1.35
72.5	-1.07	70.5	-1.06	68	-1.14	68.5	-1.45
73.5	-1.06	71.5	-1.11	69	-1.09	69.5	-1.40
74.5	-1.04	72.5	-1.11	70	-1.01	70.5	-1.45
75.5	-1.04	73.5	-1.09	71	-0.98	71.5	-1.43
76.5	-0.95	74.5	-1.12	72	-0.91	72.5	-1.42
77.5	-0.95	75.5	-1.06	73	-0.89	73.5	-1.47
78.5	-0.91	76.5	-1.07	74	-0.95	74.5	-1.45
79.5	-0.89	77.5	-1.14	75	-0.97	75.5	-1.46

Table A.1 continued from previous page

64PE304-8		64PE304-34		64PE303-16		64PE303-15	
depth (cm)	Log (Ca/Ti)	depth (cm)	Log(Ti/Ca)	depth (cm)	Log Ti/Ca	depth (cm)	log Ti/Ca
80.5	-0.86	78.5	-1.14	76	-0.99	76.5	-1.44
81.5	-0.83	79.5	-1.11	77	-0.98	77.5	-1.51
82.5	-0.87	80.5	-1.20	78	-1.01	78.5	-1.53
83.5	-0.90	81.5	-1.19	79	-1.03	79.5	-1.49
84.5	-0.86	82.5	-1.15	80	-1.11	80.5	-1.45
85.5	-0.88	83.5	-1.23	81	-1.10	81.5	-1.44
86.5	-0.77	84.5	-1.23	82	-1.22	82.5	-1.40
87.5	-0.76	85.5	-1.23	83	-1.12	83.5	-1.39
88.5	-0.78	86.5	-1.22	84	-1.21	84.5	-1.44
89.5	-0.77	87.5	-1.23	85	-1.24	85.5	-1.47
90.5	-0.78	88.5	-1.27	86	-1.33	86.5	-1.41
91.5	-0.76	89.5	-1.31	87	-1.29	87.5	-1.44
92.5	-0.73	90.5	-1.27	88	-1.27	88.5	-1.42
93.5	-0.71	91.5	-1.28	89	-1.24	89.5	-1.40
94.5	-0.73	92.5	-1.25	90	-1.20	90.5	-1.40

Table A.1 continued from previous page

64PE304-8		64PE304-34		64PE303-16		64PE303-15	
depth (cm)	Log (Ca/Ti)	depth (cm)	Log(Ti/Ca)	depth (cm)	Log Ti/Ca	depth (cm)	log Ti/Ca
95.5	-0.75	93.5	-1.24	91	-1.26	91.5	-1.42
96.5	-0.73	94.5	-1.28	92	-1.28	92.5	-1.45
97.5	-0.73	95.5	-1.27	93	-1.33	93.5	-1.45
98.5	-0.76	96.5	-1.28	94	-1.32	94.5	-1.42
99.5	-0.75	97.5	-1.28	95	-1.29	95.5	-1.41
100.5	-0.77	98.5	-1.30	96	-1.28	96.5	-1.41
101.5	-0.76	99.5	-1.27	97	-1.29	97.5	-1.39
102.5	-0.75	100.5	-1.29	98	-1.26	98.5	-1.39
103.5	-0.79	101.5	-1.25	99	-1.28	99.5	-1.39
104.5	-0.79	102.5	-1.29	100	-1.33	100.5	-1.39
105.5	-0.81	103.5	-1.23	101	-1.31	101.5	-1.39
106.5	-0.82	104.5	-1.25	102	-1.27	102.5	-1.37
107.5	-0.77	105.5	-1.28	103	-1.28	103.5	-1.40
108.5	-0.79	106.5	-1.28	104	-1.28	104.5	-1.41
109.5	-0.78	107.5	-1.24	105	-1.24	105.5	-1.40

Table A.1 continued from previous page

64PE304-8		64PE304-34		64PE303-16		64PE303-15	
depth (cm)	Log (Ca/Ti)	depth (cm)	Log(Ti/Ca)	depth (cm)	Log Ti/Ca	depth (cm)	log Ti/Ca
110.5	-0.80	108.5	-1.25	106	-1.18	106.5	-1.39
111.5	-0.79	109.5	-1.25	107	-1.18	107.5	-1.39
112.5	-0.89	110.5	-1.23	108	-1.22	108.5	-1.38
113.5	-0.82	111.5	-1.24	109	-1.22	109.5	-1.36
114.5	-0.82	112.5	-1.23	110	-1.24	110.5	-1.35
115.5	-0.84	113.5	-1.23	111	-1.21	111.5	-1.34
116.5	-0.83	114.5	-1.22	112	-1.24	112.5	-1.35
117.5	-0.92	115.5	-1.21	113	-1.28	113.5	-1.36
118.5	-0.95	116.5	-1.19	114	-1.28	114.5	-1.31
119.5	-0.91	117.5	-1.19	115	-1.23	115.5	-1.30
120.5	-0.94	118.5	-1.21	116	-1.19	116.5	-1.30
121.5	-0.94	119.5	-1.22	117	-1.18	117.5	-1.32
122.5	-0.96	120.5	-1.18	118	-1.21	118.5	-1.27
123.5	-0.97	121.5	-1.16	119	-1.21	119.5	-1.27
124.5	-1.03	122.5	-1.17	120	-1.24	120.5	-1.25

Table A.1 continued from previous page

64PE304-8		64PE304-34		64PE303-16		64PE303-15	
depth (cm)	Log (Ca/Ti)	depth (cm)	Log(Ti/Ca)	depth (cm)	Log Ti/Ca	depth (cm)	log Ti/Ca
125.5	-1.05	123.5	-1.15	121	-1.20	121.5	-1.25
126.5	-1.01	124.5	-1.17	122	-1.23	122.5	-1.26
127.5	-1.04	125.5	-1.22	123	-1.22	123.5	-1.31
128.5	-1.04	126.5	-1.21	124	-1.21	124.5	-1.28
129.5	-1.09	127.5	-1.14	125	-1.22	125.5	-1.26
130.5	-1.08	129.5	-1.21	126	-1.19	126.5	-1.27
131.5	-1.05	130.5	-1.22	127	-1.20	127.5	-1.27
132.5	-1.08	131.5	-1.22	128	-1.22	128.5	-1.23
133.5	-1.10	132.5	-1.21	129	-1.23	129.5	-1.22
135	-1.13	133.5	-1.18	130	-1.22	130.5	-1.25
136	-1.11	134.5	-1.14	131	-1.20	131.5	-1.26
137	-1.11	135.5	-1.13	132	-1.20	132.5	-1.32
138	-1.10	136.5	-1.15	133	-1.17	133.5	-1.32
139	-1.11	137.5	-1.13	134	-1.16	134.5	-1.28
140	-1.12	138.5	-1.13	135	-1.14	135.5	-1.26

Table A.1 continued from previous page

64PE304-8		64PE304-34		64PE303-16		64PE303-15	
depth (cm)	Log (Ca/Ti)	depth (cm)	Log(Ti/Ca)	depth (cm)	Log Ti/Ca	depth (cm)	log Ti/Ca
141	-1.18	139.5	-1.12	136	-1.10	137.5	-1.23
142	-1.17	140.5	-1.16	137	-1.10	138.5	-1.24
143	-1.24	141.5	-1.12	138	-1.14	139.5	-1.23
144	-1.27	142.5	-1.12	139	-1.25	140.5	-1.24
145	-1.29	143.5	-1.15	140	-1.09	141.5	-1.20
146	-1.42	144.5	-1.19	141	-1.09	142.5	-1.22
147	-1.34	145.5	-1.16	142	-1.07	143.5	-1.20
148	-1.42	146.5	-1.18	143	-1.09	144.5	-1.14
149	-1.43	147.5	-1.20	144	-1.08	145.5	-1.13
150	-1.29	148.5	-1.20	145	-1.09	146.5	-1.14
151	-1.45	149.5	-1.15	146	-1.07	147.5	-1.14
152	-1.35	150.5	-1.15	147	-1.04	148.5	-1.11
153	-1.29	151.5	-1.16	148	-1.12	149.5	-1.12
154	-1.34	152.5	-1.17	149	-1.12	150.5	-1.17
155	-1.34	153.5	-1.18	150	-1.13	151.5	-1.11

Table A.1 continued from previous page

64PE304-8		64PE304-34		64PE303-16		64PE303-15	
depth (cm)	Log (Ca/Ti)	depth (cm)	Log(Ti/Ca)	depth (cm)	Log Ti/Ca	depth (cm)	log Ti/Ca
156	-1.33	154.5	-1.18	151	-1.11	152.5	-1.11
157	-1.30	155.5	-1.18	152	-1.14	153.5	-1.12
158	-1.33	156.5	-1.17	153	-1.13	154.5	-1.11
159	-1.31	157.5	-1.13	154	-1.14	155.5	-1.13
160	-1.27	158.5	-1.16	155	-1.13	156.5	-1.16
161	-1.32	159.5	-1.19	156	-1.13	157.5	-1.12
162	-1.27	160.5	-1.20	157	-1.12	158.5	-1.16
163	-1.24	161.5	-1.20	158	-1.12	159.5	-1.11
164	-1.24	162.5	-1.22	159	-1.11	160.5	-1.16
165	-1.30	163.5	-1.22	160	-1.09	161.5	-1.20
166	-1.34	164.5	-1.22	161	-1.07	162.5	-1.28
167	-1.37	165.5	-1.20	162	-1.08	163.5	-1.19
168	-1.26	166.5	-1.19	163	-1.07	164.5	-1.18
169	-1.26	167.5	-1.21	164	-1.06	165.5	-1.25
170	-1.27	168.5	-1.21	165	-1.14	166.5	-1.26

Table A.1 continued from previous page

64PE304-8		64PE304-34		64PE303-16		64PE303-15	
depth (cm)	Log (Ca/Ti)	depth (cm)	Log(Ti/Ca)	depth (cm)	Log Ti/Ca	depth (cm)	log Ti/Ca
171	-1.34	169.5	-1.19	166	-1.07	167.5	-1.27
172	-1.26	170.5	-1.17	167	-1.04	168.5	-1.25
173	-1.32	171.5	-1.18	168	-1.01	169.5	-1.34
174	-1.20	172.5	-1.17	169	-1.03	170.5	-1.28
175	-1.15	173.5	-1.16	170	-1.02	171.5	-1.25
176	-1.17	174.5	-1.16	171	-1.04	172.5	-1.25
177	-1.18	175.5	-1.16	172	-1.05	173.5	-1.23
178	-1.17	176.5	-1.17	173	-1.04	174.5	-1.24
179	-1.20	177.5	-1.16	174	-1.05	175.5	-1.25
180	-1.31	178.5	-1.19	175	-1.00	176.5	-1.24
181	-1.26	179.5	-1.21	176	-1.00	177.5	-1.23
182	-1.27	180.5	-1.20	177	-1.00	178.5	-1.18
183	-1.23	181.5	-1.26	178	-1.01	179.5	-1.21
184	-1.19	182.5	-1.27	179	-0.99	180.5	-1.26
185	-1.20	183.5	-1.25	180	-1.01	181.5	-1.27

Table A.1 continued from previous page

64PE304-8		64PE304-34		64PE303-16		64PE303-15	
depth (cm)	Log (Ca/Ti)	depth (cm)	Log(Ti/Ca)	depth (cm)	Log Ti/Ca	depth (cm)	log Ti/Ca
186	-1.23	184.5	-1.26	181	-1.05	182.5	-1.30
187	-1.17	185.5	-1.28	182	-1.08	183.5	-1.24
188	-1.22	186.5	-1.26	183	-1.06	184.5	-1.22
189	-1.21	187.5	-1.25	184	-1.08	185.5	-1.15
190	-1.21	188.5	-1.30	185	-1.07	186.5	-1.22
191	-1.19	189.5	-1.28	186	-1.12	187.5	-1.22
192	-1.20	190.5	-1.27	187	-1.12	188.5	-1.15
193	-1.21	191.5	-1.27	188	-1.09	189.5	-1.15
194	-1.23	192.5	-1.29	189	-1.04	190.5	-1.19
195	-1.23	193.5	-1.29	190	-1.05	191.5	-1.20
196	-1.21	194.5	-1.29	191	-1.09	192.5	-1.24
197	-1.24	195.5	-1.25	192	-1.08	193.5	-1.24
198	-1.25	196.5	-1.27	193	-1.12	194.5	-1.29
199	-1.21	197.5	-1.28	194	-1.07	195.5	-1.24
200	-1.23	198.5	-1.27	195	-1.11	196.5	-1.23

Table A.1 continued from previous page

64PE304-8		64PE304-34		64PE303-16		64PE303-15	
depth (cm)	Log (Ca/Ti)	depth (cm)	Log(Ti/Ca)	depth (cm)	Log Ti/Ca	depth (cm)	log Ti/Ca
201	-1.25	199.5	-1.27	196	-1.12	197.5	-1.24
202	-1.22	200.5	-1.27	197	-1.09	198.5	-1.23
203	-1.18	201.5	-1.26	198	-1.08	199.5	-1.18
204	-1.15	202.5	-1.25	199	-1.08	200.5	-1.18
205	-1.17	203.5	-1.27	200	-1.10	201.5	-1.16
206	-1.29	204.5	-1.25	201	-1.14	202.5	-1.16
207	-1.19	205.5	-1.19	202	-1.17	203.5	-1.19
208	-1.20	206.5	-1.20	203	-1.09	204.5	-1.21
209	-1.16	207.5	-1.28	204	-1.06	205.5	-1.22
210	-1.17	208.5	-1.22	205	-1.05	206.5	-1.04
211	-1.22	209.5	-1.21	206	-1.00	207.5	-0.99
212	-1.23	210.5	-1.20	207	-1.05	208.5	-1.32
213	-1.25	211.5	-1.19	208	-1.09	209.5	-1.33
214	-1.20	212.5	-1.21	209	-1.12	210.5	-1.35
215	-1.24	213.5	-1.20	211	-1.09	211.5	-1.45

Table A.1 continued from previous page

64PE304-8		64PE304-34		64PE303-16		64PE303-15	
depth (cm)	Log (Ca/Ti)	depth (cm)	Log(Ti/Ca)	depth (cm)	Log Ti/Ca	depth (cm)	log Ti/Ca
216	-1.26	214.5	-1.27	212	-1.08	212.5	-1.37
217	-1.25	215.5	-1.28	213	-1.10	213.5	-1.36
218	-1.26	216.5	-1.28	214	-1.12	214.5	-1.32
219	-1.26	217.5	-1.26	215	-1.14	215.5	-1.29
220	-1.29	218.5	-1.26	216	-1.09	216.5	-1.26
221	-1.32	219.5	-1.24	217	-1.10	217.5	-1.26
222	-1.28	220.5	-1.25	218	-1.09	218.5	-1.26
223	-1.25	221.5	-1.28	219	-1.05	219.5	-1.33
224	-1.26	222.5	-1.26	220	-1.05	220.5	-1.33
225	-1.25	223.5	-1.25	221	-0.98	221.5	-1.32
226	-1.27	224.5	-1.25	222	-0.96	222.5	-1.24
227	-1.30	225.5	-1.24	223	-0.97	223.5	-1.21
228	-1.35	226.5	-1.27	224	-1.00	224.5	-1.20
229	-1.31	227.5	-1.24	225	-0.97	225.5	-1.20
230	-1.36	228.5	-1.26	226	-0.99	226.5	-1.21

Table A.1 continued from previous page

64PE304-8		64PE304-34		64PE303-16		64PE303-15	
depth (cm)	Log (Ca/Ti)	depth (cm)	Log(Ti/Ca)	depth (cm)	Log Ti/Ca	depth (cm)	log Ti/Ca
231	-1.34	229.5	-1.23	227	-0.99	227.5	-1.20
232	-1.34	230.5	-1.26	228	-1.05	228.5	-1.19
233	-1.27	231.5	-1.25	229	-1.01	229.5	-1.22
234	-1.32	232.5	-1.25	230	-0.97	230.5	-1.22
235	-1.32	233.5	-1.23	231	-0.99	231.5	-1.23
236	-1.31	234.5	-1.25	232	-1.01	232.5	-1.19
237	-1.28	235.5	-1.24	233	-1.00	233.5	-1.23
238	-1.26	236.5	-1.24	234	-1.05	234.5	-1.20
239	-1.24	237.5	-1.26	235	-1.07	235.5	-1.22
240	-1.29	238.5	-1.28	236	-1.07	236.5	-1.21
241	-1.31	240.5	-1.27	237	-1.05	237.5	-1.24
242	-1.28	241.5	-1.19	238	-1.05	238.5	-1.25
243	-1.26	242.5	-1.21	239	-1.06	239.5	-1.26
245	-1.28	243.5	-1.28	240	-1.05	240.5	-1.28
246	-1.22	244.5	-1.27	241	-1.03	241.5	-1.34

Table A.1 continued from previous page

64PE304-8		64PE304-34		64PE303-16		64PE303-15	
depth (cm)	Log (Ca/Ti)	depth (cm)	Log(Ti/Ca)	depth (cm)	Log Ti/Ca	depth (cm)	log Ti/Ca
247	-1.23	245.5	-1.26	242	-0.88	242.5	-1.34
248	-1.23	246.5	-1.26	243	-0.83	243.5	-1.34
249	-1.24	247.5	-1.23	244	-0.82	244.5	-1.34
250	-1.27	248.5	-1.24	245	-0.81	245.5	-1.36
251	-1.24	249.5	-1.26	246	-0.72	247.5	-1.35
252	-1.18	250.5	-1.21	247	-0.75	248.5	-1.37
253	-1.15	251.5	-1.12	248	-0.96	249.5	-1.39
254	-1.18	252.5	-1.18	249	-0.96	250.5	-1.43
255	-1.15	253.5	-1.13	250	-1.03	251.5	-1.33
256	-1.16	254.5	-1.14	251	-1.03	252.5	-1.35
257	-1.17	255.5	-1.17	252	-1.07	253.5	-1.33
258	-1.12	256.5	-1.17	253	-1.07	254.5	-1.34
259	-1.12	257.5	-1.16	254	-1.11	255.5	-1.35
260	-1.12	258.5	-1.18	255	-1.08	256.5	-1.39
261	-1.15	259.5	-1.18	256	-1.11	257.5	-1.39

Table A.1 continued from previous page

64PE304-8		64PE304-34		64PE303-16		64PE303-15	
depth (cm)	Log (Ca/Ti)	depth (cm)	Log(Ti/Ca)	depth (cm)	Log Ti/Ca	depth (cm)	log Ti/Ca
262	-1.19	260.5	-1.18	257	-1.09	258.5	-1.41
263	-1.14	261.5	-1.19	258	-1.07	259.5	-1.39
264	-1.17	262.5	-1.20	259	-1.01	260.5	-1.40
265	-1.15	263.5	-1.19	260	-1.08	261.5	-1.39
266	-1.15	264.5	-1.21	261	-1.02	262.5	-1.44
267	-1.16	265.5	-1.20	262	-1.03	263.5	-1.35
268	-1.19	266.5	-1.19	263	-1.07	264.5	-1.37
269	-1.17	267.5	-1.19	264	-1.05	265.5	-1.31
270	-1.15	268.5	-1.19	265	-1.06	266.5	-1.34
271	-1.17	269.5	-1.22	266	-1.02	267.5	-1.33
272	-1.16	270.5	-1.19	267	-1.04	268.5	-1.39
273	-1.17	271.5	-1.18	268	-1.00	269.5	-1.40
274	-1.18	272.5	-1.18	269	-1.01	270.5	-1.43
275	-1.18	273.5	-1.18	270	-0.98	271.5	-1.47
276	-1.16	274.5	-1.20	271	-1.05	272.5	-1.43

Table A.1 continued from previous page

64PE304-8		64PE304-34		64PE303-16		64PE303-15	
depth (cm)	Log (Ca/Ti)	depth (cm)	Log(Ti/Ca)	depth (cm)	Log Ti/Ca	depth (cm)	log Ti/Ca
277	-1.21	275.5	-1.19	272	-0.95	273.5	-1.39
278	-1.20	276.5	-1.18	273	-0.90	274.5	-1.41
279	-1.17	277.5	-1.17	274	-0.99	275.5	-1.46
280	-1.17	278.5	-1.20	275	-1.08	276.5	-1.46
281	-1.17	279.5	-1.16	276	-1.10	277.5	-1.45
282	-1.16	280.5	-1.20	277	-1.09	278.5	-1.45
283	-1.17	281.5	-1.18	278	-1.08	279.5	-1.43
284	-1.16	282.5	-1.17	279	-1.05	280.5	-1.42
285	-1.16	283.5	-1.17	280	-0.99	281.5	-1.37
286	-1.17	284.5	-1.21	281	-0.91	282.5	-1.36
287	-1.19	285.5	-1.18	282	-0.89	283.5	-1.30
288	-1.16	286.5	-1.21	283	-0.89	284.5	-1.33
289	-1.17	287.5	-1.18	284	-0.89	285.5	-1.31
290	-1.16	288.5	-1.17	285	-0.90	286.5	-1.27
291	-1.17	289.5	-1.20	286	-0.89	287.5	-1.15

Table A.1 continued from previous page

64PE304-8		64PE304-34		64PE303-16		64PE303-15	
depth (cm)	Log (Ca/Ti)	depth (cm)	Log(Ti/Ca)	depth (cm)	Log Ti/Ca	depth (cm)	log Ti/Ca
292	-1.20	290.5	-1.18	287	-0.97	288.5	-1.28
293	-1.21	291.5	-1.17	288	-0.91	289.5	-1.26
294	-1.25	292.5	-1.20	289	-0.93	290.5	-1.23
295	-1.20	293.5	-1.21	290	-0.94	291.5	-1.20
296	-1.19	294.5	-1.21	291	-0.92	292.5	-1.22
297	-1.17	295.5	-1.23	292	-0.89	293.5	-1.25
298	-1.17	296.5	-1.18	293	-0.88	294.5	-1.24
299	-1.16	297.5	-1.17	294	-0.90	295.5	-1.20
300	-1.18	298.5	-1.18	295	-0.95	296.5	-1.24
301	-1.16	299.5	-1.19	296	-0.97	297.5	-1.25
302	-1.20	300.5	-1.18	297	-0.98	298.5	-1.28
303	-1.15	301.5	-1.14	298	-0.98	299.5	-1.24
304	-1.14	302.5	-1.21	299	-0.99	300.5	-1.36
305	-1.14	303.5	-1.15	300	-0.99	301.5	-1.33
306	-1.06	304.5	-1.15	301	-1.06	302.5	-1.33

Table A.1 continued from previous page

64PE304-8		64PE304-34		64PE303-16		64PE303-15	
depth (cm)	Log (Ca/Ti)	depth (cm)	Log(Ti/Ca)	depth (cm)	Log Ti/Ca	depth (cm)	log Ti/Ca
307	-1.08	305.5	-1.19	302	-1.07	303.5	-1.35
308	-1.16	306.5	-1.15	303	-1.10	304.5	-1.32
309	-1.08	307.5	-1.16	304	-1.02	305.5	-1.30
310	-1.09	308.5	-1.16	305	-1.11	306.5	-1.26
311	-1.06	309.5	-1.15	306	-1.07	307.5	-1.29
312	-1.01	310.5	-1.16	307	-1.03	308.5	-1.31
313	-1.03	311.5	-1.19	308	-1.02	309.5	-1.32
314	-1.04	312.5	-1.19	309	-1.02	310.5	-1.35
315	-1.04	313.5	-1.14	310	-1.07	311.5	-1.38
316	-1.06	314.5	-1.14	311	-1.05	312.5	-1.34
317	-1.03	315.5	-1.15	312	-1.06	313.5	-1.37
318	-1.05	316.5	-1.19	313	-1.10	314.5	-1.34
319	-1.02	317.5	-1.17	314	-1.12	315.5	-1.32
320	-1.10	318.5	-1.17	315	-1.12	316.5	-1.39
321	-1.00	319.5	-1.16	316	-1.14	317.5	-1.37

Table A.1 continued from previous page

64PE304-8		64PE304-34		64PE303-16		64PE303-15	
depth (cm)	Log (Ca/Ti)	depth (cm)	Log(Ti/Ca)	depth (cm)	Log Ti/Ca	depth (cm)	log Ti/Ca
322	-1.07	320.5	-1.13	317	-1.15	318.5	-1.35
323	-1.03	321.5	-1.08	318	-1.15	319.5	-1.37
324	-1.05	322.5	-1.10	319	-1.14	320.5	-1.36
325	-1.04	323.5	-1.12	321	-1.13	321.5	-1.35
326	-1.06	324.5	-1.12	322	-1.16	322.5	-1.34
327	-1.06	325.5	-1.11	323	-1.10	323.5	-1.35
328	-1.04	326.5	-1.06	324	-1.14	324.5	-1.32
329	-1.12	327.5	-1.10	325	-1.17	325.5	-1.32
330	-1.11	328.5	-1.16	326	-1.13	326.5	-1.33
331	-1.20	329.5	-1.14	327	-1.12	327.5	-1.31
332	-1.16	330.5	-1.13	328	-1.09	328.5	-1.28
333	-1.14	331.5	-1.07	329	-1.08	329.5	-1.27
334	-1.16	332.5	-1.02	330	-1.08	330.5	-1.28
335	-1.05	333.5	-1.02	331	-1.07	331.5	-1.28
336	-1.18	334.5	-1.03	332	-1.10	332.5	-1.28

Table A.1 continued from previous page

64PE304-8		64PE304-34		64PE303-16		64PE303-15	
depth (cm)	Log (Ca/Ti)	depth (cm)	Log(Ti/Ca)	depth (cm)	Log Ti/Ca	depth (cm)	log Ti/Ca
337	-1.19	335.5	-1.05	333	-1.10	333.5	-1.25
338	-1.16	336.5	-0.94	334	-1.08	334.5	-1.21
339	-1.16	337.5	-0.94	335	-1.10	335.5	-1.14
340	-1.20	338.5	-0.96	336	-1.13	336.5	-1.20
341	-1.19	339.5	-0.94	337	-1.15	337.5	-1.23
342	-1.20	340.5	-0.97	338	-1.18	338.5	-1.18
343	-1.18	341.5	-0.98	339	-1.18	339.5	-1.18
344	-1.16	342.5	-0.98	340	-1.20	340.5	-1.21
345	-1.15	343.5	-1.01	341	-1.19	341.5	-1.26
346	-1.11	344.5	-0.90	342	-1.19	342.5	-1.25
347	-1.13	345.5	-0.90	343	-1.18	343.5	-1.27
348	-1.13	346.5	-0.94	344	-1.16	344.5	-1.27
349	-1.12	347.5	-0.90	345	-1.16	345.5	-1.25
350	-1.14	349.5	-0.93	346	-1.18	346.5	-1.26
351	-1.17	350.5	-0.90	347	-1.17	347.5	-1.27

Table A.1 continued from previous page

64PE304-8		64PE304-34		64PE303-16		64PE303-15	
depth (cm)	Log (Ca/Ti)	depth (cm)	Log(Ti/Ca)	depth (cm)	Log Ti/Ca	depth (cm)	log Ti/Ca
352	-1.16	351.5	-0.87	348	-1.23	348.5	-1.30
353	-1.18	352.5	-0.84	349	-1.23	349.5	-1.31
355	-1.15	353.5	-0.78	350	-1.18	350.5	-1.21
356	-1.17	354.5	-0.83	351	-1.15	351.5	-1.25
357	-1.17	355.5	-0.82	352	-1.12	352.5	-1.24
358	-1.18	356.5	-0.82	353	-1.09	353.5	-1.23
359	-1.21	357.5	-0.87	354	-1.06	354.5	-1.25
360	-1.21	358.5	-0.89	355	-1.06	356.5	-1.15
361	-1.19	359.5	-0.78	356	-1.08	357.5	-1.19
362	-1.20	360.5	-0.76	357	-1.19	358.5	-1.15
363	-1.25	361.5	-0.77	358	-1.14	359.5	-1.20
364	-1.20	362.5	-0.78	359	-1.24	360.5	-1.18
365	-1.20	363.5	-0.76	360	-1.18	361.5	-1.18
366	-1.23	364.5	-0.81	361	-1.18	362.5	-1.23
367	-1.21	365.5	-0.80	362	-1.20	363.5	-1.26

Table A.1 continued from previous page

64PE304-8		64PE304-34		64PE303-16		64PE303-15	
depth (cm)	Log (Ca/Ti)	depth (cm)	Log(Ti/Ca)	depth (cm)	Log Ti/Ca	depth (cm)	log Ti/Ca
368	-1.26	366.5	-0.80	363	-1.23	364.5	-1.25
369	-1.20	367.5	-0.79	364	-1.19	365.5	-1.15
370	-1.29	368.5	-0.82	365	-1.18	366.5	-1.18
371	-1.24	369.5	-0.76	366	-1.18	367.5	-1.24
372	-1.24	370.5	-0.77	367	-1.22	368.5	-1.28
373	-1.28	371.5	-0.76	368	-1.21	369.5	-1.28
374	-1.27	372.5	-0.76	369	-1.20	370.5	-1.23
375	-1.26	373.5	-0.77	370	-1.16	371.5	-1.25
376	-1.30	374.5	-0.76	371	-1.13	372.5	-1.25
377	-1.37	375.5	-0.74	372	-1.16	373.5	-1.18
378	-1.25	376.5	-0.73	373	-1.12	374.5	-1.19
379	-1.28	377.5	-0.71	374	-1.16	375.5	-1.20
380	-1.27	378.5	-0.78	375	-1.18	376.5	-1.19
381	-1.30	379.5	-0.73	376	-1.13	377.5	-1.25
382	-1.34	380.5	-0.78	377	-1.16	378.5	-1.16

Table A.1 continued from previous page

64PE304-8		64PE304-34		64PE303-16		64PE303-15	
depth (cm)	Log (Ca/Ti)	depth (cm)	Log(Ti/Ca)	depth (cm)	Log Ti/Ca	depth (cm)	log Ti/Ca
383	-1.21	381.5	-0.80	378	-1.15	379.5	-1.17
384	-1.19	382.5	-0.71	379	-1.13	380.5	-1.15
385	-1.22	383.5	-0.67	380	-1.16	381.5	-1.15
386	-1.22	384.5	-0.70	381	-1.18	382.5	-1.19
387	-1.13	385.5	-0.71	382	-1.14	383.5	-1.24
388	-1.14	386.5	-0.71	383	-1.13	384.5	-1.25
389	-1.13	387.5	-0.77	384	-1.09	385.5	-1.24
390	-1.17	388.5	-0.76	385	-1.09	386.5	-1.18
391	-1.13	389.5	-0.78	386	-1.11	387.5	-1.17
392	-1.12	390.5	-0.81	387	-1.05	388.5	-1.15
393	-1.10	391.5	-0.79	388	-1.10	389.5	-1.16
394	-1.12	392.5	-0.81	389	-1.07	390.5	-1.20
395	-1.09	393.5	-0.81	390	-1.04	391.5	-1.16
396	-1.12	394.5	-0.78	391	-1.03	392.5	-1.10
397	-1.13	395.5	-0.81	392	-1.04	393.5	-1.06

Table A.1 continued from previous page

64PE304-8		64PE304-34		64PE303-16		64PE303-15	
depth (cm)	Log (Ca/Ti)	depth (cm)	Log(Ti/Ca)	depth (cm)	Log Ti/Ca	depth (cm)	log Ti/Ca
398	-1.10	396.5	-0.79	393	-1.01	394.5	-1.04
399	-1.11	397.5	-0.79	394	-1.05	395.5	-0.98
400	-1.16	398.5	-0.76	395	-1.00	396.5	-0.98
401	-1.10	399.5	-0.79	396	-1.10	397.5	-1.04
402	-1.13	400.5	-0.81	397	-1.10	398.5	-1.06
403	-1.07	401.5	-0.76	398	-1.11	399.5	-1.06
404	-1.08	402.5	-0.79	399	-1.12	400.5	-1.05
405	-1.11	403.5	-0.73	400	-1.16	401.5	-1.03
406	-1.10	404.5	-0.80	401	-1.17	402.5	-1.04
407	-1.11	405.5	-0.74	402	-1.18	403.5	-1.04
408	-1.05	406.5	-0.69	403	-1.16	404.5	-1.04
409	-1.04	407.5	-0.74	404	-1.17	405.5	-1.00
410	-1.05	408.5	-0.71	405	-1.14	406.5	-0.94
411	-1.11	409.5	-0.68	406	-1.11	407.5	-0.96
412	-1.09	410.5	-0.74	407	-1.14	408.5	-1.05

Table A.1 continued from previous page

64PE304-8		64PE304-34		64PE303-16		64PE303-15	
depth (cm)	Log (Ca/Ti)	depth (cm)	Log(Ti/Ca)	depth (cm)	Log Ti/Ca	depth (cm)	log Ti/Ca
413	-1.07	411.5	-0.72	408	-1.16	409.5	-1.00
414	-1.09	412.5	-0.76	409	-1.14	410.5	-0.97
415	-1.05	413.5	-0.74	410	-1.15	411.5	-1.03
416	-1.02	414.5	-0.81	411	-1.18	412.5	-0.98
417	-1.05	415.5	-0.86	412	-1.10	413.5	-0.98
418	-1.10	416.5	-0.93	413	-1.12	414.5	-1.04
419	-1.07	417.5	-0.94	414	-1.09	415.5	-1.00
420	-1.09	418.5	-1.01	415	-1.07	416.5	-1.00
421	-1.09	419.5	-1.00	416	-1.05	417.5	-0.97
422	-1.12	420.5	-0.94	417	-1.03	418.5	-1.01
423	-1.08	421.5	-0.92	418	-1.07	419.5	-0.99
424	-1.22	422.5	-0.89	419	-1.08	420.5	-1.04
425	-1.12	423.5	-0.85	420	-1.03	421.5	-1.09
426	-1.11	424.5	-0.88	421	-1.07	422.5	-1.12
427	-1.14	425.5	-0.86	422	-1.08	423.5	-1.15

Table A.1 continued from previous page

64PE304-8		64PE304-34		64PE303-16		64PE303-15	
depth (cm)	Log (Ca/Ti)	depth (cm)	Log(Ti/Ca)	depth (cm)	Log Ti/Ca	depth (cm)	log Ti/Ca
428	-1.12	426.5	-0.83	423	-1.10	424.5	-1.08
429	-1.16	427.5	-0.87	424	-1.15	425.5	-1.16
430	-1.17	428.5	-0.85	425	-1.19	426.5	-1.17
431	-1.18	429.5	-0.90	426	-1.23	427.5	-1.12
432	-1.35	430.5	-0.91	427	-1.21	428.5	-1.07
433	-1.28	431.5	-0.89	428	-1.21	429.5	-1.09
434	-1.17	432.5	-0.95	429	-1.21	430.5	-0.98
435	-1.13	433.5	-0.97	430	-1.15	431.5	-0.99
436	-1.15	434.5	-1.02	432	-1.13	432.5	-0.93
437	-1.14	435.5	-1.14	433	-1.14	433.5	-0.90
438	-1.18	436.5	-1.15	434	-1.11	434.5	-0.91
439	-1.20	437.5	-1.19	435	-1.09	435.5	-0.93
440	-1.20	438.5	-1.26	436	-1.05	436.5	-0.98
441	-1.18	439.5	-1.24	437	-1.03	437.5	-1.18
442	-1.20	440.5	-1.26	438	-1.09	438.5	-1.23

Table A.1 continued from previous page

64PE304-8		64PE304-34		64PE303-16		64PE303-15	
depth (cm)	Log (Ca/Ti)	depth (cm)	Log(Ti/Ca)	depth (cm)	Log Ti/Ca	depth (cm)	log Ti/Ca
443	-1.21	441.5	-1.27	439	-1.08	439.5	-1.22
444	-1.32	442.5	-1.25	440	-1.06	440.5	-1.23
445	-1.27	443.5	-1.28	441	-1.09		
446	-1.32	444.5	-1.28	442	-1.07		
447	-1.47	445.5	-1.29	443	-1.03		
448	-1.27	446.5	-1.24	444	-1.02		
449	-1.24	447.5	-1.20	445	-1.01		
450	-1.21	448.5	-1.16	446	-1.03		
451	-1.24	449.5	-1.11	447	-1.08		
452	-1.22	450.5	-1.08	448	-1.12		
453	-1.23	451.5	-1.09	449	-1.08		
454	-1.23	452.5	-1.05	450	-1.06		
455	-1.22	453.5	-1.09	451	-1.07		
456	-1.21	454.5	-1.11	452	-1.09		
457	-1.41	455.5	-1.13	453	-1.05		

Table A.1 continued from previous page

64PE304-8		64PE304-34		64PE303-16		64PE303-15	
depth (cm)	Log (Ca/Ti)	depth (cm)	Log(Ti/Ca)	depth (cm)	Log Ti/Ca	depth (cm)	log Ti/Ca
458	-1.32	456.5	-1.16	454	-0.96		
459	-1.31	459.5	-0.95	455	-0.97		
460	-1.30	460.5	-0.96	456	-0.94		
461	-1.29	461.5	-0.98	457	-1.01		
462	-1.32	462.5	-0.99	458	-0.97		
463	-1.33	463.5	-0.97	459	-1.01		
464.5	-1.33	464.5	-0.97	460	-1.08		
465.5	-1.35	465.5	-0.95	461	-1.04		
466.5	-1.34	466.5	-0.96	462	-1.08		
467.5	-1.35	467.5	-0.99	463	-1.10		
468.5	-1.36	468.5	-0.98	464	-1.01		
469.5	-1.35	469.5	-0.99	465	-0.96		
470.5	-1.36	470.5	-1.11	466	-0.96		
471.5	-1.37	471.5	-1.06	467	-0.96		
472.5	-1.35	472.5	-1.04	468	-1.02		

Table A.1 continued from previous page

64PE304-8		64PE304-34		64PE303-16		64PE303-15	
depth (cm)	Log (Ca/Ti)	depth (cm)	Log(Ti/Ca)	depth (cm)	Log Ti/Ca	depth (cm)	log Ti/Ca
473.5	-1.33	473.5	-1.05	469	-1.00		
474.5	-1.37	474.5	-1.04	470	-0.82		
475.5	-1.36	475.5	-1.03	471	-0.87		
476.5	-1.38	476.5	-1.03	472	-0.97		
477.5	-1.32	477.5	-1.04	473	-0.96		
478.5	-1.36	478.5	-1.06	474	-1.00		
479.5	-1.34	479.5	-1.17	475	-0.99		
480.5	-1.34	480.5	-1.18	476	-1.00		
481.5	-1.36	481.5	-1.12	477	-0.92		
482.5	-1.35	482.5	-1.11	478	-0.95		
483.5	-1.39	483.5	-1.08	479	-1.04		
484.5	-1.37	484.5	-1.08	480	-1.07		
485.5	-1.39	485.5	-1.05	481	-1.08		
486.5	-1.39	486.5	-1.02	482	-1.07		
487.5	-1.41	487.5	-1.03	483	-1.07		

Table A.1 continued from previous page

64PE304-8		64PE304-34		64PE303-16		64PE303-15	
depth (cm)	Log (Ca/Ti)	depth (cm)	Log(Ti/Ca)	depth (cm)	Log Ti/Ca	depth (cm)	log Ti/Ca
488.5	-1.43	488.5	-1.04	484	-1.02		
489.5	-1.44	489.5	-1.03	485	-1.03		
490.5	-1.44	490.5	-1.03	486	-1.10		
491.5	-1.44	491.5	-0.99	487	-1.09		
492.5	-1.43	492.5	-1.01	488	-1.07		
493.5	-1.44	493.5	-1.03	489	-1.06		
494.5	-1.56	494.5	-1.02	490	-1.07		
495.5	-1.57	495.5	-1.02	491	-1.09		
496.5	-1.49	496.5	-0.97	492	-1.12		
497.5	-1.52	497.5	-1.03	493	-1.12		
498.5	-1.59	498.5	-1.19	494	-1.10		
499.5	-1.64	499.5	-1.01	495	-1.12		
500.5	-1.66	500.5	-1.03	496	-1.12		
501.5	-1.67	501.5	-1.03	497	-1.07		
502.5	-1.67	502.5	-1.04	498	-1.07		

Table A.1 continued from previous page

64PE304-8		64PE304-34		64PE303-16		64PE303-15	
depth (cm)	Log (Ca/Ti)	depth (cm)	Log(Ti/Ca)	depth (cm)	Log Ti/Ca	depth (cm)	log Ti/Ca
503.5	-1.70	503.5	-0.98	499	-1.12		
504.5	-1.61	504.5	-0.96	500	-1.13		
505.5	-1.76	505.5	-1.02	501	-1.09		
506.5	-1.81	506.5	-0.96	502	-1.14		
507.5	-1.84	507.5	-0.95	503	-1.16		
508.5	-1.86	508.5	-1.00	504	-1.18		
509.5	-1.78	509.5	-0.98	505	-1.17		
510.5	-1.73	510.5	-0.98	506	-1.14		
511.5	-1.62	511.5	-1.01	507	-1.11		
512.5	-1.56	512.5	-0.99	508	-1.10		
513.5	-1.48	513.5	-1.02	509	-1.09		
514.5	-1.34	514.5	-1.03	510	-1.01		
515.5	-1.42	515.5	-0.97	511	-1.07		
516.5	-1.38	516.5	-0.99	512	-1.10		
517.5	-1.38	517.5	-1.03	513	-1.09		

Table A.1 continued from previous page

64PE304-8		64PE304-34		64PE303-16		64PE303-15	
depth (cm)	Log (Ca/Ti)	depth (cm)	Log(Ti/Ca)	depth (cm)	Log Ti/Ca	depth (cm)	log Ti/Ca
518.5	-1.43	518.5	-0.98	514	-1.14		
519.5	-1.45	519.5	-1.02	515	-1.16		
520.5	-1.49	520.5	-1.01	516	-1.14		
521.5	-1.58	521.5	-0.97	517	-1.03		
522.5	-1.57	522.5	-0.98	518	-1.07		
523.5	-1.51	523.5	-0.97	519	-1.04		
524.5	-1.48	524.5	-1.02	520	-1.03		
525.5	-1.53	525.5	-1.02	521	-1.05		
526.5	-1.45	526.5	-1.03	522	-1.01		
527.5	-1.46	527.5	-1.01	523	-1.01		
528.5	-1.49	528.5	-1.02	524	-1.00		
529.5	-1.46	529.5	-1.07	525	-1.00		
530.5	-1.45	530.5	-1.10	526	-1.00		
531.5	-1.43	531.5	-1.16	527	-0.99		
532.5	-1.48	532.5	-1.13	528	-0.99		

Table A.1 continued from previous page

64PE304-8		64PE304-34		64PE303-16		64PE303-15	
depth (cm)	Log (Ca/Ti)	depth (cm)	Log(Ti/Ca)	depth (cm)	Log Ti/Ca	depth (cm)	log Ti/Ca
533.5	-1.46	533.5	-1.13	529	-0.99		
534.5	-1.40	534.5	-1.19	530	-0.99		
535.5	-1.40	535.5	-1.20	531	-0.99		
536.5	-1.42	536.5	-1.21	532	-1.00		
537.5	-1.50	537.5	-1.21	533	-1.03		
538.5	-1.38	538.5	-1.24	534	-0.98		
539.5	-1.40	539.5	-1.26	535	-1.01		
540.5	-1.44	540.5	-1.25	536	-0.94		
541.5	-1.38	541.5	-1.24	537	-0.95		
542.5	-1.33	542.5	-1.20	538	-1.02		
543.5	-1.23	543.5	-1.18				
544.5	-1.31	544.5	-1.09				
545.5	-1.19	545.5	-1.12				
546.5	-1.28	546.5	-1.21				
547.5	-1.22	547.5	-1.01				

Table A.1 continued from previous page

64PE304-8		64PE304-34		64PE303-16		64PE303-15	
depth (cm)	Log (Ca/Ti)	depth (cm)	Log(Ti/Ca)	depth (cm)	Log Ti/Ca	depth (cm)	log Ti/Ca
548.5	-1.22	548.5	-1.14				
549.5	-1.27	549.5	-0.99				
550.5	-1.35	550.5	-0.97				
551.5	-1.24	551.5	-0.95				
552.5	-1.34	552.5	-1.03				
553.5	-1.20	553.5	-0.99				
554.5	-1.28	554.5	-1.14				
555.5	-1.24	555.5	-0.97				
556.5	-1.23	556.5	-0.96				
557.5	-1.21	557.5	-0.98				
558.5	-1.21	558.5	-0.96				
559.5	-1.22	559.5	-0.97				
560.5	-1.25	560.5	-0.97				
561.5	-1.27	561.5	-0.98				
562.5	-1.23	562.5	-1.00				

Table A.1 continued from previous page

64PE304-8		64PE304-34		64PE303-16		64PE303-15	
depth (cm)	Log (Ca/Ti)	depth (cm)	Log(Ti/Ca)	depth (cm)	Log Ti/Ca	depth (cm)	log Ti/Ca
563.5	-1.24	563.5	-1.01				
564.5	-1.22	564.5	-1.00				
565.5	-1.21	565.5	-1.05				
566.5	-1.26	566.5	-1.06				
567.5	-1.21	567.5	-1.10				
568.5	-1.20	569.5	-1.06				
569.5	-1.22	570.5	-1.13				
570.5	-1.24	571.5	-1.11				
571.5	-1.17	572.5	-1.12				
572.5	-1.22	573.5	-1.08				
574	-1.13	574.5	-1.09				
575	-1.26	575.5	-1.10				
576	-1.15	576.5	-1.13				
577	-1.16	577.5	-1.16				
578	-1.18	578.5	-1.19				

Table A.1 continued from previous page

64PE304-8		64PE304-34		64PE303-16		64PE303-15	
depth (cm)	Log (Ca/Ti)	depth (cm)	Log(Ti/Ca)	depth (cm)	Log Ti/Ca	depth (cm)	log Ti/Ca
579	-1.17	579.5	-1.20				
580	-1.23	580.5	-1.21				
581	-1.27	581.5	-1.21				
582	-1.27	582.5	-1.22				
583	-1.26	583.5	-1.23				
584	-1.27	584.5	-1.25				
585	-1.36	585.5	-1.24				
586	-1.40	586.5	-1.22				
587	-1.36	587.5	-1.25				
588	-1.40	588.5	-1.25				
589	-1.32	589.5	-1.28				
590	-1.29	590.5	-1.28				
591	-1.29	591.5	-1.26				
592	-1.29	592.5	-1.28				
593	-1.23	593.5	-1.25				

Table A.1 continued from previous page

64PE304-8		64PE304-34		64PE303-16		64PE303-15	
depth (cm)	Log (Ca/Ti)	depth (cm)	Log(Ti/Ca)	depth (cm)	Log Ti/Ca	depth (cm)	log Ti/Ca
594	-1.28	594.5	-1.24				
595	-1.27	595.5	-1.28				
596	-1.31	596.5	-1.39				
597	-1.33	597.5	-1.49				
598	-1.32	598.5	-1.58				
599	-1.32	599.5	-1.64				
600	-1.32	600.5	-1.60				
601	-1.35	601.5	-1.56				
602	-1.30	602.5	-1.60				
603	-1.32	603.5	-1.48				
604	-1.28	604.5	-1.35				
605	-1.28	605.5	-1.38				
606	-1.27	606.5	-1.38				
607	-1.23	607.5	-1.32				
608	-1.23	608.5	-1.31				

Table A.1 continued from previous page

64PE304-8		64PE304-34		64PE303-16		64PE303-15	
depth (cm)	Log (Ca/Ti)	depth (cm)	Log(Ti/Ca)	depth (cm)	Log Ti/Ca	depth (cm)	log Ti/Ca
609	-1.21	609.5	-1.41				
610	-1.25	610.5	-1.44				
611	-1.25	611.5	-1.51				
612	-1.25	612.5	-1.47				
613	-1.29	613.5	-1.47				
614	-1.17	614.5	-1.52				
615	-1.24	615.5	-1.48				
616	-1.22	616.5	-1.49				
617	-1.23	617.5	-1.46				
618	-1.21	618.5	-1.44				
619	-1.23	619.5	-1.46				
620	-1.25	620.5	-1.45				
621	-1.27	621.5	-1.43				
622	-1.28	622.5	-1.43				
623	-1.28	623.5	-1.35				

Table A.1 continued from previous page

64PE304-8		64PE304-34		64PE303-16		64PE303-15	
depth (cm)	Log (Ca/Ti)	depth (cm)	Log(Ti/Ca)	depth (cm)	Log Ti/Ca	depth (cm)	log Ti/Ca
624	-1.30	624.5	-1.38				
625	-1.20	625.5	-1.37				
626	-1.19	626.5	-1.32				
627	-1.18	627.5	-1.26				
628	-1.15	628.5	-1.26				
629	-1.16	629.5	-1.27				
630	-1.22	630.5	-1.25				
631	-1.20	631.5	-1.30				
632	-1.26	632.5	-1.26				
633	-1.23	633.5	-1.28				
634	-1.23	634.5	-1.22				
635	-1.23	635.5	-1.20				
636	-1.22	636.5	-1.19				
637	-1.25	637.5	-1.20				
638	-1.23	638.5	-1.18				

Table A.1 continued from previous page

64PE304-8		64PE304-34		64PE303-16		64PE303-15	
depth (cm)	Log (Ca/Ti)	depth (cm)	Log(Ti/Ca)	depth (cm)	Log Ti/Ca	depth (cm)	log Ti/Ca
639	-1.22	639.5	-1.28				
640	-1.29	640.5	-1.13				
641	-1.28	641.5	-1.22				
642	-1.29	642.5	-1.21				
643	-1.32	643.5	-1.21				
644	-1.29	644.5	-1.27				
645	-1.25	645.5	-1.22				
646	-1.25	646.5	-1.22				
647	-1.24	647.5	-1.27				
648	-1.23	648.5	-1.21				
649	-1.31	649.5	-1.23				
650	-1.35	650.5	-1.20				
651	-1.35	651.5	-1.20				
652	-1.35	652.5	-1.16				
653	-1.35	653.5	-1.22				

Table A.1 continued from previous page

64PE304-8		64PE304-34		64PE303-16		64PE303-15	
depth (cm)	Log (Ca/Ti)	depth (cm)	Log(Ti/Ca)	depth (cm)	Log Ti/Ca	depth (cm)	log Ti/Ca
654	-1.34	654.5	-1.21				
655	-1.38	655.5	-1.22				
656	-1.38	656.5	-1.24				
657	-1.41	657.5	-1.22				
658	-1.41	658.5	-1.22				
659	-1.55	659.5	-1.24				
660	-1.50	660.5	-1.27				
661	-1.50	661.5	-1.25				
662	-1.35	662.5	-1.23				
663	-1.38	663.5	-1.23				
664	-1.35	664.5	-1.25				
665	-1.36	665.5	-1.29				
666	-1.31	666.5	-1.25				
667	-1.32	667.5	-1.32				
668	-1.21	668.5	-1.28				

Table A.1 continued from previous page

64PE304-8		64PE304-34		64PE303-16		64PE303-15	
depth (cm)	Log (Ca/Ti)	depth (cm)	Log(Ti/Ca)	depth (cm)	Log Ti/Ca	depth (cm)	log Ti/Ca
669	-1.23	669.5	-1.32				
670	-1.24	670.5	-1.31				
671	-1.26	671.5	-1.32				
672	-1.15	672.5	-1.28				
673	-0.99	673.5	-1.34				
674	-1.02	674.5	-1.35				
675	-0.99	675.5	-1.36				
676	-1.06	676.5	-1.39				
677	-1.09						
678	-1.18						
679	-1.28						
680	-1.22						
681	-1.27						

Appendix B

Stable Isotope data

TABLE B.1: Stable Isotope Data for core 64PE304-8

G. ruber			*N. dutertrei*			*C wuellerstorfi*		
Depth (cm)	$\delta^{13}C$ (‰)	$\delta^{18}O$ (‰)	Depth (cm)	$\delta^{13}C$ (‰)	$\delta^{18}O$ (‰)	Depth (cm)	$\delta^{13}C$ (‰)	$\delta^{18}O$ (‰)
0.5	1.34	-1.97	0.5	1.19	-1.10	0.5	0.80	1.58
1.5	1.07	-2.21	1.5	1.06	-1.28	2.5	0.82	1.43
2.5	1.63	-1.93	2.5	1.17	-1.23	4.5	0.98	1.83
2.5	1.25	-2.07	2.5	0.98	-1.10	6.5	1.07	1.73
2.5	1.42	-2.15	3.5	1.34	-0.86	7.5	0.97	1.80
2.5	1.63	-1.93	4.5	1.09	-1.09	8.5	1.00	1.89
3.5	1.26	-2.26	5.5	1.05	-1.24	9.5	1.09	1.83
4.5	1.34	-2.24	6.5	1.07	-1.10	10.5	0.95	1.92
5.5	1.28	-2.15	7.5	0.88	-1.30	12.5	1.02	1.90
6.5	1.37	-2.02	8.5	1.13	-1.15	14.5	0.87	1.88
7.5	1.24	-2.12	9.5	1.36	-1.40	15.5	1.12	1.77
8.5	1.19	-1.90	10.5	1.15	-1.16	16.5	0.86	1.89
9.5	1.55	-1.88	12.5	0.99	-1.01	17.5	1.06	1.67
10.5	1.50	-1.90	14.5	1.26	-1.06	18.5	0.91	1.74
12.5	1.18	-2.26	15.5	0.97	-1.23	19.5	0.96	1.86

Table B.1 continued from previous page

G. ruber			*N. dutertrei*			*C wuellerstorfi*		
Depth (cm)	$\delta^{13}C$	$\delta^{18}O$	Depth (cm)	$\delta^{13}C$	$\delta^{18}O$	Depth (cm)	$\delta^{13}C$	$\delta^{18}O$
14.5	1.24	-2.05	16.5	0.97	-1.17	20.5	1.00	1.38
15.5	1.29	-2.15	17.5	1.09	-0.93	28.5	1.12	1.83
16.5	1.44	-2.17	18.5	1.44	-1.03	31.5	0.74	1.86
17.5	1.36	-2.03	19.5	0.80	-1.11	32.5	1.20	1.85
18.5	1.50	-2.12	20.5	0.85	-1.59	33.5	1.04	1.88
18.5	1.50	-2.12	26.5	1.26	-1.15	34.5	1.42	1.67
19.5	1.45	-2.20	28.5	1.15	-1.23	35.5	1.06	1.82
20.5	1.24	-2.11	31.5	0.86	-1.17	36.5	1.03	1.78
28.5	1.41	-2.17	32.5	1.24	-1.21	38.5	1.08	1.88
29.5	1.26	-2.18	33.5	1.03	-1.00	39.5	1.14	1.93
31.5	1.73	-2.09	34.5	1.18	-1.10	40.5	1.00	1.85
31.5	1.73	-2.09	35.5	1.14	-1.11	41.5	0.78	1.71
32.5	1.64	-2.20	36.5	1.24	-0.99	42.5	1.13	1.76
33.5	1.38	-2.08	38.5	1.29	-1.10	47.5	1.04	1.82
34.5	1.16	-2.10	39.5	1.18	-1.19	51.5	0.72	1.54

Table B.1 continued from previous page

G. ruber			*N. dutertrei*			*C wuellerstorfi*		
Depth (cm)	$\delta^{13}C$	$\delta^{18}O$	Depth (cm)	$\delta^{13}C$	$\delta^{18}O$	Depth (cm)	$\delta^{13}C$	$\delta^{18}O$
36.5	1.13	-1.98	40.5	1.21	-1.15	54.5	1.10	1.81
38.5	1.42	-2.00	41.5	1.46	-1.09	55.5	1.16	1.92
39.5	1.19	-1.93	42.5	1.11	-0.91	55.5	1.03	1.84
40.5	1.39	-1.97	47.5	1.03	-1.22	57.5	0.69	1.96
41.5	1.58	-2.16	51.5	1.26	-1.12	58.5	1.05	1.89
42.5	1.37	-2.21	54.5	1.09	-0.98	59.5	0.92	1.93
47.5	1.28	-2.05	55.5	1.12	-1.05	60.5	0.91	2.06
51.5	1.59	-2.03	56.5	1.12	-1.14	61.5	0.88	1.73
51.5	1.59	-2.03	57.5	1.18	-1.05	65.5	0.92	1.98
54.5	1.27	-2.04	58.5	1.22	-0.91	65.5	1.15	1.71
55.5	1.16	-1.97	59.5	1.26	-1.09	66.5	0.84	1.96
56.5	1.55	-2.20	60.5	1.13	-1.15	70.5	0.83	2.12
57.5	1.21	-1.82	61.5	1.16	-1.28	71.5	0.65	1.65
58.5	1.26	-1.95	65.5	1.50	-1.04	72.5	0.89	1.93
59.5	1.30	-2.18	66.5	1.00	-0.86	73.5	0.69	2.21

Table B.1 continued from previous page

G. ruber			*N. dutertrei*			*C wuellerstorfi*		
Depth (cm)	$\delta^{13}C$	$\delta^{18}O$	Depth (cm)	$\delta^{13}C$	$\delta^{18}O$	Depth (cm)	$\delta^{13}C$	$\delta^{18}O$
60.5	1.02	-2.07	67.5	0.99	-0.85	74.5	0.63	2.08
61.5	0.89	-1.99	70.5	1.04	-0.66	75.5	0.76	2.12
65.5	1.47	-2.21	71.5	1.04	-0.84	76.5	0.73	2.24
66.5	1.21	-1.94	73.5	1.02	-0.76	77.5	0.74	2.31
67.5	1.38	-1.85	74.5	1.18	-0.73	78.5	0.54	2.22
70.5	1.10	-2.16	75.5	1.14	-0.90	79.5	0.95	2.11
71.5	1.22	-2.02	76.5	1.14	-0.49	80.5	0.83	2.72
71.5	1.22	-2.02	77.5	0.97	-0.59	80.5	0.62	2.26
72.5	1.00	-1.86	78.5	0.97	-0.75	81.5	0.68	2.19
74.5	1.00	-1.75	79.5	0.94	-0.86	82.5	0.67	2.02
75.5	1.07	-1.84	80.5	0.93	-0.61	83.5	0.83	2.12
76.5	1.13	-1.91	81.5	0.79	-0.71	84.5	0.58	2.01
78.5	0.91	-2.07	82.5	0.95	-0.81	85.5	0.66	2.34
80.5	1.41	-1.98	83.5	1.16	-0.51	86.5	0.46	2.12
81.5	1.09	-1.96	84.5	0.72	-0.61	87.5	0.68	2.02

Table B.1 continued from previous page

G. ruber			*N. dutertrei*			*C wuellerstorfi*		
Depth (cm)	$\delta^{13}C$	$\delta^{18}O$	Depth (cm)	$\delta^{13}C$	$\delta^{18}O$	Depth (cm)	$\delta^{13}C$	$\delta^{18}O$
82.5	0.91	-2.21	85.5	1.11	-0.66	88.5	0.48	2.38
84.5	1.06	-1.83	86.5	0.75	-0.80	89.5	0.62	2.17
84.5	1.14	-1.80	87.5	0.93	-0.63	90.5	0.80	2.01
85.5	0.95	-1.98	88.5	1.03	-0.56	91.5	0.69	2.37
86.5	1.05	-1.95	89.5	1.07	-0.89	92.5	0.75	2.00
88.5	0.94	-2.04	90.5	0.89	-0.68	93.5	0.77	2.21
89.5	1.15	-1.67	91.5	1.01	-0.44	94.5	0.67	2.11
90.5	0.90	-1.91	92.5	1.12	-0.71	96.5	0.90	2.24
91.5	1.21	-1.93	93.5	1.15	-0.74	98.5	0.43	2.09
91.5	1.21	-1.93	94.5	1.27	-0.83	100.5	0.58	2.16
92.5	0.89	-1.95	96.5	1.08	-0.68	101.5	0.39	2.14
93.5	0.79	-1.78	98.5	0.77	-0.59	102.5	0.54	2.24
94.5	1.14	-1.86	100.5	0.95	-0.51	104.5	0.48	2.22
96.5	1.13	-1.91	101.5	0.81	-0.56	106.5	0.44	2.12
100.5	1.06	-1.77	102.5	0.83	-0.63	108.5	0.51	2.28

Table B.1 continued from previous page

G. ruber			*N. dutertrei*			*C wuellerstorfi*		
Depth (cm)	$\delta^{13}C$	$\delta^{18}O$	Depth (cm)	$\delta^{13}C$	$\delta^{18}O$	Depth (cm)	$\delta^{13}C$	$\delta^{18}O$
101.5	0.83	-1.80	104.5	0.90	-0.73	109.5	0.69	2.36
104.5	1.01	-1.77	106.5	1.14	-0.67	110.5	0.45	2.12
106.5	1.10	-1.83	108.5	0.71	-0.45	111.5	0.43	2.07
108.5	0.93	-1.74	109.5	0.93	-0.22	112.5	0.38	2.26
109.5	1.00	-1.67	110.5	0.73	-0.42	114.5	0.53	2.47
110.5	0.96	-1.72	111.5	0.77	-0.15	115.5	1.12	2.48
111.5	1.09	-1.44	112.5	0.87	-0.46	117.5	1.07	2.62
111.5	1.09	-1.44	114.5	0.82	-0.02	120.5	1.09	2.32
112.5	0.80	-1.53	115.5	1.21	0.06	121.5	1.09	2.40
114.5	0.95	-1.59	116.5	0.93	-0.19	122.5	0.89	2.78
115.5	0.97	-1.22	117.5	1.01	-0.15	123.5	0.95	2.56
116.5	1.04	-1.22	118.5	0.63	0.04	124.5	0.79	2.92
117.5	1.05	-1.20	120.5	0.96	-0.29	125.5	1.22	2.72
118.5	1.10	-1.50	121.5	0.98	-0.09	126.5	0.94	3.13
120.5	0.94	-1.22	122.5	1.10	0.08	128.5	0.83	3.20

Table B.1 continued from previous page

G. ruber			*N. dutertrei*			*C wuellerstorfi*		
Depth (cm)	$\delta^{13}C$	$\delta^{18}O$	Depth (cm)	$\delta^{13}C$	$\delta^{18}O$	Depth (cm)	$\delta^{13}C$	$\delta^{18}O$
121.5	0.87	-1.04	123.5	0.95	-0.07	129.0	1.37	3.19
122.5	0.92	-1.20	124.5	0.82	-0.08	130.0	0.87	2.82
123.5	0.80	-1.38	125.5	0.91	-0.12	131.0	0.90	2.97
124.5	1.00	-1.24	126.5	1.12	0.17	132.0	0.81	2.71
125.5	0.98	-1.00	128.5	0.99	-0.17	133.0	0.77	2.82
126.5	1.12	-1.11	129.0	1.17	0.19	134.0	0.79	2.57
128.5	1.24	-1.21	130.0	1.12	0.20	135.0	0.79	3.09
129.0	1.11	-1.12	131.0	1.11	-0.04	136.0	0.71	2.91
130.0	0.94	-0.99	132.0	1.05	-0.18	137.0	1.14	3.15
131.0	1.04	-0.93	133.0	1.07	0.15	138.0	0.71	2.92
131.0	1.04	-0.93	134.0	1.06	-0.05	139.0	1.10	3.55
132.0	1.06	-1.02	135.0	1.31	0.55	140.0	1.06	3.29
133.0	0.94	-0.82	136.0	0.79	0.29	141.0	0.98	3.05
134.0	0.95	-1.15	137.0	0.82	0.07	142.0	1.15	3.17
135.0	1.16	-0.28	138.0	1.10	0.48	143.0	1.36	3.49

Table B.1 continued from previous page

G. ruber			*N. dutertrei*			*C wuellerstorfi*		
Depth (cm)	$\delta^{13}C$	$\delta^{18}O$	Depth (cm)	$\delta^{13}C$	$\delta^{18}O$	Depth (cm)	$\delta^{13}C$	$\delta^{18}O$
136.0	1.08	-0.77	139.0	1.26	0.47	144.0	0.90	3.31
137.0	0.98	-0.48	140.0	1.28	0.34	145.0	1.01	3.62
138.0	1.15	-0.62	141.0	1.18	0.36	147.0	0.95	3.44
140.0	1.23	-0.51	142.0	1.54	0.39	148.0	0.97	3.42
141.0	1.16	-0.54	143.0	1.07	0.54	149.0	1.04	3.66
142.0	0.84	-0.92	144.0	1.03	0.67	150.0	1.20	3.27
143.0	0.63	-0.33	145.0	1.23	0.59	151.0	1.17	3.43
144.0	1.06	-0.47	146.0	1.30	0.69	152.0	0.94	3.09
145.0	0.92	-0.31	147.0	1.07	0.36	153.0	1.16	3.28
146.0	0.97	-0.59	148.0	1.33	0.75	154.0	0.94	3.26
147.0	1.01	-0.55	149.0	1.40	0.49	155.0	0.92	3.41
149.0	1.12	-0.71	150.0	1.18	0.53	156.0	1.06	3.35
150.0	0.93	-0.67	151.0	1.50	0.61	157.0	0.98	3.42
151.0	1.20	-0.70	152.0	1.19	0.33	158.0	0.98	3.14
151.0	1.20	-0.70	153.0	0.82	0.45	159.0	1.13	2.99

Table B.1 continued from previous page

G. ruber			*N. dutertrei*			*C wuellerstorfi*		
Depth (cm)	$\delta^{13}C$	$\delta^{18}O$	Depth (cm)	$\delta^{13}C$	$\delta^{18}O$	Depth (cm)	$\delta^{13}C$	$\delta^{18}O$
152.0	1.42	-0.61	154.0	1.28	0.51	160.0	0.87	3.35
153.0	1.05	-0.49	155.0	1.17	0.77	162.0	0.93	3.18
154.0	1.07	-0.50	156.0	1.54	0.38	163.0	1.16	3.05
155.0	1.21	-0.44	157.0	1.31	0.56	164.0	0.86	3.24
156.0	1.21	-0.51	158.0	1.52	0.47	165.0	1.33	3.14
157.0	0.50	-1.03	159.0	1.21	0.41	166.0	0.92	3.19
158.0	1.05	-0.85	160.0	1.34	0.22	167.0	0.90	3.08
159.0	0.92	-0.67	161.0	1.32	0.52	168.0	0.92	3.28
160.0	1.05	-0.62	162.0	1.29	0.45	169.0	0.64	3.16
161.0	1.07	-0.70	163.0	1.23	0.46	171.0	0.98	2.76
162.0	0.93	-0.60	164.0	1.60	0.33	172.0	1.11	3.08
163.0	1.09	-0.63	165.0	1.11	0.72	173.0	0.90	3.26
165.0	0.96	-0.74	166.0	1.45	0.27	174.0	0.86	3.11
166.0	1.29	-0.63	167.0	1.34	0.27	175.0	1.18	3.38
167.0	1.35	-0.70	168.0	1.47	0.40	176.0	1.00	3.13

Table B.1 continued from previous page

G. ruber			*N. dutertrei*			*C wuellerstorfi*		
Depth (cm)	$\delta^{13}C$	$\delta^{18}O$	Depth (cm)	$\delta^{13}C$	$\delta^{18}O$	Depth (cm)	$\delta^{13}C$	$\delta^{18}O$
169.0	1.17	-0.59	169.0	1.42	0.05	177.0	1.25	3.51
170.0	1.27	-0.75	170.0	1.37	0.16	178.0	0.86	3.03
171.0	1.25	-0.79	171.0	1.20	0.11	179.0	1.25	3.41
171.0	1.25	-0.79	172.0	1.66	0.32	180.0	1.07	3.16
173.0	0.91	-0.78	173.0	1.20	0.18	182.0	1.09	2.96
175.0	1.05	-0.82	175.0	1.31	0.42	183.0	1.06	3.11
176.0	1.19	-0.79	176.0	1.65	0.34	184.0	0.87	3.00
177.0	0.76	-0.82	177.0	1.08	0.24	185.0	1.22	3.11
178.0	1.41	-0.82	178.0	1.50	0.11	186.0	1.25	3.05
179.0	1.16	-0.83	179.0	1.35	0.31	187.0	1.12	3.02
180.0	0.77	-0.91	180.0	1.52	-0.05	188.0	1.10	3.17
181.0	1.06	-0.72	181.0	1.31	0.14	189.0	1.20	3.14
183.0	1.22	-0.82	182.0	1.22	0.13	190.0	0.79	2.86
184.0	1.22	-0.95	183.0	1.27	0.15	191.0	0.70	2.91
185.0	1.07	-0.72	184.0	1.54	0.28	192.0	1.07	2.94

Table B.1 continued from previous page

G. ruber			*N. dutertrei*			*C wuellerstorfi*		
Depth (cm)	$\delta^{13}C$	$\delta^{18}O$	Depth (cm)	$\delta^{13}C$	$\delta^{18}O$	Depth (cm)	$\delta^{13}C$	$\delta^{18}O$
186.0	1.03	-0.92	185.0	1.61	0.40	193.0	1.19	2.99
187.0	1.28	-0.89	186.0	1.73	0.24	194.0	0.89	2.95
188.0	1.12	-0.89	187.0	1.24	0.19	195.0	1.10	2.96
189.0	1.12	-0.83	188.0	1.77	0.08	196.0	0.90	2.87
190.0	1.21	-0.83	189.0	1.60	0.18	197.0	1.00	3.20
191.0	1.29	-0.69	190.0	1.24	0.20	198.0	0.89	2.94
191.0	1.29	-0.69	191.0	1.49	0.04	199.0	1.07	2.44
193.0	0.86	-1.12	192.0	1.41	0.05	200.0	0.92	2.96
194.0	1.35	-1.16	193.0	1.27	0.21	201.0	0.97	2.86
195.0	0.90	-0.99	193.0	1.28	0.09	202.0	0.93	2.91
197.0	1.19	-0.96	194.0	1.01	-0.06	203.0	0.76	2.99
198.0	1.19	-0.93	195.0	1.20	-0.10	204.0	0.95	2.87
199.0	1.18	-1.05	196.0	1.40	0.00	205.0	1.07	3.13
201.0	0.89	-0.82	197.0	1.05	-0.14	206.0	1.06	3.11
202.0	1.30	-0.70	198.0	1.22	-0.10	207.0	1.40	3.11

Table B.1 continued from previous page

G. ruber			*N. dutertrei*			*C wuellerstorfi*		
Depth (cm)	$\delta^{13}C$	$\delta^{18}O$	Depth (cm)	$\delta^{13}C$	$\delta^{18}O$	Depth (cm)	$\delta^{13}C$	$\delta^{18}O$
203.0	1.27	-0.95	199.0	1.12	-0.03	208.0	0.82	2.92
204.0	0.98	-1.13	200.0	1.36	-0.23	209.0	0.85	2.70
205.0	1.15	-0.98	201.0	1.18	-0.04	210.0	0.90	2.89
206.0	1.04	-0.89	203.0	0.83	-0.26	211.0	0.74	2.90
207.0	1.13	-0.87	204.0	1.21	-0.10	212.0	0.94	2.97
209.0	0.94	-0.89	205.0	1.16	0.08	213.0	1.01	3.03
210.0	1.22	-1.01	206.0	1.44	0.05	214.0	0.94	2.79
211.0	0.91	-0.90	207.0	1.13	0.19	215.0	1.19	2.92
211.0	0.91	-0.90	208.0	1.13	0.05	216.0	1.22	2.83
212.0	1.56	-1.00	209.0	1.56	-0.10	217.0	1.16	2.97
213.0	1.19	-1.01	211.0	1.36	-0.09	218.0	1.21	3.10
214.0	1.15	-0.87	212.0	1.06	-0.35	219.0	1.03	2.95
215.0	1.23	-0.90	213.0	1.15	-0.23	220.0	1.08	2.91
216.0	1.37	-1.04	214.0	0.91	-0.37	221.0	1.48	3.19
217.0	1.14	-0.88	215.0	0.90	-0.11	222.0	0.86	2.88

Table B.1 continued from previous page

G. ruber			*N. dutertrei*			*C wuellerstorfi*		
Depth (cm)	$\delta^{13}C$	$\delta^{18}O$	Depth (cm)	$\delta^{13}C$	$\delta^{18}O$	Depth (cm)	$\delta^{13}C$	$\delta^{18}O$
218.0	0.90	-0.84	216.0	1.03	-0.04	223.0	1.02	2.98
219.0	0.92	-0.99	217.0	1.00	-0.05	224.0	1.22	2.90
220.0	1.23	-0.88	218.0	0.86	0.17	225.0	0.90	3.09
221.0	0.89	-0.98	219.0	1.06	0.00	226.0	0.81	2.87
222.0	1.39	-1.08	220.0	1.41	-0.05	227.0	1.03	2.84
223.0	1.39	-0.98	221.0	0.86	-0.10	228.0	0.80	2.76
224.0	1.42	-0.96	222.0	1.38	-0.08	229.0	0.97	3.16
225.0	1.09	-0.92	223.0	1.06	-0.11	230.0	0.76	2.91
226.0	1.12	-0.92	224.0	1.45	-0.15	231.0	0.65	2.68
227.0	1.15	-1.13	225.0	1.02	-0.06	232.0	0.99	2.79
228.0	1.30	-1.00	226.0	1.37	-0.08	233.0	0.96	2.88
229.0	1.21	-0.98	227.0	0.91	0.16	235.0	1.17	2.93
231.0	1.34	-1.02	228.0	1.19	-0.22	236.0	1.00	2.81
231.0	1.34	-1.02	230.0	1.04	-0.07	237.0	1.05	3.01
232.0	1.08	-1.10	231.0	1.12	-0.11	238.0	0.87	2.84

Table B.1 continued from previous page

G. ruber			*N. dutertrei*			*C wuellerstorfi*		
Depth (cm)	$\delta^{13}C$	$\delta^{18}O$	Depth (cm)	$\delta^{13}C$	$\delta^{18}O$	Depth (cm)	$\delta^{13}C$	$\delta^{18}O$
233.0	0.70	-1.33	232.0	1.13	0.07	240.0	0.68	2.66
234.0	1.11	-1.03	233.0	0.99	0.12	242.0	0.78	2.77
235.0	1.03	-1.22	234.0	0.93	0.08	244.0	0.93	2.92
236.0	1.37	-1.15	235.0	1.00	-0.08	246.0	0.75	2.80
237.0	1.45	0.14	236.0	1.04	-0.35	248.0	0.73	2.57
238.0	1.10	-1.01	237.0	0.88	-0.04	250.0	0.53	2.55
240.0	1.09	-1.28	238.0	0.83	0.02	251.0	0.83	2.86
242.0	1.02	-1.41	240.0	0.84	-0.03	271.0	0.52	3.01
244.0	1.25	-1.15	242.0	0.91	-0.04	628.0	0.69	2.85
246.0	1.23	-1.31	244.0	1.12	-0.16			
251.0	1.11	-1.12	246.0	0.78	-0.12			
251.0	1.11	-1.12	248.0	0.79	-0.01			
271.0	1.09	-1.16	250.0	0.72	-0.12			
271.0	1.09	-1.16	251.0	0.92	-0.19			
291.0	0.86	-1.19	267.0	1.20	-0.64			

Table B.1 continued from previous page

G. ruber			*N. dutertrei*			*C wuellerstorfi*		
Depth (cm)	$\delta^{13}C$	$\delta^{18}O$	Depth (cm)	$\delta^{13}C$	$\delta^{18}O$	Depth (cm)	$\delta^{13}C$	$\delta^{18}O$
291.0	0.86	-1.19	271.0	0.76	-0.26			
311.0	1.51	-1.39	628.0	0.62	-0.35			
311.0	1.51	-1.39						
331.0	1.29	-1.63						
331.0	1.29	-1.63						
350.0	1.34	-1.38						
350.0	1.34	-1.38						
370.0	1.43	-1.17						
370.0	1.43	-1.17						
390.0	1.36	-1.52						
390.0	1.36	-1.52						
410.0	1.22	-1.64						
410.0	1.22	-1.64						
418.0	1.57	-0.96						
430.0	1.38	-1.62						

Table B.1 continued from previous page

G. ruber			*N. dutertrei*			*C wuellerstorfi*		
Depth (cm)	$\delta^{13}C$	$\delta^{18}O$	Depth (cm)	$\delta^{13}C$	$\delta^{18}O$	Depth (cm)	$\delta^{13}C$	$\delta^{18}O$
430.0	1.38	-1.62						
450.0	1.11	-1.52						
450.0	1.11	-1.52						
468.5	1.01	-1.68						
468.5	1.01	-1.68						
488.5	0.88	-2.18						
488.5	0.88	-2.18						
507.5	0.68	-1.05						
508.5	0.68	-1.05						
528.5	0.96	-0.75						
528.5	0.96	-0.75						
547.5	0.86	-0.42						
548.5	0.86	-0.42						
568.0	0.72	-0.70						
568.0	0.72	-0.70						

Table B.1 continued from previous page

G. ruber			*N. dutertrei*			*C wuellerstorfi*		
Depth (cm)	$\delta^{13}C$	$\delta^{18}O$	Depth (cm)	$\delta^{13}C$	$\delta^{18}O$	Depth (cm)	$\delta^{13}C$	$\delta^{18}O$
588.0	0.89	-0.41						
588.0	0.89	-0.41						
608.0	0.69	-1.19						
608.0	0.69	-1.19						
628.0	0.93	-1.16						
628.0	0.93	-1.16						
648.0	0.57	-0.86						
648.0	0.57	-0.86						
668.0	0.91	-1.34						
668.0	0.91	-1.34						

TABLE B.2: Stable Isotope Data for core 64PE303-16

G. ruber			*N. dutertrei*			*C wuellerstorfi*		
Depth (cm)	$\delta^{13}C$ (‰)	$\delta^{18}O$ (‰)	Depth (cm)	$\delta^{13}C$ (‰)	$\delta^{18}O$ (‰)	Depth (cm)	$\delta^{13}C$ (‰)	$\delta^{18}O$ (‰)
2.5	1.10	-2.22	2.5	1.19	-0.96	4.5	0.70	2.58
2.5	1.10	-1.59	3.5	0.85	-0.85	7.5	0.64	2.35
3.5	1.59	-1.46	4.5	1.27	-1.05	8.5	0.51	2.50
3.5	1.47	-2.07	6.5	1.18	-1.19	9.5	0.62	2.57
4.5	1.43	-2.16	7.5	1.42	-1.17	11.5	0.49	2.55
6.5	1.29	-2.07	8.5	1.09	-1.02	14.5	0.60	2.32
7.5	1.49	-2.12	9.5	0.97	-1.20	16.5	0.67	2.46
8.5	1.58	-2.11	11.5	1.21	-0.90	17.5	0.55	2.52
9.5	1.37	-2.12	12.5	1.23	-1.03	18.5	0.94	2.25
11.5	1.30	-2.18	13.5	1.35	-1.07	22.5	0.64	2.48
12.5	1.31	-2.10	14.5	1.32	-0.92	24.5	0.97	1.56
13.5	1.34	-2.05	16.5	1.08	-1.11	26.5	0.37	2.84
16.5	1.25	-2.22	17.5	1.19	-0.94	28.5	0.70	2.64
17.5	1.17	-2.10	18.5	1.12	-0.99	31.5	0.48	2.89
18.5	1.25	-2.14	19.5	1.11	-0.99	32.5	0.35	2.84

Table B.2 continued from previous page

G. ruber			*N. dutertrei*			*C wuellerstorfi*		
Depth (cm)	$\delta^{13}C$	$\delta^{18}O$	Depth (cm)	$\delta^{13}C$	$\delta^{18}O$	Depth (cm)	$\delta^{13}C$	$\delta^{18}O$
19.5	1.16	-2.27	21.5	1.24	-0.86	34.5	0.38	2.91
21.5	1.07	-2.24	22.5	1.24	-0.88	37.5	0.14	3.17
22.5	1.67	-2.08	24.5	1.16	-0.72	43.5	0.91	1.98
26.5	0.97	-1.87	26.5	1.08	-0.55	44.5	0.39	3.29
27.5	1.11	-1.74	27.5	0.91	-0.53	45.5	0.33	3.58
28.5	1.04	-1.85	28.5	1.04	-0.64	47.5	0.50	2.79
29.5	0.72	-1.77	29.5	0.80	-0.33	52.5	0.33	3.03
31.5	0.97	-1.84	31.5	1.32	-0.28	57.5	0.41	3.08
32.5	0.75	-1.60	32.5	0.76	-0.53	58.5	1.17	2.23
33.5	0.84	-1.65	33.5	1.12	-0.30	59.5	0.45	3.04
34.5	1.10	-1.82	34.5	1.09	-0.07	61.5	0.40	3.24
36.5	1.08	-1.49	36.5	1.15	-0.42	63.5	0.39	3.33
37.5	1.07	-1.68	37.5	0.87	-0.42	64.5	0.50	2.75
38.5	0.92	-1.68	38.5	1.03	-0.41	66.5	0.68	2.98
39.5	1.03	-1.49	39.5	0.83	-0.38	67.5	0.45	2.92

Table B.2 continued from previous page

G. ruber			*N. dutertrei*			*C wuellerstorfi*		
Depth (cm)	$\delta^{13}C$	$\delta^{18}O$	Depth (cm)	$\delta^{13}C$	$\delta^{18}O$	Depth (cm)	$\delta^{13}C$	$\delta^{18}O$
41.5	0.74	-1.34	41.5	0.98	-0.48	68.5	0.26	3.38
42.5	1.08	-1.37	42.5	1.07	-0.17	69.5	0.31	3.40
43.5	0.85	-1.43	43.5	1.23	0.06	72.5	0.31	3.41
44.5	0.93	-1.20	44.5	1.25	0.06	73.5	0.20	3.34
46.5	1.04	-1.14	46.5	1.02	-0.02	74.5	0.44	2.97
47.5	1.36	-0.85	47.5	0.99	0.01	76.5	0.70	2.99
48.5	0.70	-1.31	48.5	1.03	-0.19	78.5	0.31	3.12
51.5	0.96	-1.06	49.5	0.95	0.05	82.5	0.52	3.22
51.5	0.94	-1.32	51.5	0.83	0.05	85.5	0.48	3.54
52.5	0.99	-1.38	52.5	0.92	0.00	87.5	0.51	3.94
53.5	1.22	-1.27	53.5	0.99	0.20	88.5	0.40	3.42
54.5	0.82	-1.05	54.5	1.13	-0.09	89.5	0.53	3.61
56.5	1.15	-1.35	56.5	0.89	0.07	92.5	0.04	3.22
57.5	0.83	-1.23	57.5	0.88	0.13	93.5	0.39	3.70
58.5	1.10	-1.43	58.5	1.01	0.05	94.5	0.80	3.01

Table B.2 continued from previous page

G. ruber			*N. dutertrei*			*C wuellerstorfi*		
Depth (cm)	$\delta^{13}C$	$\delta^{18}O$	Depth (cm)	$\delta^{13}C$	$\delta^{18}O$	Depth (cm)	$\delta^{13}C$	$\delta^{18}O$
61.5	1.05	-1.25	59.5	0.84	-0.06	97.5	0.65	3.69
62.5	0.96	-1.34	61.5	0.77	-0.05	98.5	0.83	2.47
63.5	0.84	-1.19	62.5	1.03	-0.12	101.5	0.28	3.49
66.5	0.80	-1.35	63.5	0.84	0.45	102.5	0.38	3.77
67.5	1.05	-1.16	63.5	0.73	0.16	103.5	0.68	3.86
68.5	0.59	-1.41	64.5	1.05	0.03	104.5	0.36	4.05
69.5	0.89	-1.25	66.5	1.10	0.01	106.5	0.23	4.06
72.5	0.78	-1.44	67.5	0.86	0.05	107.5	0.20	3.73
73.5	0.98	-1.38	69.5	1.02	-0.15	108.5	0.18	3.79
76.5	0.81	-1.10	72.5	1.08	-0.12	112.5	0.22	3.91
77.5	0.96	-1.05	73.5	0.79	-0.27	113.5	0.23	4.16
78.5	0.58	-1.17	74.5	0.99	0.09	114.5	0.15	3.94
79.5	0.78	-1.02	76.5	0.52	0.24	116.5	0.22	3.97
81.5	0.86	-1.02	77.5	0.90	0.25	117.5	0.24	4.13
82.5	0.71	-0.81	79.5	0.69	0.28	119.5	0.73	3.41

Table B.2 continued from previous page

G. ruber			*N. dutertrei*			*C wuellerstorfi*		
Depth (cm)	$\delta^{13}C$	$\delta^{18}O$	Depth (cm)	$\delta^{13}C$	$\delta^{18}O$	Depth (cm)	$\delta^{13}C$	$\delta^{18}O$
83.5	1.11	-0.83	81.5	0.89	0.34	121.5	0.22	4.06
84.5	1.04	-0.73	82.5	0.76	0.56	122.5	0.13	3.96
86.5	0.76	-0.95	83.5	1.11	0.19	123.5	0.33	3.92
87.5	1.11	-0.55	84.5	1.10	0.39	124.5	0.14	3.97
88.5	0.76	-0.64	86.5	0.84	0.07	127.5	0.23	4.04
89.5	0.96	-0.60	87.5	0.82	0.55	128.5	0.16	4.08
91.5	0.88	-0.71	88.5	1.00	0.59	129.5	0.21	4.02
92.5	0.73	-0.27	89.5	0.96	0.64	131.5	0.24	3.91
93.5	1.03	-0.52	91.5	1.02	0.19	132.5	0.25	3.94
94.5	0.99	-0.58	92.5	0.75	0.51	133.5	0.03	4.00
96.5	0.62	-0.43	93.5	1.28	0.70	134.5	-0.02	3.86
97.5	1.06	-0.49	96.5	1.18	0.79	136.5	0.22	3.89
98.5	0.92	-0.84	97.5	1.08	0.76	137.5	0.21	3.83
99.5	0.88	-0.53	98.5	1.01	0.22	138.5	0.18	4.05
101.5	1.05	-0.55	99.5	1.13	0.76	139.5	0.23	3.86

Table B.2 continued from previous page

G. ruber			*N. dutertrei*			*C wuellerstorfi*		
Depth (cm)	$\delta^{13}C$	$\delta^{18}O$	Depth (cm)	$\delta^{13}C$	$\delta^{18}O$	Depth (cm)	$\delta^{13}C$	$\delta^{18}O$
102.5	1.14	-0.07	101.5	1.27	0.79	141.5	0.09	3.92
103.5	1.15	-0.74	102.5	1.30	0.47	142.5	0.22	3.69
104.5	0.99	-0.45	103.5	1.38	0.72	143.5	0.19	3.98
106.5	1.31	-0.42	104.5	1.26	0.68	144.5	0.18	3.85
107.5	1.05	-0.35	106.5	1.35	0.68	148.5	0.38	3.81
108.5	1.21	-0.42	107.5	1.10	0.61	149.5	0.36	3.50
109.5	0.79	-0.39	108.5	1.26	0.63	151.5	0.37	3.73
111.5	1.13	-0.47	109.5	1.38	0.67	152.5	0.50	4.10
112.5	0.89	-0.40	111.5	1.18	0.64	156.5	0.41	3.86
113.5	1.18	-0.46	112.5	1.28	0.65	157.5	0.65	3.78
114.5	1.02	-0.43	113.5	1.29	0.64	158.5	0.16	3.97
116.5	1.10	-0.50	114.5	1.41	0.57	159.5	0.42	3.96
117.5	1.02	-0.52	116.5	1.23	0.56	162.5	0.40	3.80
118.5	1.25	-0.57	117.5	1.23	0.61	163.5	0.31	4.03
119.5	0.91	-0.49	118.5	1.34	0.70	166.5	0.09	3.88

Table B.2 continued from previous page

G. ruber			*N. dutertrei*			*C wuellerstorfi*		
Depth (cm)	$\delta^{13}C$	$\delta^{18}O$	Depth (cm)	$\delta^{13}C$	$\delta^{18}O$	Depth (cm)	$\delta^{13}C$	$\delta^{18}O$
121.5	1.00	-0.34	119.5	0.98	0.81	167.5	0.76	3.80
122.5	1.03	-0.60	121.5	1.51	0.56	169.5	0.03	3.90
123.5	1.02	-0.42	122.5	1.45	0.62	171.5	0.36	3.83
124.5	1.04	-0.35	123.5	1.37	0.61	172.5	0.30	3.77
127.5	1.14	-0.55	124.5	1.17	0.66	173.5	0.28	3.66
128.5	1.08	-0.43	127.5	1.43	0.57	174.5	0.39	3.74
129.5	1.02	-0.60	128.5	1.39	0.57	176.5	0.43	3.69
131.5	1.13	-0.37	129.5	1.38	0.60	178.5	0.26	3.72
132.5	0.77	-0.65	131.5	1.42	0.51	181.5	0.34	3.79
133.5	0.98	-0.60	132.5	1.39	0.41	182.5	0.44	3.77
136.5	1.16	-0.52	133.5	1.26	0.43	183.5	0.35	3.93
137.5	1.18	-0.45	136.5	1.33	0.32	184.5	0.60	3.81
138.5	1.06	-0.80	137.5	1.24	0.57	187.5	0.47	3.49
139.5	1.24	-0.50	138.5	1.48	0.36	189.5	0.61	3.70
141.5	1.03	-0.86	139.5	1.17	0.36	197.5	0.31	3.84

Table B.2 continued from previous page

G. ruber			*N. dutertrei*			*C wuellerstorfi*		
Depth (cm)	$\delta^{13}C$	$\delta^{18}O$	Depth (cm)	$\delta^{13}C$	$\delta^{18}O$	Depth (cm)	$\delta^{13}C$	$\delta^{18}O$
142.5	1.35	-0.60	141.5	1.37	0.42	202.5	0.48	3.78
143.5	1.00	-0.67	142.5	1.15	0.54	206.5	0.45	3.64
144.5	1.38	-0.40	143.5	1.26	0.59	211.5	0.29	3.74
146.5	1.12	-0.84	144.5	1.31	0.45	212.5	0.35	3.69
147.5	1.09	-0.38	146.5	1.13	0.69	213.5	0.43	3.63
148.5	1.24	-0.86	147.5	1.25	0.51	214.5	0.49	3.86
149.5	1.22	-0.53	148.5	1.49	0.53	216.5	0.28	3.49
151.5	1.29	-0.65	149.5	1.13	0.20	218.5	0.45	3.73
152.5	1.09	-0.56	151.5	1.35	0.48	219.5	0.27	3.52
153.5	1.40	-0.64	152.5	1.38	0.62	222.5	0.33	3.87
154.5	1.39	-0.44	153.5	1.35	0.44	223.5	0.34	3.59
156.5	1.26	-0.53	156.5	1.32	0.48	224.5	0.32	3.74
157.5	1.35	-0.73	157.5	1.42	0.43	227.5	0.40	3.80
158.5	1.12	-0.59	158.5	1.02	0.50	228.5	0.35	3.56
159.5	1.08	-0.69	159.5	1.29	0.57	229.5	0.41	3.48

Table B.2 continued from previous page

G. ruber			*N. dutertrei*			*C wuellerstorfi*		
Depth (cm)	$\delta^{13}C$	$\delta^{18}O$	Depth (cm)	$\delta^{13}C$	$\delta^{18}O$	Depth (cm)	$\delta^{13}C$	$\delta^{18}O$
161.5	1.19	-0.43	162.5	1.34	0.36	231.5	0.43	3.57
162.5	1.39	-0.60	164.5	1.10	0.54	233.5	0.43	3.73
164.5	1.30	-0.72	166.5	1.25	0.48	234.5	0.51	3.66
166.5	1.01	-0.62	167.5	1.60	0.42	236.5	0.37	3.48
167.5	1.08	-0.39	168.5	1.54	0.66	237.5	0.42	3.60
168.5	1.15	-0.44	171.5	1.19	0.54	238.5	0.38	3.50
171.5	1.22	-0.78	172.5	1.33	0.19	239.5	0.41	3.76
172.5	1.28	-0.79	173.5	1.63	0.37	241.5	0.18	3.62
173.5	0.98	-0.76	174.5	1.31	0.29	244.5	0.18	3.51
174.5	0.96	-0.57	176.5	1.30	0.18	246.5	0.40	3.57
174.5	0.88	-1.03	177.5	1.43	0.54	247.5	0.67	3.59
176.5	1.30	-0.71	178.5	1.64	0.12	248.5	0.55	3.64
177.5	1.37	-0.87	179.5	1.28	0.56	249.5	0.20	3.09
178.5	1.24	-0.52	181.5	1.24	0.41	251.5	0.43	3.59
179.5	1.31	-0.86	182.5	1.64	0.06	252.5	0.51	3.36

Table B.2 continued from previous page

G. ruber			*N. dutertrei*			*C wuellerstorfi*		
Depth (cm)	$\delta^{13}C$	$\delta^{18}O$	Depth (cm)	$\delta^{13}C$	$\delta^{18}O$	Depth (cm)	$\delta^{13}C$	$\delta^{18}O$
181.5	1.27	-0.68	183.5	1.19	0.10	254.5	0.15	3.09
182.5	1.28	-0.74	184.5	1.35	0.21	256.5	0.33	3.62
183.5	1.26	-0.71	186.5	1.09	0.34	257.5	0.23	3.44
184.5	1.16	-0.70	187.5	1.21	0.37	261.5	0.23	3.55
186.5	1.14	-0.61	188.5	1.30	0.22	262.5	0.40	3.40
187.5	1.04	-0.40	189.5	1.45	0.58	263.5	0.22	3.45
188.5	1.27	-0.56	192.5	1.13	0.46	264.5	0.38	3.58
189.5	1.36	-0.74	193.5	1.34	0.54	267.5	0.26	3.57
191.5	0.75	-0.83	194.5	1.33	0.33	268.5	0.58	3.68
192.5	0.98	-0.69	196.5	1.18	0.62	271.5	0.39	3.62
192.5	0.76	-0.98	197.5	1.39	0.33	272.5	0.33	3.45
193.5	1.13	-0.54	198.5	1.14	0.67	273.5	0.29	3.66
194.5	0.96	-0.73	199.5	1.22	0.26	274.5	0.53	3.14
196.5	0.97	-0.68	201.5	1.33	0.68	276.5	0.51	3.52
197.5	1.13	-0.73	203.5	1.09	0.78	277.5	0.57	3.40

Table B.2 continued from previous page

G. ruber			*N. dutertrei*			*C wuellerstorfi*		
Depth (cm)	$\delta^{13}C$	$\delta^{18}O$	Depth (cm)	$\delta^{13}C$	$\delta^{18}O$	Depth (cm)	$\delta^{13}C$	$\delta^{18}O$
198.5	1.07	-0.75	206.5	1.37	0.64	278.5	0.32	3.74
199.5	1.07	-0.70	208.5	1.21	0.20	282.5	0.20	3.66
201.5	1.05	-0.58	211.5	1.56	0.28	286.5	0.31	3.59
202.5	1.00	-0.57	212.5	1.11	0.25	287.5	0.22	3.66
203.5	0.97	-0.41	213.5	1.73	0.30	296.5	0.63	3.37
204.5	0.95	-0.71	214.5	1.39	0.36	297.5	0.43	3.45
206.5	1.34	-0.64	216.5	1.25	0.41	298.5	0.55	3.54
207.5	1.14	-0.76	217.5	1.17	0.31	301.5	0.37	3.21
208.5	1.04	-0.80	218.5	1.24	0.36	302.5	0.17	3.22
211.5	0.89	-0.91	219.5	1.27	0.17	303.5	0.36	3.39
212.5	1.17	-0.72	221.5	1.22	0.24	304.5	0.16	3.37
213.5	1.00	-0.70	222.5	1.23	0.39	307.5	0.63	3.43
214.5	0.99	-0.60	223.5	0.90	0.37	309.5	1.04	2.78
216.5	1.07	-0.75	224.5	1.28	0.40	321.5	0.86	3.51
217.5	1.11	-0.75	226.5	1.14	0.28	322.5	0.39	3.76

Table B.2 continued from previous page

G. ruber			*N. dutertrei*			*C wuellerstorfi*		
Depth (cm)	$\delta^{13}C$	$\delta^{18}O$	Depth (cm)	$\delta^{13}C$	$\delta^{18}O$	Depth (cm)	$\delta^{13}C$	$\delta^{18}O$
218.5	1.01	-0.66	227.5	1.31	0.16	323.5	0.33	3.57
219.5	0.97	-0.70	228.5	1.35	0.05	324.5	0.34	3.52
221.5	1.20	-0.69	229.5	1.30	0.35	326.5	0.30	3.61
222.5	0.90	-0.80	231.5	1.14	0.16	327.5	0.28	3.33
223.5	1.15	-0.85	232.5	1.28	0.35	328.5	0.22	3.59
224.5	1.14	-0.78	233.5	1.35	0.18	329.5	0.37	3.51
226.5	0.73	-0.91	234.5	1.44	0.36	331.5	0.43	3.53
227.5	0.93	-0.97	236.5	1.16	0.15	333.5	0.25	3.39
228.5	0.99	-0.74	237.5	1.22	0.04	334.5	-0.01	3.27
229.5	1.02	-0.82	238.5	1.39	0.14	336.5	0.20	3.68
231.5	1.27	-1.10	239.5	1.77	0.04	337.5	0.08	3.49
232.5	1.08	-0.78	241.5	1.38	0.14	338.5	0.44	3.59
233.5	0.95	-0.92	242.5	1.19	0.32	339.5	0.54	3.56
234.5	1.01	-0.72	243.5	1.50	0.31	341.5	0.39	3.22
236.5	0.96	-0.77	244.5	1.40	0.29	342.5	0.26	3.46

Table B.2 continued from previous page

G. ruber			*N. dutertrei*			*C wuellerstorfi*		
Depth (cm)	$\delta^{13}C$	$\delta^{18}O$	Depth (cm)	$\delta^{13}C$	$\delta^{18}O$	Depth (cm)	$\delta^{13}C$	$\delta^{18}O$
237.5	1.05	-0.99	246.5	1.34	0.10	343.5	0.40	3.64
238.5	1.08	-0.88	247.5	1.49	-0.14	344.5	0.53	3.39
239.5	1.07	-0.81	248.5	1.19	0.19	346.5	0.31	3.18
241.5	1.01	-1.00	249.5	1.45	-0.09	347.5	0.51	3.37
242.5	0.87	-1.05	251.5	1.59	0.58	348.5	0.33	3.36
243.5	1.13	-0.97	252.5	1.29	0.14	349.5	0.29	3.35
244.5	1.32	-0.86	253.5	1.19	-0.02			
246.5	1.18	-0.97	254.5	1.39	0.13			
247.5	1.09	-0.95	256.5	1.55	-0.01			
248.5	0.87	-0.69	257.5	1.32	0.13			
249.5	1.04	-0.88	258.5	1.30	0.02			
251.5	1.35	-0.92	259.5	1.23	0.19			
252.5	0.95	-0.73	261.5	1.33	-0.09			
253.5	0.89	-1.22	262.5	1.26	0.07			
254.5	1.22	-0.91	263.5	1.21	-0.12			

Table B.2 continued from previous page

G. ruber			*N. dutertrei*			*C wuellerstorfi*		
Depth (cm)	$\delta^{13}C$	$\delta^{18}O$	Depth (cm)	$\delta^{13}C$	$\delta^{18}O$	Depth (cm)	$\delta^{13}C$	$\delta^{18}O$
256.5	1.23	-0.85	264.5	1.41	0.10			
257.5	0.97	-0.68	266.5	1.90	0.57			
258.5	0.93	-0.94	267.5	1.36	-0.01			
259.5	1.03	-0.90	268.5	1.86	0.63			
261.5	1.25	-0.84	269.5	1.31	0.12			
262.5	0.88	-0.94	271.5	1.18	0.58			
263.5	0.84	-0.98	273.5	1.44	0.20			
264.5	0.87	-1.09	273.5	1.30	0.12			
266.5	1.05	-1.08	274.5	1.26	0.10			
267.5	1.30	-0.81	276.5	1.23	0.08			
268.5	1.19	-0.91	277.5	1.11	0.37			
269.5	0.68	-1.18	278.5	1.27	0.16			
271.5	0.97	-0.89	279.5	1.41	0.05			
272.5	0.94	-0.76	282.5	1.04	-0.08			
273.5	1.24	-0.90	283.5	1.42	0.18			

Table B.2 continued from previous page

G. ruber			*N. dutertrei*			*C wuellerstorfi*		
Depth (cm)	$\delta^{13}C$	$\delta^{18}O$	Depth (cm)	$\delta^{13}C$	$\delta^{18}O$	Depth (cm)	$\delta^{13}C$	$\delta^{18}O$
274.5	0.93	-0.80	284.5	1.13	-0.17			
276.5	1.02	-0.98	286.5	1.12	0.07			
277.5	1.16	-0.73	287.5	0.91	-0.04			
278.5	0.89	-1.01	288.5	0.97	-0.30			
279.5	1.26	-1.03	289.5	1.03	0.22			
282.5	1.20	-0.89	292.5	1.08	0.39			
283.5	1.00	-0.93	293.5	0.99	0.58			
284.5	1.02	-0.91	294.5	0.92	-0.20			
286.5	1.01	-0.97	294.5	1.00	-0.27			
287.5	0.96	-0.76	296.5	1.33	0.11			
288.5	0.85	-1.06	296.5	1.16	0.12			
289.5	1.09	-1.08	297.5	1.17	0.04			
292.5	1.00	-1.18	298.5	1.08	0.24			
293.5	0.82	-1.13	299.5	1.01	-0.10			
294.5	0.95	-0.99	301.5	1.10	0.00			

Table B.2 continued from previous page

G. ruber			*N. dutertrei*			*C wuellerstorfi*		
Depth (cm)	$\delta^{13}C$	$\delta^{18}O$	Depth (cm)	$\delta^{13}C$	$\delta^{18}O$	Depth (cm)	$\delta^{13}C$	$\delta^{18}O$
296.5	0.84	-1.15	302.5	0.98	0.11			
297.5	1.05	-0.86	303.5	0.85	-0.03			
298.5	0.83	-1.02	304.5	1.05	-0.04			
299.5	0.71	-0.93	306.5	1.20	0.07			
301.5	0.98	-1.07	307.5	1.14	0.20			
302.5	0.89	-0.92	309.5	1.09	0.19			
303.5	0.93	-0.98	311.5	0.80	0.16			
304.5	0.98	-0.77	312.5	1.21	-0.13			
306.5	1.26	-0.78	319.5	1.02	-0.06			
307.5	0.80	-0.86	321.5	1.02	0.05			
309.5	0.85	-0.91	322.5	1.02	0.17			
312.5	0.99	-0.95	323.5	1.27	0.44			
312.5	1.03	-0.94	324.5	1.34	0.01			
319.5	1.07	-0.93	326.5	1.08	-0.06			
322.5	1.00	-0.98	327.5	1.12	-0.11			

Table B.2 continued from previous page

G. ruber			*N. dutertrei*			*C wuellerstorfi*		
Depth (cm)	$\delta^{13}C$	$\delta^{18}O$	Depth (cm)	$\delta^{13}C$	$\delta^{18}O$	Depth (cm)	$\delta^{13}C$	$\delta^{18}O$
324.5	1.16	-0.83	328.5	0.87	-0.11			
326.5	1.35	-0.86	329.5	1.51	0.06			
327.5	1.08	-0.82	331.5	1.38	0.09			
328.5	1.13	-0.83	332.5	1.23	0.00			
329.5	1.06	-0.76	333.5	0.85	-0.15			
331.5	1.20	-0.86	334.5	1.15	0.10			
332.5	1.28	-0.81	336.5	1.16	-0.20			
333.5	0.85	-0.83	337.5	1.23	0.58			
334.5	1.07	-0.99	338.5	0.89	0.34			
337.5	1.23	-0.46	339.5	1.44	-0.33			
341.5	1.34	-0.88	341.5	0.92	-0.26			
342.5	1.07	-0.88	342.5	1.30	0.08			
344.5	1.10	-0.86	343.5	1.21	-0.05			
346.5	1.25	-1.02	344.5	1.08	-0.06			
348.5	1.14	-0.92	346.5	1.46	-0.24			

Table B.2 continued from previous page

G. ruber		*N. dutertrei*			*C wuellerstorfi*		
Depth (cm)	$\delta^{13}C$	$\delta^{18}O$	Depth (cm)	$\delta^{13}C$	$\delta^{18}O$	Depth (cm)	$\delta^{13}C$	$\delta^{18}O$
349.5	1.27	-0.93	347.5	1.54	-0.07			
			348.5	0.99	-0.10			
			349.5	1.03	-0.05			

TABLE B.3: Stable Isotope Data for core 64PE303-15

G. ruber			*N. dutertrei*			*C wuellerstorfi*		
Depth (cm)	$\delta^{13}C$ (‰)	$\delta^{18}O$ (‰)	Depth (cm)	$\delta^{13}C$ (‰)	$\delta^{18}O$ (‰)	Depth (cm)	$\delta^{13}C$ (‰)	$\delta^{18}O$ (‰)
0.5	1.78	-2.22	0.5	1.24	-1.26	0.5	0.30	2.34
0.5	1.43	-2.12	1.5	1.19	-0.58	1.5	0.70	2.62
1.5	1.30	-2.20	2.5	1.32	-0.99	2.5	0.69	2.73
2.5	1.56	-2.10	3.5	1.24	-0.66	3.5	0.60	2.64
3.5	1.48	-2.07	4.5	1.27	-0.91	4.5	0.74	2.66
4.5	1.46	-2.10	5.5	1.30	-1.00	6.5	0.76	2.72
5.5	1.31	-2.05	6.5	1.36	-1.08	7.5	0.66	2.57
6.5	1.30	-2.17	7.5	1.27	-1.03	8.5	0.70	2.54
7.5	1.40	-2.03	8.5	1.22	-0.86	9.5	0.61	2.64
8.5	1.14	-1.93	9.5	1.14	-0.97	10.5	0.84	1.40
9.5	1.51	-1.66	11.5	1.04	-1.04	11.5	-0.12	1.68
11.5	1.46	-2.07	12.5	1.13	-1.07	12.5	0.81	2.42
12.5	1.42	-2.03	13.5	1.22	-0.74	13.5	0.83	2.78
13.5	1.37	-2.17	14.5	1.27	-0.75	14.5	0.55	2.64
14.5	1.34	-2.02	15.5	1.33	-0.95	15.5	0.01	2.21

Table B.3 continued from previous page

G. ruber			*N. dutertrei*			*C wuellerstorfi*		
Depth (cm)	$\delta^{13}C$	$\delta^{18}O$	Depth (cm)	$\delta^{13}C$	$\delta^{18}O$	Depth (cm)	$\delta^{13}C$	$\delta^{18}O$
15.5	1.40	-2.11	16.5	1.51	-1.24	16.5	0.69	2.78
16.5	1.52	-2.04	17.5	1.41	-1.27	17.5	0.06	1.94
17.5	1.43	-1.84	18.5	1.26	-0.97	18.5	0.54	2.13
18.5	1.35	-2.19	20.5	1.26	-0.91	20.5	0.59	2.97
20.5	1.47	-2.01	21.5	1.42	-1.26	21.5	0.56	2.34
21.5	1.54	-2.29	22.5	1.22	-1.09	22.5	0.65	2.37
22.5	1.05	-2.30	23.5	1.15	-0.84	23.5	0.73	2.84
23.5	1.31	-2.10	24.5	1.67	-1.23	24.5	1.05	2.29
24.5	1.62	-2.34	25.5	1.45	-0.80	25.5	0.57	1.94
25.5	1.37	-1.87	30	0.97	-0.93	28	0.61	2.61
30	1.28	-2.08	33	1.23	-0.76	29	0.63	2.75
33	0.76	-2.08	37	1.29	-0.84	30	0.78	2.55
37	1.13	-1.85	38	1.60	-1.09	31	0.47	2.40
38	1.19	-1.86	41	0.91	-0.64	32	0.36	3.20
41	1.14	-1.90	43	1.06	-0.45	33	0.49	2.42

Table B.3 continued from previous page

G. ruber			*N. dutertrei*			*C wuellerstorfi*		
Depth (cm)	$\delta^{13}C$	$\delta^{18}O$	Depth (cm)	$\delta^{13}C$	$\delta^{18}O$	Depth (cm)	$\delta^{13}C$	$\delta^{18}O$
43	1.03	-1.81	44	1.27	-0.78	34	0.46	2.56
44	1.13	-1.90	46	1.15	-0.47	36	0.36	2.93
46	1.09	-1.88	48	1.12	-0.37	39	0.30	2.89
48	1.11	-1.80	49	1.15	-0.57	40	0.25	2.84
49	1.12	-1.96	50	1.22	0.02	41	0.63	2.91
50	1.30	-2.05	52	1.06	-0.47	43	0.59	2.85
51	1.09	-1.46	53	1.00	-0.18	44	-0.07	2.06
52	1.60	-1.54	54	1.04	-0.19	46	-0.07	2.31
53	0.99	-1.69	56	1.14	-0.35	48	0.80	2.97
54	0.89	-1.45	57	0.87	-0.25	49	1.18	2.93
55	0.88	-1.57	58	1.42	-0.20	50	-0.08	2.45
57	1.06	-1.46	59	0.88	-0.27	51	0.17	3.00
58	1.11	-1.77	60	1.06	-0.39	52	0.36	2.98
59	1.01	-1.32	61	1.02	-0.03	53	0.29	2.66
60	0.99	-0.99	62	0.87	-0.13	54	0.36	3.12

Table B.3 continued from previous page

G. ruber			*N. dutertrei*			*C wuellerstorfi*		
Depth (cm)	$\delta^{13}C$	$\delta^{18}O$	Depth (cm)	$\delta^{13}C$	$\delta^{18}O$	Depth (cm)	$\delta^{13}C$	$\delta^{18}O$
61	0.83	-1.29	64	0.98	-0.24	55	0.38	2.85
62	0.77	-1.22	66	1.29	-0.12	57	0.24	3.14
64	0.95	-1.24	67	1.03	-0.24	58	0.35	2.88
66	0.80	-1.29	68	0.88	-0.15	59	0.46	2.85
67	0.87	-1.18	69	1.01	0.07	60	0.50	3.08
68	0.96	-1.34	70	0.91	0.55	60	0.29	3.02
69	1.09	-0.89	72	1.56	0.29	61	0.14	3.33
72	0.88	-0.95	74	1.11	0.28	63	0.09	3.84
74	0.93	-0.84	75	1.07	0.62	66	0.25	3.45
75	0.94	-0.62	76	1.00	0.54	67	0.44	3.16
76	1.22	-0.57	78	0.59	0.61	68	0.63	3.54
78	0.84	-0.48	79	1.12	0.58	70	0.15	3.57
79	1.14	-0.57	80	1.39	0.71	73	0.34	3.41
80	1.29	-0.63	81	1.22	0.79	74	0.49	3.40
81	1.19	-0.61	82	1.34	0.58	75	-0.29	2.79

Table B.3 continued from previous page

G. ruber			*N. dutertrei*			*C wuellerstorfi*		
Depth (cm)	$\delta^{13}C$	$\delta^{18}O$	Depth (cm)	$\delta^{13}C$	$\delta^{18}O$	Depth (cm)	$\delta^{13}C$	$\delta^{18}O$
82	0.84	-0.73	83	1.18	0.64	76	0.22	3.57
83	1.18	-0.53	84	1.42	0.32	78	0.41	3.45
84	1.00	-0.46	86	1.45	0.50	79	0.45	3.50
86	1.29	-0.70	88	1.29	0.61	80	0.87	3.16
88	1.18	-0.52	89	1.34	0.67	81	0.33	3.83
89	1.19	-0.48	90	1.05	0.82	82	0.41	3.89
90	1.11	-0.58	92	1.05	0.43	82	0.31	3.77
92	0.91	-0.57	93	1.40	0.65	83	0.24	4.27
93	0.79	-0.55	94	1.28	0.49	84	0.44	3.24
94	0.90	-0.45	95	1.51	0.71	84	0.15	3.90
95	1.12	-0.57	96	1.34	0.67	86	0.43	3.61
96	1.15	-0.59	97	1.32	0.46	88	0.13	4.12
97	1.13	-0.49	98	0.95	0.56	89	0.28	4.18
98	1.11	-0.49	99	1.25	0.67	90	0.05	4.27
99	1.01	-0.73	100	1.40	0.46	91	0.09	4.24

Table B.3 continued from previous page

G. ruber			*N. dutertrei*			*C wuellerstorfi*		
Depth (cm)	$\delta^{13}C$	$\delta^{18}O$	Depth (cm)	$\delta^{13}C$	$\delta^{18}O$	Depth (cm)	$\delta^{13}C$	$\delta^{18}O$
100	1.21	-0.35	101	1.30	0.46	92	-0.21	4.01
101	1.01	-0.47	102	1.22	0.56	92	0.11	4.13
102	1.16	-0.46	103	1.41	0.74	93	0.32	4.14
103	1.09	-0.85	104	1.16	0.55	94	0.06	4.17
104	1.23	-0.37	105	1.43	0.66	95	0.24	4.48
105	1.30	-0.46	106	1.47	0.58	96	-0.04	4.12
106	1.33	-0.39	108	1.26	0.47	97	0.23	4.28
108	1.17	-0.56	110	0.96	0.49	98	0.03	4.28
110	1.27	-0.45	112	1.08	0.45	99	0.13	4.10
112	1.06	-0.65	114	1.49	0.40	100	0.03	4.17
117	1.12	-0.52	116	1.44	0.56	101	0.57	4.29
118	1.08	-0.66	117	1.49	0.82	102	-0.04	3.91
120	1.10	-0.64	118	1.33	0.57	103	0.11	4.31
121	1.57	-0.61	119	1.33	0.41	104	-0.04	4.12
122	1.07	-0.49	120	1.27	0.66	105	-0.19	4.37

Table B.3 continued from previous page

G. ruber			*N. dutertrei*			*C wuellerstorfi*		
Depth (cm)	$\delta^{13}C$	$\delta^{18}O$	Depth (cm)	$\delta^{13}C$	$\delta^{18}O$	Depth (cm)	$\delta^{13}C$	$\delta^{18}O$
123	1.16	-0.41	122	1.32	0.47	106	-0.20	4.07
125	1.55	-0.54	123	1.59	0.51	107	-0.08	3.82
126	1.04	-0.57	124	1.32	0.43	108	-0.07	4.04
127	1.47	-0.67	125	1.52	0.49	110	-0.07	3.96
128	1.08	-0.55	126	1.40	0.62	111	0.05	4.21
129	1.01	-0.66	127	1.56	0.61	115	-0.04	3.87
130	1.17	-0.55	128	1.15	0.41	117	0.00	4.01
131	1.27	-0.50	129	1.07	0.55	118	0.02	4.22
132	1.01	-0.60	130	1.29	0.33	119	-0.10	4.09
134	1.29	-0.44	131	1.44	0.59	120	-0.42	4.04
135	1.23	-0.58	132	1.32	0.38	121	-0.24	3.91
136	1.03	-0.49	133	1.38	0.68	122	-0.15	4.19
137	0.90	-0.54	134	1.45	0.38	123	-0.25	4.01
138	1.46	-0.52	135	1.75	0.37	124	-0.08	4.09
139	1.30	-0.59	136	1.43	0.57	125	-0.12	3.87

Table B.3 continued from previous page

G. ruber			*N. dutertrei*			*C wuellerstorfi*		
Depth (cm)	$\delta^{13}C$	$\delta^{18}O$	Depth (cm)	$\delta^{13}C$	$\delta^{18}O$	Depth (cm)	$\delta^{13}C$	$\delta^{18}O$
140	1.28	-0.55	137	1.16	0.58	126	-0.06	4.01
141	1.38	-0.65	138	1.28	0.24	127	-0.16	3.98
142	1.07	-0.54	139	1.32	0.51	128	0.06	4.06
143	1.08	-0.45	140	1.35	0.34	129	-0.01	4.15
144	1.12	-0.60	141	1.66	0.55	130	0.11	4.05
146	1.60	-0.38	142	1.44	0.41	131	0.15	4.32
147	1.24	-0.54	143	1.65	0.61	132	0.08	3.82
148	0.90	-0.68	144	1.47	0.35	133	0.03	3.98
150	1.12	-0.50	146	1.15	0.46	134	0.14	4.07
152	1.18	-0.55	147	1.37	0.77	135	-0.03	4.18
153	1.23	-0.66	148	1.59	0.49	136	-0.02	3.74
154	1.02	-0.53	150	1.20	0.51	137	0.12	3.81
155	1.25	-0.76	152	1.30	0.58	138	-0.07	4.09
156	1.21	-0.71	153	1.17	0.54	139	0.07	4.04
157	1.35	-0.80	154	1.40	0.53	140	-0.01	3.90

Table B.3 continued from previous page

G. ruber			*N. dutertrei*			*C wuellerstorfi*		
Depth (cm)	$\delta^{13}C$	$\delta^{18}O$	Depth (cm)	$\delta^{13}C$	$\delta^{18}O$	Depth (cm)	$\delta^{13}C$	$\delta^{18}O$
158	1.07	-0.73	155	1.37	0.38	141	0.23	4.18
159	1.01	-0.68	156	1.22	0.23	142	0.10	4.15
160	1.03	-0.77	157	1.49	0.20	143	0.19	4.10
161	1.02	-0.69	158	1.29	0.43	144	0.17	4.17
162	1.18	-0.79	159	1.48	0.31	146	0.05	4.10
164	1.11	-0.59	160	1.32	0.33	148	-0.10	4.13
165	1.18	-0.78	161	1.36	0.39	149	-0.12	3.95
166	1.23	-0.60	162	0.98	0.29	150	0.15	4.04
167	1.33	-0.80	164	1.40	0.32	151	0.14	4.22
168	1.65	-0.90	165	1.59	0.18	152	-0.08	3.86
169	1.07	-0.76	166	1.21	0.48	153	-0.24	3.98
171	1.28	-0.90	167	1.26	0.52	154	0.11	4.14
172	1.38	-0.69	168	1.41	0.28	155	-0.21	4.16
173	1.28	-0.81	169	1.39	0.39	156	-0.42	3.62
174	1.11	-0.81	170	1.57	0.23	157	-0.24	3.93

Table B.3 continued from previous page

G. ruber			*N. dutertrei*			*C wuellerstorfi*		
Depth (cm)	$\delta^{13}C$	$\delta^{18}O$	Depth (cm)	$\delta^{13}C$	$\delta^{18}O$	Depth (cm)	$\delta^{13}C$	$\delta^{18}O$
175	1.09	-0.87	171	1.76	0.53	158	0.06	4.03
176	1.41	-0.75	172	1.53	0.46	159	-0.07	3.98
177	1.28	-0.89	173	1.18	0.37	160	0.08	3.81
178	1.11	-0.70	174	1.23	0.25	163	0.20	4.09
180	1.23	-0.82	175	1.68	0.45	164	0.22	3.78
181	1.23	-0.73	176	1.39	0.25	165	0.34	4.16
182	1.42	-0.64	177	1.65	0.22	166	0.10	3.92
183	1.09	-0.60	178	1.33	0.25	167	0.05	3.44
184	1.13	-0.63	180	1.43	0.41	168	0.63	3.25
185	1.00	-0.77	181	1.41	0.21	169	0.03	3.65
186	1.27	-0.56	182	1.07	0.16	170	0.03	3.92
187	1.13	-0.86	183	1.47	0.27	171	0.00	3.88
189	1.42	-0.81	184	2.00	0.20	172	0.14	3.87
190	1.14	-0.77	185	1.60	0.31	173	0.33	3.81
191	1.47	-0.94	186	1.35	0.49	174	-0.01	3.67

Table B.3 continued from previous page

G. ruber			*N. dutertrei*			*C wuellerstorfi*		
Depth (cm)	$\delta^{13}C$	$\delta^{18}O$	Depth (cm)	$\delta^{13}C$	$\delta^{18}O$	Depth (cm)	$\delta^{13}C$	$\delta^{18}O$
192	1.27	-0.85	187	1.42	0.31	175	0.19	3.65
193	1.17	-0.82	188	1.32	0.09	176	0.27	3.92
194	1.22	-0.88	189	1.29	0.45	177	0.05	3.87
195	1.09	-1.00	190	1.08	0.37	178	0.12	3.90
196	0.99	-0.82	191	1.36	0.25	180	0.27	3.79
197	0.93	-0.84	192	1.42	0.31	181	0.26	3.99
198	1.03	-0.76	193	1.35	0.50	182	0.24	3.90
200	1.52	-0.97	194	1.45	0.09	183	0.13	4.00
201	1.03	-0.80	195	1.45	-0.17	184	0.17	4.04
202	0.92	-0.88	196	1.20	0.11	185	0.52	3.62
204	1.30	-0.94	197	1.44	0.10	186	-0.08	3.56
205	1.36	-0.95	198	1.34	0.18	187	0.23	3.82
208	1.38	-0.72	200	1.31	0.45	188	0.23	3.98
209	1.55	-0.92	201	1.42	0.26	189	0.29	3.84
210	1.20	-0.66	202	1.37	0.17	191	0.28	3.80

Table B.3 continued from previous page

G. ruber			*N. dutertrei*			*C wuellerstorfi*		
Depth (cm)	$\delta^{13}C$	$\delta^{18}O$	Depth (cm)	$\delta^{13}C$	$\delta^{18}O$	Depth (cm)	$\delta^{13}C$	$\delta^{18}O$
212	1.17	-0.85	204	1.60	0.15	192	0.16	3.80
214	1.22	-0.99	205	1.43	0.18	193	0.25	3.69
215	1.31	-0.82	206	1.65	0.06	194	0.23	3.96
216	1.05	-0.82	208	1.50	-0.16	195	0.33	3.52
218	1.02	-0.87	209	1.53	0.02	196	-0.07	3.71
220	1.05	-1.08	210	1.21	-0.01	197	0.15	4.05
222	1.33	-1.00	212	1.04	0.17	198	0.23	3.93
223	1.38	-0.84	214	1.54	-0.09	200	-0.16	3.61
225	1.25	-1.11	215	1.56	-0.04	201	0.44	3.71
226	1.05	-1.05	216	1.53	0.09	202	-0.09	3.60
228	0.89	-1.11	218	1.33	0.00	204	0.10	3.83
229	1.23	-0.99	220	1.25	0.08	205	0.34	3.78
230	1.02	-1.07	222	1.47	-0.18	206	0.05	3.72
232	1.39	-0.94	224	1.48	-0.08	208	0.19	3.87
234	0.98	-1.00	225	1.42	-0.03	210	-0.05	3.58

Table B.3 continued from previous page

G. ruber			*N. dutertrei*			*C wuellerstorfi*		
Depth (cm)	$\delta^{13}C$	$\delta^{18}O$	Depth (cm)	$\delta^{13}C$	$\delta^{18}O$	Depth (cm)	$\delta^{13}C$	$\delta^{18}O$
236	1.16	-0.90	226	1.41	-0.27	212	0.11	3.75
238	1.06	-0.84	228	1.72	-0.26	214	0.23	3.62
240	1.19	-0.76	229	1.44	0.04	215	0.22	3.72
242	1.15	-0.60	230	1.03	0.18	216	0.23	3.74
243	1.14	-0.97	232	0.96	-0.02	221	0.19	3.69
244	1.27	-0.87	234	1.25	0.09	222	0.14	3.78
246	1.41	-0.85	236	0.95	0.12	223	0.17	3.78
247	1.33	-0.74	238	1.50	0.00	224	0.09	3.23
248	1.25	-0.88	239	1.02	-0.24	225	0.09	3.46
250	1.42	-0.99	240	1.73	0.18	226	-0.32	2.81
260	1.07	-0.87	242	1.34	0.13	228	0.10	2.93
265	1.32	-0.84	244	1.26	-0.04	229	0.31	3.80
268	1.30	-1.03	246	1.13	-0.18	230	0.02	3.64
279	0.99	-0.95	247	1.28	0.04	234	0.31	3.46
283	0.89	-0.90	248	1.33	-0.01	235	0.51	3.58

Table B.3 continued from previous page

G. ruber			*N. dutertrei*			*C wuellerstorfi*		
Depth (cm)	$\delta^{13}C$	$\delta^{18}O$	Depth (cm)	$\delta^{13}C$	$\delta^{18}O$	Depth (cm)	$\delta^{13}C$	$\delta^{18}O$
285	1.47	-0.94	250	1.20	-0.17	236	0.32	3.59
287	1.30	-0.96	251	1.52	0.25	238	0.37	3.75
288	1.20	-0.98	252	1.04	-0.06	239	0.37	3.82
289	1.78	-1.42	253	1.36	0.09	240	0.28	3.66
290	1.03	-0.95	255	1.38	0.01	241	0.23	3.37
293	1.16	-0.78	256	0.98	-0.12	242	0.12	3.49
296	1.51	-1.12	260	1.16	-0.08	243	0.23	3.90
297	1.14	-1.20	265	1.35	0.05	245	0.25	3.85
305	1.13	-0.94	271	1.42	-0.06	246	0.36	3.76
305	1.53	-0.81	272	1.45	0.01	247	0.32	3.86
307	1.16	-0.98	279	1.38	-0.09	248	0.09	3.71
310	1.06	-1.09	283	1.57	0.33	250	0.13	3.80
314	1.21	-1.40	287	1.09	0.12	251	0.17	3.83
318	1.09	-1.30	288	1.26	0.15	252	0.26	3.90
324	1.20	-1.34	289	1.45	0.23	253	0.68	3.86

Table B.3 continued from previous page

G. ruber			*N. dutertrei*			*C wuellerstorfi*		
Depth (cm)	$\delta^{13}C$	$\delta^{18}O$	Depth (cm)	$\delta^{13}C$	$\delta^{18}O$	Depth (cm)	$\delta^{13}C$	$\delta^{18}O$
325	1.07	-1.27	290	1.30	0.18	255	0.28	3.83
329	0.98	-1.34	293	1.15	0.12	256	0.54	3.58
332	1.23	-1.11	296	1.52	-0.09	260	0.24	3.74
335	1.07	-1.12	297	1.10	0.16	264	0.12	3.62
340	1.16	-1.12	303	1.13	0.19	265	0.34	3.71
343	0.82	-0.83	305	1.16	0.23	268	0.36	3.86
344	0.86	-1.00	306	1.13	-0.17	271	0.42	3.92
345	1.07	-1.22	307	1.29	-0.11	272	0.24	3.76
345	0.72	-1.12	310	1.23	-0.12	279	0.34	3.63
349	1.07	-1.37	314	1.13	-0.09	283	0.51	3.63
350	1.27	-1.21	316	1.00	-0.06	287	0.75	2.99
351	1.10	-1.21	318	0.99	-0.01	288	0.40	3.59
353	1.13	-0.97	324	1.16	-0.12	289	0.40	3.71
354	0.75	-1.21	329	1.03	0.06	290	0.73	3.63
356	1.42	-1.02	332	1.18	-0.06	293	0.57	3.76

Table B.3 continued from previous page

G. ruber			*N. dutertrei*			*C wuellerstorfi*		
Depth (cm)	$\delta^{13}C$	$\delta^{18}O$	Depth (cm)	$\delta^{13}C$	$\delta^{18}O$	Depth (cm)	$\delta^{13}C$	$\delta^{18}O$
376	1.05	-0.86	335	1.11	0.09	296	0.35	3.85
396	1.13	-0.88	340	0.93	-0.12	297	0.26	3.79
416	1.33	-0.88	341	1.13	0.30	303	0.36	3.81
419	1.37	-1.20	343	0.70	-0.03	305	0.23	4.07
424	1.17	-1.21	344	1.22	-0.04	306	0.26	3.77
427	1.45	-1.25	345	0.90	-0.04	307	0.34	3.45
428	1.30	-1.38	348	1.00	-0.12	314	0.31	1.03
429	1.52	-1.46	349	1.01	-0.06	316	0.38	2.84
433	1.43	-1.20	350	1.01	-0.23	318	0.28	3.00
435	2.02	-1.27	351	0.91	-0.06	330	0.24	3.70
436	1.41	-1.08	353	0.87	0.00	332	0.80	3.01
			354	0.98	0.05	333	0.36	3.55
			376	1.36	-0.02	335	0.77	2.56
			416	1.45	-0.31	340	0.24	3.68
			419	1.19	-0.16	341	0.25	3.64

Table B.3 continued from previous page

G. ruber			*N. dutertrei*			*C wuellerstorfi*		
Depth (cm)	$\delta^{13}C$	$\delta^{18}O$	Depth (cm)	$\delta^{13}C$	$\delta^{18}O$	Depth (cm)	$\delta^{13}C$	$\delta^{18}O$
			424	1.45	-0.38	343	0.25	3.72
			427	1.29	-0.40	344	0.44	3.76
			428	1.40	-0.36	345	0.22	4.35
			429	1.57	-0.39	348	0.52	2.66
			433	1.31	0.19	349	0.81	3.14
			435	1.39	-0.38	350	0.09	3.70
			436	1.28	-0.38	351	0.10	3.55
						353	0.36	3.55
						376	0.04	3.50
						416	0.14	3.86
						419	0.11	3.61
						424	0.25	3.77
						428	1.60	1.98
						429	0.34	3.40
						433	0.36	3.53

Table B.3 continued from previous page

G. ruber			*N. dutertrei*			*C wuellerstorfi*		
Depth (cm)	$\delta^{13}C$	$\delta^{18}O$	Depth (cm)	$\delta^{13}C$	$\delta^{18}O$	Depth (cm)	$\delta^{13}C$	$\delta^{18}O$
						435	0.72	3.36
						436	0.51	3.56

Appendix C

Counting Data

TABLE C.1: Counting data for core 64PE304-8. Samples selected for dating are indicated in bold and underlined.

Depth (cm)	No. Splits	No. Ruber	No. Total Planktics	Adjusted Ruber	Adjusted Total	Ratio
58.5	5	9	141	288	4512	0.06
61.5	**5**	**21**	**121**	**672**	**3872**	**0.17**
70.5	5	15	113	480	3616	0.13
72.5	3	10	143	80	1144	0.07
74.5	4	14	118	224	1888	0.12
76.5	3	8	98	64	784	0.08
78.5	3	19	151	152	1208	0.13
80.5	4	7	107	112	1712	0.07
81.5	4	14	107	224	1712	0.13
82.5	4	28	128	448	2048	0.22
83.5	4	10	119	160	1904	0.08
84.5	4	18	131	288	2096	0.14
85.5	4	10	111	160	1776	0.09
86.5	4	12	91	192	1456	0.13
87.5	4	10	79	160	1264	0.13

Table C.1 continued from previous page

Depth (cm)	No. Splits	No. Ruber	No. Total Planktics	Adjusted Ruber	Adjusted Total	Ratio
88.5	4	24	92	384	1472	0.26
89.5	3	6	102	48	816	0.06
90.5	4	15	95	240	1520	0.16
108.5	4	26	145	416	2320	0.18
109.5	4	14	93	224	1488	0.15
110.5	5	10	81	320	2592	0.12
111.5	4	33	161	528	2576	0.20
112.5	5	15	93	480	2976	0.16
114.5	5	11	109	352	3488	0.10
115.5	**6**	**23**	**129**	**1472**	**8256**	**0.18**
116.5	4	24	83	384	1328	0.29
118.5	6	15	94	960	6016	0.16
120.5	5	20	132	640	4224	0.15
121.5	6	9	84	576	5376	0.11
122.5	5	19	90	608	2880	0.21

Table C.1 continued from previous page

Depth (cm)	No. Splits	No. Ruber	No. Total Planktics	Adjusted Ruber	Adjusted Total	Ratio
123.5	6	13	68	832	4352	0.19
124.5	5	16	108	512	3456	0.15
124.5	6	18	199	1152	12736	0.09
126.5	6	11	95	704	6080	0.12
128.5	6	26	103	1664	6592	0.25
130	5	32	99	1024	3168	0.32
131	5	15	123	480	3936	0.12
132	5	13	85	416	2720	0.15
134	6	27	103	1728	6592	0.26
144	5	35	120	1120	3840	0.29
146	**7**	**22**	**105**	**2816**	**13440**	**0.21**
148	6	34	145	2176	9280	0.23
150	6	30	168	1920	10752	0.18
176	6	34	107	2176	6848	0.32
178	5	61	222	1952	7104	0.27

Table C.1 continued from previous page

Depth (cm)	No. Splits	No. Ruber	No. Total Planktics	Adjusted Ruber	Adjusted Total	Ratio
180	6	29	124	1856	7936	0.23
182	6	19	104	1216	6656	0.18
184	6	21	102	1344	6528	0.21
186	**6**	**29**	**93**	**1856**	**5952**	**0.31**
188	5	47	175	1504	5600	0.27
190	5	19	80	608	2560	0.24
215	7	15	98	2976	11008	0.27
216	**5**	**93**	**344**	**2496**	**11712**	**0.21**
220	6	39	183	2240	11648	0.19
222	6	35	182	3712	18432	0.20
224	7	29	144	2944	18816	0.16
226	7	23	147	2368	11968	0.20
228	6	37	187	960	6656	0.14
230	6	15	104	4224	17792	0.24
231	7	33	139	752	2864	0.26

Table C.1 continued from previous page

Depth (cm)	No. Splits	No. Ruber	No. Total Planktics	Adjusted Ruber	Adjusted Total	Ratio
232	4	47	179	3328	16000	0.21

TABLE C.2: Counting data for core 64PE303-16. Samples selected for dating are indicated in bold and underlined.

Depth (cm)	No. Splits	No. ruber	No. total planktics	Adjusted ruber	adjusted total	Ratio
16.5	4	17	107	272	1712	0.16
18.5	3	18	133	144	1064	0.14
19.5	5	8	66	256	2112	0.12
21.5	4	21	120	336	1920	0.18
23.5	**5**	**19**	**139**	**608**	**4448**	**0.14**
24.5	4	22	173	352	2768	0.13
26.5	4	15	109	240	1744	0.14
28.5	4	29	194	464	3104	0.15
31.5	5	15	114	480	3648	0.13
31.5	5	15	114	480	3648	0.13
33.5	4	20	130	320	2080	0.15
33.5	4	20	130	320	2080	0.15
34.5	5	21	125	672	4000	0.17
34.5	5	21	125	672	4000	0.17

Table C.2 continued from previous page

Depth (cm)	No. Splits	No. ruber	No. total planktics	Adjusted ruber	adjusted total	Ratio
36.5	5	13	103	416	3296	0.13
36.5	5	13	103	416	3296	0.13
61.5	5	13	163	416	5216	0.08
62.5	5	22	133	704	4256	0.17
63.5	5	14	139	448	4448	0.10
64.5	5	26	160	832	5120	0.16
66.5	5	15	151	480	4832	0.10
67.5	5	13	135	416	4320	0.10
68.5	5	18	143	576	4576	0.13
69.5	5	14	129	448	4128	0.11
71.5	**5**	**18**	**156**	**576**	**4992**	**0.12**
73.5	5	13	85	416	2720	0.15
76.5	5	19	105	608	3360	0.18
78.5	5	16	78	512	2496	0.21
79.5	5	14	83	448	2656	0.17

Table C.2 continued from previous page

Depth (cm)	No. Splits	No. ruber	No. total planktics	Adjusted ruber	adjusted total	Ratio
82.5	5	29	181	928	5792	0.16
83.5	6	6	128	384	8192	0.05
86.5	5	20	133	640	4256	0.15
88.5	6	14	111	896	7104	0.13
92.5	6	17	143	1088	9152	0.12
106.5	5	39	302	1248	9664	0.13
108.5	5	35	227	1120	7264	0.15
111.5	5	49	256	1568	8192	0.19
113.5	6	20	205	1280	13120	0.10
116.5	6	15	147	960	9408	0.10
118.5	4	29	178	464	2848	0.16
121.5	6	20	129	1280	8256	0.16
123.5	6	24	121	1536	7744	0.20
124.5	7	11	102	1408	13056	0.11
126.5	**6**	**23**	**156**	**1472**	**9984**	**0.15**

Table C.2 continued from previous page

Depth (cm)	No. Splits	No. ruber	No. total planktics	Adjusted ruber	adjusted total	Ratio
128.5	6	22	143	1408	9152	0.15
271.5	5	32	138	1024	4416	0.23
273.5	5	34	167	1088	5344	0.20
276.5	5	44	215	1408	6880	0.20
277.5	6	21	79	1344	5056	0.27
279.5	5	14	109	448	3488	0.13
283.5	4	19	98	304	1568	0.19
286.5	5	18	127	576	4064	0.14
288.5	5	32	243	1024	7776	0.13
291.5	**6**	**22**	**167**	**1408**	**10688**	**0.13**
293.5	5	34	174	1088	5568	0.20
296.5	5	25	125	800	4000	0.20
298.5	5	29	189	928	6048	0.15
301.5	5	23	203	736	6496	0.11
302.5	6	15	80	960	5120	0.19

Table C.2 continued from previous page

Depth (cm)	No. Splits	No. ruber	No. total planktics	Adjusted ruber	adjusted total	Ratio
304.5	4	23	162	368	2592	0.14
307.5	4	45	257	720	4112	0.18

TABLE C.3: Counting data for core 64PE303-15. Samples selected for dating are indicated in bold and underlined.

Depth (cm)	No. Splits	No. Ruber	No. Total Planktics	Adjusted ruber	Adjusted total planks	ratio
17.5	7	19	115	2432	14720	0.17
18.5	6	30	172	1920	11008	0.17
21.5	5	30	125	960	4000	0.24
22.5	5	18	113	576	3616	0.16
24.5	6	22	151	1408	9664	0.15
25.5	6	19	154	1216	9856	0.12
30	6	9	77	576	4928	0.12
35	6	8	73	512	4672	0.11
42	5	26	181	832	5792	0.14
43	5	8	86	256	2752	0.09
44	6	13	80	832	5120	0.16
45	6	6	67	384	4288	0.09
46	**6**	**16**	**115**	**1024**	**7360**	**0.14**
47	6	33	243	2112	15552	0.14

Table C.3 continued from previous page

Depth (cm)	No. Splits	No. Ruber	No. Total Planktics	Adjusted ruber	Adjusted total planks	ratio
48	5	21	134	672	4288	0.16
49	5	18	179	576	5728	0.10
50	5	24	159	768	5088	0.15
51	5	23	179	736	5728	0.13
52	6	13	73	832	4672	0.18
53	5	21	132	672	4224	0.16
54	5	21	148	672	4736	0.14
56	5	14	87	448	2784	0.16
57	5	18	109	576	3488	0.17
58	4	13	111	208	1776	0.12
59	5	23	129	736	4128	0.18
60	**6**	**19**	**95**	**1216**	**6080**	**0.20**
61	6	7	57	448	3648	0.12
62	6	9	57	576	3648	0.16
64	5	14	69	448	2208	0.20
66	5	21	104	672	3328	0.20

Table C.3 continued from previous page

Depth (cm)	No. Splits	No. Ruber	No. Total Planktics	Adjusted ruber	Adjusted total planks	ratio
67	6	9	45	576	2880	0.20
68	6	3	56	192	3584	0.05
70	5	26	93	832	2976	0.28
74	5	26	121	832	3872	0.21
76	6	24	84	1536	5376	0.29
78	5	28	106	896	3392	0.26
81	5	30	113	960	3616	0.27
82	5	32	91	1024	2912	0.35
83	5	38	129	1216	4128	0.29
84	5	27	186	864	5952	0.15
86	6	19	84	1216	5376	0.23
88	5	39	144	1248	4608	0.27
90	**5**	**47**	**176**	**1504**	**5632**	**0.27**
92	5	37	172	1184	5504	0.22
94	5	31	164	992	5248	0.19

Table C.3 continued from previous page

Depth (cm)	No. Splits	No. Ruber	No. Total Planktics	Adjusted ruber	Adjusted total planks	ratio
96	5	32	150	1024	4800	0.21
98	6	28	127	1792	8128	0.22
201	6	18	70	1152	4480	0.26
220	5	52	172	1664	5504	0.30
221	6	48	169	3072	10816	0.28
222	**7**	**32**	**117**	**4096**	**14976**	**0.27**
224	6	29	146	1856	9344	0.20
225	5	32	131	1024	4192	0.24
226	6	28	129	1792	8256	0.22
228	6	19	109	1216	6976	0.17
229	6	25	100	1600	6400	0.25
230	6	38	131	2432	8384	0.29
234	6	38	146	2432	9344	0.26
236	5	44	161	1408	5152	0.27
238	4	38	177	608	2832	0.21

Table C.3 continued from previous page

Depth (cm)	No. Splits	No. Ruber	No. Total Planktics	Adjusted ruber	Adjusted total planks	ratio
240	5	58	206	1856	6592	0.28
310	5	27	130	864	4160	0.21
312	6	15	101	960	6464	0.15
314	**6**	**24**	**85**	**1536**	**5440**	**0.28**
315	6	16	69	1024	4416	0.23
316	5	28	122	896	3904	0.23
318	5	48	173	1536	5536	0.28
319	6	25	95	1600	6080	0.26
323	6	12	77	768	4928	0.16
329	5	20	120	640	3840	0.17
332	5	33	148	1056	4736	0.22
333	5	18	96	576	3072	0.19
334	5	33	116	1056	3712	0.28
339	5	26	149	832	4768	0.17
340	5	21	103	672	3296	0.20

Appendix D

Data used to create Indian Ocean stable isotope time slices

TABLE D.1: Details of sediment cores and stable isotope data used to produce modern time slice presented in chapter 5. Reference provided in table 5.1.

Station	**Longitude**	**Latitude**	**Water depth (m)**	$\delta^{18}O$ **(‰)**	$\delta^{13}C$ **(‰)**
64PE303-15	39.8220	-9.0125	1985		
64PE303-16	39.7295	-8.9703	1350		
64PE304-8	39.6655	-8.9505	752		
GeoB3004-1 (M31/3-107_GC)	52.9200	14.6050	1803	2.55	0.19
MD01-2378	121.7880	-13.0825	1783	2.32	0.59
MD02-2488	88.0200	-46.4800	3420	2.94	0.18
MD02-2589	25.2550	-41.4333	2660		
MD73-025	51.3167	-43.8167	3284	2.93	0.22
MD76-125	75.2000	8.3500	1877	2.62	0.29
MD76-127	73.9000	12.0833	1610	2.48	0.22
MD76-128	73.1900	13.0800	1712	2.49	0.09
MD76-129	72.3333	15.0000	1954	2.56	0.19
MD76-135	50.3100	14.2700	1895	2.35	-0.16
MD77-171	94.0900	11.4600	1760	1.46	0.40
MD77-178	93.0833	17.2000	2459		

Table D.1 continued from previous page

Station	Longitude	Latitude	Water depth (m)	$\delta^{18}O$ (‰)	$\delta^{13}C$ (‰)
MD77-181	90.4833	17.4000	2271	1.92	0.27
MD77-182	91.0000	16.0200	2455	2.38	-0.13
MD77-184	92.2000	13.9833	2843		
MD77-191	76.7167	7.5000	1254	1.23	0.10
MD77-200	67.9000	16.5500	2910	2.60	0.15
MD79-254	38.4000	-17.5300	1934	2.74	0.71
MD79-256	37.0333	-19.5667	1222	2.41	0.68
MD79-257	36.3333	-20.4000	1262	1.50	0.39
MD84-527	51.1900	-43.4900	3262	3.09	0.28
MD88-769	90.1112	-46.0693	3420	2.87	0.51
MD88-770	96.4607	-46.0220	3290	2.42	0.13
MD98-2165	118.3400	-9.6500	2100	2.46	0.19
Meteor5-422	59.0472	24.3944	2732	2.38	-0.09
NIOP905	51.9500	10.7667	1575	2.26	0.00
NIOP929	53.2460	13.7035	2490	3.04	-0.12
ODP121-758	90.3612	5.3841	2935		

Table D.1 continued from previous page

Station	Longitude	Latitude	Water depth (m)	$\delta^{18}O$ (‰)	$\delta^{13}C$ (‰)
OROGON4-KS8	59.1972	23.4667	2900	2.79	-0.05
PS2082-1	11.7383	-43.2202	4610		
PS2561-2 (PS30/030	28.5417	-41.8583	4465	3.13	0.09
RC09-150	114.5500	-31.2800	2703		
RC11-120	79.8670	-43.5200	3193	2.92	0.39
RC12-339	90.0330	9.1330	3010		
RC12-344	96.0670	12.7670	2140		
RS102-GC09	128.0300	-33.5000	769	1.49	1.45
RS102-GC13	130.8000	-33.8300	1008	1.95	1.11
RS102-GC14	130.4200	-34.3800	1502	2.37	0.66
RS102-GC15	130.2600	-34.5900	2003	2.40	0.53
RS102-GC16	130.1400	-34.7500	2495	2.35	0.36
RS102-GC17	130.0600	-34.8900	3001	2.70	0.47
RS102-GC18	130.0100	-34.9600	3504	2.43	0.35
RS53-GC04	113.5400	-19.5900	956	1.85	0.73
RS53-GC06	112.7500	-19.0500	1979	2.44	0.66

Table D.1 continued from previous page

Station	Longitude	Latitude	Water depth (m)	$\delta^{18}O$ (‰)	$\delta^{13}C$ (‰)
RS53-GC07	112.6300	-18.9100	2256	2.37	0.77
RS53-GC09	112.9300	-20.0100	962	1.63	0.70
RS53-GC11	112.3300	-20.9000	1432	2.33	0.74
RS57-GC15	113.2200	-29.3800	2750		
RS57-GC19	111.6300	-27.3200	2755		
RS67-GC13	140.1667	-38.4650	2525		
RS67-GC3	138.5833	-37.5500	1467		
SK-129-CR2	76.0000	3.0000	3800	2.88	0.53
SK-157-14	90.0833	5.1833	3304	2.64	0.50
SK157-18	90.0200	11.9800	3069		
SO42-74Kl	57.3470	14.3210	3212	2.46	-0.01
SO93-22KL	83.3333	0.7500	4420		
V29-29	77.5833	5.1167	2673	2.63	0.20
V34-51	89.9700	-6.1900	4382	2.71	0.03
V34-53	89.5800	-6.1200	3812	2.51	0.27
V34-54	89.1700	-6.0800	3254	2.25	0.24

Table D.1 continued from previous page

Station	Longitude	Latitude	Water depth (m)	$\delta^{18}O$ (‰)	$\delta^{13}C$ (‰)
V34-55	88.9600	-6.0400	2992	2.44	0.04
WIND28K	51.0128	-10.1538	4157		

TABLE D.2: Details of sediment cores and stable isotope data used to produce LGM time slice presented in chapter 5. Reference provided in table 5.1.

Station	**Longitude**	**Latitude**	**Water depth (m)**	$\delta^{18}O$ **(‰)**	$\delta^{13}C$ **(‰)**
64PE303-15	39.8220	-9.0125	1985	4.07	-0.07
64PE303-16	39.7295	-8.9703	1350	3.94	0.21
64PE304-8	39.6655	-8.9505	752	3.35	1.05
GeoB3004-1 (M31/3-107_GC)	52.9200	14.6050	1803	3.67	-0.09
MD01-2378	121.7880	-13.0825	1783	3.98	0.08
MD02-2488	88.0200	-46.4800	3420	4.55	-0.85
MD02-2589	25.2550	-41.4333	2660	4.68	0.07
MD73-025	51.3167	-43.8167	3284	4.28	-0.94
MD76-125	75.2000	8.3500	1877	3.94	-0.10
MD76-127	73.9000	12.0833	1610		
MD76-128	73.1900	13.0800	1712		
MD76-129	72.3333	15.0000	1954		
MD76-135	50.3100	14.2700	1895	4.06	-0.06
MD77-127	75.9000	12.0800	1610	3.83	-0.12
MD77-169	10.1300	95.0300	1600	3.69	0.00

Table D.2 continued from previous page

Station	Longitude	Latitude	Water depth (m)	$\delta^{18}O$ (‰)	$\delta^{13}C$ (‰)
MD77-171	94.0900	11.4600	1760		
MD77-176	93.1000	14.5000	1357	3.23	0.04
MD77-178	93.0833	17.2000	2459	2.89	-0.21
MD77-181	90.4833	17.4000	2271	3.62	-0.41
MD77-182	91.0000	16.0200	2455	3.83	-1.08
MD77-183	15.1700	91.7500	2632	4.34	-1.09
MD77-184	92.2000	13.9833	2843	3.32	-0.60
MD77-191	76.7167	7.5000	1254	2.21	0.19
MD77-194	75.2333	10.4667	1222	3.46	0.26
MD77-200	67.9000	16.5500	2910		
MD77-202	60.6817	19.2217	2427	4.08	-0.23
MD77-203	59.5683	20.6983	2442	3.98	-0.35
MD79-254	38.4000	-17.5300	1934	4.19	-0.02
MD79-256	37.0333	-19.5667	1222		
MD79-257	36.3333	-20.4000	1262	2.88	0.12
MD84-527	51.1900	-43.4900	3262	4.34	-0.56

Table D.2 continued from previous page

Station	Longitude	Latitude	Water depth (m)	$\delta^{18}O$ (‰)	$\delta^{13}C$ (‰)
MD88-769	90.1112	-46.0693	3420	4.37	-0.64
MD88-770	96.4607	-46.0220	3290	4.04	-0.90
MD98-2165	118.3400	-9.6500	2100	4.18	-0.32
Meteor5-422	59.0472	24.3944	2732		
NIOP905	51.9500	10.7667	1575	3.63	-0.12
NIOP929	53.2460	13.7035	2490	4.00	-0.32
ODP121-758	90.3612	5.3841	2935	4.26	-0.04
OROGON4-KS8	59.1972	23.4667	2900	4.20	-0.52
PS2082-1	11.7383	-43.2202	4610		
PS2561-2 (PS30030)	28.5417	-41.8583	4465	4.59	-0.76
RC09-150	114.5500	-31.2800	2703	4.12	-0.12
RC11-120	79.8670	-43.5200	3193	4.45	-0.48
RC11-147	112.4500	-19.0400	1953	3.93	0.29
RC11-83	9.8000	-41.6000	4718	3.98	-0.96
RC12-339	90.0330	9.1330	3010	3.87	-0.18
RC12-344	96.0670	12.7670	2140	3.37	-0.24

Table D.2 continued from previous page

Station	Longitude	Latitude	Water depth (m)	$\delta^{18}O$ (‰)	$\delta^{13}C$ (‰)
RS102-GC09	128.0300	-33.5000	769	3.28	1.73
RS102-GC13	130.8000	-33.8300	1008	3.70	1.01
RS102-GC14	130.4200	-34.3800	1502	3.62	0.43
RS102-GC15	130.2600	-34.5900	2003	3.63	0.31
RS102-GC16	130.1400	-34.7500	2495	3.83	0.11
RS102-GC17	130.0600	-34.8900	3001	3.83	0.11
RS102-GC18	130.0100	-34.9600	3504	3.83	0.07
RS53-GC04	113.5400	-19.5900	956	3.40	0.51
RS53-GC06	112.7500	-19.0500	1979	3.90	0.27
RS53-GC07	112.6300	-18.9100	2256	4.02	0.20
RS53-GC09	112.9300	-20.0100	962	3.27	0.69
RS53-GC11	112.3300	-20.9000	1432	3.17	0.51
RS57-GC15	113.2200	-29.3800	2750	3.71	0.17
RS57-GC19	111.6300	-27.3200	2755	4.14	0.10
RS67-GC13	140.1667	-38.4650	2525	3.87	-0.37
RS67-GC3	138.5833	-37.5500	1467	3.63	0.49

Table D.2 continued from previous page

Station	Longitude	Latitude	Water depth (m)	$\delta^{18}O$ (‰)	$\delta^{13}C$ (‰)
SK-129-CR2	76.0000	3.0000	3800	4.18	-0.12
SK-157-14	90.0833	5.1833	3304	4.24	-0.23
SK157-18	90.0200	11.9800	3069	4.43	-0.31
SO28-57KL	63.1200	20.9000	3422	4.30	-0.49
SO42-74KI	57.3470	14.3210	3212	4.01	-0.39
SO93-22KL	83.3333	0.7500	4420		
V29-29	77.5833	5.1167	2673		
V34-51	89.9700	-6.1900	4382	3.94	-0.45
V34-53	89.5800	-6.1200	3812	3.87	-0.35
V34-54	89.1700	-6.0800	3254	3.70	-0.16
V34-55	88.9600	-6.0400	2992	3.84	-0.16
WIND28K	51.0128	-10.1538	4157	4.22	-0.03